MATERIALS FOR ADAPTIVE STRUCTURAL ACOUSTIC CONTROL

Period February 1, 1996 to January 31, 1997

Final Report

VOLUME VI

OFFICE OF NAVAL RESEARCH
Contract No.: N00014-92-J-1510

APPROVED FOR PUBLIC RELEASE — DISTRIBUTION UNLIMITED

L. Eric Cross

PENNSTATE

1855

THE MATERIALS RESEARCH LABORATORY
UNIVERSITY PARK, PA

REPORT DOCUMENTATION PAGE

Form Approved
OMB No. 0704-0188

1. AGENCY USE ONLY (Leave blank)	2. REPORT DATE	3. REPORT TYPE AND DATES COVERED
	4/14/97	FINAL REPORT 2/1/96-1/31/97

4. TITLE AND SUBTITLE

MATERIALS FOR ADAPTIVE STRUCTURAL ACOUSTIC CONTROL

5. FUNDING NUMBERS

ONR CONTRACT NO:
N00014-92-J-1510

6. AUTHOR(S)

L. ERIC CROSS

7. PERFORMING ORGANIZATION NAME(S) AND ADDRESS(ES)

MATERIALS RESEARCH LABORATORY
THE PENNSYLVANIA STATE UNIVERSITY
UNIVERSITY PARK, PA 16802-4800

8. PERFORMING ORGANIZATION REPORT NUMBER

9. SPONSORING/MONITORING AGENCY NAME(S) AND ADDRESS(ES)

OFFICE OF NAVAL RESEARCH
CODE 1513:NRJ
800 NORTH QUINCY STREET
ARLINGTON, VA 22217-5660

GERALD T. SMITH
OFFICE OF NAVAL RESEARCH RES.
536 SOUTH CLARK STREET, RM 286
CHICAGO, ILLINOIS 60606-1588

10. SPONSORING/MONITORING AGENCY REPORT NUMBER

REP.

11. SUPPLEMENTARY NOTES

12a. DISTRIBUTION/AVAILABILITY STATEMENT

12b. DISTRIBUTION CODE

13. ABSTRACT *(Maximum 200 words)*

SEE FOLLOWING TWO PAGES.

14. SUBJECT TERMS

15. NUMBER OF PAGES

16. PRICE CODE

17. SECURITY CLASSIFICATION OF REPORT	18. SECURITY CLASSIFICATION OF THIS PAGE	19. SECURITY CLASSIFICATION OF ABSTRACT	20. LIMITATION OF ABSTRACT

GENERAL INSTRUCTIONS FOR COMPLETING SF 298

The Report Documentation Page (RDP) is used in announcing and cataloging reports. It is important that this information be consistent with the rest of the report, particularly the cover and title page. Instructions for filling in each block of the form follow. It is important to ***stay within the lines*** to meet ***optical scanning requirements***.

Block 1. Agency Use Only *(Leave blank)*.

Block 2. Report Date. Full publication date including day, month, and year, if available (e.g. 1 Jan 88). Must cite at least the year.

Block 3. Type of Report and Dates Covered. State whether report is interim, final, etc. If applicable, enter inclusive report dates (e.g. 10 Jun 87 - 30 Jun 88).

Block 4. Title and Subtitle. A title is taken from the part of the report that provides the most meaningful and complete information. When a report is prepared in more than one volume, repeat the primary title, add volume number, and include subtitle for the specific volume. On classified documents enter the title classification in parentheses.

Block 5. Funding Numbers. To include contract and grant numbers; may include program element number(s), project number(s), task number(s), and work unit number(s). Use the following labels:

C	- Contract	PR	- Project
G	- Grant	TA	- Task
PE	- Program Element	WU	- Work Unit Accession No.

Block 6. Author(s). Name(s) of person(s) responsible for writing the report, performing the research, or credited with the content of the report. If editor or compiler, this should follow the name(s).

Block 7. Performing Organization Name(s) and Address(es). Self-explanatory.

Block 8. Performing Organization Report Number. Enter the unique alphanumeric report number(s) assigned by the organization performing the report.

Block 9. Sponsoring/Monitoring Agency Name(s) and Address(es). Self-explanatory.

Block 10. Sponsoring/Monitoring Agency Report Number. *(If known)*

Block 11. Supplementary Notes. Enter information not included elsewhere such as: Prepared in cooperation with...; Trans. of...; To be published in.... When a report is revised, include a statement whether the new report supersedes or supplements the older report.

Block 12a. Distribution/Availability Statement. Denotes public availability or limitations. Cite any availability to the public. Enter additional limitations or special markings in all capitals (e.g. NOFORN, REL, ITAR).

DOD	- See DoDD 5230.24, "Distribution Statements on Technical Documents."
DOE	- See authorities.
NASA	- See Handbook NHB 2200.2.
NTIS	- Leave blank.

Block 12b. Distribution Code.

DOD	- Leave blank.
DOE	- Enter DOE distribution categories from the Standard Distribution for Unclassified Scientific and Technical Reports.
NASA	- Leave blank.
NTIS	- Leave blank.

Block 13. Abstract. Include a brief *(Maximum 200 words)* factual summary of the most significant information contained in the report.

Block 14. Subject Terms. Keywords or phrases identifying major subjects in the report.

Block 15. Number of Pages. Enter the total number of pages.

Block 16. Price Code. Enter appropriate price code *(NTIS only)*.

Blocks 17. - 19. Security Classifications. Self-explanatory. Enter U.S. Security Classification in accordance with U.S. Security Regulations (i.e., UNCLASSIFIED). If form contains classified information, stamp classification on the top and bottom of the page.

Block 20. Limitation of Abstract. This block must be completed to assign a limitation to the abstract. Enter either UL (unlimited) or SAR (same as report). An entry in this block is necessary if the abstract is to be limited. If blank, the abstract is assumed to be unlimited.

ABSTRACT

This report documents work carried out largely over the fifth and final year of the ONR sponsored University Research Initiative (URI) entitled "Materials for Adaptive Structural Acoustic Control." This program has continued to foster the successful development of new electroceramic single crystal and composite material combinations for both sensing and actuation functions in adaptive structural systems.

For the classical perovskite relaxor, dielectrics typified by lead magnesium niobate, continuing studies of properties in the temperature region above the dielectric maximum T_m have added strong additional support to the superparaelectric/spin glass model for the behavior developed earlier in the IMRL. The most exciting and important discovery of the year has been the ultra high strain capability of relaxor ferroelectric single crystal actuators. For crystal in the lead zinc niobate:lead titanate (PZN;PT) solid solution system, at compositions in the rhombohedral phase close to the morphotropic phase boundary to the tetragonal ferroelectric phase at 9 mole % PT in PZN, crystals cut and poled along the 001 cube axis exhibit massive field induced quasi linear anhysterestic strains up to 0.6%. For this poling d_{33} values up to 2,300 pC/N and coupling coefficients k_{33} of 94% have been achieved and it was the original hypothesis that these extreme numbers must be largely due to extrinsic domain wall motion. Now however it is very clear that the exact equivalence of the effect of an 001 oriented E field on the $111, \bar{1}11, 1\bar{1}1,$ and $\bar{1}\bar{1}1$ rhombohedral domains precludes this field from driving domain wall motion so that quite contrary to our earlier expectation the polarization and associated strain phenomena are purely intrinsic. At higher field levels there is an obvious step in both polarization and strain into an induced tetragonal phase which gives total reproducible induced strains up to 1.7%. Clearly the PZN:PT crystals represent a major breakthrough into a completely new regimen for piezoelectric actuation and sensing.

For antiferroelectric:ferroelectric switching compositions in the lead lanthanum zirconated titanate stannate family, new experimental studies have proven that the induced polarization P_3 and the strain x_{33} onset at different field levels. A new domain re-orientation model has been invoked to explain this startlingly unusual behavior. Both barium and strontium additives have also been explored to control hysteresis between forward and backward switching with good success. As well as being interesting for transduction we believe these compositions are sure to be important for energy storage dielectrics.

In composite sensing it is pleasing to report that the moonie flextensional patent has now been licensed to the Input:Output Corporation who have successfully fabricated and sold more than 80,000 moonie sensors. Work is continuing on the cymbal type modification of the moonie with focus now on array structures for large area panels. This topic is transitioning to a joint study between the IMRL and Penn State's ARL, on a new MURI initiative. For the very small hollow PZT spheres produced by blowing, the emphasis has been upon both poling and driving from outer surface electrodes, and exploring both by experiment and by finite element theoretical methods, the resonant mode structures which can be induced. Studies of the 2:2 composite structures confirm the very high effective hydrostatic sensitivity and are permitting closer consonance between measurement and theoretical analysis.

Actuation studies have been dominated by the initial exploration of the fantastic strain capability of the relaxor ferroelectric MPB single crystals. Obviously the induced strains are on order of magnitude larger than for conventional PZT ceramics, but the blocking force has

not yet been determined. It is expected that d_{31} will also be large and anhysteritic in these crystals, as spontaneous strain depends on Q_{44} which is a pure shear constant. The d_{15} however may be significantly more complex as an E_1 field will certainly drive domain walls in these E_3 poled crystals.

Reliability studies of conventional actuators are continuing with emphasis on using acoustic emission to explore and separate domain wall motion and crack propagation. Most earlier studies were indeterminate and difficult to interpret, recently for these strongly piezoelectric samples we have shown that electrical noise in the power supply induces very strong mechanical noise in the sample giving high spurious emission counts. New studies using a long time constant filter in the supply have permitted clear and effective separation. Over the last few years there has been a strong re-awakening of interest in bimorph type transducer amplifiers with new concepts like rainbow, cerambow and thunder appearing. Under our ONR program with Virginia Polytechnic it has been necessary to sort out the conflicting claims for these 'morph' types and these data are included for completeness. We have also begun serious study of the large electrostriction in the soft polyurethane elastomers where it has been necessary to derive new techniques to measure strain with ultra low constraint on the films.

Processing studies now involved both single crystal flux growth and a wide range of powder and ceramic processing. Current needs for integrity and better mechanical properties are driving new needs for fine grained PZT piezoceramics and new processing is permitting retention of excellent properties down to submicron grain sizes.

From the wide range of thin ferroelectric film activities in the laboratory, only those which refer to the thicker films being produced on silicon for MEMS devices are included.

MATERIALS FOR ADAPTIVE STRUCTURAL ACOUSTIC CONTROL

Period February 1, 1996 to January 31, 1997

Final Report

VOLUME VI

OFFICE OF NAVAL RESEARCH
Contract No.: N00014-92-J-1510

L. Eric Cross

TABLE OF CONTENTS

APPENDICES

VOLUME I

General Summary Papers

1. Cross, L.E., "Ferroelectric Materials for Electromechanical Transducer Applications." *Mat. Chem. Phys* **43**, 108-115 (1996).

2. Cross, L.E., "Ferroelectric Ceramics: Materials and Application Issues." *Ceramic Transactions* **68**, 15-55 (1996).

3. Li. S., J.A. Eastman, Z. Li, C.M. Foster, R.E. Newnham, and L.E. Cross, " Size Effects in Ferroelectrics." *Phys. Lett. A* **212**, 341 (1996).

4. Li, Shaoping, J.A. Eastman, R.E. Newnham, and L.E. Cross, "Susceptibility of Nanostructured Ferroelectrics." *Japanese J. Appl. Physics* **35** (Part 2) [No. 4B], L502-L504 (1996).

5. Newnham, R.E., Chapter: Crystal Chemistry and Crystal Physics, in Innovative Ideas in Ceramics and Materials Curricula, edited by T. Stoebe and W. Huebner. Published by the *American Ceramic Society*, pp. 65-72 (1996).

6. Uchino, K., "New Applications of Photostriction." *Innovations in Mater. Res.* **1** (1), 11-22 (1996).

7. Aburatani, H. and K. Uchino, "Acoustic Emission (AE) Measurement Technique in Piezoelectric Ceramics." *Jpn. J. Appl. Phys.* **35** (2) [4B], L516-L518 (1996).

Materials Studies

8. Choi, S., J.M. Jung, and A.S. Bhalla, "Dielectric, Pyroelectric and Piezoelectric Properties of Calcium-Modified Lead Magnesium Tantalate-Lead Titanate Ceramics." *Ferroelectric Letters* **21**, 27-33 (1996).

9. Alberta, E. and A.S. Bhalla, "Preparation of Phase Pure Perovskite Lead Indium Niobate Ceramic." *Mater. Lett.* **29**, 127-129 (1996).

10. Zhang, Q.M., J. Zhao, T.R. Shrout, and L.E. Cross, "The Effect of Ferroelastic Coupling in Controlling the Abnormal Aging Behavior in Lead Magnesium Niobate-Lead Titanate Relaxor Ferroelectrics." *J. Mater. Res.* **12** (7), (1997).

11. Alberta, E., A.S. Bhalla, and T. Takenaka, "Piezoelectric, elastic and Dielectric Constants for Ceramics in the Solids Solution: $xPbZrO_3$ - $(1-x-z)Pb(Zn_{1/3}Nb_{2/3})\ O_3$ - $zPbTiO_3$." *Ferroelectrics* **188**, 109-124 (1996).

Materials Studies–continued

12. Zhang, Q.M. and J. Zhao, "Polarization Responses in Lead Magnesium Niobate Based Relaxor Ferroelectrics." *Applied Physics Letters* (submitted).

13. Müeller, V. and Q.M. Zhang, "Nonlinearity and Scaling Behavior in Donor Doped Lead Zirconate Titanate Piezoceramic." *Physics Review Letters* (submitted).

14. Zhang, Q.M., J. Zhao, K. Uchino, and J. Zheng, "Change of the Weak-Field Properties of $Pb(ZrTi)O_3$ Piezoceramics with Compressive Uniaxial Stresses and Its Links to the Effect of Dopants on the Stability of the Polarizations in the Materials." *J. Mat. Res.* **12**, 226 (1997).

15. Markowski, K., S.-E. Park, S. Yoshikawa, and L.E. Cross, "The Effect of Compositional Variations in the Lead Lanthanum Zirconate Stannate Titanate System on Electrical Properties." *J. Amer. Ceram.* **79** (12), 3297-3304 (1996).

16. Park, S.-E., K. Markowski, S. Yoshikawa, and L.E. Cross, "The Effect of Barium and Strontium Additions in the Lead Lanthanum Zirconate Stannate Titanate System on Electrical Properties." *J. Amer. Ceram.* **80** (2), 407-412 (1997).

VOLUME II

17. Yoshikawa, S., K. Markowski, S.-E. Park, M.-J. Pan, and L.E. Cross, "Antiferroelectric-to-Ferroelectric Phase Switching Lead Lanthanum Zirconate Stannate Titanate (PLZST) Ceramics." *SPIE Proceedings* **IV** (1997).

18. Blue, C.T., J.C. Hicks, S.-E. Park, S. Yoshikawa, and L.E. Cross, "In-situ X-ray Diffraction Study of the Antiferroelectric-Ferroelectric Phase Transition in PLSnZT." *Applied Physics Letter* **68** (21), 2942-2944 (1996).

19. Pan, M.-J., S.-E. Park, K. Markowski, and S. Yoshikawa, "Antiferroelectric-to-Ferroelectric PLZST Ceramics-II: The Effect of Pre-Stress Conditions on the Strain Behavior." Submitted *Proceedings of IEEE International Symposium on the Applications of Ferroelectrics*, Rutgers University, East Brunswick, New Jersey (August 1996).

20. M.-J. Pan, Markowski, K., S.-E. Park, S. Yoshikawa, and L.E. Cross. "Antiferroelectric-to Ferroelectric PLZSnT Ceramics-I: Structure, Compositional Modification and Electric Properties." Submitted *Proceedings of IEEE International Symposium on the Applications of Ferroelectrics*, Rutgers University, East Brunswick, New Jersey (August 1996).

Materials Studies–continued

21. Lopath, P.D., K.K. Shung, S.-E. Park, and T.R. Shrout, "Ultrasonic Transducers Using Piezoelectric Single Crystals Perovskites." Submitted *Proceedings of IEEE International Symposium on the Applications of Ferroelectrics*, Rutgers University, East Brunswick, New Jersey (August 1996).

22. Park, S.-E. and T.R. Shrout, "Characteristics of Relaxor-Based Piezoelectric Single Crystals for Ultrasonic Transducers." Proceedings of 1996 IEEE Ultrasonics Symposium, San Antonio, Texas (November 1996).

23. Park, S.-E., P.D. Lopath, K.K. Shung, and T.R. Shrout, "Relaxor-Based Single Crystal Materials for Ultrasonic Transducer Applications." Proceedings on SPIE's International Symposium on Medical Imaging, Newport Beach, California (February 1997).

24. Lopath, P.D., S.-E. Park, K.K. Shung, and T.R. Shrout, "$Pb(Zn_{1/3}Nb_{2/3})O_3/PbTiO_3$ Single Crystal Piezoelectrics for Ultrasonic Transducers." Proceedings on SPIE's International Symposium on Medical Imaging, Newport Beach, California (February 1997).

25. Park, S.-E. and T.R. Shrout, "Relaxor Based Ferroelectric Single Crystals for Electro-Mechanical Actuators." *Innovations in Materials Research* (accepted).

26. Park, S.-E. and T.R. Shrout, "Characteristics of Relaxor-Based Piezoelectric Single Crystals for Ultrasonic Transducers," *IEEE Trans. on Ultrasonics, Ferroelectric and Frequency Control Special Issue on Ultrasonic Transducers* (to be published).

27. Jin, B., R. Guo, and A.S. Bhalla, "Piezoelectric Properties and Equivalent Circuits of Ferroelectric Relaxor Single Crystals."

28. Mulvihill, M.L., K. Uchino, Z. Li, and W. Cao, "In-situ Observation of the Domain Configurations during the Phase Transitions in Barium Titanate." *Phil. Mag. B.* **74** (1), 25-36 (1996).

29. Mulvihill, M.L., L.E. Cross, and K. Uchino, "Dynamic Motion of the Domain Configuration in Relaxor Ferroelectric Single Crystals as a Function of Temperature and Electric Field." *Ferroelectrics* **186**, 325-328 (1996).

30. Sundar, V. and R.E. Newnham, "Conversion Method Measurements of Electrostriction Coefficients in Low-K Dielectrics." *Mat. Res. Bull.* **31** (5), 545-554 (1996).

31. Sundar, V., J.-F., Li, D. Viehland, and R.E. Newnham, "Interferometric Evaluation of Electrostriction Coefficients." *Mat. Res. Bull.* **31** (5), 555-563 91996).

Materials Studies–continued

32. Sundar, V., N. Kim, C. Randall, R. Yimnirun, and R.E. Newnham, "The Effect of Doping and Grain Size on Electrostriction in $PbZr_{0.52}Ti_{0.48}O_3$." Submitted *Proceedings of IEEE International Symposium on the Applications of Ferroelectrics*, Rutgers University, East Brunswick, New Jersey (August 1996).

33. Erdei, S., L. Galambos, I. Tanaka, L. Hesselik, F.W. Ainger, L.E. Cross, and R.S. Feigelson, "Segregation and Inhomogenities in Photorefractive SBN Fibers." *SPIE Proceedings V–Photorefractive Fiber and Crystal Devices: Materials, Optical Properties, and Applications II*, **2849**, 168-173 (1996).

34. Li, Shaoping, J.A. Eastman, J.M. Vertrone, R.E. Newnham, and L.E. Cross, "Coherent Coupling in Ferroelectric Superlattices." (1996).

35. Su, J., Q.M. Zhang, and R.Y. Ting, "Space Charge Enhanced Electromechanical Response in Thin Film Polyurethane Elastomers." *Applied Physics Letters* (submitted).

36. Zhang, Q.M., J. Su, and C.-H. Kim, "An Experimental Investigation of Electromechanical Responses in a Polyurethane Elastomer." *J. Appl. Phys.* **81** (6), 2770 (1997).

VOLUME III

37. Su, J., Q.M. Zhang, C.H. Kim, R.Y. Ting, and R. Capps, "Effects of Transitional Phenomena on the Electric Field Induced Strain-Electrostrictive Response of a Segmented Polyurethane Elastomer." *J. Appl. Polymer Sci.* (accepted).

Composite Sensors

38. Fernandez, J.F., A. Dogan, Q.M. Zhang, J.F. Tressler, and R.E. Newnham, "Hollow Piezoelectric Composites, Sensors and Actuators." *A: Physical* **51** (2,3), 183-192 (1996).

39. Fernandez, J.F., A. Dogan, Q.M. Zhang, and R.E. Newnham, "Piezoelectric Composites with Enclosed Hollow Spaces." Proceedings 4th Euroceramics Conference, *Electroceramics* **5**, 39-46 (1996).

40. Fernandez, J.F., A. Dogan, J.T. Fielding, K. Uchino, and R.E. Newnham, "Temperature Dependence of New Design Ceramic-Metal Piezocomposites Actuators." Proceeding 4th Euroceramics Conference, *Electroceramics* **5**, 133-138 (1996).

Composite Sensors–continued

41. Newnham, R.E., "Composite Sensors and Actuators," Disordered Materials, edited by G. Milton, K. Godlen, G. Grimmett, and P. Sen, Springer-Verlag, NY (accepted January 1997).

42. Tressler, J.F. and R.E. Newnham, "Doubly Resonant Cymbal Transducers, *IEEE Transactions of UFFC*, Special Issue on Transducers (accepted 1996).

43. Tressler, J.F., W. Cao, K. Uchino, and R.E. Newnham, "Ceramic Metal Composite Transducers for Underwater Acoustic Applications." Submitted *Proceedings of IEEE International Symposium on the Applications of Ferroelectrics*, Rutgers University, East Brunswick, New Jersey (August 1996).

44. Alkoy, S., A. Dogan, A.C. Hladky, J.K. Cochran, and R.E. Newnham, "Vibration Modes of PZT Hollow Sphere Transducers." Submitted *Proceedings of IEEE International Symposium on the Applications of Ferroelectrics*, Rutgers University, East Brunswick, New Jersey (August 1996).

45. Alkoy, S., A. Dogan, A.C. Hladky, and R.E. Newnham, "Miniature Piezoelectric Hollow Sphere Transducers (BBs)." 1996 Proceeding of IEEE International Frequency Control Symposium, pp. 586-594, Honolulu, Hawaii (1996).

46. Alkoy, S., A. Dogan, A.C. Hladky, and R.E. Newnham, "Piezoelectric Hollow Spheres." 1996 Proceeding 3rd Turkish Ceramic Society Meeting., Eds. V. Günay, H. Mandel, S. Ozgen. Istanbul, Turkey (October 1996).

47. Koc, B., A. Dogan, J.F. Fernandez, R.E. Newnham, and K. Uchino, "Accelerometer Application of the Modified Moonie (Cymbal) Transducer." *J. App. Phys.* **35**, 65-67 (1996).

VOLUME IV

48. Kumar, S., A. Bhalla, and L.E. Cross, "Underwater Acoustic Absorption by Collocated Smart Materials." *Ferroelectric Letters* **21**, 11-16 (1996).

49. Geng, X. and Q.M. Zhang, "Evaluation of Piezocomposites for Ultrasonic Transducer Applications–Influence of the Unit Cell Dimensions and the Properties of Constituents the Performance of 2-2 Piezocomposites." *IEEE Transactions of UFFC* (accepted).

50. Zhang, Q.M. and X. Geng, "Acoustic Properties of the Interface of a Uniform Medium-2-2 Piezocomposite and the Field Distributions in the Composite." *J. Appl. Phys.* (accepted).

Actuator Studies

51. Park, S.-E., and T.R. Shrout, "Ultrahigh Strain and Piezoelectric Behavior in Relaxor Based Ferroelectric Single Crystals."

52. Uchino, K. and S. Takahashi, "Multilayer Ceramic Actuators." *Current Opinion, Ceramic, Composites and Intergrowths*, p. 98-705 (1996).

53. Zheng, J., S. Takahashi, S. Yoshikawa, and K. Uchino, "Heat Generation in Multilayer Piezoelectric Actuators." *J. Amer. Ceram.* **79** (12), 3193-3198 (1996).

54. Dogan, A., J.F. Fernandez, K. Uchino, and R.E. Newnham, "New Piezoelectric Composite Actuator Designs for Displacement Amplification." *Proceeding Euroceramic Conference, Electroceramics* (5), 127-132 (1995) (in press).

VOLUME V

55. Poosanaas, P., A. Dogan., A.V. Prasadarao, S. Komarneni, and K. Uchino, "Photostriction of Sol-Gel Processed PLZT Ceramics." *J. Electroceramics* (1996) (in press).

56. Uchino, K., "Reliability of Ceramic Actuators." Submitted *Proceedings of IEEE International Symposium on the Applications of Ferroelectrics*, Rutgers University, East Brunswick, New Jersey (August 1996).

57. Uchino, K., "High Electromechanical Coupling Piezoelectrics-How High Energy Conversion Rate is Possible?-." *Proceeding MRS 1996* (1996) (in press).

58. Uchino, K., "Recent Developments in Ceramic Actuators-Comparison Among USA, Japan and Europe."

59. Xu, B., Q.M. Zhang, V.D. Kugel, Q. M. Wang, and L.E. Cross, "Optimization of Bimorph Based Double Amplifier Actuator under Quasistatic Situation." Submitted *Proceedings of IEEE International Symposium on the Applications of Ferroelectrics*, Rutgers University, East Brunswick, New Jersey (August 1996).

60. Kugel, V.D., S. Chandran, and L.E. Cross, "Caterpillar-Type Piezoelectric d_{33} Bimorph Transducer." *Appl. Phys. Lett.* **69** (14), 2021-2023 (1996).

61. Kugel, V.D., Q.M. Zhang, B. Xu, Q.-M. Wang, S. Chandran, and L.E. Cross, "Behavior of Piezoelectric Actuators under High Electric Field." Submitted *Proceedings of IEEE International Symposium on the Applications of Ferroelectrics*, Rutgers University, East Brunswick, New Jersey (August 1996).

62. Kugel, V.D., B. Xu, Q.M. Zhang, and L.E. Cross, "Bimorph-Based Piezoelectric Air Acoustic Transducer Model." *Sensors and Actuators A* (submitted 1996).

Actuator Studies–continued

63. Chandran, S., V.D. Kugel, and L.E. Cross, "CRESCENT: A Novel Piezoelectric Bending Actuator." *Proceeding SPIE's 4th Annual Symposium on Smart Structures* accepted 1997).

64. Kugel, V.D., S. Chandran, and L.E. Cross, "A Comparative Analysis of Piezoelectric Bending-Mode Actuators." Submitted *SPIE Proceedings*, Smart Structures and Materials: Smart Materials Technologies, 3040, 70-80 (1997).

65. Wang, Q.M., B. Xu, V.D. Kugel, and L.E. Cross, "Characteristics of Shear Mode Piezoelectric Actuators," Submitted *Proceedings of IEEE International Symposium on the Applications of Ferroelectrics*, Rutgers University, East Brunswick, New Jersey (August 1996).

Integration Studies

66. Elissalde, C., L.E. Cross, and C.A. Randall, "Structural-Property Relations in a Reduced and Internally Biased Oxide Wafer (RAINBOW) Actuator Material." *J. Amer. Ceram.* **79** (8), 2041-2048 (1996).

67. Xu. B., Q.M. Zhang, V.D. Kugel, Q. Wang, and L.E. Cross, "Optimization of Bimorph Based Double Amplifier Transducer under Quasistatic Conditions." Submitted *Proceedings of IEEE International Symposium on the Applications of Ferroelectrics*, Rutgers University, East Brunswick, New Jersey (August 1996).

68. Xu, B., Q. M. Zhang, V.D. Kugel, and L.E. Cross, "Piezoelectric Air Transducer for Active Noise Control." *Proceeding SPIE, Smart Structures and Integrated Systems* **271** (7), 388 (1996).

VOLUME VI

69. Chandran, S., V.D. Kugel, and L.E. Cross, "Characterization of the Linear and Non-Linear Dynamic Performance of RAINBOW Actuator." Submitted *Proceedings of IEEE International Symposium on the Applications of Ferroelectrics*, Rutgers University, East Brunswick, New Jersey (August 1996).

70. Wang, H., Q.M. Zhang, L.E. Cross, and C.M. Trottier, "Tailoring Material Properties by Structure Design–Radially Poled Piezoelectric Cylindrical Tube." *Ferroelectrics* **173**, 181-189 (1995).

Processing Studies

71. Park, S.-E., M. Mulvihill, P.D. Lopath, M. Zipparo, and T.R. Shrout, "Crystal Growth and Ferroelectric Related Properties of (1-x) Pb $(A_{1/3}Nb_{1/3})O_3$ - $xPbTiO_3$(A=Zn^{2+}, Mg^{2+})." Submitted *Proceedings of IEEE International Symposium on the Applications of Ferroelectrics*, Rutgers University, East Brunswick, New Jersey (August 1996).

72. Mulvihill, M., S.-E. Park, G. Risch, Z. Li, K. Uchino, and T.R. Shrout, "The Role of Processing Variables in the Flux Growth of PZN-PT Relaxor Ferroelectric Single Crystals." *Jpn. J. Appl. Phys.* **35** (Pt. 1; No. 7), 3984-3990 (1996).

73. Pan, M.-J., S.-E. Park, C.W. Park, K.A. Markowski, S. Yoshikawa, and C. Randall, "Superoxidation and Electrochemical Reactions during Switching in $Pb(Zr,Ti)O_3$ Ceramics." *J. Amer. Ceram.* **79** (11), 2971-2974 (1996).

74. Park, S.-E., M.L. Mulvihill, G. Risch, and T.R. Shrout, "The Effect of Growth Condition on Dielectric Properties of $Pb(Zn_{1/3}Nb_{2/3})O_3$ Crystal." *Jpn. J. Appl. Phys.* **36** (1) (1997).

75. Yoshikawa, Y. and K. Uchino, "Chemical Preparation of Lead-Containing Niobate Powders." *J. Amer. Ceram.* **79** (9), 2417-2421 (1996).

76. Ravindrathan, P., V. Srikanth, S. Komarneni, and A.S. Bhalla, "Processing of $Pb(Zn_{1/3}Nb_{2/3})O_3$: Ceramics at High Pressure." *Ferroelectrics* **188**, 135-141 (1996).

77. Ravindrathan, P., S. Komarneni, A.S. Bhalla, and R. Roy, "Low Temperature Chemical Routes to Smart Materials." *Ferroelectrics* **188**, 125-133 (1996).

78. Alberta, E.F. and A.S. Bhalla, "A Processing and Electrical Property Investigation of the Solid Solution: (x) $Pb(In_{1/2}Nb_{1/2})O_3$ - (1-x)$Pb(Sc_{1/2}Ta_{1/2})O_3$." *Ferroelectrics* **188**, 95-107 (1996).

Thin Film Ferroelectrics

79. Chen, H.D., K.R. Udayakumar, C.J. Gaskey, and L.E. Cross, "Fabrication and Electrical Properties of Lead Zirconate Titanate Thick Films." *J. Amer. Ceram.* **79** (8), 2189-2192 (1996).

80. Chen, H.D., K.K. Li, C.J. Gaskey, and L.E. Cross, "Thickness-Dependent Electrical Properties in Lanthanum-Doped PZT Thick Films." *Mat. Res. Soc. Symp. Proc.* **433**, 325-332 (1996).

81. Ravichandran, D., R. Meyer, Jr., R. Roy, R. Guo, A.S. Bhalla, and L.E. Cross, "Sol-Gel Synthesis of $Ba(Mg_{1/3}Ta_{2/3})O_3$: Phase Pure Powder and Thin Films." *Mat. Res. Bull.* **31** (7), 817-825 (1996).

82. Ravichandran, D., K. Yamakawa, R. Roy, A.S. Bhalla, S. Trolier-McKinstry, R. Guo, and L.E. Cross, "The Effect of Annealing Temperature on the Formation of $SrBi_2Ta_2O_9$ (SBT) Thin Films." Submitted *Proceedings of IEEE International Symposium on the Applications of Ferroelectrics*, Rutgers University, East Brunswick, New Jersey (August 1996).

Instrumentation

83. Su, J., P. Moses, and Q.M. Zhang, "A Bimorph Based Dilatometer for Field Induced Strain Measurement in Soft and Tin Free Standing Polymer Films." *Reviews of Scientific Instruments* (submitted).

INTEGRATION STUDIES

(continued)

APPENDIX 69

Accepted into the Proceedings of the 10th Annual International Symposium on Applications of Ferroelectrics (ISAF), 1996.

Characterization of the linear and non-linear dynamic performance of RAINBOW actuator

Sanjay Chandran, V. D. Kugel and L. E. Cross
Intercollege Materials Research Laboratory, The Pennsylvania State University
University Park, PA 16802, USA

Abstract- In the last few years the technology of using piezoelectric actuators for applications requiring large displacements such as loudspeakers and noise-canceling devices has undergone significant development. The RAINBOW (Reduced and INternally Biased Oxide Wafer) is a novel high displacement actuator and knowledge of its dynamic response is indeed essential for these applications. In an attempt to characterize the RAINBOW, measurements were made of important lumped mechanical and electrical parameters. Cantilevers of different dimensions were cut from RAINBOW discs. The data include measurements of the mechanical displacement (under both quasistatic conditions and electromechanical resonance), and its hysteresis, mechanical quality factor and the electrical impedance of RAINBOW cantilevers. These measurements demonstrate the macroscopic effects of the sinusoidal applied electric field and indicate significant non-linearities in the RAINBOW device.

I. Introduction

For many years, piezoelectric and electrostrictive ceramic materials are being increasingly investigated for use as solid-state actuators for small displacements (<10μ) and precise mechanical movement devices. However, many applications like loudspeakers and noise-canceling devices require actuators producing larger displacements (>1mm). The direct extensional strain in most active ceramic materials is quite small (<1%) and hence novel techniques of strain amplification are required to satisfy these demands for high displacement actuation. Recently, a new type of monolithic ceramic bender called RAINBOW was developed by Haertling [1]. Key features of the RAINBOW include quick processing, ease of fabrication, surface mountable configurations and above all, its ability to produce very high displacements at reasonable driving fields. A good knowledge of the dynamic behavior of the device is indeed essential for many applications. The purpose of this work is to study the dynamic characteristics of the RAINBOW.

II. Experimental Methods

A. Sample Preparation

As it is known, piezoelectric PLZT ceramics are prepared by a conventional mixed oxide process. During the processing, an additional important step for making the RAINBOW is the high temperature chemical reduction process which involves the local reduction of one surface of the ceramic thereby achieving an anisotropic, stress-biased, dome-shaped wafer with significant internal tensile and compressive stresses which act to increase the overall strength of the material [1]. The thickness of the electrically conducting reduced layer is about 1/3 of the sample thickness. The RAINBOW ceramics used in this work were supplied by Aura Ceramics Inc. The original wafers were 50.8mm in diameter and 0.38mm in thickness. Cantilevers of various dimensions were cut from the original wafers using a Motional Diamond Saw. One end of the cantilever was clamped in a plastic support using Superglue, the other end was free.

B. Measurements

Frequency measurements under low electric field were performed using a HP4194A Impedance/Gain Phase analyzer in the frequency range 100 Hz - 4 MHz. To investigate the response of the RAINBOW cantilevers under varying frequency and amplitude of the driving field (RMS), sinusoidal signals varying in amplitude and frequency were applied with the signal generator. The current flowing through the sample was determined from the voltage drop across a small resistance which was measured on a lock-in amplifier. Hence impedance of the sample was determined. The tip displacement of the RAINBOW cantilever was measured by an optical fiber sensor. The amplitude of the tip displacement (RMS) was measured by a lock-in amplifier while the sinusoidal signal corresponding to the tip displacement was monitored on an oscilloscope. Complete description of the measurement setup used can be found in [2].

III. RESULTS

A. Resonance modes

The frequency spectrum of the electrical impedance of the RAINBOW cantilever with one end clamped shows four resonance modes in the frequency range 100 Hz - 4 MHz [3]. The lowest resonant mode is the bending mode. All the results discussed subsequently are pertinent to this bending mode. The resonant frequency of the bending mode can be expressed as [4] :

$$f_R = (m^2/2\pi\sqrt{12}) \cdot (t/L^2) \cdot (1/\sqrt{(\rho \times s_{11}^E)}) \qquad (1)$$

where m = eigen value of the resonant mode = 1.875
t = thickness of the sample
l = length of the sample
ρ = density of the sample
s_{11}^E = elastic compliance of the sample

It is assumed in (1) that the elastic compliance values of both reduced and unreduced layers are equal. Work by Elissalde [3] confirmed this aspect.

B. Determination of Q

The sharpness of the peak in the impedance frequency spectrum in the neighborhood of resonance is determined by losses in the material. Near the resonance the dominant factor may be related to the mechanical losses. Hence the mechanical quality factor Q is an important parameter to be determined in the characterization of resonating systems: it gives an idea of the damping, a narrow peak surrounding f_R suggests light damping and vice-versa. Q can be calculated from the minimum impedance $|Z_M|$ at resonance as follows [4] :

$$Q = 1/[\, 4\pi(C_o + C_1) \cdot (f_p - f_s) \cdot |Z_M| \,] \qquad (2)$$

where $(C_o + C_1)$ = capacitance measured at frequency well below fundamental resonance
f_p , f_s = frequencies corresponding to the maximum values of resistance R and conductance G respectively.

As evident from Fig. 1, Q (calculated from (2)) decreases almost linearly with the driving field over the 2 kV/cm range. This behavior can be attributed to the increase in the losses in the material.

C. Variation of f_r with driving voltage

Fig. 2 shows that the resonant frequency f_R decreases with increasing electric field. This can be attributed to change in the elastic properties of the material due to the increasing driving voltage, increasing losses and a change in the effective length of the curved RAINBOW cantilever. The curvature of the RAINBOW slightly decreases with increasing magnitude of the driving voltage resulting in a longer effective length. s_{11}^E of the RAINBOW also may increase as a result of temperature increase due to Joule heating [3].

D. Variation of tip displacement w at resonant frequency with driving field

Fig. 3 shows the variation of the tip displacement of the RAINBOW cantilever with increasing driving field at resonant frequency. The tip displacement w increases in a non-linear manner with increasing field. The lower curve indicates increasing field and upper curve decreasing field. A 5% hysteresis is observed and the slope of the curve shows a monotonic decrease over the 2 kV/cm field range. It can be observed that w is as high as 0.6 mm at a driving field slightly less than 2 kV/cm. This confirms the high displacement actuation of the RAINBOW.

E. Variation of tip displacement w^* under quasistatic conditions with driving field

As seen from Fig. 4, the quasistatic tip displacement w^* (at 10 Hz) increases non-linearly with electric field. The curve shows hysteresis and the slope of the curve monotonically decreases with increasing field.

F. Signal distortions

While traversing the frequency range 100 Hz to 1 kHz, small output signal distortions were always detectable. Significant distortions in the tip displacement signal w for a sinusoidal input were observed for frequencies close to the frequencies

$$f_d = f_R / j \qquad (3)$$

where j = 2, 3, 4 etc.

This may be due to the presence of higher harmonic components which may grow and cause significant distortions.

IV. DISCUSSION

The results discussed in the previous sections suggest the presence of significant non-linearities in the RAINBOW device. These non-linearities include a 5 % hysteresis and a change in the slope of tip displacement versus driving field curve. To understand the origin of distortions in the tip displacement signal w of the RAINBOW cantilevers it is

useful to analyze the constitutive equations of bending vibrations [5]. Externally applied voltage produces a bending moment in bimorph and unimorph cantilevers [5]. This bending moment M is related as

$$M \propto d_{31} / s_{11}^{E} \quad (4)$$

There is a linear relation between d_{31} and w^* and between $1/s_{11}^{E}$ and f_R^2 [4]. Therefore the product F^* given by

$$F^* = (f_R^2) . (w^*) \quad (5)$$

gives an idea of the component of the bending moment produced by external electric field. If F^* is a non-linear function of the sinusoidal driving voltage, the corresponding excited mechanical vibrations can be expected to have higher harmonic components. The variation of F^* as a function of the driving field is shown in Fig. 4. It is evident from Fig. 4 that F^* varies non-linearly with the driving field especially at high fields. Consequently, at such high fields, the higher harmonic components in displacement w may grow and significant distortions may result.

V. Summary

The dynamic performance of the RAINBOW under an electric field varying in amplitude and frequency has been studied. As discussed in the earlier sections, the measurements of various parameters like mechanical displacement (under both quasistatic conditions and resonance), electrical impedance, mechanical quality factor and resonant frequency indicate significant non-linearities in the behavior of the RAINBOW.

VI. References

1. G. H. Haertling, " Reduction/Oxidation effects in PLZT ceramics ", in *Proceedings of the 4th International SAMPE Electronics Conference* , 1990, pp. 699-711.

2. V. D. Kugel, Q. Zhang, B. Xu, Q. Wang, Sanjay Chandran and L.E. Cross, " Non-linear properties of piezoelectric transducers under high electric field ", in *Proceedings of the 10th International Symposium on Applications of Ferroelectrics* , 1996 (in press).

3. C. Elissalde and L. E. Cross, " Dynamic characteristics of RAINBOW ceramics ", *J. Am. Ceram. Soc.*, vol. 78, no. 8, pp. 2233-2236, 1995.

4. W. P. Mason, *Electromechanical Transducers and Wave Filters*, D. Van Nostrand Co., New York, 1942, pp. 211-236.

5. T. Ikeda, *Fundamentals of Piezoelectricity*, Oxford University Press, Oxford, 1996, pp. 105-107, pp. 246-249.

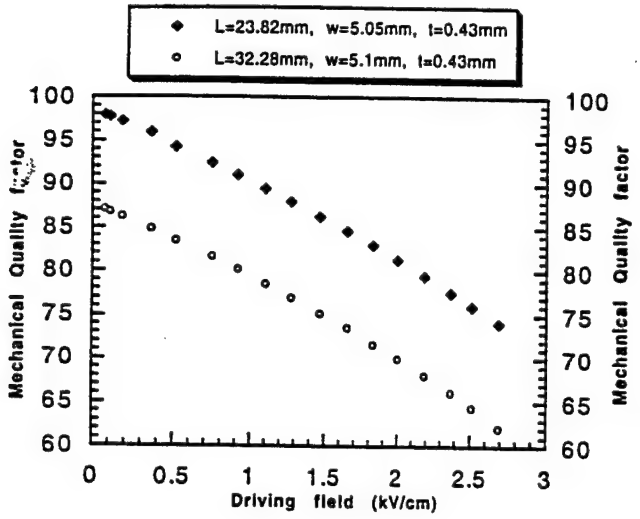

Fig. 1. Mechanical Quality factor as a function of applied field

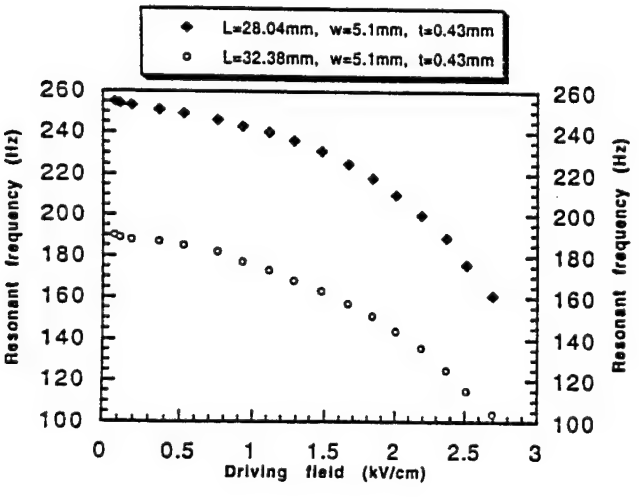

Fig. 2. Resonant frequency as a function of applied field

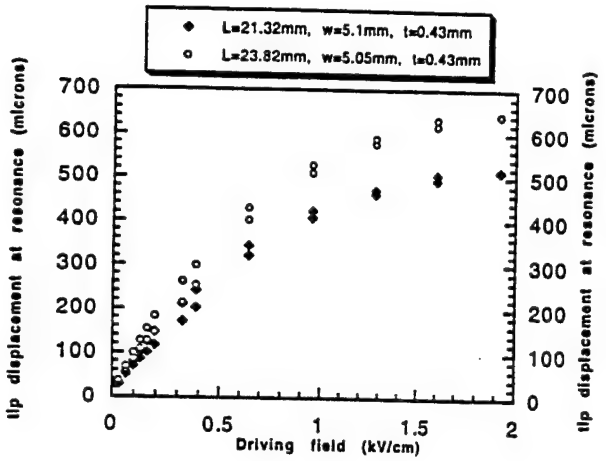

Fig. 3. Tip displacement at resonance as a function of applied field

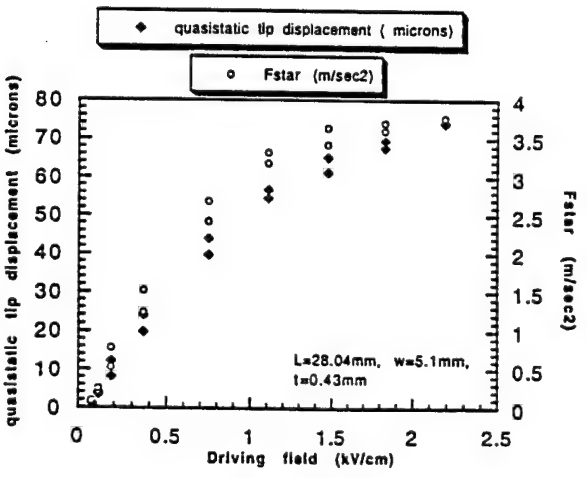

Fig. 4. Quasistatic tip displacement and F* as a function of applied field

APPENDIX 70

Ferroelectrics, 1995, Vol. 173, pp. 181–189
Reprints available directly from the publisher
Photocopying permitted by license only

TAILORING MATERIAL PROPERTIES BY STRUCTURE DESIGN—RADIALLY POLED PIEZOELECTRIC CYLINDRICAL TUBE

H. WANG, Q. M. ZHANG and L. E. CROSS
Materials Research Laboratory, The Pennsylvania State Univeristy, University Park, PA 16802, USA

and

C. M. TROTTIER
Fiber Materials Inc., Biddeford, ME 04005, USA

(Received May 1, 1995)

In many applications such as hydrophone and ultrasonic transducers, materials with large piezoelectric anisotropy are preferred in order to suppress the interfering signals from lateral modes. It has been shown that piezoelectric anisotropy can be significantly improved by structure design. For instance, for a radially poled cylindrical tube, the effective transverse piezoelectric response can be tuned to zero. In this work, the effective piezoelectric responses of lead zirconate titanate (PZT) and lead magnesium niobate-lead titanate (PMN-PT) ceramic cylindrical tubes were studied. Large piezoelectric anisotropy with a high effective uniaxial coefficient has been obtained for both materials. It has been shown that near zero effective d_{31} can be achieved for a PZT tube with a proper dimension ratio of r_0/R_0, where r_0 and R_0 are inner and outer radii of the tube, respectively. While for a PMN-PT tube, the effective piezoelectric responses can be tuned by the ratio of r_0/R_0 as well as the bias field because the induced piezoelectric coefficients d_{33} and d_{31} and their ratio $|d_{33}/d_{31}|$ are all functions of the bias field.

Keywords: piezoelectric anisotropy, relaxor ferroelectrics, cylindrical tube structure.

INTRODUCTION

Conventional piezoelectric lead zirconate titanate (PZT) ceramics are widely used in many transducer applications. The materials have high electromechanical coupling coefficients and large piezoelectric strain constants d_{33} and d_{31}. However, the piezoelectric anisotropy, which is measured by d constant ratio $|d_{33}/d_{31}|$ or coupling constant ratio k_t/k_p, where k_t and k_p are thickness and planar coupling coefficients, respectively, of the materials is quite small. In the applications where large piezoelectric anisotropy is required PZT ceramics are not favorable candidates. For example, in underwater hydrophone applications, an important material parameter is hydrostatic coefficient d_h ($=d_{33} + 2d_{31}$). In order to achieve a large d_h constant it is desirable to use materials with a large ratio of $|d_{33}/d_{31}|$ since d_{33} and d_{31} have opposite signs. Similarly, for ultrasonic transducers, materials with high piezoelectric anisotropy can transmit ultrasonic wave in the poling direction with minimal interference from lateral modes. Previous efforts to improve piezoelectric anisotropy of a device were mainly focused on the selection of materials with large ratio of $|d_{33}/d_{31}|$, including single phase ceramics and ceramic/polymer composites. For example, lead titanite (PT) ceramic possesses large lattice anisotropy. Under certain processing

conditions modified PT ceramics showed unusually large ratio of the thickness to the planar coupling coefficients and, consequently, a large ratio of $|d_{33}/d_{31}|$.[1,2] Piezoelectric ceramic/polymer composites can also be engineered to exhibit high piezoelectric anisotropy.[3]

Another approach to increase piezoelectric anisotropy is by material structure design. Even for the materials with small piezoelectric anisotropy as PZT ceramics, by proper design of material structure it is possible to enhance the effective longitudinal coefficient d_{33} meanwhile to suppress the effective transverse coefficient d_{31}. Piezoelectric ceramic cylindrical tubes are commonly employed as stress sensors. Recently it has been shown that when poled in the radial direction, the effective d_{33} constant of a ceramic tube with a large ratio of length to wall thickness can reach an exceptionally large value.[4] In addition, analysis has indicated that the effective d_{31} constant can be tuned from positive to zero, and to negative by varying the ratio r_0/R_0 of the tube, where r_0 and R_0 are inner and outer radii, respectively, and/or by changing the ratio $|d_{33}/d_{31}|$ of the ceramic. Besides providing large piezoelectric anisotropy, the structure is also very attractive in the applications where large surface displacement is required since the effective d_{33} constant is proportional to the ratio of the length to the wall thickness and can be much higher than those of PZT and PT based ceramics.

In this paper, the results of recent investigations of the effective piezoelectric responses of lead magnesium niobate-lead titanate (PMN-PT) and PZT ceramic cylindrical tubes are reported. High piezoelectric anisotropy and large uniaxial coefficients have been obtained. The effects of non-uniformity of electric field and bias-field dependence of induced piezoelectric coefficients on the effective piezoelectric responses of PMN-PT tubes are discussed.

PIEZOELECTRIC RESPONSES OF A CYLINDRICAL TUBE

Piezoelectricity can be described by the constitutive equations. When mechanical stress (T) and electric field (E) are chosen as independent variables, the mechanical strain (S) and electric displacement (D) responses are described by:

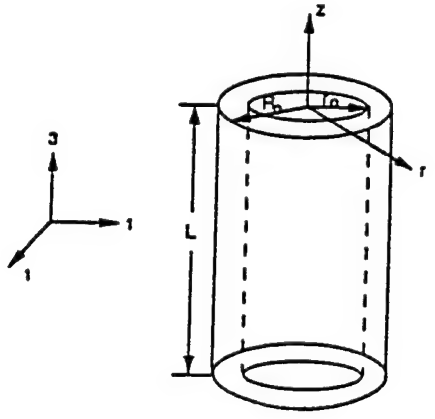

FIGURE 1 Schematic drawing of a cylindrical tube.

$$S_i = s_{ij}T_j + d_{in}E_n \tag{1a}$$

$$D_m = d_{mj}T_j + \varepsilon_0 K_{mn}E_n \tag{1b}$$

where s_{ij} are elastic compliances, K_{mn} are dielectric constants, ε_0 is free space permittivity and d_{mj} are piezoelectric strain coefficients. Equation (1b) describes the direct effect, where electric charges are induced by a stress while Equation (1a) describes the converse effect, where strains are induced by an electric field.

Shown in Figure 1 is a schematic drawing of a piezoelectric cylindrical tube and its coordinate system. Electrodes are on the inner and outer wall surfaces and the polarization of the material is along the radial direction. The piezoelectric responses from the direct and the converse effects of such system were analyzed by several authors.[5-10] In their works, the voltage developed in the system by pressure or transmitting responses induced by an electric field were obtained. Recently, the analytical results of the effective piezoelectric strain constants d_{33} and d_{31} of a radially poled ceramic tube have been reported.[4] It has also been shown that for such a system, the effective piezoelectric d constants determined from the converse effect are equal to those from the direct effect. For the cylindrical tube structure, the effective d constants are defiend as:

$$\frac{\Delta L}{L} = d_{33}^{\text{eff}} \frac{V}{L} \tag{2a}$$

$$\frac{\Delta D}{2R_0} = d_{31}^{\text{eff}} \frac{V}{L} \tag{2b}$$

where ΔL and ΔD are the displacements in the axial and radial directions under an applied voltage V, respectively, and L is the length of the tube. The effective piezoelectric d constants have the expressions:

$$d_{33}^{\text{eff}} = d_{31} \frac{2L}{(R_0 + r_0)\ln(R_0/r_0)} \tag{3a}$$

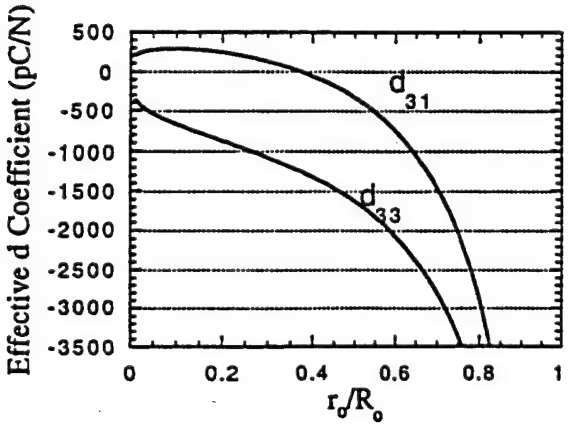

FIGURE 2 Calculated effective d constants of a PZT ceramic tube as functions of the dimension ratio.

$$d_{31}^{\text{eff}} = \frac{L}{(R_0 + r_0)\ln(R_0/r_0)}\left[\left(1 + \frac{r_0}{R_0}\right)d_{31} + \left(1 - \frac{r_0}{R_0}\right)d_{33}\right] \tag{3b}$$

Two assumptions were used in the derivations of above equations. First, it was assumed that the material is elastically isotropic and the material parameters d_{33} and d_{31} are constant throughout the sample. Secondly, the strain responses in axial and radial directions are independent. Therefore, the requirements for the sample geometry are thin-wall ($R_0 >> (R_0 - r_0)$) or long tube ($L >> (R_0 - r_0)$).

It can be seen from Equations (3a) and (3b) that the effective longitudinal response of a tube depends only on the piezoelectric d_{31} constant of the material while the effective transverse response of a tube is a competition between the piezoelectric d_{33} and d_{31} modes through the tube dimensions. For piezoelectric ceramics such as PZT and PT, material parameters d_{33} and d_{31} are fixed after the poling. Therefore, the only way to tune the transverse response of a piezoelectric ceramic tube is to change the ratio of r_0/R_0. In Figure 2, the calculated effective d_{33} and d_{31} constants of PZT-500[11] ceramic tube are depicted as functions of the ratio of r_0/R_0. The outer radius and the length of the tube are 5.08 mm and 12.70 mm, respectively. As can be seen, when ratio r_0/R_0 is near 0.38, the effective d_{31} of the tube is almost zero and the effective d_{33} constant is around -1200 pC/N resulting in large piezoelectric anisotropy.

As illustrated by Equation (3b), the transverse piezoelectric response of a radially poled cylindrical tube depends not only on the ratio of r_0/R_0 of the tube, but also on the ratio of $|d_{33}/d_{31}|$ of the material. For relaxor ferroelectrics, of which piezoelectric d_{33} and d_{31} coefficients can be induced by a DC bias field, the ratio of $|d_{33}/d_{31}|$ changes with the bias field. Therefore, the effective d_{31} constant of a cylindrical tube made of relaxor ferroelectric ceramic can be tuned by the bias field.

EXPERIMENTAL DETAILS

The major aims of this work were to experimentally investigate the piezoelectric responses of a radially poled ceramic cylindrical tube and to increase the piezoelectric anisotropy by structure design. For most PZT ceramics, the d constant ratio $|d_{33}/d_{31}|$ is around 2.2. Therefore, when the dimension ratio r_0/R_0 of a PZT ceramic tube is close to 0.38, near zero transverse response can be obtained as seen from Figure 2. In this work, normal piezoelectric ceramic PZT-500 and relaxor ferroelectric ceramic PMN-PT (90/10) were used. To achieve high piezoelectric anisotropy, the tube dimensions were designed based on Equations (3a) and (3b). The sample dimensions are listed in Table I. PMN-PT tubes were purchased from TRS Ceramic Inc. and poled PZT-500 tubes were purchased from Piezo Kinetic Inc. Gold sputtering and

TABLE I

Sample dimension of cylindrical ceramic tubes

Sample	R_o (mm)	r_o (mm)	L (mm)
PZT-500	2.56	1.01	12.70
PMN-PT-1	2.54	1.27	12.70
PMN-PT-2	2.54	1.02	12.70

silver paste were used for the electrodes of PMN-PT samples. Low frequency dielectric constant and polarization of PMN-PT ceramics as functions of temperature were measured by a LCR meter (HP4274A) and a pA meter (HP4140B), respectively, with a computer controlled temperature regulation system. Material parameters d_{33} and d_{31} and the effective piezoelectric responses of the tube samples were measured by a double-beam laser interferometer.

RESULTS AND DISCUSSION

Material Properties

The induced d_{33} and d_{31} of an electrostrictive material are functions of the electric bias field and are proportional to the dielectric constant ($\varepsilon/\varepsilon_0$) and polarization ($P$) of the material. In order to obtain high induced piezoelectricity, materials with high dielectric constants and large polarization are preferred. For relaxor ferroelectrics, in the temperatures above T_d and near T_m, where T_m is the temperature of maximum dielectric constant and T_d is the depolarization temperature, large reversible polarization and high dielectric constant are achievable. Consequently, large material parameters d_{33} and d_{31} can be obtained.

PMN ceramics are relaxor-type ferroelectrics with a broad and frequency-dispersive dielectric constant peak. Near the diffuse transition region, its dielectric constant can be over 30,000. Modification of the composition by normal ferroelectrics $PbTiO_3$ can shift the transition temperature from $T_m \sim -10°C$ to that near room temperature, which is desirable for most applications. In this work, cylindrical tubes made of 0.9PMN-0.1PT ceramic were used. Plotted in Figure 3 are the dielectric constant and the polarization of the material as functions of temperature measured at frequency of 1 kHz. As can be seen from the diagram, the depolarization temperature T_d and

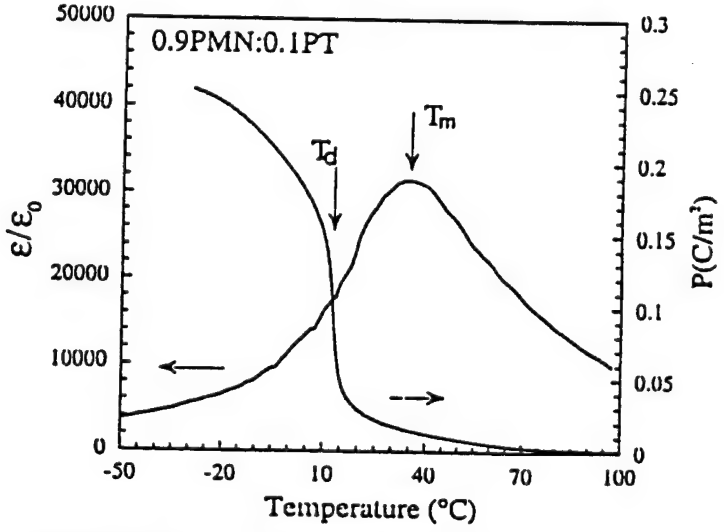

FIGURE 3 Dielectric constant and polarization of PMN-PT (90/10) ceramic as functions of temperature.

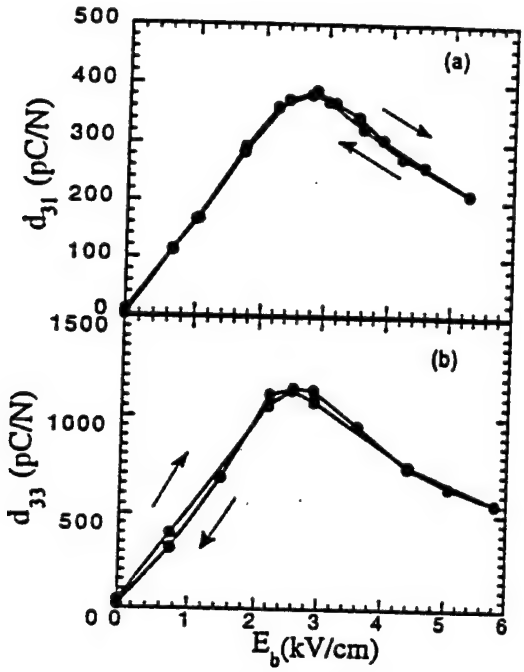

FIGURE 4 Induced piezoelectric d_{31} (a) and d_{33} (b) coefficients of PMN-PT (90/10) ceramic.

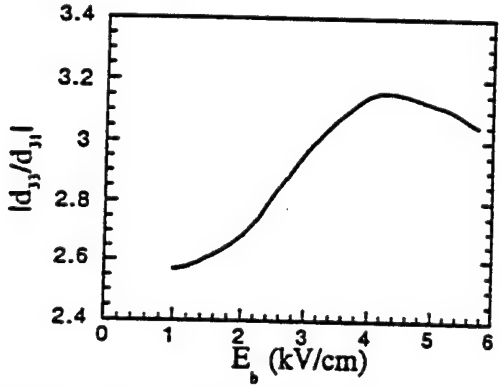

FIGURE 5 The d constant ratio as a function of bias field.

the temperature of maximum dielectric constant of the material T_m are around 10°C and 50°C, respectively. The dielectric constant is about 15,000 in room temperature.

At temperatures above T_d, piezoelectricity can be induced by a DC bias field. Shown in Figures 4(a) and 4(b) are the induced transverse and longitudinal piezoelectric constants of 0.9PMN-0.1PT ceramic as functions of bias field, respectively, measured at frequency of 500 Hz. Clearly, induced d_{33} and d_{31} coefficients increase linearly with bias field until they reach a peak. Depicted in Figure 5 is the change of the ratio $|d_{33}/d_{31}|$ with the bias field. The overall ratio of the material is higher than those of most PZT ceramics, which are around the value of 2.2. In addition, in the field range of 1–4 kV/cm, this ratio increases with the bias field. Therefore, even

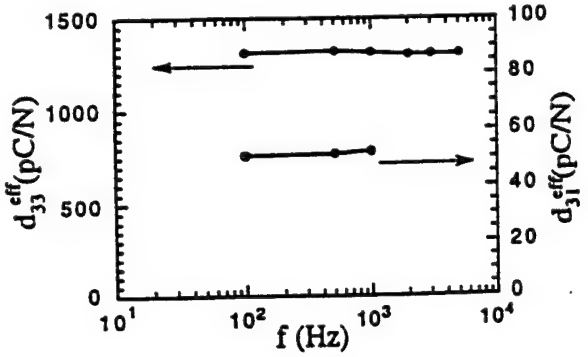

FIGURE 6 Effective d constants of the PZT-500 tube as a function of frequency.

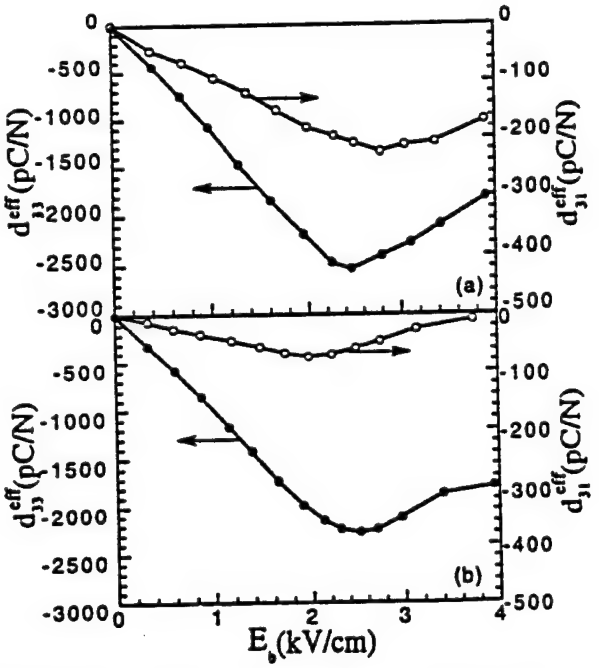

FIGURE 7 DC bias field dependence of the effective d constants of PMN-PT sample #1 (a) and sample #2(b).

for fixed dimensions (r_0/R_0) the effective d_{31} constant of a PMN-PT tube can be adjusted by the bias field.

Effective Piezoelectric Response of a Radially Poled Tube

The material parameters d_{33} and d_{31} of PZT ceramics are fixed after the ceramics are poled. Therefore, the transverse piezoelectric response of a radially poled PZT cylindrical tube only depends on its dimensions. As indicated in Figure 2, when the ratio of r_0/R_0 is 0.372, the calculated effective d_{31} constant of a PZT-500 tube is zero.

For the PZT-500 samples used in this study, the ratio of r_0/R_0 was 0.395. Shown in Figure 6 are effective d_{33} and d_{31} coefficients of a PZT-500 tube measured at low frequencies. The effective d_{33} constant is about -1300 pC/N and the effective d_{31} constant is about -50 PC/N. Obviously, compared with the material parameters (d_{33} = 374 pC/N and $d_{31} = -171$ pC/N), piezoelectric anisotropy is greatly enhanced in this structure. For PMN-PT ceramic tubes the effective responses also depend on the DC bias field because the induced piezoelectric parameters d_{33} and d_{31} and their ratio $|d_{33}/d_{31}|$ are functions of the bias field. The bias field dependence of effective d_{33} and d_{31} constants of PMN-PT ceramic tubes #1 and #2 is illustrated in Figure 7(a) and 7(b), respectively. Several features can be seen from the results presented in Figures 6, 7(a) and 7(b). (1) For all samples, the effective longitudinal and transverse d constants have the same sign, which indicates that in hydrostatic applications, both longitudinal and transverse effects make positive contribution to the total response. (2) The uniaxial piezoelectric response (d_{33}^{eff}) is greatly enhanced. This parameter can be further improved by using samples with a larger ratio of $L/(R_0 - r_0)$. Hence, a piezoelectric ceramic tube with appropriate dimensions is a good candidate for uniaxial actuator applications. (3) As indicated by Equation (3b) the effective d_{31} constant of a tube strongly depends on the ratio r_0/R_0. For the PMN-PT samples, when the ratio r_0/R_0 is reduced by 20%, the effective d_{31} constant decreases about 70%. Consequently, strong piezoelectric anisotropy is obtained. (4) Comparing the results of the PMN-PT ceramic, it is found that at the same bias voltage level, radially poled tubular structure can provide much higher d_{33} constant than that of the material parameter. Therefore, the requirements for the power supply equipment are greatly reduced.

Listed in Table II is a comparison between experimental results and the calculations by Equations (3a) and (3b). It can be seen that for PZT samples the experimental results of the effective d constants are in good agreement with those from the analytical calculations. For PMN-PT samples, the discrepancy between the measured and the calculated values is more obvious (beyond the data scattering). This is because for relaxor ferroelectric materials, induced piezoelectricity strongly depends on the DC bias field as indicated in Figures 4(a) and 4(b). For the structure of a cylindrical tube, DC bias field is not uniform in the radial direction. Thus, the induced piezoelectric d_{33} and d_{31} coefficients are not constant in the material. The bias field in the calculations and in Figures 7(a) and 7(b) was taken as the bias voltage divided by the tube wall thickness. For the samples employed in this work the electric field at inner wall surface of the samples is more than double of that at

TABLE II

Effective d coefficients of the ceramic tubes

Sample	d_{33} (pC/N)		d_{31} (pC/N)	
	Measured	Calculated	Measured	Calculated
PZT-500	-1310	-1308	-51	-46
PMN-PT-1*	-2500	-3558	-210	72
PMN-PT-2*	-2280	-2893	-55	617

* Both measured and calculated d coefficients are at bias field of 2.5 kV/cm.

outer wall surface. For example, with a DC bias voltage of 200 V, the actual electric fields are 0.86 kV/cm and 2.15 kV/cm at the outer and inner surfaces of sample #2, respectively. From Figure 4(a), the corresponding induced d_{33} constants are 390 pC/N and 1070 pC/N, respectively. Apparently, this inhomogeneity of piezoelectric constants in the material is quite significant. Moreover, due to the nonlinear relation between induced piezoelectric constants and the bias field, the induced piezoelectric constants are not monotonically decreasing in the radial direction. Hence, it is not surprising that there is a discrepancy between the predictions of Equations (3a) and (3b) and the experimental results for relaxor ferroelectrics. For quantitative predictions of the effective piezoelectric responses of a relaxor ferroelectric ceramic tube, the inhomogeneity of induced piezoelectric coefficients due to the non-uniform bias field needs to be considered.

CONCLUSIONS

Piezoelectric anisotropy can be significantly improved by an appropriate structure design. The experimental results presented above demonstrate that for a radially poled cylindrical tube, practically, a zero transverse d_{31} coefficient has been obtained for both piezoelectric PZT ceramic and relaxor ferroelectric PMN-PT ceramic, which confirms the predictions from the early analytical calculations. Moreover, the effective uniaxial coefficients have been greatly enhanced compared with the material parameters. Besides the dependence of effective piezoelectric constants on the tube dimensions, the effective transverse coefficient of a relaxor ferroelectric ceramic tube can also be tuned by the material parameters d_{33} and d_{31}, which are functions of bias field. Due to the non-uniform bias field in the radial direction, the inhomogeneity of induced piezoelectric constants in a tube made of relaxor ferroelectrics needs to be considered in the calculations of the total piezoelectric responses. The structure is promising in applications where large surface displacement and high piezoelectric anisotropy are required.

ACKNOWLEDGEMENT

This work was supported by a SBIR grant from ARPA through Fiber Materials Inc. and by the Office of Naval Research.

REFERENCES

1. D. Damjanovic, T. R. Gururaja, S. J. Jang and L. E. Cross, *Ultrason. Symp. Proc.*, 633 (1986).
2. D. Damjanovic, T. R. Gururaja, S. J. Jang and L. E. Cross, *Am. Ceram. Soc. Bull.*, **66**, 699 (1987).
3. T. R. Gururaja, A. Safari, R. E. Newnham and L. E. Cross, in "Electronic Ceramics," edited by L. M. Levinson, Marcel Dekker Inc., New York, 1988, p. 92.
4. Q. M. Zhang, H. Wang and L. E. Cross, *Proc. SPIE Smart Struc. Mater.*, **1916**, 244 (1993).
5. R. A. Langevin, *J. Acoust. Soc. Amer.*, **26**, 421 (1954).
6. C. P. Germano, *J. Acoust. Soc. Amer.*, **34**, 1139–1141 (1962).
7. W. D. Wilder, *J. Acoust. Soc. Amer.*, **62**, 769–771 (1977).
8. A. A. Anan'eva, "Ceramic Acoustic Detectors," Consultants Bureau, New York, 1965.
9. J. A. Burt, *J. Acoust. Soc. Amer.*, **64**, 1640 (1978).
10. P. H. *Rogers, J. Acoust. Soc. Amer.*, **80**, 13 (1986).
11. Trademark of Piezo Kinetic Inc., Belloefont, PA.

PROCESSING STUDIES

APPENDIX 71

Crystal Growth and Ferroelectric Related Properties of (1-x) $Pb(A_{1/3}Nb_{2/3})O_3$ - x $PbTiO_3$ ($A=Zn^{2+}$, Mg^{2+})

Seung-Eek Park[1], Maureen L. Mulvihill[1], Patrick D. Lopath[2], Mike Zipparo[2] and Thomas R. Shrout[1]
[1] Materials Research Laboratory
[2] Bioengennering Department
The Pennsylvania State Univerity, University Park, PA 16802

Abstract - Crystals of (1-x) $Pb(A_{1/3}Nb_{2/3})O_3$ - x $PbTiO_3$ ($A=Zn^{2+}$,Mg^{2+}) were grown by the flux technique. The dielectric and piezoelectric properties as a function of composition and crystal orientation have been evaluated. Both MPB and non-MPB crystals were found to possess high piezoelectric properties. Values of longitudinal electromechanical coupling coefficients (k_{33}) > 90%, dielectric constants ranging from 3000 to 5000 with low dielectric loss < 1% were observed for rhombohedral crystals. Tetragonal crystals with increased $PbTiO_3$ content exhibited large thickness coupling coefficients (k_T) > 63% with relatively low dielectric constant (~1000). Ultrahigh values of piezoelectric coefficients (d_{33}) > 2000 pC/N were also measured for non-MPB crystals and confirmed by direct E-field strain measurements. These properties are briefly discussed in relation to device performance.

I. Introduction

Relaxor ferroelectrics such as $Pb(Zn_{1/3}Nb_{2/3})O_3$ (PZN), $Pb(Mg_{1/3}Nb_{2/3})O_3$ (PMN) and their solid solutions with normal ferroelectric $PbTiO_3$ (PT) have been investigated for high performance transducer applications. [1,2,3] In spite of poor phase stability during solid state reaction, crystals of these materials can be readily grown by high temperature flux technique. It is the single crystal form of these solid solutions that exhibit ultrahigh piezoelectric properties not currently available with piezoelectric ceramics such as PZTs. Longitudinal electromechanical coupling (k_{33}) values as high as ~90% and piezoelectric coefficients (d_{33}) ~1500 pC/N have been reported for crystals of PZN-PT [2] and PMN-PT [3], making them attractive for both actuator and ultrasonic transducer applications. According to reported data, the properties of these crystals are critically dependent upon the composition and crystallographic direction. Compositionally these crystals were engineered to lie near morphotropic phase boundaries (MPBs) as in the case of polycrystalline ceramics and crystallographically have been poled along <001> direction.

In this study, dielectric and piezoelectric properties as a function of composition and crystal orientation are further investigated for PZN-PT and PMN-PT crystals. Crystals of various compositions were grown by high temperature solution technique. Optimum growth conditions and their effect on dielectric properties are discussed, respresentatively for pure PZN crystals. Specifically the properties of rhombohedral or tetragonal crystals near MPB compositions were evaluated for PZN-PT crystals. The relatively low PT content for MPB PZN-PT (~9% PT) allows for more uniform crystal compositions, compared with the case of PMN-PT (PMB ~35% PT). It will be shown that a MPB to obtain high dielectric and piezoelectric properties is not required.

II. Experimental Procedure

Crystals of PZN-PT and PMN-PT were grown by high temperature flux technique, using PbO and $PbO-B_2O_3$ fluxes, respectively. Important parameters were flux to composition ratio (7:3-6:4), soaking temperature (1150-1200°C), cooling rate (1-5°C/hr), and the low temperature limit to which the melt cooled down (T_L, 850-900°C). Raw powder was mixed and loaded into a Pt crucible. The Pt crucible was then placed in an alumina crucible which was sealed with an alumina lid and alumina cement to minimize volatilization of the Pb rich phases. Crucible and powder was placed in the furnace and held at a soaking temperature for 10 hr, followed by slow cooling down to T_L (850 -900°C). The crucible was then furnace-cooled to room temperature. Selected crystals were chemically analyzed using inductively coupled plasma spectrophotometer (ICP, Leeman Labs PS30000UV) to check crystal stoichiometry and the impurities such as Pt. Pt was not detectable within detection limits (80 ppm).

Crystals were oriented along pseudocubic <111> and <001> directions using a Laue back reflection camera. Samples for dielectric and piezoelectric measurements were then prepared based on IEEE standards. [4] Crystals were polished with silicon carbide and alumina polishing powders to achieve flat and parallel surfaces onto which gold was sputtered as an electrode. Impedence analyzer (HP 4194) and multi-frequency LCR meters (HP 4274A and 4275A) with a computer controlled temperature chamber were used to measure piezoelectric properties and temperature dependence of capacitance, respectively. Polarization and strain as a function of E-field were measured using modified Sawyer Tower system and linear variable displacement transducer (LVDT) sensor.

This research has been supported by Office of Naval research and Whitaker Center for Ultrasonic Imaging.

TABLE 1 GROWTH CONDITIONS AND DIELECTRIC (1KHZ) PROPERTIES OF PZN CRYSTALS.

Growth Run	PZN-A	PZN-B	PZN-C
Flux:Composition	7:3	7:3	6:4
Soaking Temperature (°C)	1150	1150	1200
Cooling Rate (°C/hr)	5	1	1
Crystal Color	Colorless	Yellow	Brown
Zn/Nb	0.27	0.30	0.28
Impurity (Pt)	n. d.*	n. d.	n. d.
K_{RT} (virgin)	3490	5350	3140
loss (virgin)	0.0543	0.0662	0.0515
K_{RT} (poled)	2540	2980	1260
loss (poled)	0.0466	0.0131	0.0148
T_{max} (°C)	145	126	135
K_{max}	39700	44600	57000

* not detectable

III. RESULT AND DISCUSSION

A. Crystal Growth

Although perovksite crystals of both PZN-PT and PMN-PT could be obtained using the growth conditions mentioned above, it was found that crystals could decompose into pyrochlore crystals even after they were grown in PbO rich flux. For example, the amount of pyrochlore phase was critically dependent upon the temperature limit of slow cooling (T_L). T_L was determined by D. T. A., detecting the thermal anomaly caused by decomposition of perovskite into pyrochlore.[5] Slow cooling down to a temperature lower than this temperature limit (T_L) resulted in an increased amount of pyrochlore phase. Although average crystal size did not vary critically on processing conditions, crystal quality and associated dielectric properties were dependent on the growth conditions not only for crystals of solid solutions but also for crystals of end members such as PZN. Example chemical compositions and dielectric properties of three different PZN crystals associated with different growth conditions are given in table 1. Figure 1 shows the dielectric constant as a function of temperature and frequency for various PZN crystals. Although broad and frequency dispersive dielectric maxima are observed for all crystals as a characteristic of relaxors, different T_{max} values occurred. It can be found in table 1 that increased cooling rate and soaking temperature caused the Zn/Nb ratio to decrease. Increased soaking temperature was related to the volatilization of Zn rich phase as well as Pb rich phase during crystal growth. A decreased Zn/Nb ratio induced T_{max} to shift to higher temperatures associated with a decreased dielectric constant at room temperature. Crystal color also varied with the change in growth parameters. The degree of coloration correlated to the ferroelectric-relaxor transition temperature. The importance of this temperature was associated with the depolarization temperature, determining the temperature usage range of the crystal. Details on this coloration are reported elsewhere. [6]

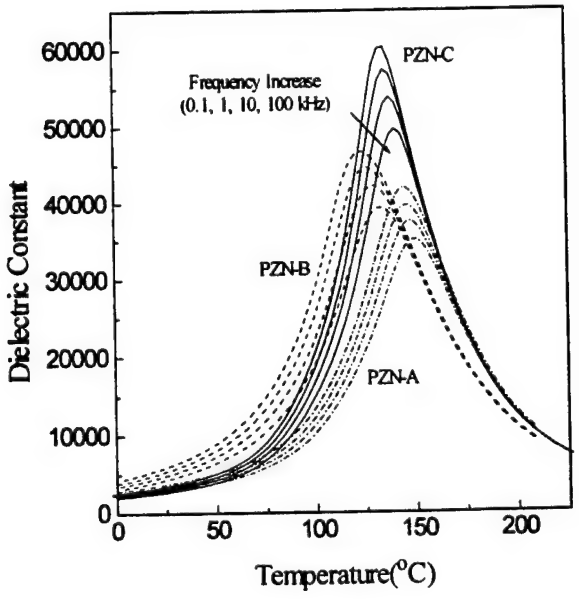

Figure 1 K vs. T curves for (111) oriented PZN crystals

B. Dielectric and Piezoelectric Properties

Figure 2 shows the dielectric constant as a function of temperature and frequency for PZN-PT crystals with varying PT content. Increased PT content resulted in the ferroelectric transition to become more 1st-order. Increased temperature range of the intermediate tetragonal phase was also observed with increased PT content a consequence of the curved MPB.[7] The rhombohedral to tetragonal phase transition

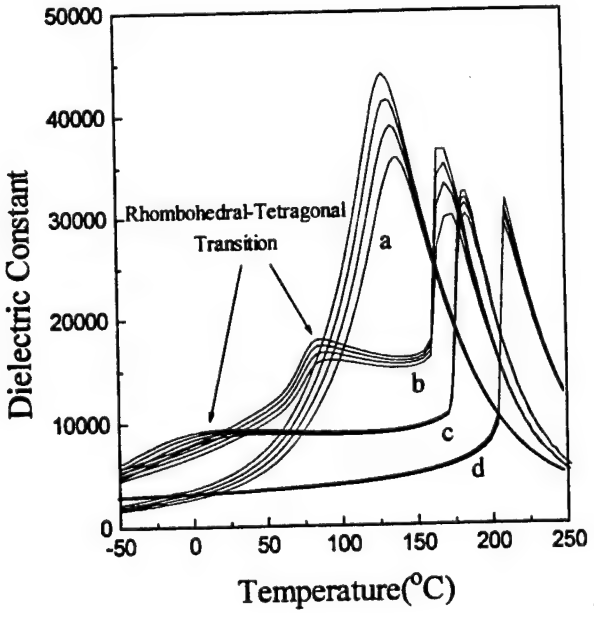

Figure 2 K vs. T curves for (001) oriented crystals for (a) PZN, (b) PZN-8%PT, (c) PZN-9.5%PT, and (d) PZN-15% PT

Table 2 Dielectric and Piezoelectric Properties of $Pb(A_{1/3}Nb_{2/3})O_3$ -$PbTiO_3$ crystals (A=Zn, Mg) from k_{33} mode sample.

Crystal	Cut	Tmax (°C)	Dielectric Constant (Loss)	Coupling	s_{33}^D ($\times 10^{-12}$ m^2/N)	d_{33} (pC/N)	Nt (Hz m)
PZN	111	~140	900 (0.012)	0.377	7.2	83	2058
	001		3600 (0.008)	0.852	13.2	1100	1521
PZN-8%PT	111	~170	2150 (0.012)	0.395	6.3	82	2205
	001		4200 (0.012)	0.938	15.5	2070	1401
PZN-9.5%PT	111	~176	4300 (0.007)	0.644	6.1	405 (600*)	2240
	001		1400 (0.004)	0.894	15.5	880 (1600*)	1403
PMN-30%PT	001	~150	2890 (0.014)	0.808	11.6	730	1608
PMN-35%PT	001	~160	3100 (0.014)	0.923	10.2	1240	1730

* values determined by Berlincourt d_{33} meter.

occurred at ~90°C for PZN-8%PT (Figure 2(b)) and near room temperature for PZN-9.5%PT (Figure 2(c)), substantiating that PZN-9.5%PT lies on the MPB. PMN-PT exhibited the same trend as that of PZN-PT except the increased PT content.

Dielectric and piezoelectric properties of PZN-PT and PMN-PT crystals are summarized in table 2. High coupling (k_{33}) values of 89% and 93% were observed with (001) oriented MPB crystals of PZN-9.5%PT and PMN-35%PT, respectively. However, unlike the case of polycrystalline piezoelectrics such as PZT, "non-MPB crystals" also exhibited high properties. As can be seen in table 2, longitudinal coupling values (k_{33}) of 85% and 94% were determined for (001) oriented rhombohedral crystals of PZN and PZN-8%PT, respectively. These high piezoelectric properties were observed for crystals oriented and poled along the pseudocubic <001> axis. However, both PZN and PZN-8%PT poled along their polar axis <111> possessed coupling less than 40%. It was found that this apparent anisotropy was related to a lack of domain stability after poling with respect to the crystallographic direction [8].

Thickness coupling coefficients (k_T) are given in table 3. Crystals of MPB compositions (PZN-9.5%PT, PMN-30%PT and PMN-35%PT) exhibited k_Ts ~ 54%.

Table 3
Dielectric and Piezoelectric Properties of $Pb(A_{1/3}Nb_{2/3})O_3$ -$PbTiO_3$ crystals (A=Zn, Mg) from k_T mode sample.

Crystal	Cut	Coupling	K_3^T	Loss	Qm	Nt (Hz m)
PZN	001	0.493	2732	0.013	40	2056
PZN-8%PT	001	0.481	4450	0.017	39.5	1831
PZN-9.5%PT	001	0.541	1553	0.024	31.3	1967
PZN-11%PT	001	0.638	890	0.024	16.6	1576
PMN-30%PT	001	0.568	4739	0.014	43.7	2368
PMN-35%PT	001	0.541	4540	0.031	35.3	2305

Rhombohedral crystals, however, were found to possess thickness coupling (k_T) less than 50% in spite of the high longitudinal coupling (k_{33}). On the other hand, for tetragonal crystals of PZN-11%PT, k_T of ~64% was measured. This increased k_T for tetragonal crystal is a consequence of the relatively large anisotropy expected with tetragonal symmetry. Increased crystal anisotropy is associated with the decreased contribution of lateral mode coupling, resulting in decreased thickness clamping effect on coupling. The relatively low dielectric constant (k_3^T) <1000 observed with tetragonal symmetry is also indication of the large degree of anisotropy.

Ultrahigh piezoelectric coefficients (d_{33}) ~1100 and ~2000 pC/N were measured for rhombohedral PZN and PZN-8%PT crystal, respectively. (table 2) These values were confirmed by direct inspection of strain as a function of electric field as shown in figure 3. A linear response of strain as a function of electric field was observed with the piezoelectric coefficients

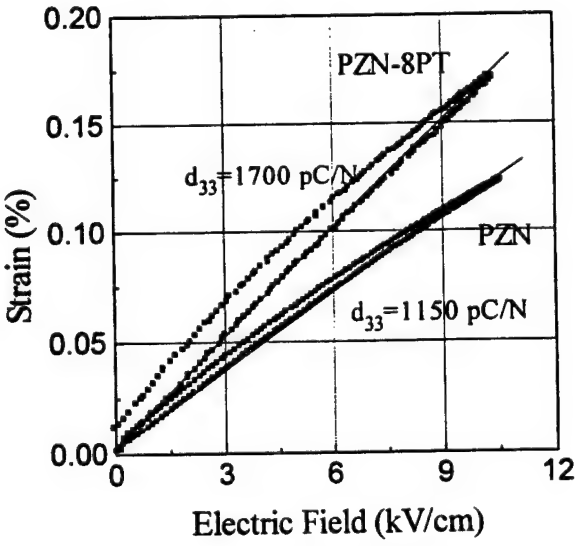

Figure 3 Strain vs. E curves for (001) oriented PZN and PZN-8%PT crystals

(d_{33}) of ~1100 pC/N ((001) oriented PZN) and ~1700 pC/N ((001) oriented PZN-8%PT). This linear response should be noted related to the observed low dielectric loss <1%, indicating that minimual domain motion was involved with this high strain behavior and that the domain state in (001) oriented rhombohedral crystals is stable.

C. Transducer Performance

The performance gain for transducer applications associated with piezoelectric materials with coupling coefficient as high as 90% are clearly evident for ultrasound transducers requiring broad bandwidth, resulting in increased axial resolution and improved sensitivity. A range of dielectric constants is also required for electrical impedence matching from the view point of transducer design. Acoustic arrays consisting of many rods or narrow plates require high k_{33} mode coupling and high dielectric constant for electrical impedence matching. Therefore, the relatively large dielectric constant ranging from 3000 to 5000 found in rhombohedral PZN-PT crystals is benificial for low to medium frequency transducers (2-5MHz). On the other hand, tetragonal crystals meet the requirements for high frequency single element transducers, where transducer shape requires a very thin plate. Thickness mode coupling (k_T) and low dielectric constant are necessary for better performance and electrical impedence matching, respectively. Further details concerning ultrasonic transducer design can be found in ref. [9].

III. SUMMARY

Crystals of PZN-PT and PMN-PT were grown by the high temperature flux technique. Growth conditions to maximize the amount of perovskite are suggested. Crystal properties were found to vary with the change of growth conditions. For example, different cooling rates and soaking temperature caused the dielectric constant and T_{max} to change for PZN crystals. In addition to high electromechanical couplings for MPB crystals, (001) oriented rhombohedral crystals also exhibited high longitudinal electromechanical coupling (k_{33}) > 90%, large dielectric constants from 3000 to 5000, ultrahigh piezoelectric coefficients from 1100 pC/N (PZN) to ~2000 pC/N (PZN-8%PT). Direct E-field strain measurements confirmed the high piezoelectric coefficients - making them attractive for actuator applications. Tetragonal PZN-11%PT crystals were found to have large thickness coupling coefficients (k_T) > 63% with decreased dielectric constant (<1000). High piezoelectric activity and a range of dielectric constant associated with the crystal compositions and their respective crystallographic structure will offer potential flexibility in transducer design.

ACKNOWLEDGEMENT

The authors would like to thank Hua Lei for her help with the preparation of samples.

REFERENCES

[1] J. Kuwata, K. Uchino, and S. Nomura, "Phase Transitions in the $Pb(Zn_{1/3}Nb_{2/3})O_3$ -$PbTiO_3$ System." Ferroelectrics, Vol. 37, pp 579-582, 1981.

[2] J. Kuwata, K. Uchino, and S. Nomura, "Dielectric and Piezoelectric Properties of $0.91Pb(Zn_{1/3}Nb_{2/3})O_3$ -$0.09PbTiO_3$ Single Crystals," Japanese Journal of Applied Physics, Vol. 21, No. 9, pp 1298-1302 1982.

[3] T. R. Shrout, Z. P. Chang, N. Kim, and S. Markgraf, "Dielectric Behavior of Single Crystals near the $(1-x)Pb(Mg_{1/3}Nb_{2/3})O_3$ - (x) $PbTiO_3$ Morphotropic Phase Boundary," Ferroelectric Letters, Vol 12, pp 63-69, 1990.

[4] IRE Standard on Piezoelectric Crystals: Proceedings of IRE, 49, 1161, 1961

[5] M. L. Mulvihill, S.-E. Park, G. Risch, Z. Li, K. Uchino, T. R. Shrout, "The Role of Processing Variables in the Flux Growth of Lead Zinc Niobate-Lead Titanate Relaxor Ferroelectric Single Crystals," Japanese Journal of Applied Physics, Vol. 35, No 7, pp 51-57, 1996.

[6] S.-E. Park, M. L. Mulvihill, G. Risch, T. R. Shrout, "The effect of growth conditions on dielectric properties of $Pb(Zn_{1/3}Nb_{2/3})O_3$ crystals," unpublished work.

[7] S. Nomura, "Ferroelectric Properties in the System $Pb(Zn_{1/3}Nb_{2/3})O_3$ - $PbTiO_3$," Journal of Physical Society of Japan, Vol. 27, p 262, 1969.

[8] S.-E. Park, M. Zipparo, and T. R. Shrout, "Apparent anisotropy and ferroelectric related propertes of $Pb(Zn_{1/3}Nb_{2/3})O_3$ crystal," unpublished work.

[9] P. D. Lopath, S.-E. Park, K. K. Shung, and T. R. Shrout, "Ultrasonic Transducers Using Piezoelectric Single Crystal Perovskites," Proceedings of ISAF 96', 1996.

APPENDIX 72

Jpn. J. Appl. Phys. Vol. 35 (1996) pp. 3984-3990
Part 1, No. 7, July 1996

The Role of Processing Variables in the Flux Growth of Lead Zinc Niobate-Lead Titanate Relaxor Ferroelectric Single Crystals

Maureen L. MULVIHILL, Seung Eek PARK, George RISCH, Zhuang LI[1], Kenji UCHINO and Thomas R. SHROUT

Materials Research Laboratory, Pennsylvania State University, University Park, PA 16802, USA
[1]*Materials Science Division, Argonne National Laboratory, Argonne, IL. 60439, USA*

(Received January 8, 1996; accepted for publication March 27, 1996)

Relaxor ferroelectric single crystals of $Pb(Zn_{1/3}Nb_{2/3})O_3$–$PbTiO_3$ (PZN-PT) are of interest as high performance transducers due to their very large piezoelectric coupling and dielectric properties. A high temperature flux solution method was used to grow $(1-x)$PZN-(x)PT, where $x = 0.0$, 0.1 and 0.15 single crystals. Processing conditions were optimized to increase the size and yield of the perovskite crystals, including variation of the flux to composition ratio, cooling rate, soak time and soak temperature. The crystals varied in size from 0.01 cm to 1.5 cm on an edge, and in color from opaque to brown due to the changes in processing conditions. The crystals were characterized by XRD, dielectric constant and dielectric loss measurements. As the content of PT increased the transition from the paraelectric to the ferroelectric phase approached first order behavior and the crystal structure transformed from rhombohedral to tetragonal. This structure transition caused the lattice constant along the c-axis to elongate as the c/a ratio increased. At room temperature, the dielectric constants for the PZN-PT compositions along the [111] or [001] axes were as great as 5000 and the dielectric losses were as low as 0.01.

KEYWORDS: lead zinc niobate, lead titanate, relaxor ferroelectric, single crystal, transducers, piezoelectrics, flux growth

1. Introduction

In contrast to a normal ferroelectric such as $PbTiO_3$ (PT), relaxor ferroelectrics exhibit a broad and frequency dispersive phase transition. $Pb(Zn_{1/3}Nb_{2/3})O_3$ (PZN) is an example of a relaxor ferroelectric material which has a disordered complex perovskite structure in which the Zn^{2+} and Nb^{5+} cations exhibit only short range order on the B-site. The maximum in the dielectric constant is obtained near 140°C. The transition temperature (T_{max}) and dielectric constant maximum (K_{max}) depend on the measurement frequency.[1-3] PZN has rhombohedral symmetry at room temperature[4,5] with space group R3m whereas the normal ferroelectric $PbTiO_3$ (PT) has tetragonal symmetry with space group P4mm and a transition temperature (T_C) at 490°C.

A complete solid solution is formed between $(1-x)$ $Pb(Zn_{1/3}Nb_{2/3})O_3$ and $xPbTiO_3$ (PZN-PT). The morphotropic phase boundary (MPB) at $x \sim 0.1$ separates the rhombohedral and tetragonal phases at 25°C.[6,7] In contrast to the $PbZrO_3$–$PbTiO_3$ (PZT) system.[8] the MPB for PZN-PT inclines as a function of temperature and composition, as shown in Fig. 1.[9]

Single crystal growth of PZN-PT by the flux technique is considerably easier than for PZT which makes PZN-PT a potential candidate material for high performance transducers. Several researchers have reported on the large piezoelectric ($d_{33}^* \sim 1500 \times 10^{-12}$C/N), dielectric ($K_{RT} \sim 3000$), and electromechanical coupling parameters ($k_{33}^* \sim 92\%$) of PZN-PT based single crystals.[6,9,10] However, most of these studies failed to discuss processing conditions such as flux to composition ratio, soak temperature, soak time, and cooling rates. In this study, the variables which affect crystal growth of PZN and 90PZN-10PT are systematically controlled to determine the effect on size, color and morphology.

2. Experimental Procedure

The PZN-PT single crystals were grown by the flux solution method.[11] The powders used were PbO, 99.9%, Pb_3O_4, 99.9%, and TiO_2, 99.99% from Aldrich Chemical Company. The ZnO and Nb_2O_5 powders were Grade 1 from Specialty Products-Johnson Matthey. PbO and Pb_3O_4 were used as the flux. Each batch was based on 450 gs of raw powder which was loaded into a 70 m*l* platinum crucible and charged several times at 900°C until the crucible was full. The platinum crucible was covered with a platinum lid and placed in an alumina crucible. The alumina crucible was then sealed with an alumina lid using alumina cement to minimize PbO volatility and then placed in a bottom loading furnace.

Differential Thermal Analysis (DTA) was used to determine the initial processing conditions for the growth of PZN single crystals. One gram of 30:70 PZN:PbO ground crystals was heated in air at a rate of 3°C per minute to 1150°C then cooled at 10°C per minute.

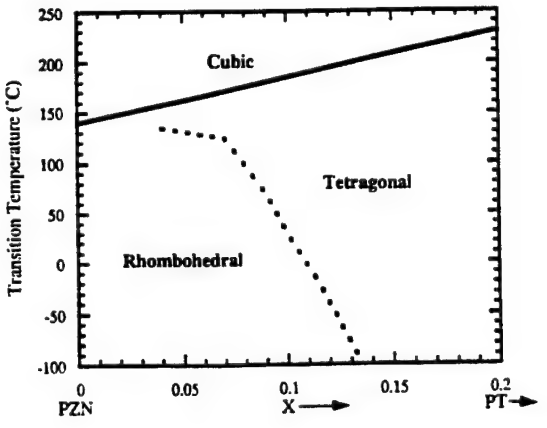

Fig. 1. Represents the PZN-PT phase diagram (after ref. 9).

The processing conditions were varied in an attempt to achieve PZN-PT single crystals which were perovskite phase pure, greater than 1 cm in size, and high optical quality. The processing conditions which were analyzed are listed below:

1. Mole ratio of solute composition to flux (C:F)
2. Soaking time (t_{soak})
3. Soaking temperature (T_{soak})
4. Slow cooling rate (C_S)
5. Transition temperature ($T_{S\text{-}F}$) between the slow (C_S) and fast (C_F) cooling rates.

The effect of compositional variation was studied by varying the mole ratio of solute composition to flux (C:F) from 26:74 to 40:60. Figure 2 illustrates the furnace profile for crystal growth. The furnace controller was programmed to reach the maximum temperature (T_{soak}) between 1150°C and 1200°C. The samples were held at a constant soak temperature (T_{soak}) for 2 to 10 h. The crucibles were then cooled at a slow rate (C_S) between 0.5 to 5°C per hour. The changes in soak temperature, time and slow cooling rate enabled the effect of these variables on the crystal color, morphology and size to be studied. After the furnace temperature cooled to a temperature between 800°C and 900°C, the furnace was cooled at the faster rate (C_F) to room temperature. The transition temperature between the slow cooling rate (C_S) and the fast cooling rate (C_F) determined the amount of pyrochlore phase formation. The fast heating (H_F) rate remained constant at 100°C per hour for every crystal run. The fast cooling (C_F) rate was held constant at −50°C per hour which will be discussed in §3.6. The single crystals were removed from the flux with the aid of a warm 25 vol% nitric acid solution.

Crystals from each batch were ground into a fine powder and examined by powder X-ray diffraction (XRD) for phase identification and lattice parameters. Single crystals were oriented along the [111] or [001] crystallographic axes using the Laué X-ray technique. The dielectric constants and losses were measured along the respective crystal structure polarization axes. The crystals were cut into thin sections and polished to a 3 μm surface finish. Circular gold electrodes were deposited with diameters ranging from 1 to 2 mm. The capacitance and loss of the crystal plates were measured as functions of temperature and frequency using a Hewlett Packard Programmable 4275A Multi-frequency LCR meter in a computer controlled furnace system.

3. Results and Discussion

The DTA data for a 30:70 PZN:PbO sample is shown in Fig. 3. On heating, an endothermic peak occurred at 850°C which signified the melting of the PbO flux. On cooling, the crystallization of the PZN resulted in an exothermic peak at 1000°C. The crystallization temperature increased as the solute content increased. The cooling curve also showed a second exothermic peak near 850°C which is assumed to be pyrochlore crystallization which will be discussed later. A third exothermic peak occurred at 700°C which was associated with the flux solidification temperature.

3.1 *Mole ratio of solute composition to flux, (C:F)*

The composition to flux ratios, C:F, were varied from 26:74 to 40:60. PbO and Pb_3O_4 were used as the PbO source to determine the best source of raw material for the flux. Pb_3O_4 was considered a better flux than PbO since the decomposition of Pb_3O_4 to PbO released O_2 which would assist in the thermal mixing of the raw powders.[12] The three crystals runs used to examine the effect of the C:F are represented in Table I. With each of the crystal runs all the growth parameters were held constant except the C:F ratio. The ratio of 35:65 produced perovskite crystals with minimal pyrochlore phase. The 30:70 ratio produced yellow perovskite single crystals with approximately 15 vol% pyrochlore phase. The 26:74 ratio produced 100% pyrochlore crystals. The stability of perovskite with respect to pyrochlore was found to be very sensitive to the C:F ratio and it was assumed that no perovskite crystals could be formed with a ratio lower that 26:74. It has been found that PZN can be formed under an excess molten PbO environment.[13] Therefore, the temperature range where PZN phase can be formed using a PbO flux depends on the C:F ratio. This temperature range is associated with both crystal-

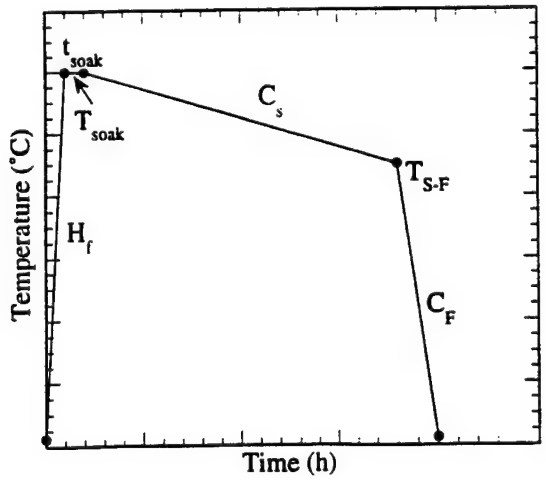

Fig. 2. An illustration of the furnace profile for the PZN-PT single crystal growth.

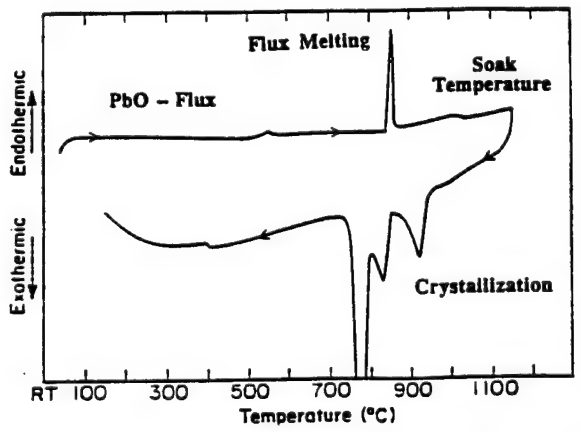

Fig. 3. A DTA measurement of a 30 mole percent PZN to 70 mole percent PbO sample.

Table I. Study of the effect of the composition to flux (C:F) ratio on a PZN perovskite crystal formation.

Run number	1	2	3
Crystal	PZN	PZN	PZN
C:F	26:74	30:70	35:65
Flux	PbO	PbO	PbO
t_{soak} (h)	2	2	2
T_{soak} (°C)	1150	1150	1150
C_S (°C/h)	2	2	2
$T_{S\text{-}F}$ (°C)	900	900	900
Color	NA	yellow	yellow
Size (cm)	NA	0.3	0.5
Perovskite (%)	0	85	95
Pyrochlore (%)	100	15	5

Table II. Study of the effect of soaking time on a 90PZN-10PT perovskite crystal formation.

Run number	1	2
Crystal	90PZN-10PT	90PZN-10PT
C:F	30:70	40:60
Flux	PbO	PbO
t_{soak} (h)	2	10
T_{soak} (°C)	1150	1150
C_S (°C/h)	2	2
$T_{S\text{-}F}$ (°C)	900	900
Color	yellow	yellow
Size (cm)	0.6	0.6

Table III. Study of the effect of the soaking temperature on a PZN perovskite crystal formation.

Run number	1	2
Crystal	PZN	PZN
C:F	40:60	40:60
Flux	PbO	PbO
t_{soak} (h)	10	10
T_{soak} (°C)	1150	1200
C_S (°C/h)	1	1
$T_{S\text{-}F}$ (°C)	900	880
Color	dark yellow	dark brown
Size (cm)	0.6	1.5

Table IV. Study of the effect of the slow cooling rate on a PZN perovskite crystal formation.

Run number	1	2	3
Crystal	PZN	PZN	PZN
C:F	30:70	30:70	30:70
Flux	PbO	PbO	PbO
t_{soak} (h)	2	2	2
T_{soak} (°C)	1150	1150	1150
C_S (°C/h)	0.5	2	5
$T_{S\text{-}F}$ (°C)	900	900	900
Color	NA	yellow	white
Size (cm)	NA	0.5	0.5
Mechanical integrity	NA	strong	weak
Pyrochlore (%)	100	15	15

lization temperature and decomposition temperature of the perovskite phase into the pyrochlore phase; therefore, decreasing the C:F ratio causes the decomposition temperature and crystallization temperature to increase and decrease, respectively. In other words, decreasing the C:F ratio caused the perovskite crystallization temperature range to decrease. Most of all, the increase of the decomposition temperature would be critical if the $T_{S\text{-}F}$ in Table I were fixed since all of the perovskite phase would decompose into the pyrochlore phase. This decomposition in to the pyrochlore phase is expected to be the case for the 26:74 ratio batch, and will be further discussed in §3.5.

3.2 *Soak time, (t_{soak})*

The soak time, t_{soak}, was changed from 2 to 10 hours, as reported in Table II, to determine the effect on crystal growth. The effect of the soak times was compared using the MPB composition, 90PZN-10PT. The single crystals for the two soak times were similar in color (yellow) and size (0.6 cm). From this, it can be assumed that soak time does not appear to have a significant effect on the crystal quality or size; therefore, a shorter soak time is recommended to reduce volatilization of PbO and ZnO.

3.3 *Soak temperature, (T_{soak})*

While the DTA data indicated a soak temperature, T_{soak}, of $\sim$ 1000°C would be sufficient to grow perovskite crystals, actual crystal runs demonstrated that higher temperatures were needed to produce crystals larger than a few 100 μm. Crystals grown using soak temperatures of 1150°C and 1200°C varied in size and color as represented in Table III. The higher soak temperature produced larger crystals ($\sim$ 1.5 cm) with a brown color and the lower soak temperature produced smaller crystals ($\sim$ 0.6 cm) with a yellow color. The growth rate at 1150°C was $\sim$ 0.0024 cm/h, compared to $\sim$ 0.0047 cm/h at 1200°C. The origin and effect of the color differences on measured dielectric properties are the subject of future investigation.

3.4 *Slow cooling rate, (C_S)*

PZN single crystals slow cooled at different rates varied in structure and color. The cooling rate, C_S, was altered from 0.5°C/h to 5°C/h as compared in Table IV. The crystals which were formed at the slowest rate, 0.5°C/h, had only pyrochlore phase present which can be attributed to the decomposition of the perovskite phase. The crystals cooled at 2°C/h had a perovskite structure with a yellow color. The crystals cooled using the fastest rate were perovskite and opaque. The opaque perovskite crystals contained many cracks; therefore, they were more brittle than the yellow perovskite crystals. The faster cooling rate supersaturated the solution and resulted in unstable growth conditions. An intermediate cooling rate $\sim$ 1 to 2°C/h was optimal to produce low defect perovskite PZN single crystals.

Table V. Study of the effect of the transition temperature on a PZN perovskite crystal formation.

Run number	1	2
Crystal	PZN	PZN
C:F	40:60	40:60
Flux	PbO	PbO
t_{soak} (h)	10	10
T_{soak} (°C)	1200	1200
C_S (°C/h)	1	1
$T_{S\text{-}F}$ (°C)	800	880
Color	Light brown	Dark brown
Size (cm)	0.4	1.5
Perovskite (%)	75	95
Pyrochlore (%)	25	5

3.5 *Lower temperature limit of slow cooling, ($T_{S\text{-}F}$)*

The crucibles were slow cooled down to the transition temperature between slow and fast cooling, $T_{S\text{-}F}$, which was varied between 900°C to 800°C. From the DTA data in Fig. 3, it was expected that the exothermic peak at 850°C was due to pyrochlore formation. From the experiments represented in Table V, it was confirmed that the second peak in Fig. 3 was the pyrochlore crystallization temperature. The percentage of pyrochlore phase formed can be reduced by setting $T_{S\text{-}F}$ above 850°C.

3.6 *Fast cooling rate, (C_F)*

It must also be noted that it is very important to cool quickly through the pyrochlore phase region to avoid pyrochlore crystal formation. The fast cooling rate, C_F, was found to be associated with the decomposition of perovskite crystals into pyrochlore crystals. The size and yield of perovskite crystals decreased and pyrochlore crystals increased as the cooling rate decreased. At a C_F of −50°C/h, the crystals maintained a high quality perovskite structure without cracking.

3.7 *Crystal morphology*

In each crystal growth run, a fraction of pyrochlore phase formed on the top layer of the crucible which depended on processing conditions. The pyrochlore phase was very easy to identify and remove since it had an orange-red color and octahedral morphology with the symmetry m3m, as illustrated in Fig. 4(a).

Perovskite PZN crystals showed an arrow-head shape, as illustrated in Fig. 4(b), as found by previous researchers.[1,3,7] The typical crystal morphologies for PZN-PT are presented in Fig. 5. Although the rhombohedral perovskite crystals did not exhibit a fully faceted well developed morphology, the {111} faces which indicates the rhombohedral morphology could be indexed. It was expected that the morphology of the crystals would have been cubic since according to Fig. 1 the crystals should have had a cubic symmetry when they were grown. This means that if perovskite crystals were grown under stable growth condition a cubic morphology should have occurred. Even though it is not obvious why PZN perovskite crystals have a rhombohedral morphology with an arrow-head shape, it can be assumed that

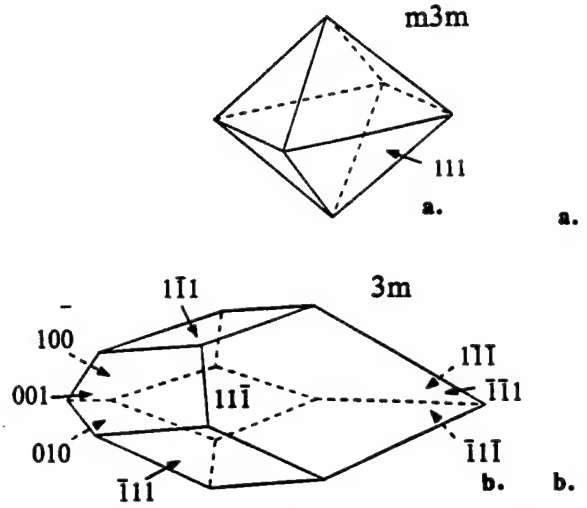

Fig. 4. Illustration of the crystal morphology. (a) pyrochlore and (b) perovskite.

the PZN perovskite crystals were not grown under stable conditions, but under metastable conditions in a PbO excess environment. From the as-grown morphology, it can be expected that the formation for the perovskite crystals under metastable conditions can be followed by the decomposition of the crystal into another phase (the other phase being pyrochlore) if appropriate growth conditions are not maintained which was supported by this work.

3.8 *Dielectric constant and loss measurements*

All single crystals characterized by dielectric measurement were confirmed as perovskite by XRD. The dielectric constant and dielectric losses were measured along the [111] and [001] directions of the pseudocubic unit cell. All of the dielectric loss values measured at high (> 225°C) and low (< 25°C) temperatures were low which suggested that the crystals had minimal number of defects.

Dielectric constant and loss variations of PZN with temperature is shown in Fig. 6. This [111] oriented crystal showed typical relaxor-type ferroelectric phase transition behaviors in which the dielectric constant maximum lowered from ~ 53000 to ~ 43000 and shifted to higher temperatures from 140°C to 150°C with increasing frequency from 100 Hz to 100 kHz.

According to previously reported work,[4-7] the 90PZN-10PT single crystal composition should lie along the morphotropic phase boundary at room temperature. In the case of PZN-PT, the MPB varies as a function of temperature and composition. Thus, the MPB is not a particular composition but a range of compositions, and therefore a mixed phase was expected for this crystal. The XRD data for the 90PZN-10PT composition is shown in Fig. 7. All peaks could be indexed as mixed rhombohedral and tetragonal phases. The lattice parameters of the rhombohedral and tetragonal phases are $a = 4.051$ Å, $\alpha = 89.93$ Å and $a = 4.033$ Å, $c = 4.080$ Å, respectively. Near room temperature a dramatic change in the dielectric loss occurred accompanied by a slight change in the

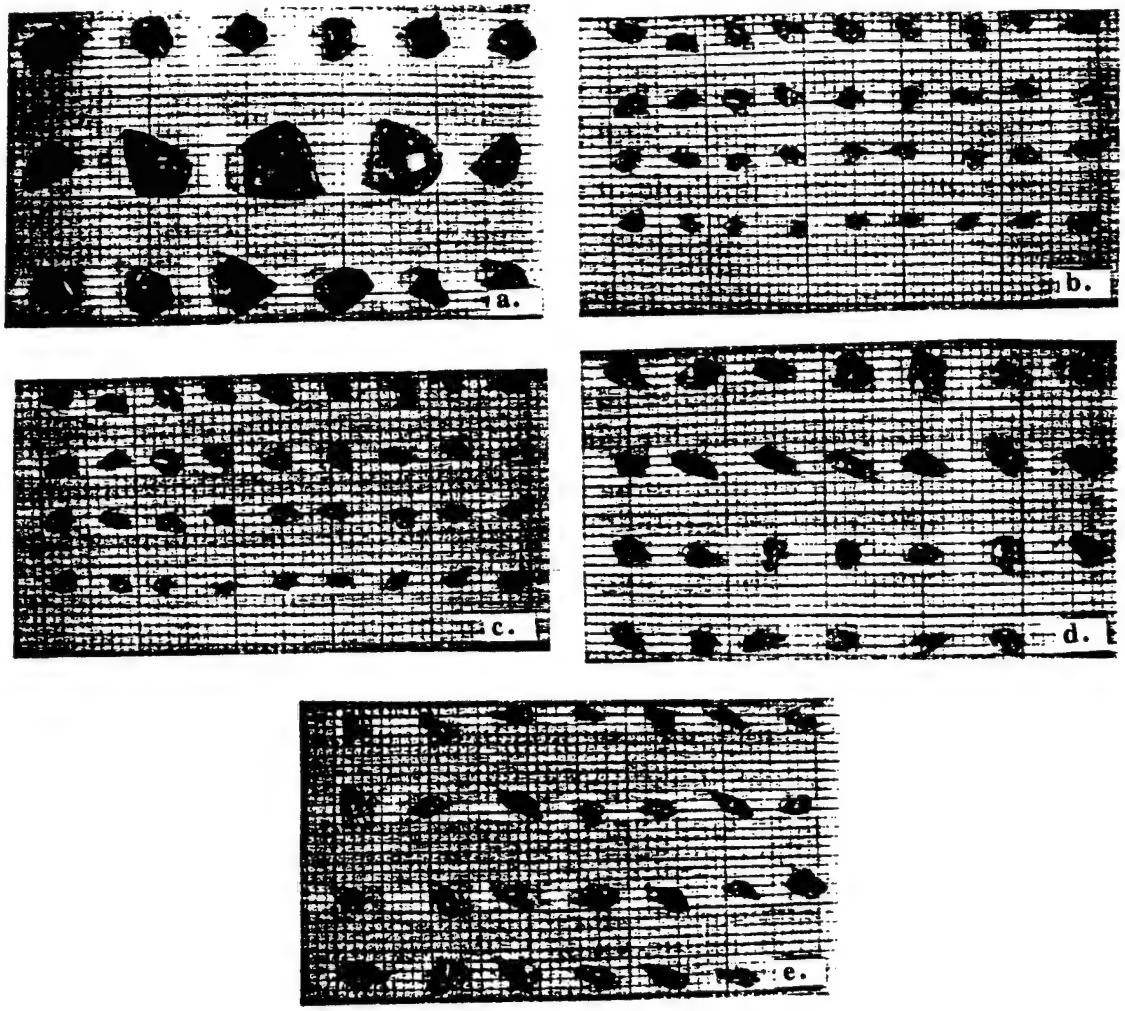

Fig. 5. PZN-PT based single crystals grown in this study. Scale: 5 grid lines ~ 6.4 mm. (a) 100% PZN (Table III, Run 2), (b) 100% PZN (Table IV, Run 2), (c) 100% PZN (Table IV, Run 3), (d) 90PZN-10PT (Table II, Run 1), and (e) 85PZN-15PT. Run numbers correspond to data in Tables I through V.

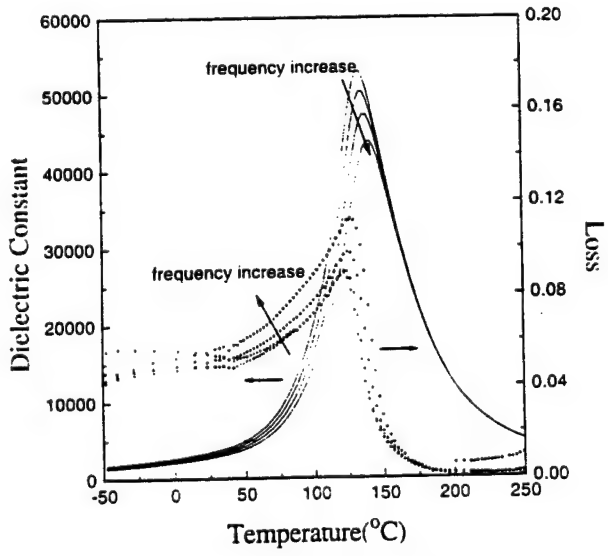

Fig. 6. The dielectric constant and loss behavior as a function of temperature for a PZN single crystal.

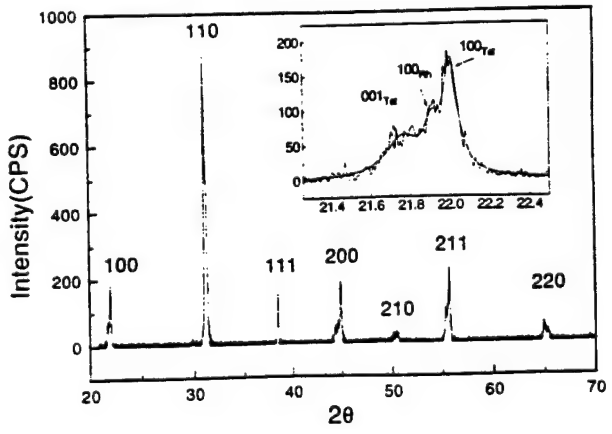

Fig. 7. X-ray diffraction patterns for the 90PZN-10PT composition.

dielectric constant. These changes signified the rhombohedral to tetragonal transition which coincides with a previous report.[10] Although the 90PZN-10PT composition showed more of a first-order phase transition than

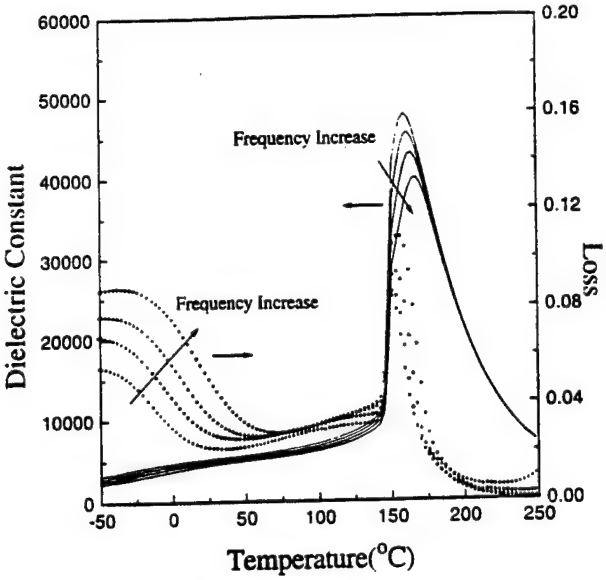

Fig. 8. The dielectric constant and loss behavior as a function of temperature for a 90PZN-10PT single crystal.

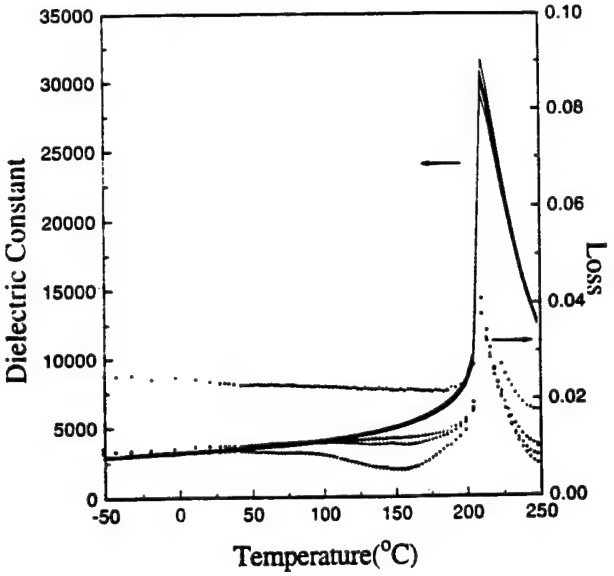

Fig. 9. The dielectric constant and loss behavior as a function of temperature for a 85PZN-15PT single crystal.

Table VI. Dielectric constant, dielectric loss and transition behavior of PZN-PT crystals at 1 kHz.

Crystal	K_{RT}	Loss	T_{max} (°C)	K_{max}	Transition type
PZN [111]	3200	0.05	~ 135	~ 50000	Relaxor
90PZN-10PT [111]	5000	0.03	~ 165	~ 45000	Mixed
85PZN-15PT [001]	2400	0.01	210	30000	First order

the PZN crystal, it still had some relaxor behavior with the onset temperature of 148°C below T_{max} as shown in Fig. 8. The T_{max} occurred near 160°C with a dielectric constant near 45000 for 100 Hz.

Single crystal XRD analysis for the 85PZN-15PT revealed that this composition had a single phase tetragonal structure. This crystal showed the first-order, Curie-Weiss behavior as expected for the tetragonal structure. Figure 9 shows the dielectric constant and loss variations on temperature for [001] oriented crystal. Sharp first order transitions were found at a temperature of 205°C with a maximum dielectric constant near 34000.

In Table VI, the dielectric constant, dielectric loss and transition behavior of the as-grown crystals are summarized. As expected, the morphotropic phase boundary crystal (90PZN-10PT) showed the highest dielectric constant at room temperature. The maximum dielectric constant (K_{max}) at the transition temperature decreased with increasing PT content.

4. Conclusions

The growth of PZN-PT single crystals using the flux method produced high quality, low defect, perovskite crystals. However, it was found that the perovskite crystals were grown under metastable conditions which could easily decompose into pyrochlore crystals with changes in processing conditions. The PZN-based crystals varied in size and color depending on the processing conditions. A solute composition to flux ratio of 30:70 to 40:60, Pb_3O_4 as the flux, and a soak time of 2 h produced perovskite crystals. Larger crystals were grown by increasing the soak temperature to 1200°C. A cooling rate between 1°C/h and 2°C/h produced perovskite crystals which were near defect-free and mechanically strong. The crystals which were slow cooled down to 900°C were nearly 100% perovskite phase since the pyrochlore crystallization which began at 850°C was avoided.

The dielectric constant and loss calculations determined by capacitance measured as a function of temperature showed a trend towards more first order behavior as the concentration of PT was increased. The increase in PT caused the dielectric constant at room temperature to peak at 10%PT. In all three crystal compositions measured, the dielectric loss was less than 0.05 at room temperature which signified high quality, low defect, single crystals.

Acknowledgements

The authors would like to thank John Yamashita from Toshiba Corporation in Kawasaki, Japan for his insightful discussions on PZN crystal growth. This work was supported by the Office of Naval Research under grant numbers N00014-91-J-4145 and N00014-93-J-0502.

1) V. A. Bokov and I. E. Myl'nikova: Sov. Phys.-Solid State **2** (1961) 2428.
2) N. P. Khuchua, V. F. Bokov, and I. E. Myl'nikova: Sov. Phys.-Solid State **10** (1968) 194.
3) J. Kuwata, K. Uchino, S. Nomura: Ferroelectrics **22** (1979) 863.

4) S. Nomura, T. Takahashi and Y. Yokomizo: J. Phys. Soc. Jpn. **27** (1969) 262.
5) Y. Yokomizo, T. Takahashi and S. Nomura: J. Phys. Soc. Jpn. **28** (1970) 1278.
6) J. Kuwata, K. Uchino and S. Nomura: Jpn. J. Appl. Phys. **21** (1982) 1298.
7) Z. P. Chang, A. S. Bhalla and L. E. Cross: 6th Proc. IEEE Int. Symp. Appl. Ferroelectrics (1986) p. 482.
8) B. Jaffe, W. R. Cook and H. Jaffe: *Piezoelectric Ceramics*, eds. J. P. Roberts and P. Popper (Academic Press, London and New York, 1971) Chap. 7, p. 136.
9) J. Kuwata, K. Uchino and S. Nomura: Ferroelectrics **37** (1981) 579.
10) Y. Yamashita: Jpn. J. Appl. Phys. **33** (1994) 5328.
11) W. Tolksdorf: *Handbook of Crystal Growth-Bulk Crystal Growth*, eds. D. T. J. Hurle, (Elsevier Science, North-Holland, Amsterdam, 1994) Vol. 2, Chap. 10, p. 563.
12) Y. Yamashita: personal communication, Toshiba Corporation, Kawasaki Japan.
13) H. M. Jang, S. H. Oh and J. H. Moon: J. Am. Ceram. Soc. **75** (1992) 82.

APPENDIX 73

journal

J. Am. Ceram. Soc., 79 [11] 2971–74 (1996)

Superoxidation and Electrochemical Reactions during Switching in $Pb(Zr,Ti)O_3$ Ceramics

Ming-Jen Pan,* Seung-Eek Park,* Colin W. Park, Kelley A. Markowski,* Shoko Yoshikawa,* and Clive A. Randall*

Intercollege Materials Research Laboratory, The Pennsylvania State University, University Park, Pennsylvania 16802

Under ferroelectric switching in $Pb(Zr,Ti)O_3$ (PZT) ceramics, we demonstrate that oxygen gas is emitted and degrades electrode microstructure. The oxygen is a direct result of the defect chemistry associated with superoxidation which is established during the processing of the ceramics. Under high alternating electric fields, electron injection into the ceramic surface induces a reduction process, and surface layers are believed to change from a *p*-type electronic compensation to an ionic compensation of oxygen vacancies and A-site lead vacancies. During this process, we noticed progressive changes in capacitance, loss, remnant polarization, and coercive field. The wider implications of this observation for PZT thin film nonvolatile memories are discussed in brief.

I. Introduction

In the past 40 years, $Pb(Zr,Ti)O_3$ ceramics, or PZT, have been extensively investigated for piezoelectric applications. Their performance, however, is critically dependent on the materials fabrication processes, both the mixing of Zr and Ti and the stoichiometry of the volatile Pb.[1,2] Even when an extra lead source is used in an undoped PZT, PbO is lost in the sintering process.[3] The loss of PbO causes the material to have high conductivity, which is undesirable for piezoelectric applications. The mechanism of defect chemistry for this phenomenon has been reported by Jaffe, Cook, and Jaffe.[4] That is, during sintering and cooling in the furnace, oxygen from the atmosphere re-enters the ceramic such that there is a net ionic imbalance of Pb-site vacancies. This process is referred to as superoxidation, and the resulting ceramic is compensated by electron holes in the valence band, producing a *p*-type PZT. The processing and associated defect chemistry of doped and undoped PZTs have been discussed by a number of authors.[5–8] Nevertheless, few works have been done on the ferroelectric behavior of PZT under dc or ac field after it experiences the superoxidation process.

The objective of this work was to determine the origin of a surprising observation of gas evolution at the surface of $Pb(Zr,Ti)O_3$ ceramics undergoing polarization switching. The subsequent change in dielectric and ferroelectric properties associated with this gas evolution at room temperature is discussed along with its defect chemistry. The defect chemistry discussed in this communication uses Kröger–Vink notation.[9]

II. Experimental Procedure

A lead-deficient PZT, namely $Pb_{0.98}(Zr_{0.52}Ti_{0.48})O_3$, was made by conventional solid-state reaction using the appropriate amounts of reagent-grade raw powders of lead carbonate, zirconium oxide, and titanium oxide. The chemical purity of each was greater than 99%. Calcined powder was examined by X-ray diffraction (XRD) to ensure phase purity. The powder showed a single phase within the detection limit of XRD (<2%). The pellets were pressed and sintered at 1250°C for 2 h with

S.-F. Wang—contributing editor

Manuscript No. 191873. Received April 22, 1996; approved September 5, 1996.
Presented at the 98th Annual Meeting of the American Ceramic Society, Indianapolis, IN, April 14–17, 1996 (Paper No. SXIX-15-96).
*Member, American Ceramic Society.

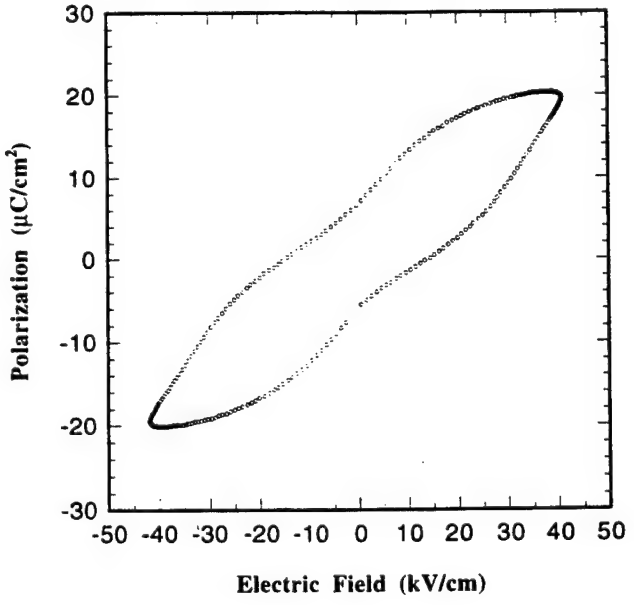

Fig. 1. As-sintered sample showed a lossy hysteresis loop with a "pinched" shape.

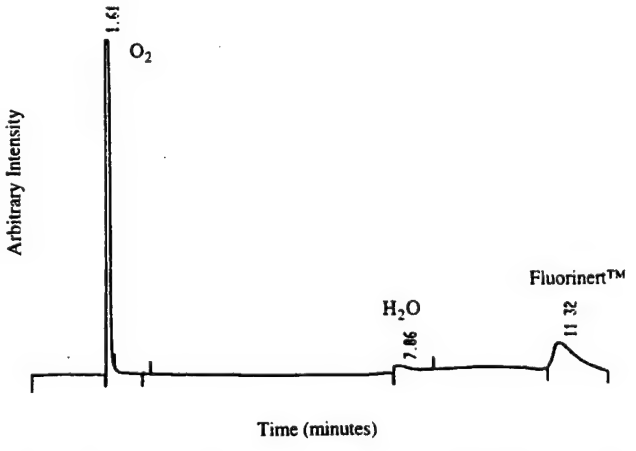

Fig. 2. Gas chromatography result confirmed the existence of oxygen.

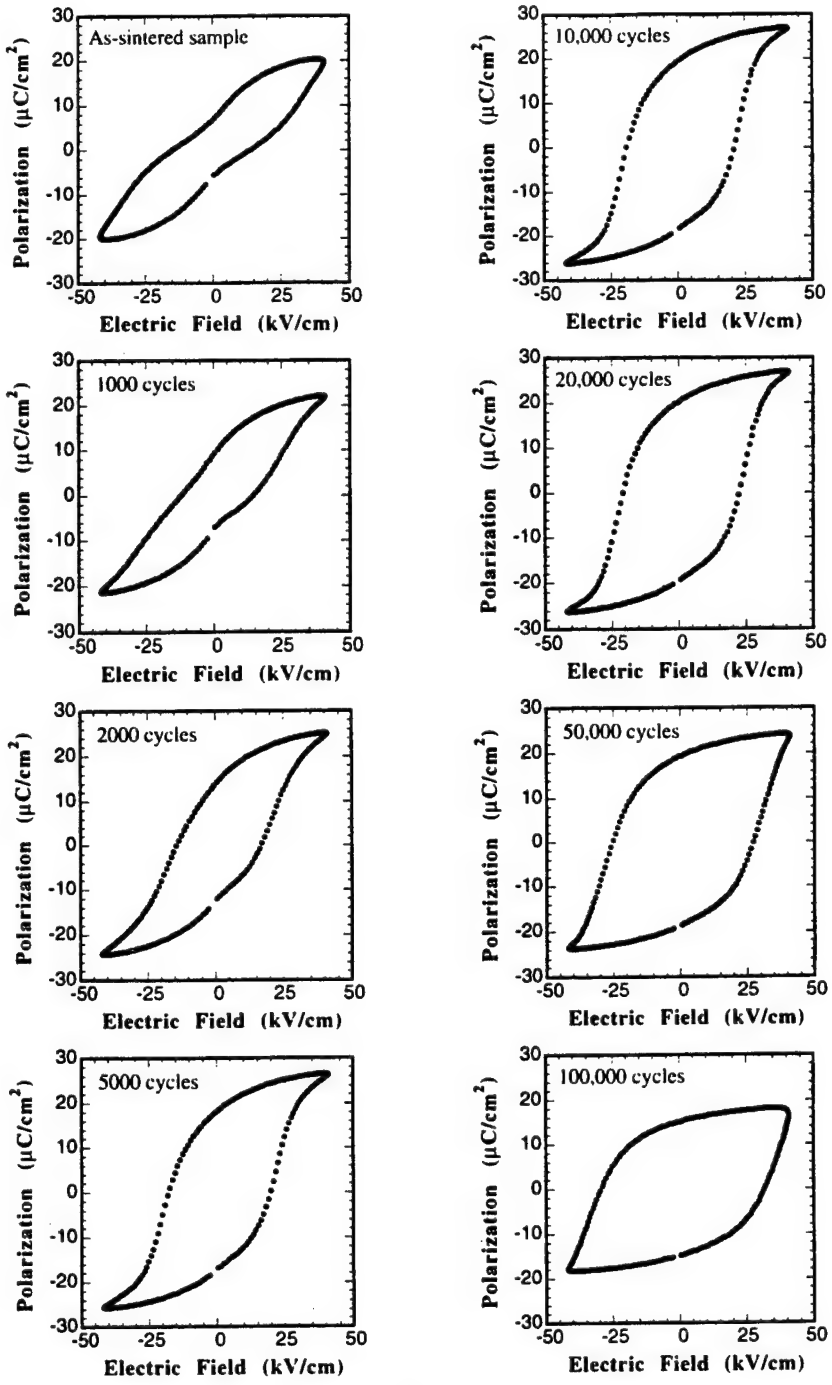

Fig. 3. Changes in P vs E hysteresis loops during the gas evolution.

10°C/min ramp rates. During sintering, 2 g of $PbZrO_3$ was used as the lead source in a crucible to minimize lead volatilization. The average density of the sintered samples was 7.58 g/cm^3 and the average weight gain was 0.74%. The sintered samples were polished and sputtered with gold electrodes.

The polarization of the samples was measured using a modified Sawyer–Tower circuit. The sample holder was placed in a plexiglass container, in which a clear liquid Fluorinert (FC-8270 Flourinert, 3M, St. Paul, MN) was provided for insulation to prevent arcing at sample edges. During cyclic driving, a 100 Hz sine wave was applied until the desired cycles were achieved, and then the polarization versus electric field loop was taken at 10 Hz for better data resolution. The capacitance and loss were immediately measured using an LCR meter (Model SR715, Stanford Research Systems) at 1 kHz. In addition, gas bubbles were observed during the measurement. An inverted glass vial filled with Fluorinert was held above the ceramic sample to collect the gas bubbles. The gas was analyzed using a 0.5 nm molecular sieve column in a Varian 3400 gas chromatography unit.

III. Results and Discussion

The proposed electrochemical reaction is based on the superoxidation process. During sintering, PbO is lost because of its high partial pressure, leaving lead and oxygen vacancies of Schottky-type point defects:

$$V''_{Pb} + V^{\cdot\cdot}_{O} \rightarrow \text{null} \quad (1)$$

During sintering and cooling, oxygen from the atmosphere is absorbed by the ceramic, and electron holes are created:

$$\tfrac{1}{2}O_2 \rightarrow V''_{Pb} + 2h^{\cdot} + O_O \quad (2)$$

This makes the sintered PZT a p-type ceramic. The direct effect

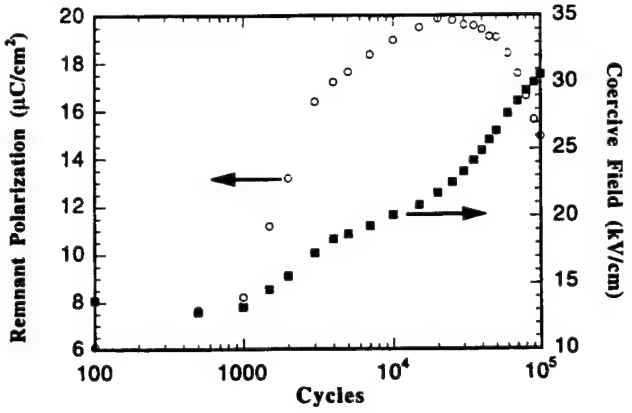

Fig. 4. Remnant polarization and coercive field during the gas evolution.

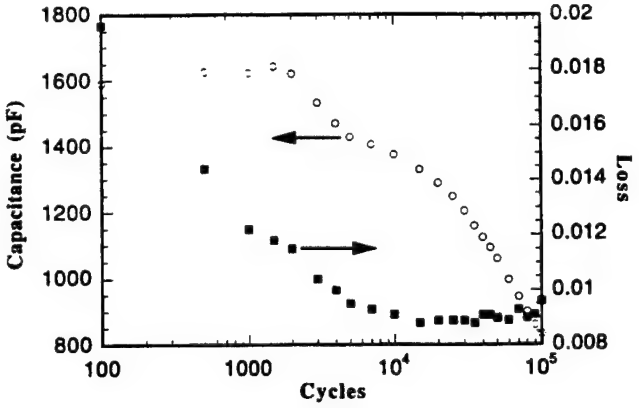

Fig. 6. Capacitance and loss showed progressive changes during the gas evolution. Note that the loss of an as-sintered sample is 0.027.

of superoxidation observed in this study is high dielectric loss and lossy hysteresis P vs E behavior, as shown in Fig. 1.

When cycling an alternating (ac) electric field to establish ferroelectric switching, it was noted that bubbles evolved at the outer electrodes of the PZT pellets. Interestingly, this gas evolution only occurred when the applied electric field was larger than 28 kV/cm, indicating an energy barrier in the process. Eventually, after a few hundred thousand cycles the gas evolution was exhausted and there were no further changes to the hysteresis loop unless breakdown occurred.

Under ac drive, electrons can be injected into the ceramic under both forward and reverse bias. The electrons can then undergo recombination with the holes in the following reaction:

$$V''_{Pb} + 2h^{\cdot} + O_O \xrightarrow{2e} V''_{Pb} + V_O^{\cdot\cdot} + \tfrac{1}{2}O_2\uparrow \qquad (3)$$

Electroneutrality is established by the reduction reaction which gives off oxygen gas. It was noted that such a reaction does not occur under unipolar driving.

The gas evolved during this process was analyzed by gas chromatography using a packed 5 nm molecular sieve column in a Varian 3400 GC. The gas analyzed consisted of oxygen (88.4%), water (1.7%), and Fluorinert (9.9%), as shown in Fig. 2. Both the water and Fluorinert originated from the syringe as it was initially filled with Fluorinert to remove the possibility of air being present when a sample of the evolved gas was removed. The gas chromatography column used to analyze the evolved gas could not distinguish between molecular and atomic oxygen, and therefore the possibility of atomic oxygen being present could not be ruled out. Note that the insulating liquid Fluorinert is a fully fluorinated carbon compound with primarily nine carbons and its boiling temperature is 130°C.[10] Therefore, oxygen could not be a product of Fluorinert even if it slowly disintegrated or boiled under high electric field. This eliminated the possibility of other gas-emitting mechanisms.

It is speculated that oxygen was evolved from the lattice of the ceramic as atomic oxygen. However, because of its reactivity, the method of collection, and limitation of the chromatography column, only molecular oxygen could be determined. The evolution of this oxygen from the ceramic was anticipated to cause point defects or clustered point defects such as crystallographic shears or dislocation loops within the lattice.

There were changes in the polarization switching behavior as the gas evolution occurred. Figure 3 shows some of the P vs E behavior changes observed during the gas evolution. An as-sintered sample showed a lossy hysteresis loop with a "pinched" shape, which resumed its normal shape after a few thousand cycles of ac driving. Continuing driving increased the remnant polarization (P_r) and coercive field (E_c), as shown in Fig. 4. Increased polarization may be caused by decreased p-type conductivity; i.e., the electric field contributes more to polarization switching rather than electric current. In addition, increased E_c suggests that the material becomes harder with gas evolution. One possible explanation is the recovery of Schottky pairs near the surface which can cause nonuniform distribution of electric field. This behavior is subject to further investigation. In Fig. 4, it is found that P_r decreases after 20 000 cycles. This implies that material damage caused by accumulation of oxygen vacancies near the surface has started. The damage became apparent after 50 000 to 60 000 cycles, as evidenced by the small black spots on the sample surface (Fig. 5).

Direct evidence of decreased conductivity was confirmed by decreased dielectric loss with respect to the number of cycles. Figure 6 shows the capacitance and loss as a function of the number of cycles. In general, both showed a continuous decrease during the cycling. In particular, the loss showed a dramatic decrease in the first 1000 cycles. This indicates that by pumping out oxygen, the contribution of electron holes to both dielectric constant and loss decreases. After 20 000 cycles, the faster decrease of capacitance and the unstable loss again suggest the accumulation of damage in the material.

The gas evolution damaged the electrode microstructure as shown in Fig. 5. All of the observations made in this study would suggest that the electrochemical reaction could be potentially damaging in degradation mechanisms in lead-based ceramics. This could be important for nonvolatile PZT thin films, high drive hard PZT multilayer actuators, and $Pb(Mg_{1/3}Nb_{2/3})O_3$:$PbTiO_3$ materials. We hope that investigators in these fields

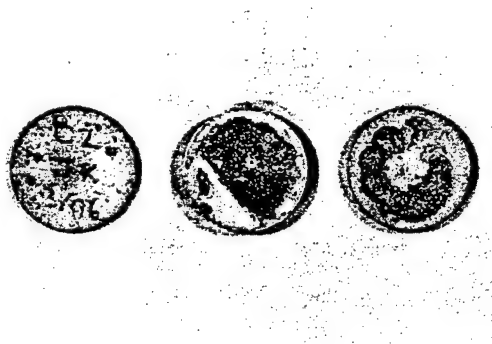

Fig. 5. Damage caused by the oxygen evolution process became apparent after 50 000 cycles.

find these observations useful toward solving degradation and fatigue problems in these technically important areas.

IV. Summary and Conclusions

We determined the origin of a surprising observation of gas evolution at the surface of PZT ceramics under ac driving. The proposed electrochemical reaction is based on the superoxidation process, and the associated defect chemistry equations have been suggested. It was predicted that oxygen gas would be released from the material with the injection of electrons. The existence of oxygen was confirmed by using gas chromatography. In addition, the ferroelectric and dielectric behavior during oxygen evolution was followed. The results imply a reduction in *p*-type conductivity with continuing ac driving. Eventually, the accumulation of oxygen vacancies near the surface caused physical damage to the material, which was evident by small black spots on the sample surface. This degradation mechanism is potentially important for PZT thin films or high drive PZT actuators.

References

[1]R. Gerson and H. Jaffe, "Electrical Conductivity in Lead Titanate Zirconate Ceramics," *J. Phys. Chem. Solids*, **24**, 979–84 (1963).

[2]D. Northrop, "Vaporization of Lead Zirconate–Lead Titanate Materials," *J. Am. Ceram. Soc.*, **50** [9] 441–45 (1967).

[3]A. I. Kingon and J. B. Clark, "Sintering of PZT Ceramics: I. Atmosphere Control," *J. Am. Ceram. Soc.*, **66** [4] 253–56 (1983).

[4]B. Jaffe, W. R. Cook, Jr., and H. Jaffe, *Piezoelectric Ceramics*; pp. 237–42. R.A.N. Publishers, Marietta, OH, 1971.

[5]R. B. Atkin and R. M. Fulrath, "Point Defects and Sintering of Lead Zirconate-Titanate," *J. Am. Ceram. Soc.*, **54** [5] 265–70 (1971).

[6]A. H. Webster, T. B. Weston, and N. F. H. Bright, "Effect of PbO Deficiency on the Piezoelectric Properties of Lead Zirconate-Titanate Ceramics," *J. Am. Ceram. Soc.*, **50** [9] 490–91 (1967).

[7]A. I. Kingon, P. J. Terblanche, and J. B. Clark, "The Control of Composition, Microstructure and Properties of $Pb(Zr,Ti)O_3$ Ceramics," *Mater. Sci. Eng.*, **71**, 391–97 (1985).

[8]K. Kakegawa, O. Matsunaga, T. Kato, and Y. Sasaki, "Compositional Change and Compositional Fluctuation in $Pb(Zr,Ti)O_3$ Containing Excess PbO," *J. Am. Ceram. Soc.*, **78** [4] 1071–75 (1995).

[9]F. A. Kröger and H. J. Vink, "Relations between the Concentration of Imperfections in Crystalline Solids," *Solid State Physics*, Vol. III; p. 307. Edited by F. Seitz and D. Turnbull. Academic Press, New York, 1956.

[10]3M material safety data sheet, C.A.S. No. 86508-42-1. □

APPENDIX 74

The Effect of Growth Conditions on the Dielectric Properties of $Pb(Zn_{1/3}Nb_{2/3})O_3$ Single Crystals

Seung-Eek Park, Maureen L. Mulvihill, George Risch, and Thomas R. Shrout

Materials Research Laboratory, The Pennsylvania State University
University Park, PA 16801

Abstract

The effect of growth conditions on the dielectric properties and ferroelectric transition of perovskite $Pb(Zn_{1/3}Nb_{2/3})O_3$ single crystals was examined. Crystals were grown by the flux technique using PbO as a self flux. Increased cooling rate and soaking temperature resulted in a decreased Zn/Nb ratio, and corresponding increased temperature of the maximum dielectric constant (T_{max}), and decreased room temperature values of the dielectric constant and loss. Different crystal colors and quality were also associated with the various growing conditions. Although dielectric properties, domain stability after poling, and associated piezoelectric properties are a function of T_{max} , it was shown that crystal quality was critical for the observed variation in these properties. [KEYWORDS: relaxor ferroelectrics, crystal growth, $Pb(Zn_{1/3}Nb_{2/3})O_3$, nonstoichimetry, phase transition]

1. Introduction

$Pb(Zn_{1/3}Nb_{2/3})O_3$ (PZN) is a prototypical relaxor ferroelectric which undergoes a diffuse phase transition around 140°C.[1] Macroscopic lattice distortion with rhombohedral symmetry can be observed at room temperature due to the high transition temperature of PZN.[2,3] In spite of the observed lattice anisotropy, as-grown PZN crystals do not show ferroelectric macrodomains.[4] However PZN switches into a stable ferroelectric macrodomain state with the application of an E-field, and effectively exhibits piezoelectric characteristics.[5] High dielectric and piezoelectric properties were reported for PZN [6] and $Pb(Zn_{1/3}Nb_{2/3})O_3$ - $PbTiO_3$ (PZN-PT) [7,8] single crystals, making them promising candidates for various transducer applications.

It is known that perovskite PZN or PZN-PT with low PT content can not be prepared by conventional solid state reaction. The reason for this phase instability has been investigated from both the viewpoints of crystal chemistry [9] and thermodynamics [10]. However, crystals of PZN and PZN-PT can be readily grown using the high temperature flux. To date, however, few studies correlating the dielectric and piezoelectric properties as a function of growth conditions for the materials have been reported, particularly with respect to nonstoichimetric variations.

It is the purpose of this study to report the variation of chemical composition, dielectric and ferroelectric properties as a function of growth conditions. PZN rather than PZN-PT was selected to eliminate the possibility of property and compositional variations caused by the change in solute concentration and ionic valence of Ti^{4+}.

2. Experimental Procedure

2.1 Crystal growth

PZN crystals were grown using the high temperature flux technique. High purity (>99.9%) powders of Pb_3O_4 (Aldrich, WI), ZnO (Johnson Matthey, MA), and Nb_2O_5 (Aldrich, WI) were used. Raw powders were mixed and loaded into a 30cc Pt crucible. The Pt crucible was then placed in an alumina crucible which was sealed with an alumina lid and alumina cement to minimize PbO volatilization. The crucible and powder were then placed in a furnace and held at a soak temperature of 1150 to 1200°C for 10 hrs, followed by cooling at a rate of 1°C/hr to 5°C/hr down to 900°C. The crucible was then furnace-cooled to room temperature. The flux was leached out with hot HNO_3 (20%) and the crystals removed for characterization. These growing conditions were determined based on several preliminary experiments including differential thermal analysis. Further details concerning the crystal growth can be found in ref. 11.

2.2 X-ray diffraction (XRD) and chemical analysis

Single crystals were ground into a fine powder for XRD analysis ranging from 20° - 80° 2θ with a step size of 0.01 and a counting time of 3 sec. Individual crystals were oriented along their polar axis <111> using a Laue back reflection camera. Crystals were chemically analyzed using inductively coupled plasma spectrophotometer (ICP, Leeman Labs PS30000UV). To determine reproducibility, chemical analysis was performed at least twice with different crystals from the same batch. The detection limit was ~ 80ppm due to the low solute concentration caused by the inherent difficulty in dissolving niobate crystals. Nonstoichiometry with the crystal growth was

observed mainly associated with B-site cation variation, as crystals were grown in the PbO self flux.

2.3 Electrical characterization - polarization and dielectric properties

For electrical characterization, samples were then prepared by polishing with silicon carbide and alumina polishing powders to achieve flat and parallel surfaces onto which gold electrodes were sputtered. Samples were rectangular plates with the thickness ranged from 0.2 to 0.5 mm and edge to thickness ratio > 10. To determine reproducibility, all dielectric and piezoelectric measurements were performed with at least three different crystals for each grown batch. Polarization vs. E-field behavior was measured at 0.2 Hz using a computer controlled Sawyer Tower system. During testing, the samples were submerged in Fluorinert (FC-40, 3M, St. Paul, MN), an insulating liquid to prevent arcing. For piezoelectric measurements, crystals were poled by applying either 10kV/cm at room temperature or by field (10kV/cm) cooling from 200°C. The piezoelectric coefficient (d_{33}) was measured using d_{33} meter (Institute of acoustics, Academia Sinica). The dielectric properties were determined with multifrequency LCR meters (Hewlett Packard 4274A and 4275A) in conjunction with a computer controlled temperature chamber (Delta Design Inc., Model MK 2300) over the frequency range of 100Hz, 1kHz, 10kHz and 100kHz.

3. Results and Discussion

3.1 Crystal growth and stoichiometry

Table 1 summarizes the various conditions used for the growth of three different PZN crystals. XRD patterns of the various crystals are shown in Fig. 1. All crystals were found to be phase pure perovskite with rhombohedral symmetry (a=4.056 (±0.001) Å and α=89°55′). Rhombohedral distortion (α) was determined from the peak split observed in the {220} peaks in Fig. 2. Lattice constants of the crystals were found to be not significantly different as a function of growth condition.

As presented in table 1, growth parameters remained constant for the growth runs of PZN-A and PZN-B with the exception of the cooling rate. A flux to composition molar ratio of 70:30 and a soak temperature of 1150°C as determined by preliminary DTA analysis [11], were employed. Cooling rates were 5°C/hr and 1°C/hr for run PZN-A and PZN-B, respectively. For PZN crystals obtained from growth run PZN-A and those from growth run PZN-B, crystal size was not significantly different. This indicates that the variation in cooling rate from 1 to 5°C/hr does not significantly affect the nucleation behavior with a soak temperature of 1150°C. This would occur if the majority of nucleation occurred on heterogeneous sites such as the crucible wall. However, the chemical composition was found to be dependent on the cooling rate as presented in table 2. Nonstoichiometry in Pb-based compounds is usually the result of Pb volatilization, which results in Pb vacancies on the A-site [12,13]. In this study, crystals were grown under a Pb-rich condition using PbO as a self flux. Therefore, it was expected that the observed nonstoichiometry, if any, would be caused by the compositional variation of the B-site cations. In table 2, the Pb content did not change significantly with growth conditions whereas the variation

in the Zn/Nb ratio was observed. Increased cooling rate resulted in a decreased Zn/Nb ratio to decrease (PZN-A and PZN-B in table 2). The different cooling rate and subsequent growth rate changes may have affected the composition at the boundary layers on the crystal. Additional investigations as to the actual origin of the compositional variation are required.

Crystals grown with the flux to composition ratio of 60:40 (designated PZN-C (table 2)) required an increase in soak temperature to 1200°C. As can be seen in table 1, the decreased flux:composition ratio resulted in relatively increased size of the PZN crystals. This could be ascribed to the increased temperature range of crystallization for PZN (PZN + liquid). In contrast with the PZN-B crystals grown at a cooling rate of 1°C/hr, the PZN-C crystals also showed decreased Zn/Nb ratio. In this case, the higher soaking temperature may have been responsible for a Zn-deficient composition owing to the volatilization of Zn-rich phase. The 1°C/hr cooling also efficiently allows the batches to stay at a higher temperature longer inducing more volatilization of Zn-rich phase.

The color of the crystals varied significantly with respect to growing conditions, as presented in table 1. PZN-A crystals were colorless whereas PZN-B crystals were slightly yellow, and PZN-C crystals dark brown for both as-grown crystals and dielectric/piezoelectric measurement samples (thickness 0.2 to 0.5 mm). One possible explanation of coloration is the role of defects involved with oxygen vacancies or interstitials both of which are common in perovskite crystals. [14] However, direct inspection such as high temperature annealing in order to check that possibility could not be employed because perovskite PZN crystal transforms into pyrochlore. [10] Figure 3 utilizes XRD to demonstrate the decomposition of PZN crystal powder annealed for 2hrs at the temperatures of 500°C, 700°C, 900°C, and 1050°C in the air. Transformation to the pyrochlore phase were initiated at only 2hr annealing at temperatures of 700°C with 100% pyrochlore phase after 2hr annealing at 1050°C. This confirmed the perovskite phase instability without the presence of the PbO flux.

Another possible explanation of coloration is the role of impurities caused by the reaction between the solution and crucible at high temperature. However, no impurities such as Pt could be found within the detection limit of ICP as presented in table 2. Additional studies are required to investigate the origin of the coloration.

3.2 Dielectric and polarization behavior

One of the direct effects of compositional variation on the dielectric properties of relaxor ferroelectrics is the shift of the temperature where the dielectric constant is maximum (T_{max}).[15,16,17] Figure 4 shows the temperature dependence of dielectric constant for the various PZN crystals. T_{max} of the PZN crystals was found to be dependent on composition as shown in Fig. 4. The decreased Zn/Nb ratio was associated with an increase in T_{max}. The opposite obervation, decreased T_{max} with decreased Zn/Nb ratio, had been reported by Matsuo[17]. This might be ascribed to the different growth conditions. Faster cooling rate (25°C.hr) in ref. 17 might be associated with the second phase inclusions. All the crystals followed the quadratic law, $1/K \sim (T-T_{max})^2$ at temperatures higher than T_{max}. Table 3 presents the T_{max} and dielectric constant (K,

1kHz) at room temperature. PZN-B crystals showed the lowest T_{max} (126°C, 1kHz), the room temperature dielectric constant being higher than both PZN-A and PZN-C crystals. For the case of as-grown crystals, higher dielectric loss was observed with PZN-B, which can be also ascribed to a low T_{max} . All the PZN crystals exhibited a linear dependency of $1/T_{max} = f(\ln \omega)$ (ω : measuring frequency) as observed for other relaxor-ferroelectrics, shown in Fig. 5. The frequency behavior of T_{max} for PZN crystal in ref. 3 is compared, ranging between those of PZN-A and PZN-C. However, growth conditions could not be directly compared due to the lack of specific conditions reported in the literature. It could be found from the slopes in Fig. 5 that T_{max} was more dependent on measurement frequency as T_{max} decreases. A decrease of T_{max} would induce the increase of frequency-dependent contributions (reorientation of polar regions) to polarization through the temperature range of the diffuse phase transition.

Figure 6 shows P vs. E behavior for the various PZN crystals at room temperature. Remnant polarization (P_r) and coercive field (E_c) are reported in table 3. An increased Curie temperature (T_c , here translated into T_{max}) corresponds to an increase in P_r at room temperature. PZN-C crystal (T_{max} = 135°C, 1kHz) exhibited larger P_r than PZN-B (T_{max} = 126°C), but in case of PZN-A crystal (T_{max} = 145°C), small P_r was observed in spite of highest T_{max} among the crystals. This may be ascribed to the poor crystal quality of PZN-A, probably a subsequence of relatively fast cooling rate during crystal growth. It should be noted that mechanical failure happened most frequently during the sample preparation of PZN-A crystal. Therefore, it could be said that the inferior crystal quality of PZN-A is responsible for low Ps in spite of high T_{max}.

3.3 Relaxor-ferroelectric transition

In table 3, decreased dielectric constant (K) and loss are reported for the poled crystals. However, the ratio of K_{poled}/K_{virgin} varied from ~0.75 (PZN-A) to ~0.4 (PZN-C). The piezoelectric coefficient (d_{33}) also varied from values as low as ~10 pC/N (PZN-A) to ~80 pC/N (PZN-B, PZN-C). The low value of d_{33} for (111) oriented PZN crystals was also reported by Kuwata. [7] These observed low values of d_{33} are belived to be associated with domain instability with respect to crystal orientation, reported elsewhere. [6]

It has been suggested that as grown PZN crystals do not exhibit a macrodomain state before poling. [5] Therefore, poling of PZN crystals can be also translated into switching of the relaxor state to macrodomain state. The poled crystals transform to relaxor with the increase of temperature at T_{FR} (ferroelectric-relaxor transition temperature). The T_{FR} was reported to be ~ -60°C and ~ 100°C for $Pb(Mg_{1/3}Nb_{2/3})O_3$ [18,19] and PZN relaxors [20], respectively. For transducer applications, relaxor based crystals should stay in the oriented macrodomain state. Transition temperature (T_{FR}) of ferroelectric-relaxor implies the temperature limit of the oriented ferroelectric macrodomain state, and that of a given transducer application. Hence, the high T_{FR} is required for increased temperature stability of piezoelectric properties.

Figure 7 shows the dielectric constant as a function of temperature with heating (no-field) from room temperature to 210°C for poled crystal. An abrupt increase of the dielectric constant (indicated by arrow) can be observed for PZN-B and PZN-C crystals, indicating ferroelectric

(macrodomain) -relaxor transition. T_{FR}'s of 72°C and 105°C were observed for PZN-B and PZN-C crystals, respectively. Different T_{FR} for PZN-B and PZN-C crystals is due to the free energy variation associated with the different T_{max}. This transition was not observable for PZN-A crystals in Fig. 7. However, ferroelectric-relaxor transition behavior for PZN-A crystal could be observed from the dielectric loss as a function of temperature for poled crystals (Fig. 8). Decreased dielectric loss by E-field exposure showed an abrupt jump at T_{FR} (indicated by arrow again) but T_{FR} of PZN-A crystal was almost same as that of PZN-C in spite of higher T_{max}. This behavior may be also ascribed to poor domain stability, resulted from inferior crystal quality.

4. Conclusions

The dielectric and ferroelectric behavior of PZN crystals grown by the flux technique were determined as a function of growth conditions. Increased cooling rate and soaking temperature caused the Zn/Nb ratio to decrease, which corresponded to a shift of both T_{max} and ferroelectric-relaxor transition to higher temperatures and various room temperature dielectric constant and loss.

Crystal quality and color were also as a function of the growing condition. Relatively fast cooling rate (>5°C/hr) may have associated with inferior crystal quality, resulting in poor domain stability after poling, lower piezoelectric coefficient, and low ferroelectric-relaxor transition temperature.

Acknowledgment

This work has been supported by the Office of Naval Research and the Whitaker Center for ultrasound transducers.

5. References

1) V. A. Bokov and I. E. Myl'nikov: Sov. Phys. - Solid State, 2 (1961), No.11, 2428.

2) S. Nomura and T. Takahashi: J. Phys. Soc. Jpn., 27 (1969), 262.

3) Y. Tokomizo, T. Takahashi, and S. Nomura, J. Phys. Soc. Jpn., 28 (1970), No. 5, 1278.

4) N. N. Krainik, L. S. Gokhberg, and I. E. Myl'nikova, Sov. Phys. - Solid State, 12 (1971), No. 8, 1885.

5) M. L. Mulvihill, L. E. Cross, and K. Uchino, J. Am. Ceram. Soc., 78 (1995), No. 12, 3345.

6) S.-E. Park, M. Zipparo, and T. R. Shrout, unpublished work.

7) J. Kuwata, K. Uchino, and S. Nomura, Ferroelectrics, 37 (1981) 579.

8) J. Kuwata, K. Uchino, and S. Nomura, Jpn. J. Appl. Phys., 21 (1982), No. 9, 1298.

9) A. Halliyal, U. Kumar, R. E. Newnham, and L. E. Cross, Am. Ceram. Soc. Bull., 66 (1987) No. 4, 671.

10) H. Jang, S. Oh, and J. Moon, J. Am. Ceram. Soc., 73 (1992) No.1, 82.

11) M . L. Mulvihill, S.-E. Park, G. Risch, Z. Li, K. Uchino, and T. R. Shrout, Jpn. J. Applied Physics, 35 [7], Pt. 1, 51 (1996).

12) R. Gerson and H. Jaffe, J. Phys. & Chem. Solids, 24 (1963) 979.

13) D. A. Northrop: J. Am. Ceram. Soc., 21 (1967) 441.

14) B. Jaffe, W. R. Cook Jr., and H. Jaffe, Piezoelectric Ceramics, (Academic Press, London and New York, 1971) Chap. 10, p.237.

15) S. L. Swartz, T. R. Shrout, W. A. Schulze, and L. E. Cross, J. Am. Ceram. Soc., 67 (1984) No. 5, 311.

16) F. Chu, I. M. Reaney, and N. Setter, J. Am. Ceram. Soc., 78 (1995), No.7, 1947.

17) Y. Matsuo, Yogyo-Kyokai-Shi, 78 (1970), No.7, 213.

18) V. A. Bokov and I. E. Myl'nikova, Sov. Phys. - Solid State, 3 (1961), No. 3, 613.

19) Z. Ye and H. Schmid, Ferroelectrics, 145 (1993) 83.

20) M. Mulvihill, L. E. Cross, and K. Uchino, to be published in Ferroelectrics.

Table Caption

Table 1 Growth condition of flux grown PZN crystals.

Table 2 Compositional analysis of PZN crystals using ICP.

Table 3 Dielectric (1kHz) and E-field induced properties of PZN crystals (<111> orientation) at room temperature.

Figure Caption

Fig. 1 XRD patterns of $Pb(Zn_{1/3}Nb_{2/3})O_3$ crystals.

Fig. 2 {220} reflections in XRD patterns of $Pb(Zn_{1/3}Nb_{2/3})O_3$ crystals.

Fig. 3 XRD patterns of $Pb(Zn_{1/3}Nb_{2/3})O_3$ crystal powder after heat treatment for 2 hr at (a) 500°C, (b) 700°C, (c) 900°C, (d) 1050°C.

Fig. 4 Temperature dependence of dielectric constant for <111> oriented $Pb(Zn_{1/3}Nb_{2/3})O_3$ crystals.

Fig. 5 $1/T_{max}$ as a function of ln f for $Pb(Zn_{1/3}Nb_{2/3})O_3$ crystals (dot line form ref. 3).

Fig. 6 Polarization as a function of electric field for <111> oriented $Pb(Zn_{1/3}Nb_{2/3})O_3$ crystals.

Fig. 7 Temperature dependence of dielectric constant for E-field exposed (10 kV) $Pb(Zn_{1/3}Nb_{2/3})O_3$ crystals (heating run, <111> orientation).

Fig. 8 Temperature dependence of dielectric loss for E-field exposed (10 kV) $Pb(Zn_{1/3}Nb_{2/3})O_3$ crystals (heating run, <111> orientation).

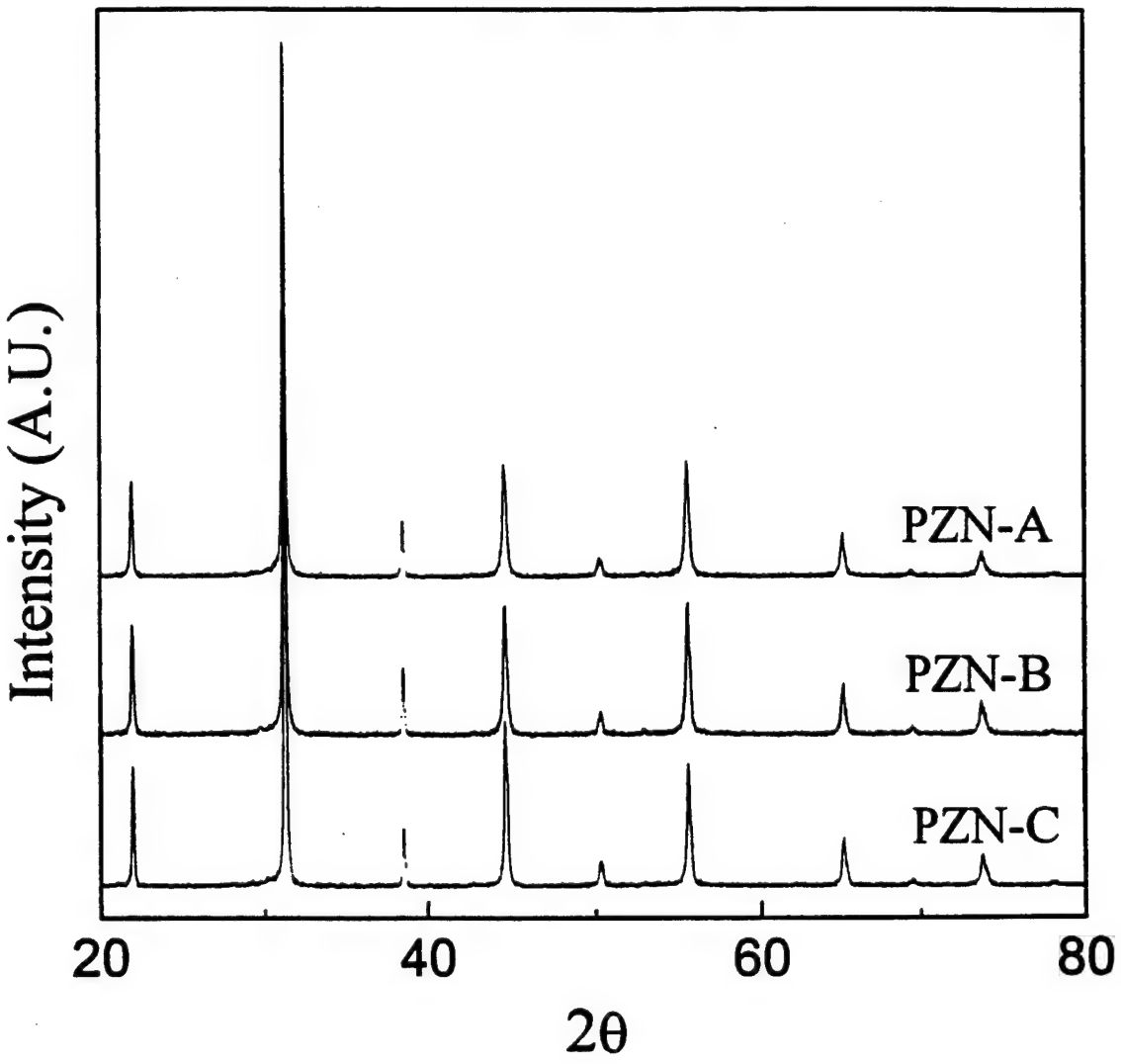

Fig. 1

Seung-Eek Park, Maureen Mulvihill, George Risch, and Thomas R. Shrout

Desired breadth undetermined, shrink so it fits and is clear to read

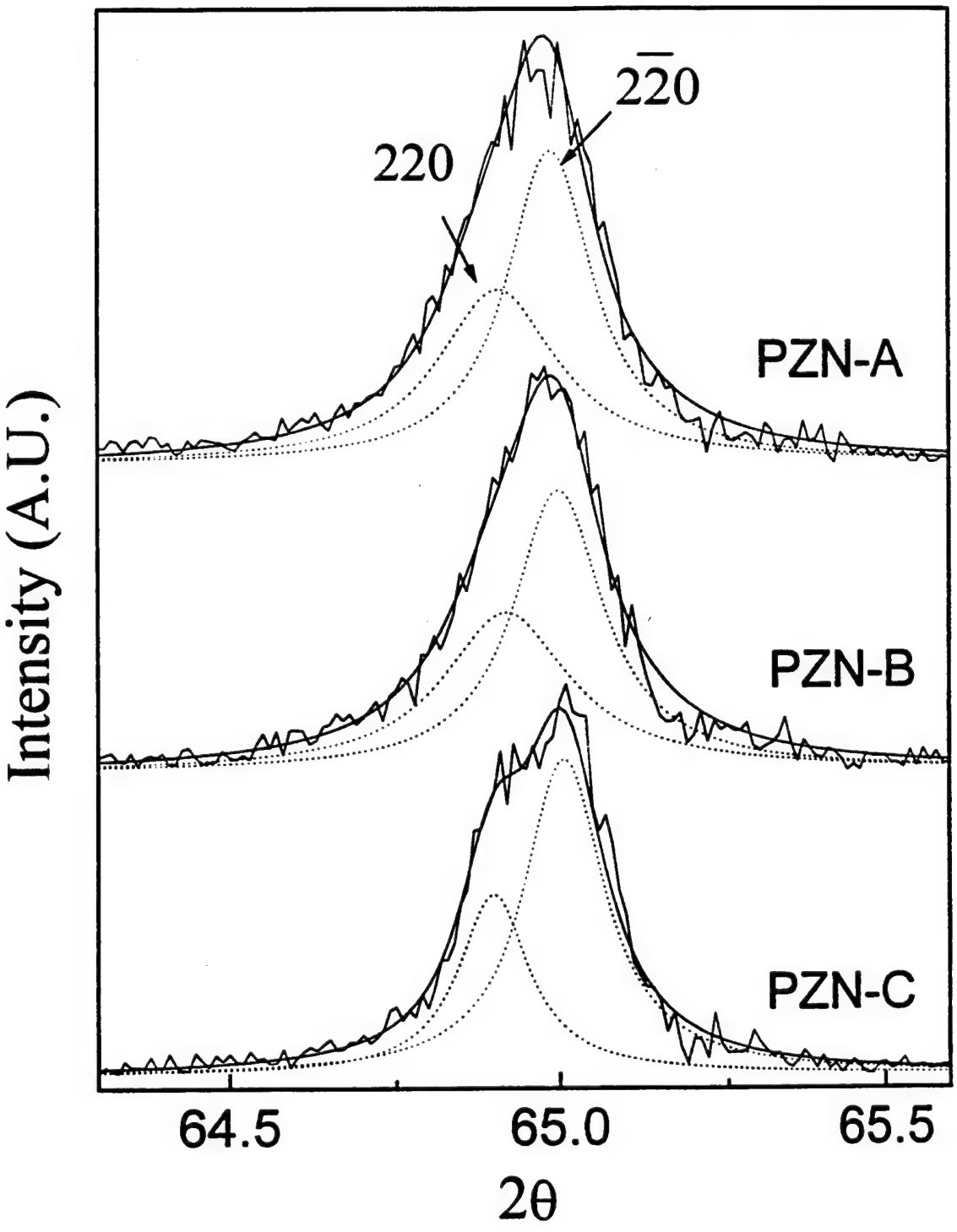

Fig. 2

Seung-Eek Park, Maureen Mulvihill, George Risch, and Thomas R. Shrout

Desired breadth undetermined, shrink so it fits and is clear to read

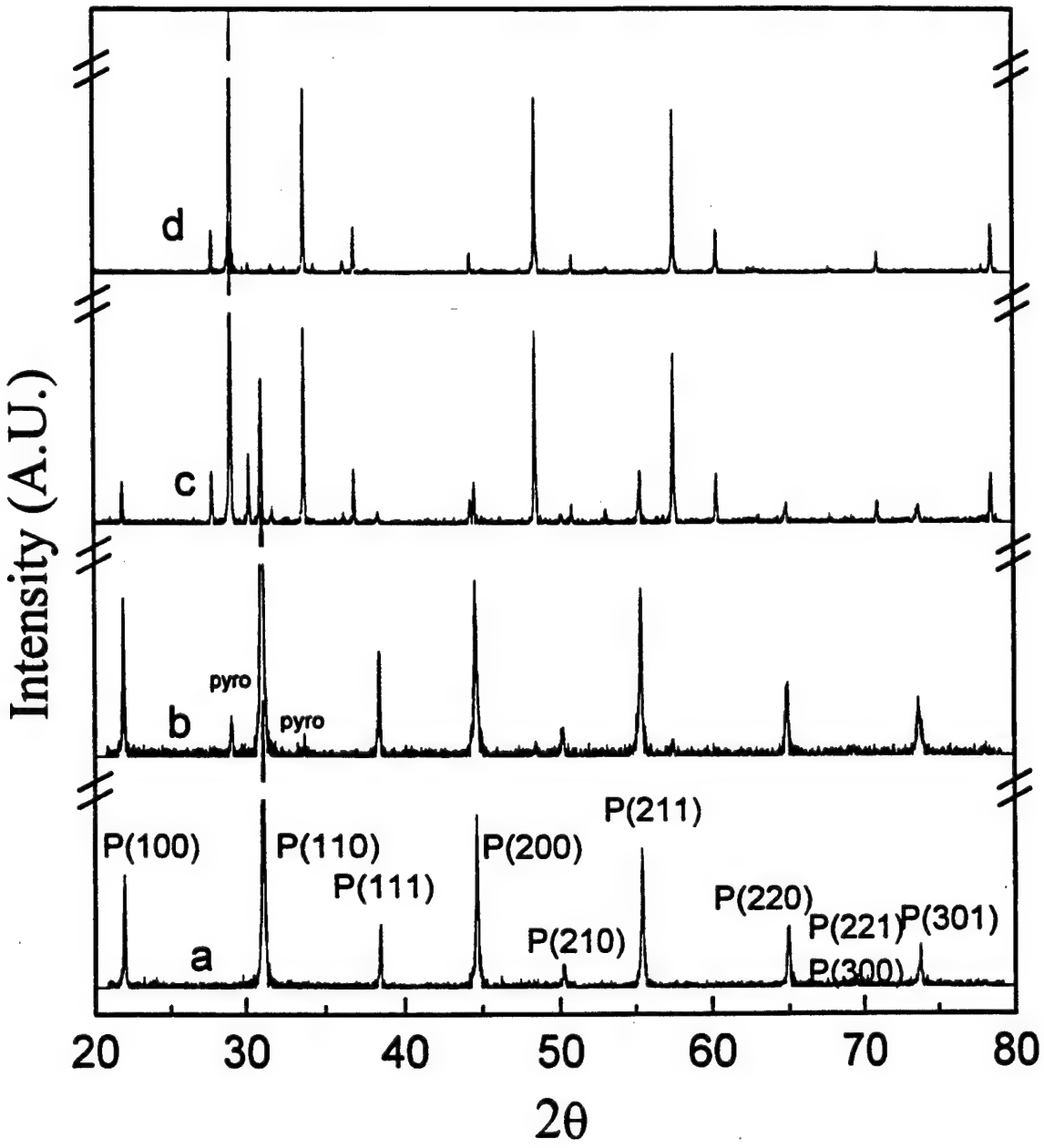

Fig. 3

Seung-Eek Park, Maureen Mulvihill, George Risch, and Thomas R. Shrout

Desired breadth undetermined, shrink so it fits and is clear to read

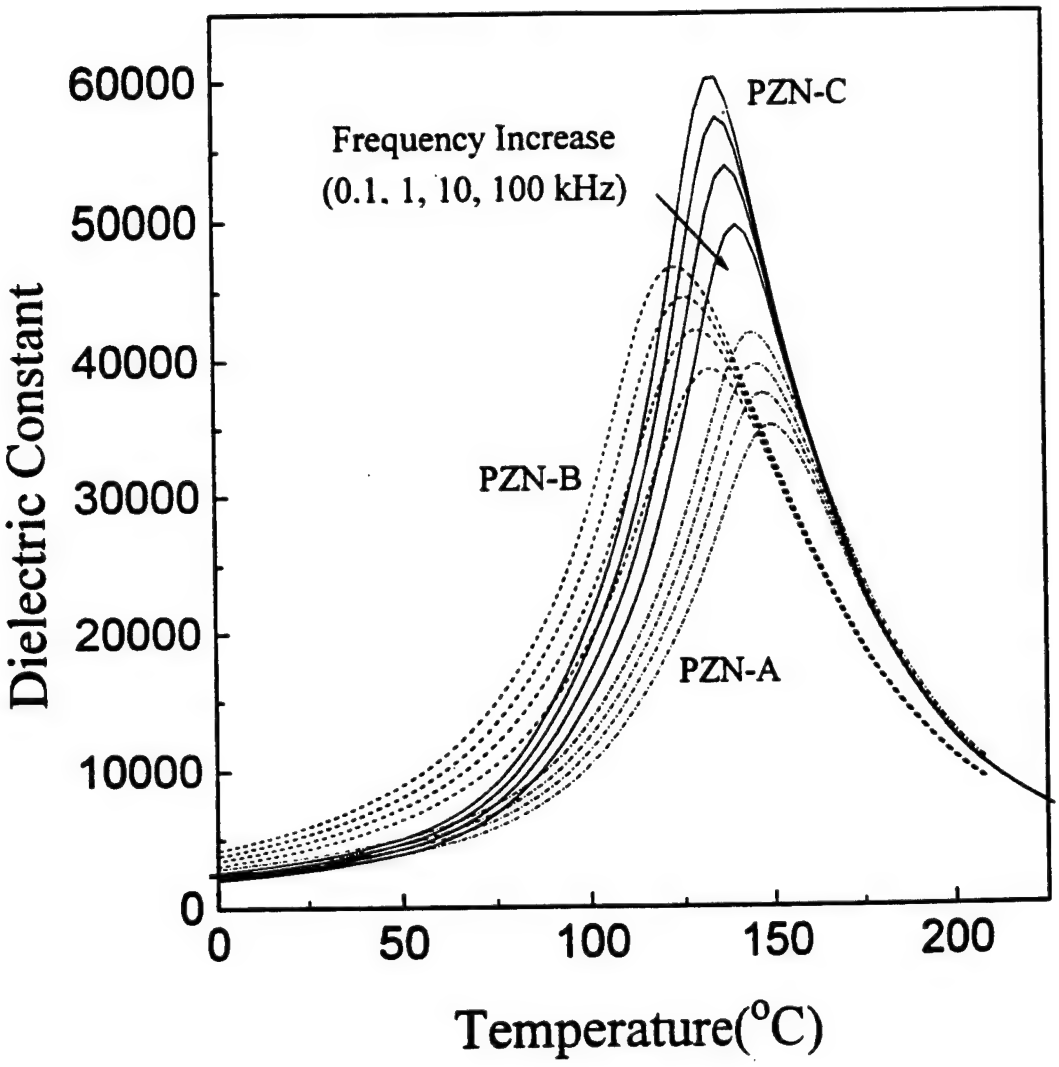

Fig. 4
Seung-Eek Park, Maureen Mulvihill, George Risch, and Thomas R. Shrout
Desired breadth undetermined, shrink so it fits and is clear to read

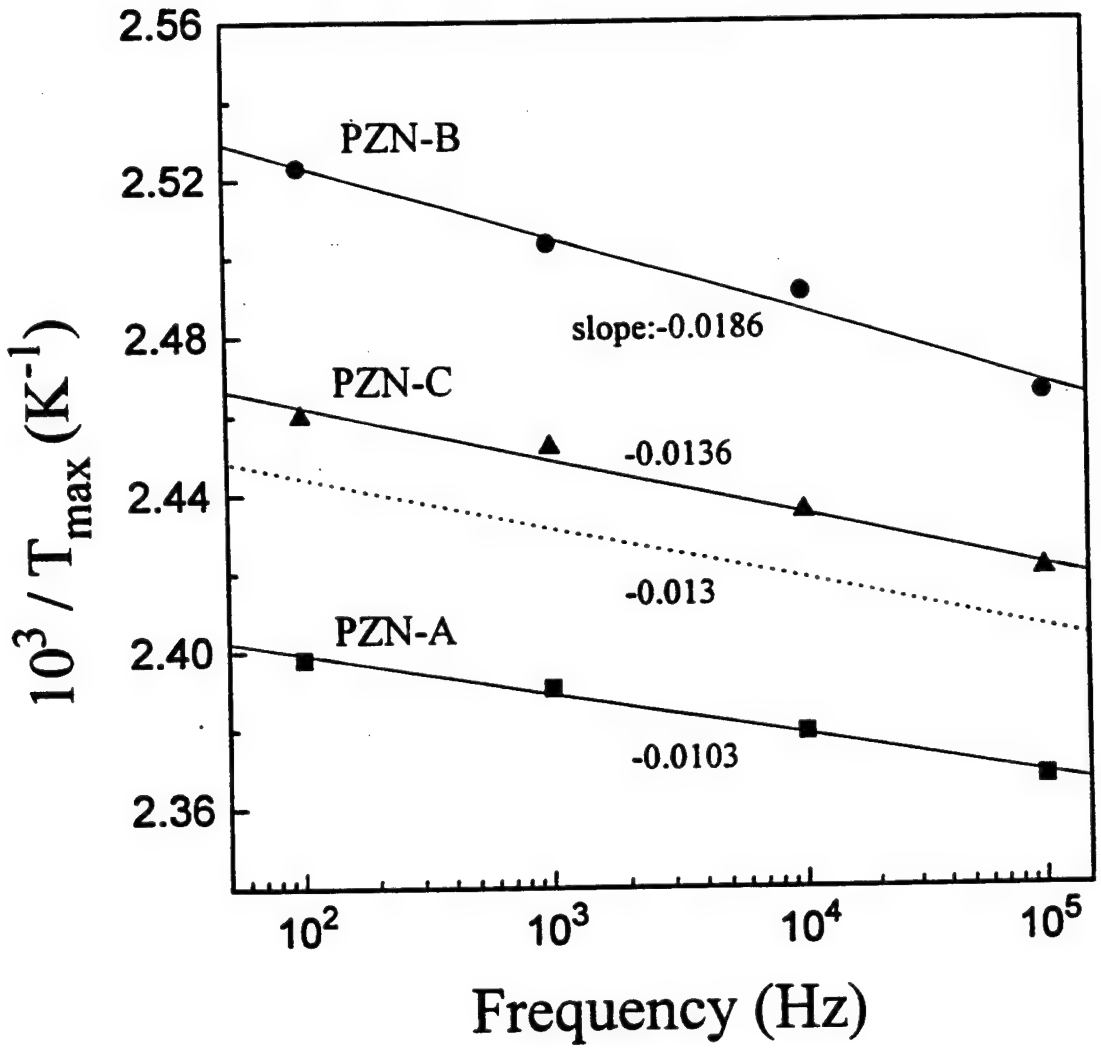

Fig. 5
Seung-Eek Park, Maureen Mulvihill, George Risch, and Thomas R. Shrout
Desired breadth undetermined, shrink so it fits and is clear to read

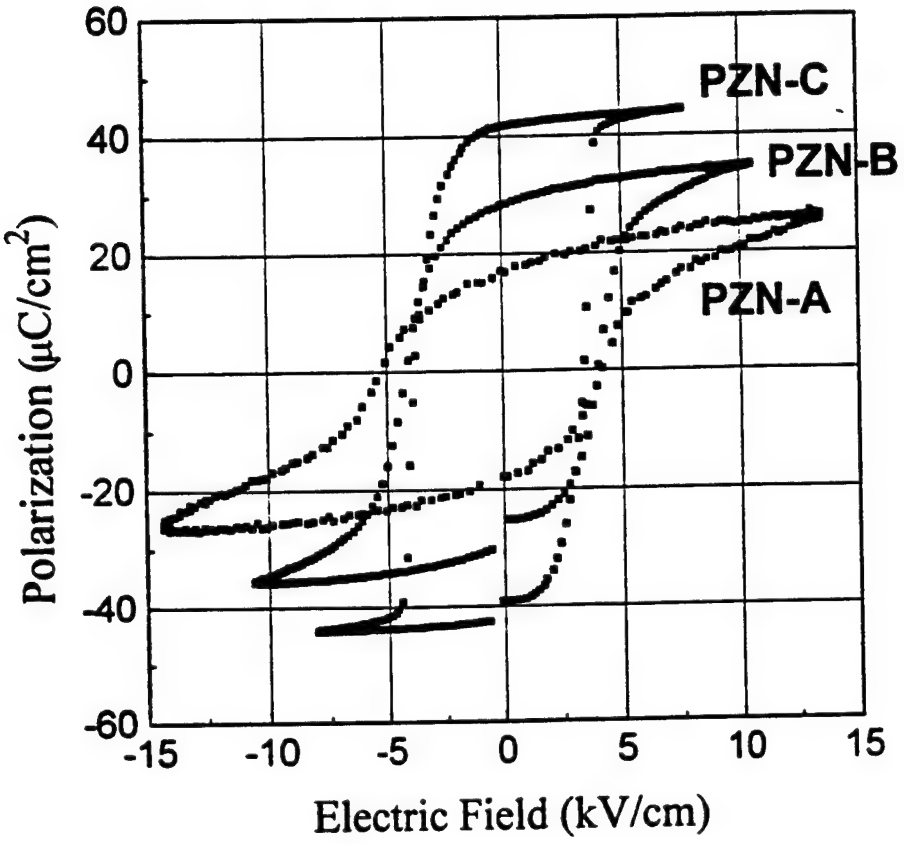

Fig. 6
Seung-Eek Park, Maureen Mulvihill, George Risch, and Thomas R. Shrout
Desired breadth undetermined, shrink so it fits and is clear to read

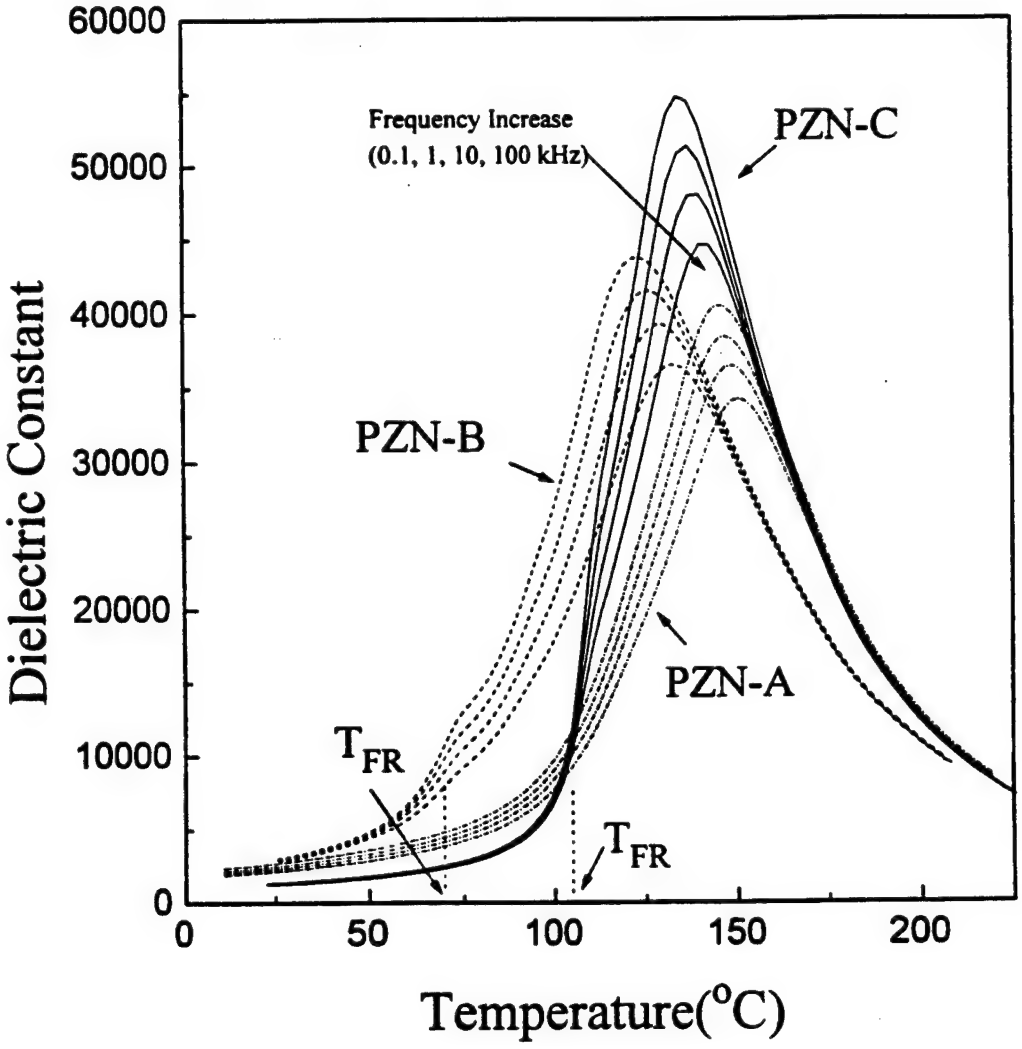

Fig. 7

Seung-Eek Park, Maureen Mulvihill, George Risch, and Thomas R. Shrout

Desired breadth undetermined, shrink so it fits and is clear to read

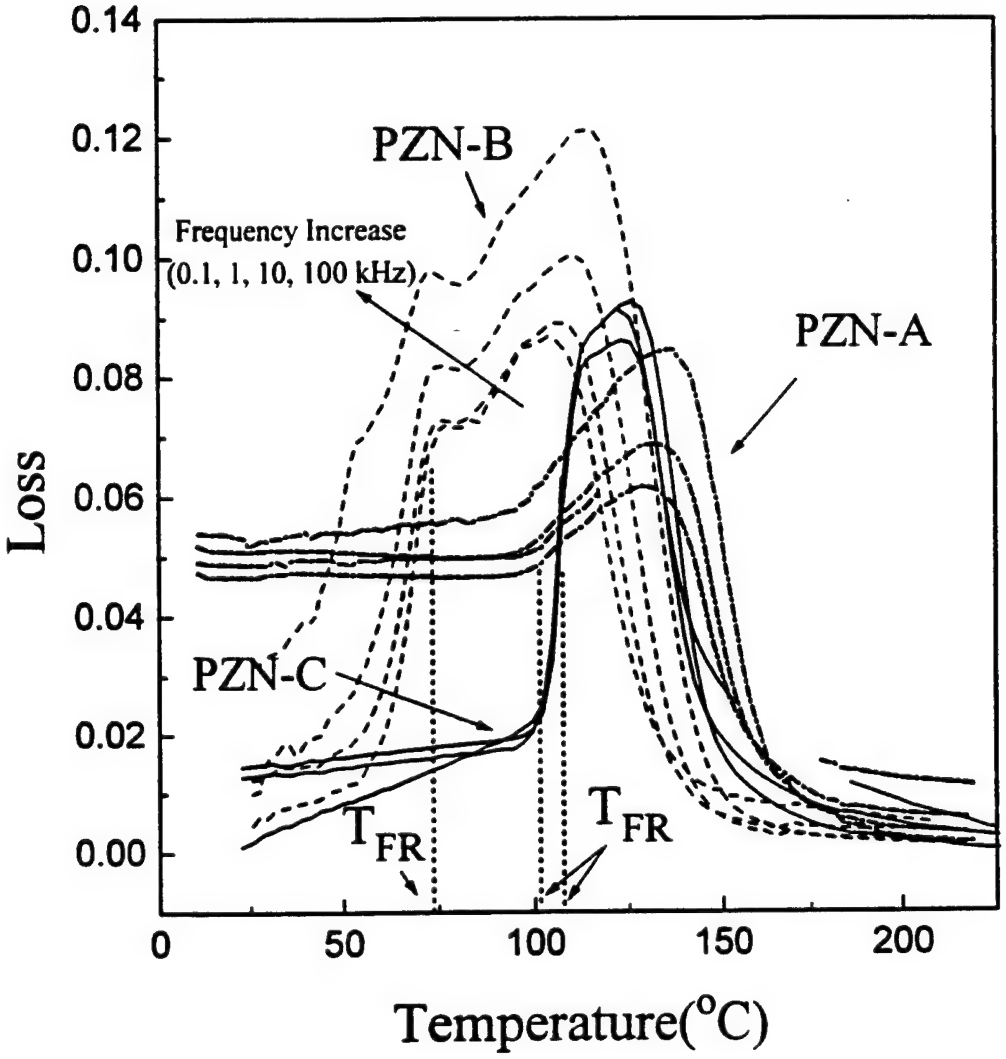

Fig. 8

Seung-Eek Park, Maureen Mulvihill, George Risch, and Thomas R. Shrout

Desired breadth undetermined, shrink so it fits and is clear to read

Table 1 Growth condition of flux grown PZN crystals.

Growth Run	*PZN-A*	*PZN-B*	*PZN-C*
Flux	PbO (Pb_3O_4)	PbO (Pb_3O_4)	PbO (Pb_3O_4)
Flux:Composition	7:3	7:3	6:4
Soaking Temperature (°C)	1150	1150	1200
Soaking Time (hr)	10	10	10
Cooling Rate (°C/hr)	5	1	1
Crystal Color	Colorless	Light Yellow	Brown
Maximum Crystal Size (cm)	0.5	0.5	1

Seung-Eek Park et al.
Desired breadth undetermined, shrink so it fits and is clear to read.

Table 2 Composition analysis of PZN crystals using ICP (wt%).

	PZN-A	*PZN-B*	*PZN-C*	*PZN**
Pb	59.5	59.9	59.9	61.1
Zn	5.5	5.8	5.7	6.4
Nb	20.2	19.3	20.7	18.3
Zn/Nb	0.27	0.30	0.28	0.35
Pt	n. d.**	n. d.	n. d.	

* expected for $Pb(Zn_{1/3}Nb_{2/3})O_3$

** not detected, detection limit 80 ppm.

Seung-Eek Park et al.

Desired breadth undetermined, shrink so it fits and is clear to read.

Table 3 Dielectric (1kHz) and E-field induced properties of PZN crystals at room temperature.

	K_{RT} (virgin)	loss (virgin)	K_{RT} (poled)	loss (poled)	T_{max} (℃)	K_{max}	Pr ($\mu C/cm^2$)	Ec (kV/cm)	d_{33} (pC/N)
PZN-A (colorless)	3490	0.054	2540	0.047	145	39700	18	4.6	10
PZN-B (light yellow)	5350	0.066	2980	0.013	126	44600	30	4.0	88
PZN-C (dark brown)	3140	0.052	1260	0.0185	135	57000	42	3.6	86

Seung-Eek Park et al.
Desired breadth undetermined, shrink so it fits and is clear to read.

APPENDIX 75

journal

J. Am. Ceram. Soc., 79 [9] 2417–21 (1996)

Chemical Preparation of Lead-Containing Niobate Powders

Yoshio Yoshikawa*

College of Engineering, Nihon University, Koriyama 963, Japan

Kenji Uchino*

International Center for Actuators and Transducers, Materials Research Laboratory, The Pennsylvania State University, University Park, Pennsylvania 16802

A chemical precipitation method was developed for synthesis of typical relaxor compounds—$Pb(Mg_{1/3}Nb_{2/3})O_3$ (PMN), $Pb(Fe_{1/2}Nb_{1/2})O_3$ (PFN), and $Pb(Sc_{1/2}Nb_{1/2})O_3$ (PSN)—from nitrate solutions. To obtain a niobium precursor compatible with the aqueous chemical routes, peroxo-niobium complex solutions were prepared by dissolving hydrated niobia precipitates in a dilute nitric acid solution with hydrogen peroxide. Powders that consisted of small particles ranging from 20 to 40 nm were successfully precipitated from the mixed nitrate solutions by hydrolysis with aqueous ammonia solutions. On calcination, these powders were highly reactive. For example, PMN precursor powder began to crystallize simultaneously to cubic pyrochlore and perovskite phases at ~400°C and yielded ~95% of the perovskite phase after calcination at 800°C for 1 h. PFN and PSN precursor powders calcined under similar conditions formed single perovskite phases.

I. Introduction

RECENTLY, lead magnesium niobate- ($Pb(Mg_{1/3}Nb_{2/3})O_3$, PMN) based ceramics prepared from mixed oxides by hot isostatic pressing[1] have been investigated for possible use in electrooptic applications. Lead scandium niobate titanate (PSNT) ceramics fabricated by advanced process technology have larger electromechanical coupling factors than that of lead zirconate titanate ($PbZr_{0.53}Ti_{0.47}O_3$), indicating that the former are suitable candidates for electromechanical bulk transducers.[2] The electrooptic and other dielectric properties—such as purity, stoichiometry, pyrochlore phase content, and grain size—of the final ceramics depend on variables related to several processes. The most-reported powder-processing method for relaxors is the calcination of mixed oxides, or the columbite method,[3] using solid-state techniques. Some problems that have occurred are the dispersability and reactivity of magnesium oxide powder, residual pyrochlore phase, and lead oxide volatilization at high temperature.

In general, chemical powder processing is an excellent technique for synthesizing high-purity multicomponent materials, because it offers good chemical homogeneity at the nanometer scale. The chemical synthesis for relaxor powders containing niobium, however, has been limited by the availability of inexpensive niobium precursors that are compatible with chemical routes. Powders prepared from alkoxides by sol–gel methods crystallize to 70% of the perovskite phase at 300°C,[4] and to 100% perovskite at 715°C[5] and 775°C.[6] Low calcination temperature is of industrial importance to fabricate high-quality and low-cost ceramics. However, the raw materials for sol–gel processing are rather expensive and normally handled under a specially controlled environment. Barium ethoxide precursor is used in the preparation of barium titanate and is an extremely moisture-sensitive material. Therefore, the relative merits and problems associated with synthesis using barium hydroxide, barium oxide, and barium metal are discussed.[7]

Lower-cost and simpler processes could be possible involving aqueous methods by the use of niobium hydrogen oxalate, a water-soluble material. In this study, peroxo-niobium complex solutions as a niobium precursor were prepared from niobium hydrogen oxalate. Several relaxor powders were prepared from mixed nitrate solutions by precipitation methods using these niobium precursors and other inorganic nitrates.

II. Experimental Procedure

(1) *Preparation of Niobium Precursor Solution*

The solubility of metal oxalates in water strongly depends on solution acidity. By acidifying with nitric acid, a clear aqueous precursor solution for PMN can be prepared from lead and magnesium nitrates and niobium oxalate ($Nb(HC_2O_4)_5 \cdot nH_2O$, Soekawa Chemical Co., Ltd., Japan). However, coprecipitation of the clear solution by hydrolysis with aqueous ammonia solutions is restricted by preferential precipitation of lead oxalate. Thus, oxalate-free niobium precursor solutions were prepared from aqueous niobium oxalate solutions by hydrolysis with aqueous ammonia solutions. The resulting hydrated niobia (25 g) was collected by a centrifuge (4000 rpm), removed, and dispersed in 500 mL of 0.1*M* aqueous ammonia solution to remove oxalic ions. Again, centrifugally collected compacts were rinsed with a small amount of water, removed, and ultrasonically dispersed in 900 mL of 0.1*M* nitric acid solution with hydrogen peroxide. The slurry was stirred by magnetic stirrer overnight until a clear solution was obtained. Niobium concentration in the precursor solutions was determined by quantitative chemical analysis.

The addition of hydrogen peroxide promoted the solubility of the hydrated niobia in 0.1*M* nitric acid solution and shortened the required time for dissolution. The appropriate amount of hydrogen peroxide to attain an acceptable hydrogen peroxide: niobium molar ratio was found to be 1.0 to 10.0. Clear, yellow-colored solutions were obtained, indicating that niobium hydroxide converted to peroxo-niobium complexes. The composition of the precipitates from the niobium precursor solutions by hydrolysis was characterized by powder X-ray diffractometry (XRD).

(2) *Preparation of Powders and Characterization*

Precursor solutions of 0.049*M* PFN ($Pb(Fe_{1/2}Nb_{1/2})O_3$) and 0.030*M* PSN ($Pb(Sc_{1/2}Nb_{1/2})O_3$) were prepared by mixing niobium precursor solutions with lead nitrate and the corresponding nitrates ($Mg(NO_3)_2 \cdot 6H_2O$ (99.0%), $Pb(NO_3)_2$ (99.5%), Koso Chemical Co., Ltd., Japan; $Sc(NO_3)_3 \cdot 4H_2O$ (99.9%),

P. P. Phule—contributing editor

Manuscript No. 192518. Received June 22, 1995; approved February 29, 1996.
*Member, American Ceramic Society.
*Author to whom correspondence should be addressed.

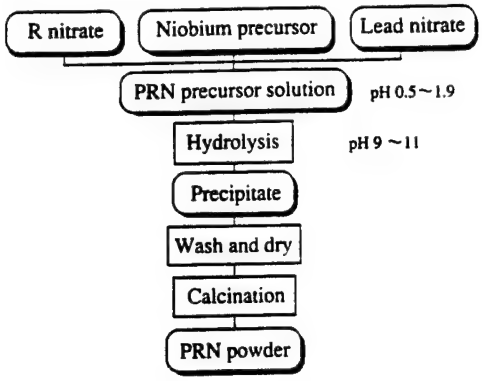

Fig. 1. Flow diagram of preparation of PRN (R = Mg, Fe, Sc) powders by precipitation method.

Soekawa Chemical Co., Ltd., Japan; $Fe(NO_3)_3 \cdot 9H_2O$, guaranteed reagent, Wako Pure Chemical Industries, Ltd., Japan) for the precipitation method shown in Fig. 1. The hydrogen peroxide content in the niobium precursor solution had a 2.5 molar ratio of hydrogen peroxide:niobium. Hydrolysis was performed by pouring 15*M* aqueous ammonia solution into 1000 mL of PFN and 500 mL of PSN precursor solutions. The final pH values of the PFN and PSN precursor solutions containing the precipitates were 10.2–11.0 and 9.1–10.4, respectively. Preliminarily 0.037*M* PMN precursor solution also was hydrolyzed by a similar method and magnesium was detected in the filtrates by precipitation of $Mg_2P_2O_7$ with $(NH_4)HPO_4$ solution. The magnesium hydroxide precipitate was partially redissolved in the ammonium nitrate solution. The composition of the precipitates was magnesium-poor. Therefore, PMN powders were prepared by another two-stage hydrolysis method, as shown in Fig. 2. 1000 mL of 0.037*M* lead nitrate precursor solution was hydrolyzed with 15*M* aqueous ammonia solution. The precipitate was filtered, washed with 400 mL of water and ultrasonically dispersed in 500 mL of water with magnesium nitrate. The slurry was again hydrolyzed with 15*M* aqueous ammonia solution. Finally, all precipitates were washed with 300 mL of water and then dried at 80°C for 12 h.

As-dried powders were characterized by scanning electron microscopy (SEM) (Model JSM-6300F, JEOL, Tokyo, Japan), X-ray diffractometry (XRD, Cu*K*α radiation) (Geigerflex SG-9, Rigaku, Japan), and thermogravimetric analysis and differential thermal analysis (TGA–DTA) (Thermoflex, TG-DTA 8112H, Rigaku, Japan). About 80 mg of as-dried powders were placed into a platinum holder and measured at a heating rate of 10°C/min in air with alumina powder as a reference. 100 mg of as-dried powder were dissolved in mixed hydrochloric and nitric acid solutions, and the cation ratios were analyzed by inductively coupled plasma atomic emission spectroscopy (ICP–AES) (SPS-1100, Seiko Electronic Co., Japan). For calcinating, an electric furnace was allowed to equilibrate at the desired calcinating temperature (400°–800°C). 1 g of as-dried powder was heated in the furnace for 1 h. The relative content of perovskite and pyrochlore phases for the calcined powders was determined from the relative intensities of the (110) perovskite peak and (222) pyrochlore peak.

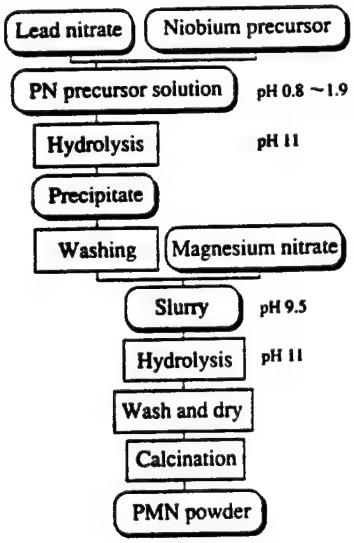

Fig. 2. Flow diagram of preparation of PMN powder by two-step hydrolysis method.

III. Results and Discussion

The niobium precursors prepared with hydrogen peroxide were clear, yellow solutions, with niobium existing as peroxo-complex ions. Peroxo-cation $Nb(OH)_4(H_2O_2)^+$, peroxo-anion $NbO_2(O\text{-}O_2)^-$, and peroxo-niobic acid ($HNbO_4 \cdot nH_2O$) were reported.[8] However, further investigation is needed to determine whether such peroxo-complex ions are present in our niobium precursor solutions. The niobium precursor solutions were prepared with a maximum niobium content of 3.2 g/L of Nb_2O_5, a hydrogen peroxide:niobium molar ratio of 3.0. When the hydrogen peroxide:niobium molar ratio exceeded 5, precipitates from the precursors by hydrolysis changed in composition and phase from a gel to a crystalline ammonium perorthoniobate ($(NH_4)_3NbO_8$). However, when the solution was mixed first with an aqueous solution of lead nitrate and then hydrolyzed, the crystalline ammonium perorthoniobate was not formed. The niobium precursor with a hydrogen peroxide:niobium molar ratio of 2.5 was used for the present powder processing.

XRD analysis revealed that the yellow precipitates obtained by the two methods from the PMN, PFN, and PSN precursor solutions were all amorphous. When lead nitrate was hydrolyzed separately, white, crystalline $Pb_3(NO_3)(OH)_5$ precipitated from the aqueous solution in the pH range of 9–11,[9] and white, crystalline $Pb(NO_3)OH$ (Ref. 10) and $Pb_7(NO_3)_4(OH)_{10}$ (Ref. 10) precipitated from nitric acid solutions in the pH range of 6–10. On addition of hydrogen peroxide to the solution prior to hydrolysis, a fine, reddish-yellow, amorphous precipitate ($3PbO \cdot 2PbO_2 \cdot 3H_2O$) was obtained as a result of oxidation of the crystalline lead hydroxides.[9] The hydrogen peroxide introduced from the niobium precursor oxidized the crystalline lead hydroxides that precipitated from the mixed nitrate solutions by hydrolysis.

This oxidation changed the lead hydroxide to higher lead oxide compounds. These higher lead oxides were smaller and less adhesive than those of lead hydroxide precipitates, because reducing hydroxo groups in the hydroxide precipitate. It is favorable for obtaining a homogeneous distribution of lead in mixed-hydroxide precipitates.

SEM observation showed that all as-dried powders consisted of agglomerates of small particles ranging in diameter from 20 to 40 nm (Fig. 3). ICP analyses of as-dried powders are shown in Table I. The results for cation ratios of as-dried powders were in agreement with the assumption that all components were precipitated completely by the precipitation methods.

Figure 4 illustrates the TGA and DTA curves of as-dried powders. The TGA curves of PMN, PFN, and PSN precursor powders show 11%, 9.1%, and 11% weight loss, respectively, below 400°–450°C because of the physical desorption of water trapped inside the powders and dehydration of hydrated precipitates with endothermic effects on DTA curves. The endothermic peak at 357°C for as-dried PMN precursor powder is due to dehydration of magnesium hydroxide. An XRD analysis was performed for as-dried PMN precursor powders heated in the TGA-DTA apparatus before and after the exothermic peak at 462°C. The XRD pattern of the powder before the peak shows only a broad peak around $2\theta = 29°$; both pyrochlore and

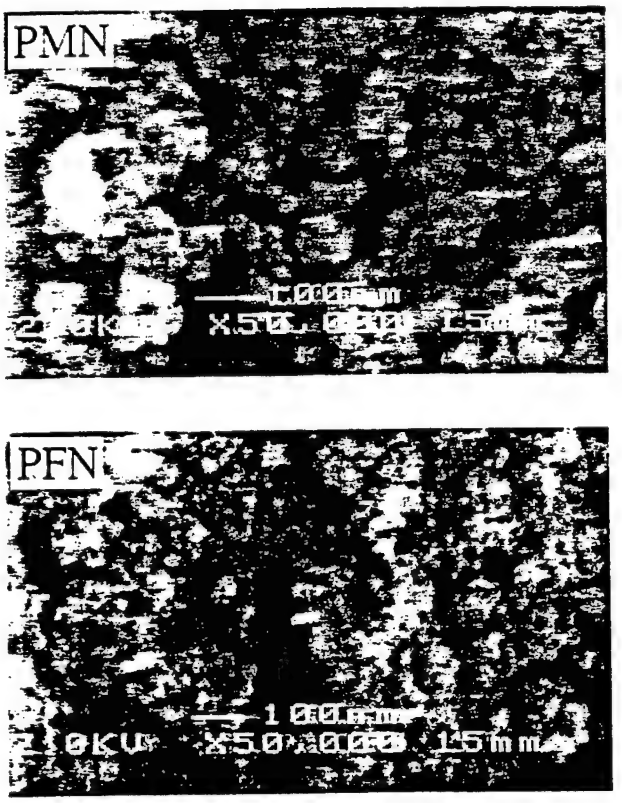

Fig. 3. SEM photographs of as-dried powders.

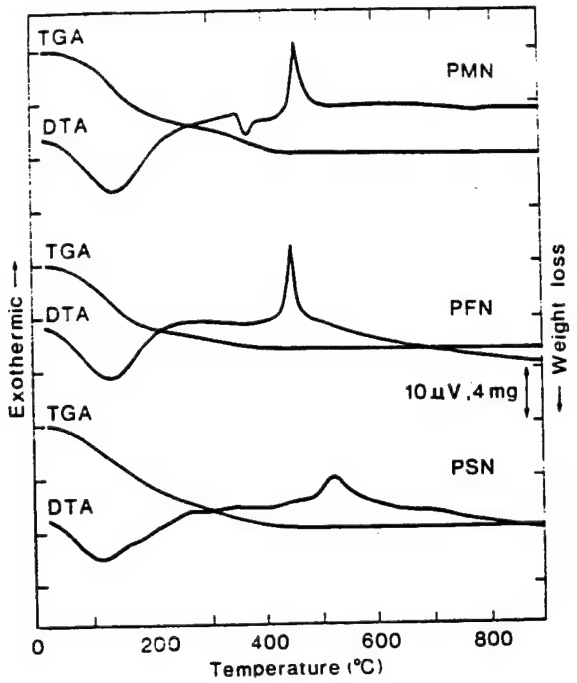

Fig. 4. TGA and DTA curves of as-dried PMN, PFN, and PSN precursor powders.

perovskite phases are detected in the XRD pattern of the powder quenched from temperature after the peak. The exotherm essentially represents crystallization, because of little weight change in the relevant temperature range. The PFN precursor powder also has a similar sharp exothermic peak for crystallization at 444°C. The main crystalline phase is perovskite. The PSN precursor powder has a broad exothermic peak at a higher temperature (520°C). The XRD analysis shows that the broad exotherm also is attributed to a similar crystallization.

XRD patterns of calcined PMN, PFN, and PSN precursor powders are shown in Figs. 5–7. For PMN precursor powder, both cubic pyrochlore and perovskite phases with broad peaks appeared simultaneously at 410°C. The broad peaks of each phase indicated that very-small-sized crystallites were formed in the fine powders. For conventional mixed-oxide powders, the formation of the perovskite phase followed the formation of pyrochlore compounds: initially, lead niobium compounds (e.g., $2PbO{\cdot}Nb_2O_5$–$3PbO{\cdot}Nb_2O_5$[11] and $3PbO{\cdot}Nb_2O_5$–$5PbO{\cdot}Nb_2O_5$[12]) were formed, and, then, from 700° to 800°C, intermediate products (e.g., $2(Pb_{1-x}Mg_{0.08})O{\cdot}Nb_2O_5$–$3(Pb_{0.92}Mg_{0.08})O{\cdot}Nb_2O_5$,[11] $5(Pb_{1-x}Mg_x)O{\cdot}2Nb_2O_5$ ($x \approx 0.02$),[12] $Pb_{1.81}Nb_{1-t}Mg_{0.25}O_{3.81}$,[13] and $Pb_2(Mg_{0.25}Nb_{0.75})O_{6.625}$[14]) were formed by the reaction of the lead niobium compounds with magnesium oxide. Such low crystallization temperatures as 462°C on DTA curves of as-dried powders and 410°C on XRD patterns of calcined powders suggest that the powders prepared chemically are highly reactive and compositionally homogeneous. Fukui *et al.*[3] reported the simultaneous formation of cubic pyrochlore and perovskite phases at a low temperature for powders prepared by the sol–gel method. Structures of precipitate nuclei occurred in aqueous or organic solutions should influence the direct formation of the perovskite phase from the precursor powders. At 700°C, the pyrochlore phase decreased and sharp perovskite peaks appeared. The ratio of the perovskite phase was 95.0% at 800°C.

The perovskite was easily formed at lower temperatures for both PFN and PSN precursor powders. They showed the formation of single perovskite phases at 800°C. The relative ease of formation of perovskites follows the sequence PFN > PSN > PMN. The thermodynamic nature and reaction kinetics should be considered in the formation of perovskite from powders.[15] The major reaction kinetic parameters—such as grain size, chemical homogeneity of components, and purity—are refined in these chemically prepared powders. Therefore, the sequence mentioned above reflects mainly the thermodynamic effects

Table I. Chemical Analysis of As-Dried Powders

PMN			PFN			PSN		
Element	Calculated	Measured	Element	Calculated	Measured	Element	Calculated	Measured
Lead	1.0	1.00 ± 0.01	Lead	1.0	1.00 ± 0.01	Lead	1.0	1.00 ± 0.01
Magnesium	0.33	0.33 ± 0.01	Iron	0.5	0.50 ± 0.01	Scandium	0.5	0.50 ± 0.01
Niobium	0.66	0.66 ± 0.01	Niobium	0.5	0.50 ± 0.01	Niobium	0.5	0.50 ± 0.01

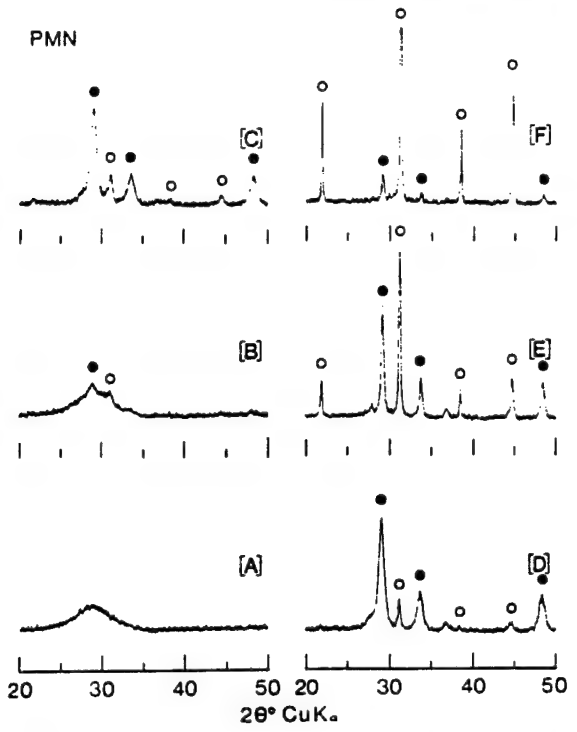

Fig. 5. XRD patterns of calcined PMN powder: (A) 400°, (B) 410°, (C) 500°, (D) 600°, (E) 700°, and (F) 800°C ((○) perovskite and (●) pyrochlore).

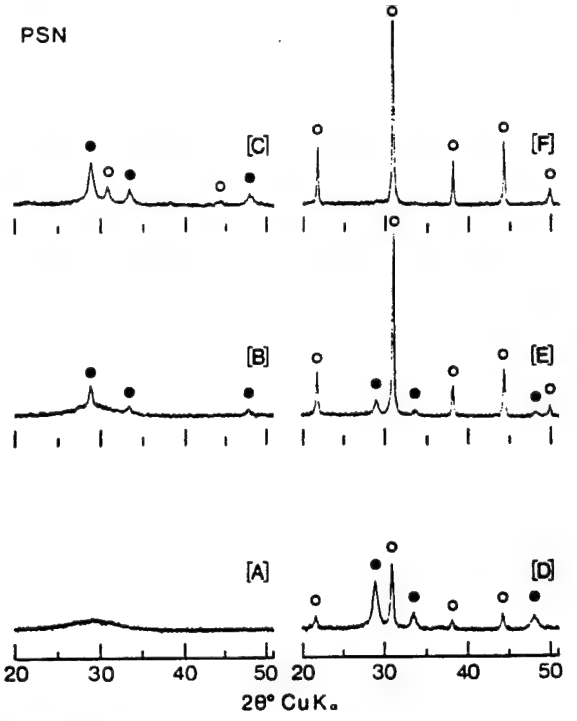

Fig. 7. XRD patterns of calcined PSN powder: (A) as-dried, (B) 400°, (C) 500°, (D) 600°, (E) 700°, and (F) 800°C ((○) perovskite and (●) pyrochlore).

on the formation of perovskite. From synthesis of perovskite $Pb(Zn_{1/3}Nb_{2/3})O_3$, it was concluded by Matsuo[16] that covalently bound Zn–O with fourfold coordination does not adapt to perovskite structure, where the B-site cation is sixfold coordinated. Thus, ionic bond M–O with sixfold coordination stabilizes the perovskite structure.[15,16] From electrostatic considerations,

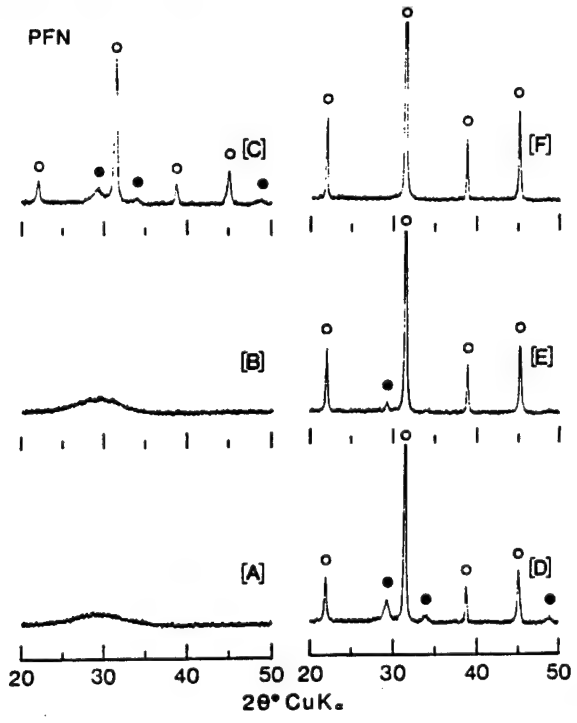

Fig. 6. XRD patterns of calcined PFN powder: (A) as-dried, (B) 400°, (C) 500°, (D) 600°, (E) 700°, and (F) 800°C ((○) perovskite and (●) pyrochlore).

trivalent ions Fe^{3+} and Sc^{3+} construct a more-ionic perovskite structure than does divalent Mg^{2+}. That the Fe^{3+} ion is smaller than the Sc^{3+} ion also is favorable for strengthening the electrostatic efforts. The perovskite constructed from the ionic components can be stabilized relative to the pyrochlore structure. However, some processing parameters should be considered in case of PMN. The magnesium:niobium ratio in PMN is smaller than that of PFN or PSN, so an inhomogeneous magnesium distribution in precipitates by the two-stage method can accelerate the formation of lead niobium compounds with pyrochlore structure.

IV. Conclusions

A chemical precipitation method was developed for synthesis of typical relaxor compounds, PMN, PFN, and PSN from nitrate solutions. The niobium precursor prepared was a clear, yellow solution with niobium existing as peroxo-complex ions. Clear PMN, PFN, and PSN precursor solutions were prepared by mixing the niobium pecursor solutions with lead nitrate and corresponding nitrates. For the PFN and PSN precursor solutions, all components were completely precipitated as hydroxides and/or hydrates by hydrolysis with aqueous ammonia solutions: for PMN precursor solutions the chemical compositions of the precipitate were magnesium-poor because magnesium hydroxide partially redissolved in the ammonium nitrate solutions. For PMN precursor solutions, a two-stage hydrolysis method was applied to avoid the problem with the redissolution of magnesium hydroxide.

On calcination, PMN precursor powders began to crystallize simultaneously to cubic pyrochlore and perovskite phases at ~400°C and yielded ~95% of perovskite phase after calcination at 800°C for 1 h. PFN and PSN powders calcined under similar conditions showed the formation of single perovskite phases.

Acknowledgments: We would like to thank the following people for their technical help in this study: N. Monma, T. Kaneko, Y. Goto, T. Takahashi, J. Tagami, and Y. Kuno.

References

[1]N. Kim, D. A. McHenry, S.-J. Jang, and T. R. Shrout, "Fabrication of Optically Transparent Lead Magnesium Niobate Polycrystalline Ceramics Using Hot Isostatic Pressing," *J. Am. Ceram. Soc.*, **73** [4] 923–28 (1990).

[2]Y. Yamashita, "Piezoelectric Properties of Niobium-Doped $(Pb(Sc_{1/2}Nb_{1/2})_{1-x}Ti_x)O_3$ Ceramics Material Near the Morphotropic Phase Boundary," *Jpn. J. Appl. Phys.*, **33**, Part 1, [8] 4652–56 (1994).

[3]S. L. Swartz and T. R. Shrout, "Fabrication of Perovskite Lead Magnesium Niobate," *Mater. Res. Bull.*, **17**, 1245–50 (1982).

[4]T. Fukui, C. Sakurai, and M. Okuyama, "Chemical Structure of a Complex Alkoxide as a Precursor of $Pb(Mg_{1/3}Nb_{2/3})O_3$," *J. Ceram. Soc. Jpn.*, **102** [4] 393–96 (1994).

[5]F. Chaput, J.-P. Boilot, M. Lejeune, R. Papiernik, and L. G. Hubert-Pfalzgraf, "Low-Temperature Route to Lead Magnesium Niobate," *J. Am. Ceram. Soc.*, **72** [8] 1335–57 (1989).

[6]P. Ravindranathan, S. Komarneni, and R. Roy, "Solid-State Epitaxial Effects in Structurally Diphasic Xerogel of $Pb(Mg_{1/3}Nb_{2/3})O_3$," *J. Am. Ceram. Soc.*, **73** [4] 1024–25 (1990).

[7]P. P. Phule, S. Raghavan, and S. H. Risbud, "Comparison of $Ba(OH)_2$, BaO, and Ba as Starting Materials for the Synthesis of Barium Titanate by the Alkoxide Method," *J. Am. Ceram. Soc.*, **70** [5] C-108–C-109 (1987).

[8]C. Alquier, M. T. Vandenborre, and M. Henry, "Synthesis of Niobium Pentoxide Gels," *J. Non-Cryst. Solids*, **79**, 383–95 (1986).

[9]Y. Yoshikawa and K. Tsuzuki, "Susceptibility of Agglomeration of Fine PLZT Powders Prepared from Nitrate Solutions," *J. Eur. Ceram. Soc.*, **6**, 227–35 (1990).

[10]W. Kwestroo, C. Langereis, and H. A. M. van Hal, "Basic Lead Nitrates," *J. Inorg. Nucl. Chem.*, **29** [1] 33–38 (1967).

[11]F. Imoto and H. Iida, "The Formation Processes of Lead Magnesio-Niobate $Pb(Mg_{1/3}Nb_{2/3})O_3$ in the Solid-State Reaction," *Yogyo-Kyokaishi*, **80** [5] 197–203 (1972).

[12]M. Dambekalne, I. Brante, and A. Sternberg, "The Formation Process of Complex Lead-Containing Niobates," *Ferroelectrics*, **90**, 1–14 (1989).

[13]T. R. Shrout and S. L. Swartz, "Dielectric Properties of Pyrochlore Lead Magnesium Niobate," *Mater. Res. Bull.*, **18**, 663–67 (1983).

[14]J. Chen and M. P. Harmer, "Microstructure and Dielectric Properties of Lead Magnesium Niobate–Pyrochlore Diphasic Mixtures," *J. Am. Ceram. Soc.*, **73** [1] 68–73 (1990).

[15]T. R. Shrout and A. Hallyal, "Preparation of Lead-Based Ferroelectric Relaxors for Capacitors," *Am. Ceram. Soc. Bull.*, **66** [4] 704–11 (1987).

[16]Y. Matsuo, "Synthesis of Perovskite-Type Complex Oxide Compound $Pb(Zn_{1/3}Nb_{2/3})O_3$," *Yogyo-Kyokaishi*, **78** [2] 46–58 (1970). □

APPENDIX 76

Ferroelectrics, 1996, Vol. 188, pp. 135–141
Reprints available directly from the publisher
Photocopying permitted by license only

PROCESSING OF $Pb(Zn_{1/3}Nb_{2/3})O_3$ CERAMICS AT HIGH PRESSURES

P. RAVINDRANATHAN, V. SRIKANTH, S. KOMARNENI† and A. S. BHALLA
Materials Research Laboratory, The Pennsylvania State University, University Park, PA 16802, USA

(Received September 6, 1995; in final form January 10, 1996)

Lead zinc niobate (PZN) with 1 mole% of $BaTiO_3$ (BT) and pure PZN, both of pyrochlore structure were synthesized by solid state and sol-gel routes respectively. The pyrochlore ceramics were subjected to high pressures (20–35 Kbars) to convert them to perovskite phases. About 80% of perovskite phase was formed from sol-gel derived PZN ceramics while only about 53% perovskite resulted from conventionally processed PZN with 1 mole% $BaTiO_3$ additive at 20 Kbar, 2 hr. A maximum dielectric constant value of 11200 was obtained at 1 kHz for the PZN ceramics processed with 20 Kbar pressure.

Keywords: Lead zinc niobate, high pressure synthesis, relaxor ferroelectric.

INTRODUCTION

Lead zirconium titanate (PZT) is the most important electromechanical transducer material because of its high piezoelectric coefficient. Through the optimization of composition and processing of this material there have been steady improvements in its properties. Extensive search to find better piezoelectric materials than PZT over the last four decades has not been fruitful, except for lead zinc niobate (PZN). PZN has been considered to be a better transducer material especially for under water applications.

Lead zinc niobate has the perovskite structure with Pb^{2+} coordinated to twelve oxygen ions and Zn^{2+} and Nb^{5+} ions in the six coordinated octahedral sites.[1] Zinc and niobium are randomly distributed over the octahedral positions, a type of disorder characteristic of the relaxor ferroelectrics. At room temperature PZN is rhombohedral with lattice parameters $a = 4.061$ Å and $\alpha = 89° 55'$. On heating it passes through a diffuse phase transition at 140°C to the ideal cubic perovskite structure. Below this temperature PZN is a ferroelectric while above this it is a paraelectric material.[2]

The preparation of PZN ceramics starting from the oxides using conventional procedure of calcining and sintering suffers from the disadvantage of the ease with which unwanted pyrochlore phases are formed at the expense of the desired perovskite phase. The stability of the perovskite phase has been investigated through structure field maps,[3] on the basis of crystal chemical parameters such as ionic radii and electronegativity differences which denote the extent of ionic bonding. On this basis it was pointed out that lead based relaxor ferroelectrics are generally less stable as perovskites when compared to simple ABO_3 compounds such as $BaTiO_3$, $KNbO_3$ etc. and that the order of the stability of the perovskite relaxors is approximately as

†Also with the Department of Agronomy.

follows: PZN < PCN < PIN < PSN < PNN < PMN < PFN < PFW < PZ < PT. In other words PZN is the most difficult relaxor ferroelectric to prepare with perovskite phase.

One approach which has been in practice to enhance the stability of the perovskite PZN is to form a solid solution of PZN with more stable perovskites such as $BaTiO_3$, $PbTiO_3$, $SrTiO_3$ etc.[4–6] Having tried all the possible ceramic processing routes Matsuo *et al.*[7] tried to use high pressure as one of the main processing parameters to synthesize PZN in perovskite form. They defined the pressure-temperature range as 25 Kbars and above and 800–1000°C to form the perovskite phase and the phase was quenched as metastable phase. Recently Fujiu *et al.*[8] reported conversion of pyrochlore PZN to perovskite phase using hot isostatic pressing at 200 MPa and 1150°C.

In the present investigation two different kinds of approaches were undertaken to synthesize the perovskite PZN in the ceramic form. In the first approach, a small amount of $BaTiO_3$ (1 mole%) was added to PZN as a stabilizer and the PZN-BT ceramic was processed with varying pressure and temperature. In the second approach pure PZN was prepared using a solution sol-gel method which has proved to be very advantageous in ceramic processing.[9,10] The PZN pyrochlore was then processed at a constant pressure and temperature for various holding periods. The objective of this paper was to find out the processing conditions to synthesize the perovskite phase and to measure the dielectric properties of these ceramics.

EXPERIMENTAL

Preparation of PZN-BT

Ceramic samples of PZN-BT were prepared using reagent grade chemicals by a two step mixed oxide technique. In the first stage a precursor columbite phase $ZnNb_2O_4$ was prepared by mixing ZnO and Nb_2O_5 in stoichiometric ratio and calcining at 1000°C for 4 hr. In the second stage the precursor was mixed in stoichiometric ratios with PbO, $BaCO_3$ and TiO_2 and ball milled for 14 hr in polyethylene bottles using zirconia balls as milling media and ethyl alcohol as wetting agent. Milled batch was dried in an oven at 80°C for 24 hr and then calcined at 900°C for 4 hr. Calcined powder was crushed, milled and 2 wt% polyvinyl alcohol binder was added prior to pressing into pellets of 1/4″ diameter and 1/4″ thick at 40000 psi. Pressed pellets were sintered at 1100°C for two hours after initial binder burn out at 600°C.

Preparation of PZN by Solution Sol-Gel Method (SSG)

Complexed alkoxide solution containing Pb, Zn and Nb was prepared using lead acetate, $Pb(CH_3COO)_2 \cdot 3H_2O$, diethyl zinc $(C_2H_5)_2Zn$, and niobium ethoxide $Nb(OC_2H_5)_5$. Lead acetate was dissolved in excess methoxyethanol at 70°C and refluxed at 125°C for a few hours. The water associated with lead acetate and the reaction product, methoxyethoxyacetate were distilled off by raising the temperature to 145°C. Stoichiometric amount of niobium ethoxide was added to the above solution and refluxed at 125°C for 6 hr. Diethyl zinc as 15 wt% solution in hexane was added to the above solution and heated first at 80°C for few hours and then the

temperature was raised to 125°C and kept for 24 hr to get a completely mixed and complexed alkoxide solution. The solution was hydrolysed with water in methoxyethanol and gelled at room temperature. The gel powder was heated at 350°C for 1 hr and then calcined at 750°C for 2 hr. The calcined powder was made into pellets and sintered at 1050°C for 4 hr.

High Pressure Processing

The above ceramics were subjected to high pressures using a piston cylinder apparatus. The specific high pressure cell used in our experiments (with slight modifications) was developed and described previously by Baker and Eggler.[11] The cylinder high pressure cells consisted of outer talc and pyrophyllite sleeves separated from the PZN specimens by an inner pyrex liner to inhibit reaction from fluids derived from dehydration at high temperature. Heating was achieved by a graphite furnace sleeve inserted directly inside the pyrex liner. The specimen was isolated from the heater assembly by boron nitride powder and crushable alumina spacer material. The temperature of the specimen was monitored by a platinum-rhodium thermocouple inserted through the steel base-plate into the alumina directly adjacent to the PZN pellet. Pressure and temperature were simultaneously increased linearly until the desired conditions were reached. This step was accomplished in five minutes. Pressure and temperature were maintained at a constant level for the period of time selected for the run (generally 30 to 240 minutes). Finally pressure was dropped at a constant temperature until contact with the furnace was broken, whereupon both pressure and temperature were dropped simultaneously.

Characterization

The above processed samples were analyzed by X-ray powder diffraction (XRD) using CuKα radiation. The relative amounts of the perovskite and pyrochlore phases were estimated from the major peak intensities using the following equation:

$$\% \text{ perovskite} = \frac{I(\text{perov}) \times 100}{I(\text{perov}) + I(\text{pyro})}$$

For measuring dielectric constant, samples were polished using diamond paste and two parallel surfaces were electroded with sputtered gold. Dielectric measurements were carried out on an automated system in which an oven (model 2300, Delts Design Inc.) and LCR meter (model 4274A, Hewlett Packard Inc.) and a digital multimeter were controlled by a desk top computer system (model 9816, Hewlett Packard Inc.). For piezoelectric measurements poling was done using an oil bath on selected samples by cooling from above the transition temperature to room temperature with an applied field of 1.5 kV/mm. The piezoelectric coefficient was measured on a Berlincourt meter (Model CPDT 3000, Channel Products, Inc.). To compare the grain size of the sol-gel derived and conventionally processed ceramics scanning electron micrographs of the fracture surfaces were obtained for both the samples using an ISI 60 scanning electron microscope.

RESULTS AND DISCUSSION

Powder X-ray diffraction of PZN-BT ceramics sintered at ambient pressure resulted in only pyrochlore phase. This is an expected result because sintering of constituent oxides at ambient pressure was well documented to form only pyrochlore phase.[3-5] After applying a pressure of 35 Kbars at 800°C the conversion of pyrochlore to perovskite phase occurred as revealed by XRD (Figure 1). The amount of perovskite formed was found to increase with increasing applied pressure at the same temperature (Figure 2).

The increased formation of perovskite phase with the applied pressure may be attributed to better kinetics at higher pressures, pressure being the catalyzing param-

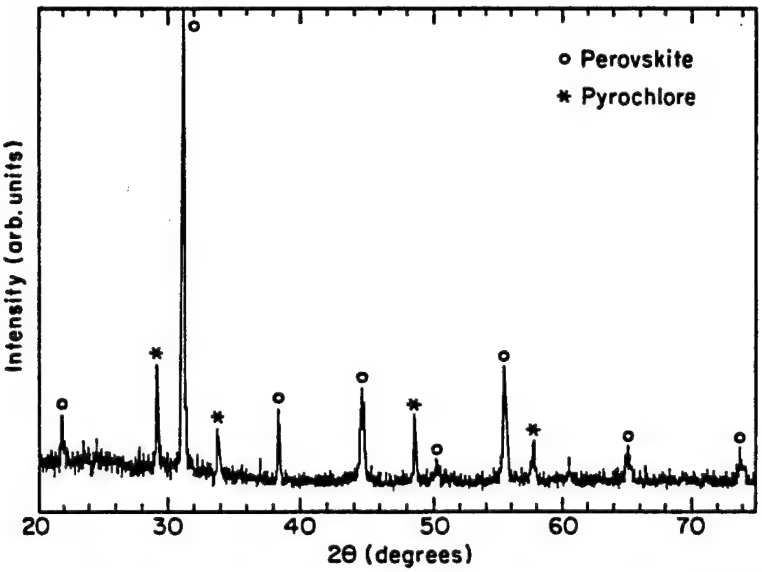

FIGURE 1 X-ray powder diffraction pattern of PZN-BT ceramics processed at 800°C, 35 Kbar.

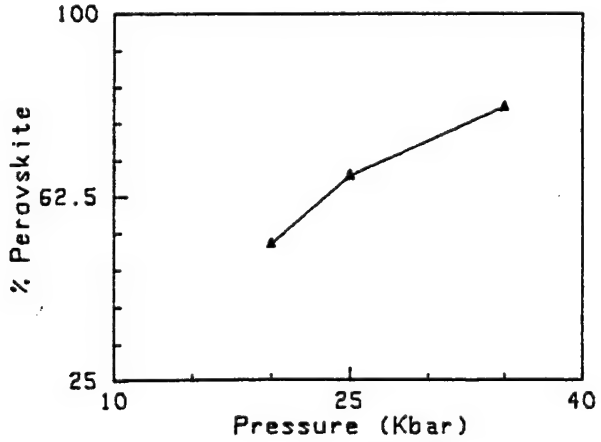

FIGURE 2 Variation of perovskite phase formation in PZN-BT ceramics at 800°C with processing pressures.

eter for the conversion. The amount of perovskite phase formed at 25 Kbar is about 60% while the amount of perovskite formed at 35 Kbar is around 80% (Figure 2).

X-ray patterns of PZN gel after sintering at 1050°C for 2 hr (Figure 3a) showed the formation of stable cubic pyrochlore as has been reported by earlier workers.[12] Because the sol-gel powders are chemically more homogeneous and much more reactive compared to the powders prepared by solid state method, the addition of $BaTiO_3$ to stabilize the perovskite was avoided. When the sol-gel powders were subjected to 20 Kbar pressure for different periods, different amounts of perovskite formed (Figure 3b and 4). The amount of perovskite formed first increased and then decreased with time (Figure 4). This result shows that there is a critical time to achieve maximum amount of perovskite beyond which the perovskite phase reverts

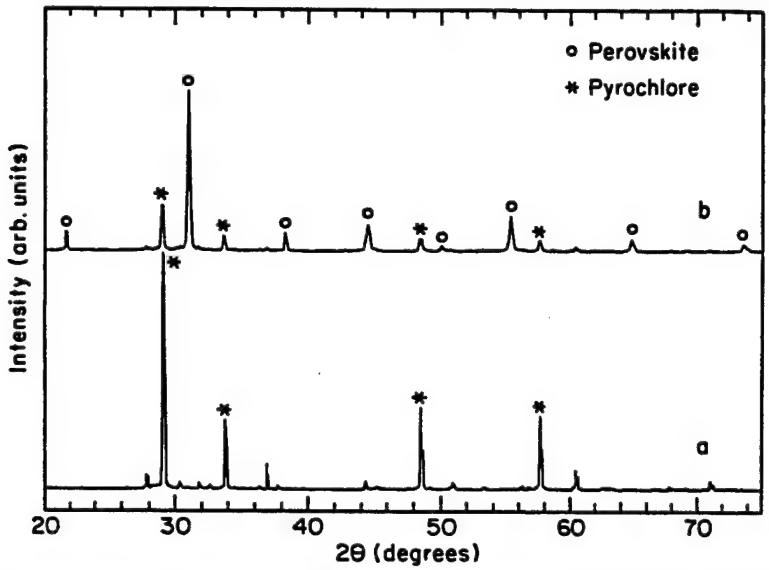

FIGURE 3 X-ray powder diffraction of (a) PZN ceramic sintered at 1050°C, 2 hr and (b) PZN ceramic processed at 20 Kbar, 2 hr.

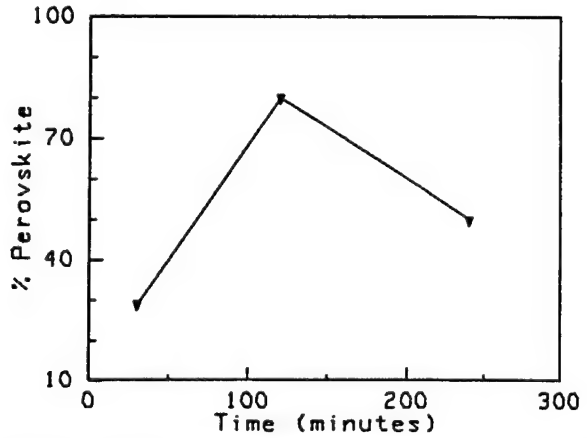

FIGURE 4 Variation of perovskite phase formation with processing time for PZN ceramics.

to pyrochlore. The reason for this transformation is not clear at present. Scanning electron micrographs of the fracture surface of the two different ceramics processed under identical conditions (20 Kbar, 2 hr) are shown in Figure 5. The grain size of sol-gel processed PZN sample is larger compared to the conventionally processed PZN ceramics because of higher reactivity in the former. The dielectric constants of the processed ceramics measured (Figure 6) here are much higher than those reported earlier.[7,8] The variation of dielectric constant with respect to temperature and frequency (Figure 6) clearly shows the relaxor nature of the material. The Curie temperature of ~170°C is a much larger value than that of the PZN single crystal (140°C) which may be because of the stresses that are built up during the processing at very high pressures. The piezoelectric constant (d_{33}) for the PZN sample prepared at 20 Kbar, 2 hr showed a value of 70×10^{-12} C/N. This value is low compared to those reported earlier and this decrease may have been caused by the presence of some pyrochlore phase in the ceramics.

FIGURE 5 Scanning electron micrographs of (a) PZN-BT ceramic and (b) PZN ceramic.

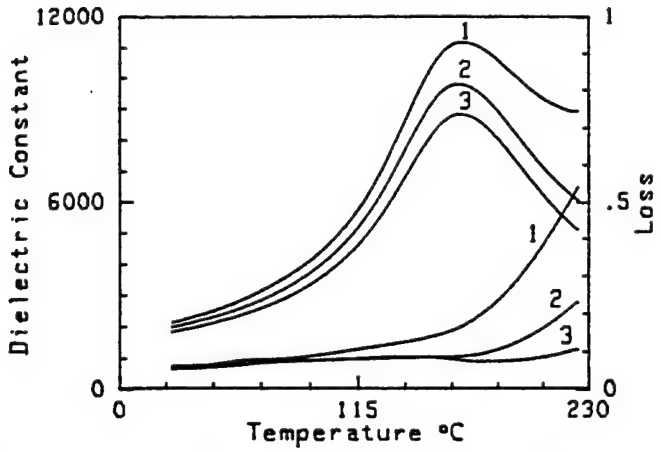

FIGURE 6 Dielectric constant and dielectric loss vs temperature for PZN ceramics processed at 20 Kbar, 2 hr: (1) 1 kHz; (2) 10 kHz; (3) 100 kHz.

CONCLUSIONS

1. Pyrochlore PZN can be converted to perovskite phase using high pressure processing (20 Kbar).

2. Perovskite conversion increases with an increase in processing pressure for PZN-BT ceramics.

3. Maximum conversion of pyrochlore to perovskite phase occurs at a critical time (2 hr) for a given pressure (20 Kbar) and temperature (800°C) conditions when sol-gel derived PZN pyrochlore is used.

4. Sol-gel derived PZN pyrochlore ceramic proved to be better than the conventionally prepared ceramic in terms of processing pressures and temperatures to convert it to the desired perovskite phase.

REFERENCES

1. V. A. Bokov and I. E. Myl'nikova, *Translation Soviet Physics Solid State*, **2**, 2428 (1961).
2. J. Kuwata, K. Uchino and S. Nomura, *Ferroelectrics*, **22**, 863 (1979).
3. T. R. Shrout and A. Halliyal, *Amer. Ceram. Soc.*, **66**, 704 (1987).
4. J. Belsick, A. Halliyal, U. Kumar, R. E. Newnham and L. E. Cross, *J. Amer. Ceram. Soc.*, **66**, 664 (1987).
5. A. Halliyal, U. Kumar, R. E. Newnham and L. E. Cross, *Amer. Ceram. Soc. Bull.*, **66**, 671 (1987).
6. A. Halliyal, U. Kumar, R. E. Newnham and L. E. Cross, *J. Amer. Ceram. Soc.*, **70**, 119 (1987).
7. Y. Matsuo, H. Sasaki, S. Hayakawa, F. Kanamaru and M. Koizumi, *J. Phys. Soc. Japan*, **28 suppl.**, 410 (1970).
8. T. Fujiu, A. Tanaka and T. Takenaka, *Jap. J. Appl. Phys.*, **30**, 1298 (1991).
9. R. Roy, *Science*, **238**, 1664 (1987).
10. K. S. Mazdiyasni, *J. Am. Ceram. Soc.*, **52**, 523 (1969).
11. D. C. Baker and D. H. Eggler, *J. Volcan. Geotherm. Res.*, **8**, 387 (1983).
12. M. Dambekalne, I. Brante and A. Sternberg, *Ferroelectrics*, **90**, 1 (1989).

APPENDIX 77

Ferroelectrics, 1996, Vol. 188, pp. 125–133
Reprints available directly from the publisher
Photocopying permitted by license only

LOW TEMPERATURE CHEMICAL ROUTES TO SMART MATERIALS

P. RAVINDRANATHAN, S. KOMARNENI,† A. S. BHALLA and R. ROY
Materials Research Laboratory, The Pennsylvania State University, University Park, PA 16802, USA

(Received October 10, 1995; in final form December 20, 1995)

The synthetic method used here to prepare smart materials utilizes simple solution chemistry to give a high degree of chemical control and reproducibility. Smart materials such as $Pb(Mg_{1/3}Nb_{2/3})O_3$ (PMN) and $0.9Pb(Mg_{1/3}Nb_{2/3})O_3$-$0.1PbTiO_3$ (PMN-PT) were prepared as bulk ceramics and thin films using sol-gel process. The importance of wet chemical method with respect to the properties of materials in device applications is highlighted.

Keywords: Smart materials, lead magnesium niobate, low temperature processing.

INTRODUCTION

Smart materials and systems are gaining importance recently because of their applications in all branches of science. Smart material systems consist of sensor, actuator and a control mechanism. A smart material senses a change in the environment and using a feed back system, makes a useful response. It is both a sensor and an actuator. Newnham and Ruschau[1] have reviewed many examples of passively smart and actively smart materials. The difference between a smart and a very smart material can be demonstrated with piezoelectric and electrostrictive ceramics. Lead zirconium titanate (PZT) is a smart material where as lead magnesium niobate-lead titanate (PMN-PT) can be considered as a very smart material because of its large non linear relationship between strain and electric field. The non linear relation between strain and electric field can be used to tune the piezoelectric coefficient. Other smart materials include lead zinc niobate, modified PT and phase transition ceramics such as $Pb(Zr,Ti,Sn)O_3$.

Newnham *et al.*[2] recently listed the various types of sensors and its functions. The reliability and reproducibility of these electronic ceramics depend upon the preparation technology. Several ways of accomplishing synthesis under mild conditions have been explored and of special importance are the energy saving routes involving low temperatures. Generally there are two methods ceramic and wet chemical which have been utilized to make ceramic powders. Wet chemical methods are of several types: co-precipitation, decomposition of metal salts, spray decomposition, freeze drying and hydrothermal and sol-gel processes. Among these, the last method namely, sol-gel process will be discussed here to make smart materials. This method involves simple solution chemistry but give a high degree of chemical homogeneity and reproducibility.

†Also with the Department of Agronomy.

Sol-Gel Process

The term "sol-gel" is used to describe chemical processes in which polymeric gels are formed from metallo-organic starting materials. The most commonly studied sol-gel systems are based on the chemistry of metal alkoxides $M(OR)_n$. There are two important key steps in the sol-gel process and can be summarized as follows:

Hydrolysis

$$\equiv M—OR + H_2O \rightarrow \equiv M—OH + R—OH$$

Condensation

$$\equiv M—OH + RO—M\equiv \rightarrow \equiv M—O—M\equiv + R—OH$$

$$\equiv M—OH + OH—M\equiv \rightarrow \equiv M—O—M\equiv + H_2O$$

where R— represents alkyl group. These reactions under controlled conditions will lead to gelation. There are many published papers on sol-gel processing of ceramics and glasses.[3,4] A recent book on sol-gel chemistry[5] gives a good account of the sol-gel process. Among the wet-chemical methods, sol-gel route has become increasingly important in the area of electroceramics because of its inherent advantages. The merits of sol-gel processing such as high purity, molecular homogeneity and lower processing temperature can be taken advantage in the electroceramics field to improve device performance. In addition to the above advantages, sol-gel method allows unique forming opportunities. Much of these driving force for the development of sol-gel thin film production has stemmed from the above mentioned advantages. The standard methods of film making such as sputtering or chemical vapor deposition (CVD) often lead to difficulties in controlling the stoichiometry of multicomponent oxide films because of differences in the sputtering rates of the constituents.

Uchino[6] has reported the importance of wet chemical methods, in particular sol-gel method, for the preparation of electroceramic powders used in electrostrictive actuators. Multilayer ceramics consist of layers of dielectrics with metal electrodes in between the layers. The volumetric efficiency (large capacitance/unit volume) in a capacitor can be achieved by decreasing the layer thickness and choosing high dielectric constant materials. Sol-gel method is expected to play an important role in miniaturization of electronic packages and also in smart material systems. Modified PT containing multi component metal ions has been used as a sensor in active vibration control and acoustic absorption systems.[8] The large thickness mode electromechanical coupling factor (K_t) and a small planar mode coupling constant (K_p) of modified PT make it a particularly promising material for ultrasonic transducers used in non destructive structural testing. Powder preparation methods, composition, homogeneity, particle size can profoundly influence the properties of the final product. In this case, uneven dopant distribution, small variations in the amount present or minute amount of other contaminants can alter the properties of ceramics. Therefore, a wet chemical method is needed to overcome these problems.

PZT and PMN-PT are used as both sensors and actuators in smart systems.[7] The critical processing issues include preparation of these materials with the desired phase and stoichiometry. One of the problems with PMN and related systems is the difficulty in producing a single phase material consisting of only perovskite.[8] Depending on the processing conditions, a second phase of pyrochlore structure may be present

which reduces the dielectric constant of the material. In addition, the processing temperature should be kept sufficiently low in order to prevent PbO loss during the preparation of lead based materials. We describe here the sol-gel processing of PMN, PMN-PT and modified PT ceramics and thin films which are used in smart material systems.

EXPERIMENTAL

PMN Fine Powder

Complex alkoxide solution was prepared by reacting lead acetate, $Pb(CH_3COO)_2 \cdot 3H_2O$, with magnesium ethoxide, $Mg(OC_2H_5)_2$, and niobium ethoxide, $Nb(OC_2H_5)_5$. The detailed experimental procedure to make the complexed alkoxide solutions was reported earlier.[9,10] The resulting solution was hydrolyzed with water in methoxyethanol and allowed to form bulk gel at room temperature. The gel was initially heated at 325°C for one hour and the resulting powder was calcined at different temperatures to study its crytallization. The powder obtained at 775°C, 2 hr showed the formation of pure perovskite phase.[9] The powders are very fine with a particle size of 200 to 500 nm size.

RESULTS AND DISCUSSION

Lowering Crystallization Temperature

A recent innovation of the sol-gel process is to make maximally heterogeneous materials.[11-13] It resulted in structurally diphasic materials with crystalline seeds in amorphous or semi crystalline gels of the same composition. These diphasic gels appear to be highly promising for densification and in radically lowering the processing temperature.[13] In order to lower the crystallization temperature of PMN gels, structurally diphasic gels with different seeds having perovskite structure were used. Fine crystalline perovskite oxides such as $SrTiO_3$ (ST), $BaTiO_3$ (BT), PMN and PT

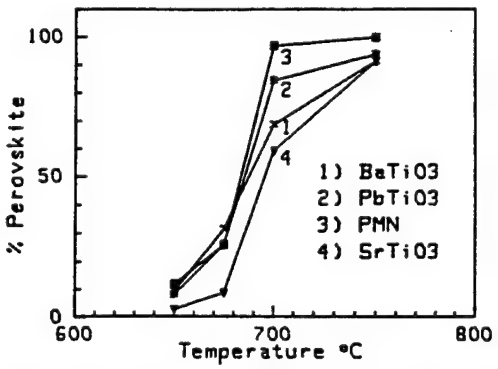

FIGURE 1 Percentage of perovskite phase vs temperature for the PMN gel with various seeds: (1) BT, (2) PT, (3) PMN, and (4) ST.

were used as seeds. The sizes of all the seeds are in the submicron range. The percentages of perovskite phase formed from the diphasic gels with various seeds heated at various temperatures were calculated from X-ray powder diffraction.[9]

The plot was given in Figure 1. The data indicates that PMN acts as a better seed in lowering the crystallization temperature compared to the other seeds. Seeding with as little as 1% PMN nuclei lowered the formation temperature of perovskite phase by about 75°C compared to the unseeded gel. With 5% seed, pure perovskite phase was obtained at a temperature as low as 675°C.[14] It is also clear from these results that a significant lowering of the crystallization temperature occurred upon seeding by solid-state epitaxial reaction. These results are in agreement with the concept of "nucleation and epitaxial growth" which is believed to govern the reactions occurring in isostructurally seeded gels.[15] By lowering the processing temperature, it is possible to make fine particles which in turn will help in lowering the sintering temperature.

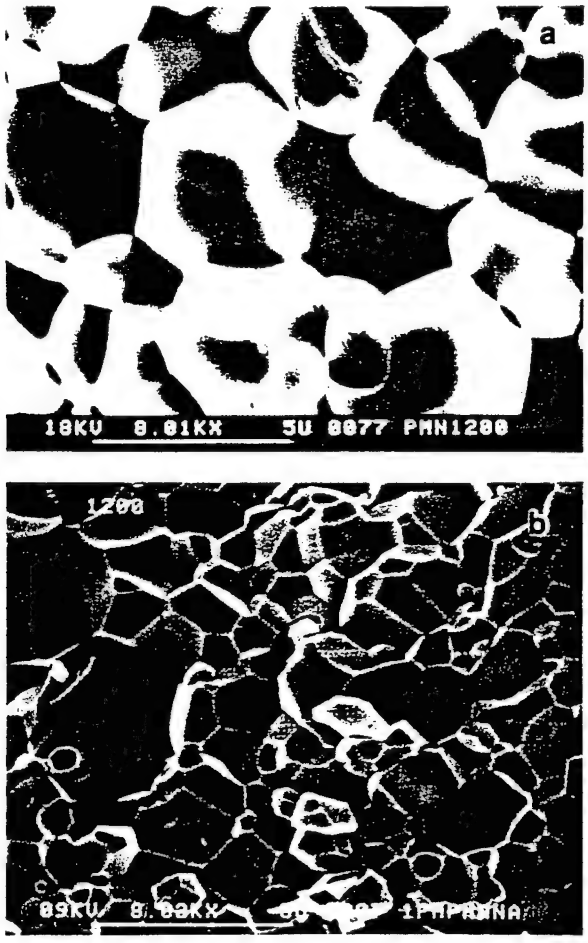

FIGURE 2 Scanning electron micrograph of the fracture surface of PMN ceramics sintered at 1200°C, 4 hr: (a) without seed and (b) with seed.

Grain Size

The dielectric properties are sensitive to microstructure and impurities either in the grain boundary or in the grain itself. In relaxor ferroelectrics, the bigger the grain size, the larger the dielectric maximum near the Curie temperature. Uchino[16] has shown the grain size effect of PLZT ceramics on strain when electric field is applied. It may be emphasized here that wet chemical methods can be utilized to control the grain size of the ceramics. Diphasic gel with seed was made similar to earlier reported procedure[15] and calcined at 750°C for 2 hr. The ceramics were made by pressing the powder into pellets and sintered at 1200°C for 4 hr with seed and without seed. Scanning electron micrograph of the fracture surface of the ceramics sintered at 1200°C for 4 hr is shown in Figure 2. There is a vast difference in the microstructure between the ceramics with seed and without seed. The grain size was found to be ~5 μm in the ceramics sintered without seed where as it is about 3–4 μm in the presence of seed. It is also possible to use hot uniaxial pressing technique to control the grain size which was reported earlier for relaxor ferroelectrics.[17]

The physical and dielectric properties of 0.9PMN-0.1PT ceramics at various sintering temperatures are presented in Table I. The dielectric constant maximum measured at 1 kHz increased as the sintering temperature increased. All of the samples exhibited frequency dispersion behavior of both dielectric constant and loss, which

TABLE I

Dependence of physical and dielectric properties of 0.9PMN-0.1PT ceramics at various sintering temperatures for 4 hr

Sintering Temp. (°C)	K (25°C) at 1 kHz	Tan δ (25°C) at 1 kHz	Grain size (μm)
900	3159	0.0062	1.0
1000	4278	0.0050	2.0-2.5
1100	8612	0.0070	3.0-3.5
1200	12144	0.0076	4.5-5.0
1250	17563	0.0077	4.5-5.5

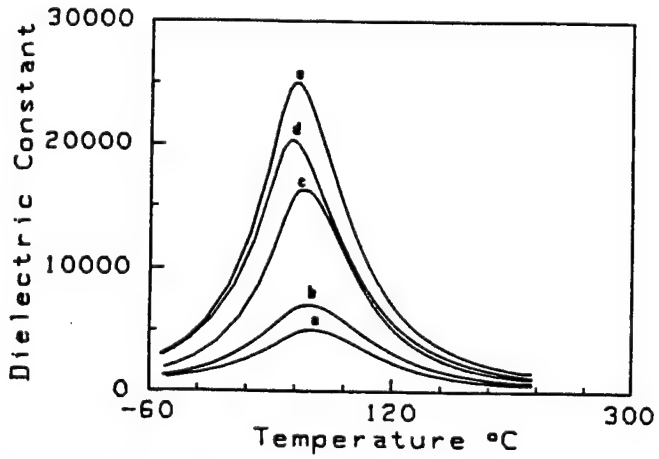

FIGURE 3 Dielectric constant vs temperature at 1 kHz for the 0.9PMN-0.1PT sintered at various temperatures: (a) 900°, (b) 1000°, (c) 1100°, (d) 1200°, and (e) 1250°C.

is a characteristic of relaxor ferroelectrics. The grain size for the ceramics increased with increase in sintering temperature as expected. A grain size variation of 1–5.5 μm was observed for the ceramics sintered from 900°C to 1250°C and this result is similar to that reported earlier for 0.93 PMN-0.07PT ceramics.[18] The sample sintered at 900°C showed a small grain size (1 μm). No abnormal grain growth was observed, probably because of the use of fine and uniform starting powders. The possible cause of the low dielectric constant (Figure 3) for the small grain size ceramics may be the existence of amorphous PbO phase along the grain boundaries and intergranular impurity phases.[18,19]

Oriented Thin Films

Much of the work on sol-gel processing of lead based ceramics has been directed at the perovskite ferroelectrics such as PT and PZT. A recent review by Swartz[20] explains the details about electronic ceramics. A limited amount of work has been done on PMN and PMN-PT thin films.[21,22] Research in the deposition of BT thin film for thin film capacitor application has been reported.[23] However, the most promising thin film material for this particular application may be PMN related materials. We have reported the solution sol-gel processing of PMN thin films recently.[22] A highly oriented film along (111) direction was obtained on silicon substrate. It was also reported that the orientation and crystallization rate were strongly influenced by the nature of the substrate and heating rates.

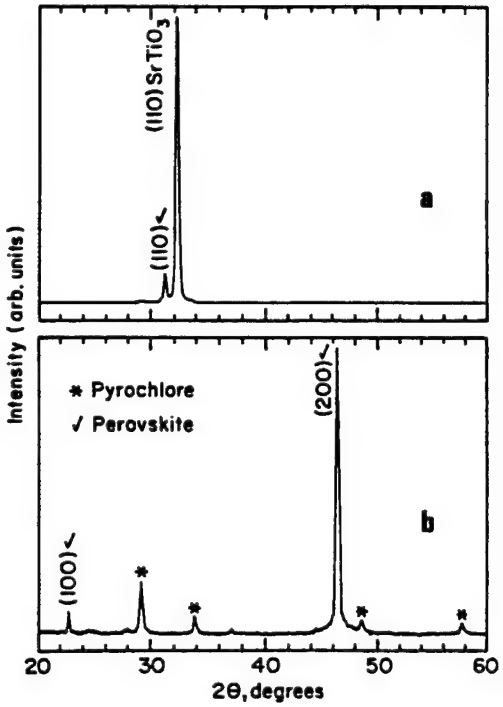

FIGURE 4 X-ray diffraction pattern of epitaxial oriented PMN thin film on $SrTiO_3$ substrate with (a) 110 and (b) 100 orientations.

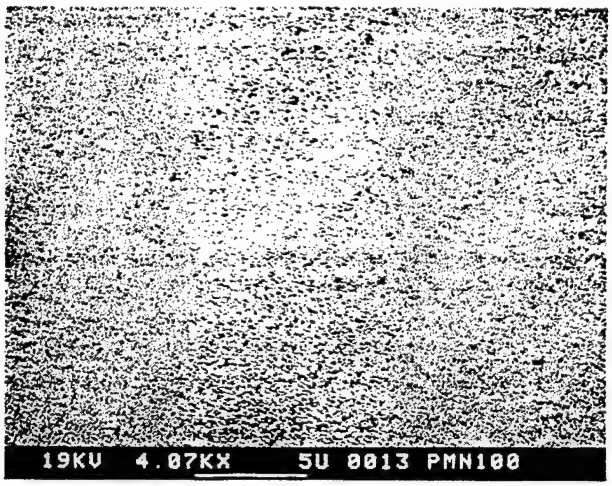

FIGURE 5 Scanning electron micrograph of PMN (100) thin film on $SrTiO_3$ substrate calcined at 750°C, 2 hr.

Recently, oriented films are gaining importance because of their performance in device applications.[20] *C*-axis oriented PT thin film was found to be better for the development of pyroelectric infrared detector and piezoelectric transducer components.[24] And also, if the ferroelectric thin films can be produced with significant crystallographic orientation, the pyroelectricity may be observed without poling.[25] PMN oriented film was made using the complexed alkoxide solution as reported earlier[22] on single crystal ST substrates. Similarly PT was also coated on different oriented (110 and 100) ST single crystal substrates. Depending upon the substrate orientation, the films were also oriented along the same direction. In many isostructurally seeded gels, the gel to ceramics conversions have been achieved at lower temperature due to epitaxial crystallization.[4] X-ray diffraction pattern of oriented PMN thin films along (110) and (100) direction are shown in Figure 4.

The microstructure of the PMN (100) oriented thin film is shown in Figure 5. A very uniform coating of few nanometers without any observable cracks and a very fine grain size was obtained. It is, however, possible to build thicker coating of a few microns using sol-gel method by modifying the process. Recently, PT films of few micrometers thickness were prepared with limited cracking by a modified sol-gel process which used acetyl acetone as chelating agent.[26] Modified PT has been used as sensors in smart systems[7] and this is a good candidate for preparation by sol-gel process. We are now in the process of preparing a modified PT of composition, $Pb_{1-x}Ca_xTi_{1-y}(Co_{0.5}W_{0.5})_yO_3 + 0.01MnO$ by the above modified sol-gel method and these results will be reported in due course.

CONCLUSION AND COMMENTS

Use of wet chemical method may be the key in advancement of electronic ceramics in various applications. The use of sol-gel method appears to be a promising route for the stabilization of the perovskite PMN phase. The formation of perovskite phase

occurs at ~700°C which is very low compared to any other technique. In the future, smart materials may be expected to be deposited as coatings by sol-gel process on silicon chips used in integrated circuits just as the PZT films are now being deposited on silicon chips for memory devices.

ACKNOWLEDGEMENTS

This research was supported by the Office of Naval Research and one of the authors (P.R.) would like to thank Drs. U. Kumar and S. Kumar for helpful discussions.

REFERENCES

1. R. E. Newnham and G. R. Ruschau, "Smart Electroceramics," *J. Am. Ceram. Soc.*, **74**, 463–80 (1991).
2. R. E. Newnham, Q. C. Xu, S. Kumar and L. E. Cross, "Smart Ceramics," *Ferroelectrics*, **102**, 259–66 (1990).
3. D. W. Johnson, Jr., "Sol-Gel Processing of Ceramics and Glass," *Am. Ceram. Soc. Bull.*, **64**, 1597–1602 (1985).
4. R. Roy, "Ceramics by the Solution-Sol-Gel Route," *Science*, **238**, 1664–69 (1987).
5. C. J. Brinker and G. W. Scherer, "Sol-Gel Science," Academic Press, New York, 1990.
6. K. Uchino, "Electrostrictive Actuators: Materials and Applications," *Am. Ceram. Soc. Bull.*, **62**, 647–52 (1986).
7. S. Kumar, "Smart Materials for Acoustic or Vibration Control," Ph.D. Thesis, Solid State Science, Pennsylvania State University, University Park, PA, 1991.
8. S. L. Swartz and T. R. Shrout, "Fabrication of Perovskite Lead Magnesium Niobate," *Mater. Res. Bull.*, **17**, 1245–50 (1982).
9. P. Ravindranathan, S. Komarneni, A. S. Bhalla, R. Roy and L. E. Cross, "Sol-Gel Processing of Lead Magnesium Niobate (PMN) Powder and its Characterization," in: "Ceramic Transactions," Vol. 1, pp. 182–89, Ceramic Powder Science, G. L. Messing, E. R. Fuller, Jr. and H. Hausner, (eds.), American Ceramic Society, Westerville, OH, 1988.
10. P. Ravindranathan, S. Komarneni, A. S. Bhalla and R. Roy, "Synthesis and Dielectric Properties of Solution Sol-Gel Derived $0.9Pb(Mg_{1/3}Nb_{2/3})O_3$-$0.1PbTiO_3$ Ceramics," *J. Am. Ceram. Soc.*, **74**, 2996–99 (1991).
11. D. Hoffman, R. Roy and S. Komarneni, "Diphasic Ceramic Composites via a Sol-Gel Method," *Mater. Lett.*, **2**, 245–47 (1984).
12. D. Hoffman, R. Roy and S. Komarneni, "Diphasic Xerogels. A New Class of Materials: Phases in the System Al_2O_3-SiO_2," *J. Am. Ceram. Soc.*, **67**, 468–71 (1984).
13. R. Roy, Y. Suwa and S. Komarneni, "Nucleation and Epitaxial Growth in Diphasic (Crystalline + Amorphous) Gels," in: "Ultrastructure Processing of Ceramics, Glasses and Composites," Vol. 2, pp. 247–58, L. L. Hench and D. R. Ulrich, (eds.), Wiley, New York, 1986.
14. P. Ravindranathan, S. Komarneni and R. Roy, "Solid-State Epitaxial Effects in Structurally Diphasic Xerogel of $Pb(Mg_{1/3}Nb_{2/3})O_3$," *J. Am. Ceram. Soc.*, **73**, 1024–25 (1990).
15. G. Vilmin, S. Komarneni and R. Roy, "Crystallization of $ThSiO_4$ from Structurally and/or Compositionally Diphasic Gels," *J. Mater. Res.*, **2**, 489–93 (1987).
16. K. Uchino, "Recent Topics in Ceramic Actuators to Improve Reliability and Durability," in: "IEEE 7th International Symposium on Applications of Ferroelectrics," pp. 153–58, S. B. Krupanidhi and S. K. Kurtz, (eds.), IEEE, New Jersey, 1990.
17. P. Papet, J. P. Dougherty and T. R. Shrout, "Particle and Grain Size Effects on the Dielectric Behavior of the Relaxor Ferroelectric $Pb(Mg_{1/3}Nb_{2/3})O_3$," *J. Mater. Res.*, **5**, 2902–09 (1990).
18. T. R. Shrout, U. Kumar, M. Megheri, N. Yang and S. J. Jang, "Grain Size Dependence of Dielectric and Electrostriction of $Pb(Mg_{1/3}Nb_{2/3})O_3$-Based Ceramics," *Ferroelectrics*, **76**, 479–87 (1987).
19. J. Chen, A. Gorten, H. M. Chen and M. P. Harmer, "Effect of Powder Purity and Second Phases on the Dielectric Properties of Lead Magnesium Niobate Ceramics," *J. Am. Ceram. Soc.*, **69**, C-303–C-305 (1986).
20. S. L. Swartz, "Topics in Electronic Ceramics," *IEEE Trans. on Electrical Insulation*, **25**, 935–87 (1990).
21. K. Okuwada, M. Imai and K. Kakuno, "Preparation of $Pb(Mg_{1/3}Nb_{2/3})O_3$ Thin Film by Sol-Gel Method," *Jpn. J. of Appl. Phys.*, **28**, L1271–L1273 (1989).

22. P. Ravindranathan, S. Komarneni, A. S. Bhalla, L. E. Cross and R. Roy, "Solution Sol-Gel Processing of Lead Magnesium Niobate Thin Films," *Ferroelectrics*, **12**, 29–34 (1990).
23. I. H. Pratt and S. Firestone, "Fabrication of rf Sputtered Barium Titanate Thin Films," *J. Vac. Sci. Tech.*, **8**, 256–60 (1971).
24. K. Kushida and H. Takeuchi, "Ferroelectric Properties of *C*-axis Oriented $PbTiO_3$ Thin Films," *Ferroelectrics*, **108**, 3–8 (1990).
25. K. Iijima, Y. Tomita, R. Takayama and I. Ueda, "Preparation of *C*-axis Oriented $PbTiO_3$ Thin Films and their Crystallographic, Dielectric and Pyroelectric Properties," *J. Appl. Phys.*, **60**, 361–67 (1986).
26. S. J. Milne and S. H. Pyke, "Modified Sol-Gel Process for the Production of Lead Titanate Films," *J. Am. Ceram. Soc.*, **74**, 1407–10 (1991).

APPENDIX 78

Ferroelectrics, 1996, Vol. 188, pp. 95–107
Reprints available directly from the publisher
Photocopying permitted by license only

A PROCESSING AND ELECTRICAL PROPERTY INVESTIGATION OF THE SOLID SOLUTION: $(x)\ Pb(In_{1/2}Nb_{1/2})O_3 - (1-x)\ Pb(Sc_{1/2}Ta_{1/2})O_3$

EDWARD F. ALBERTA and AMAR S. BHALLA
Materials Research Laboratory, The Pennsylvania State University, University Park, Pennsylvania 16802, USA

(Received September 5, 1995; in final form November 20, 1995)

Ceramics in the solid solution system $(x)\ Pb(In_{1/2}Nb_{1/2})O_3 - (1-x)\ Pb(Sc_{1/2}Ta_{1/2})O_3$ [PIN:PST(x)] with compositions ranging from $x = 0.0$ to $x = 1.0$ have been fabricated. This paper presents the processing methods for producing 100% perovskite PIN and PST ceramics, as well as those for the PIN/PST solid solution. Various electrical properties including the dielectric constant and hysteresis, the pyroelectric and piezoelectric response, are measured on these compositions.

Keywords: Relaxor ferroelectrics, lead indium niobate-scandium tantalate, synthesis & properties.

INTRODUCTION

Earlier studies have shown that both $Pb(In_{1/2}Nb_{1/2})O_3$ [PIN] and $Pb(Sc_{1/2}Ta_{1/2})O_3$ [PST] are relaxor ferroics in which the degree of B-site cation ordering can be thermally controlled. Disordered PIN has been found to have a pseudo cubic perovskite structure, specifically, a rhombohedrally distorted space group of R3m or R3. After thermal annealing, PIN has been shown to order into an antiferroelectric orthorhombic phase, isostructural with $PbZrO_3$. Disordered PST has also been found to have a pseudo cubic structure. However, after ordering, the unit cell doubles into a ferroelectric phase. It is because of this difference in ordering behavior that the PIN:PST system looks to be of both theoretical and practical interest.

EXPERIMENTAL

1. Processing

i. *Lead indium niobate ceramics.* The processing of PIN powders evolved in this paper through a number of experimental steps. The first synthesis approach was through the common mixed oxide method. The starting materials for this procedure were reagent grade PbO, Nb_2O_5, and In_2O_3. Stoichiometric amounts of the raw materials were mixed with alcohol and ball-milled in Nalgene containers. Milling times were typically longer than 12 hours, followed by drying the powders at 100°C for 18 to 24 hours. After drying, the powder was reground with a mortar and pestle to 100 mesh. The PIN powder was then calcined on a platinum foil within a closed alumina crucible. The desired reaction for the mixed oxide method is as follows:

$$4 \cdot PbO + In_2O_3 + Nb_2O_5 \rightarrow [\text{perovskite}]4 \cdot Pb(InNb)_{1/2}O_3$$

As with many other perovskite materials, a parasitic pyrochlore phase was concurrently produced. It was therefore important to determine the relative proportions of the two phases. This was accomplished using x-ray diffraction [XRD] and the method described by Swartz and Shrout (1982). From diffraction patterns the intensity of the 100% peaks of the two phases (110 and 022, respectively) were determined and the amount of perovskite present calculated by:

$$\% \text{ Perovskite} = \left(\frac{I_{110}}{I_{110} + I_{022}}\right) \times 100$$

After calcining the powders with various soak times and temperatures, it quickly became apparent that lead and/or indium volatility was a serious problem. Atmospheric control was achieved by placing boats of PbO and In_2O_3 alongside the platinum foil. Eventually, the high temperature curing cement was used for better control of the atmosphere. In no case was phase pure PIN produced for reaction times up to 10 hours. An optimum soak condition of 4 hours at 1050°C was found to result in the production of only 80% perovskite phase. Further, any increase in either time or temperature resulted in an increase of pyrochlore concentration.

Further processing steps based on a precursor method for producing an intermediate "building block" phase for the synthesis of phase pure perovskite relaxor materials was used (Swartz and Shrout, 1982). For this wolframite precursor method, $InNbO_4$ was the choice for the intermediate phase. $InNbO_4$ was synthesized using the stoichiometric mixing and milling and drying of In_2O_3 and Nb_2O_5. Von Liebertz (1972) cited a reaction temperature of 1100°C, so a sealed crucible with an indium source was employed. It was found (see Figure 1) that production of $InNbO_4$ was reasonably (~90%) complete after 4 hours at 1200°C. Using these conditions $InNbO_4$

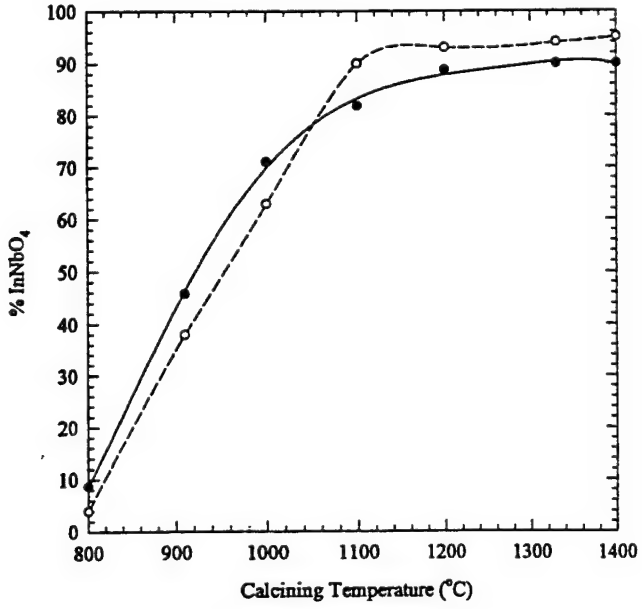

FIGURE 1 Formation of $InNbO_4$ with a soak time of 4 hours. ● → stoichiometric, ○ → 2 wt% excess In_2O_3.

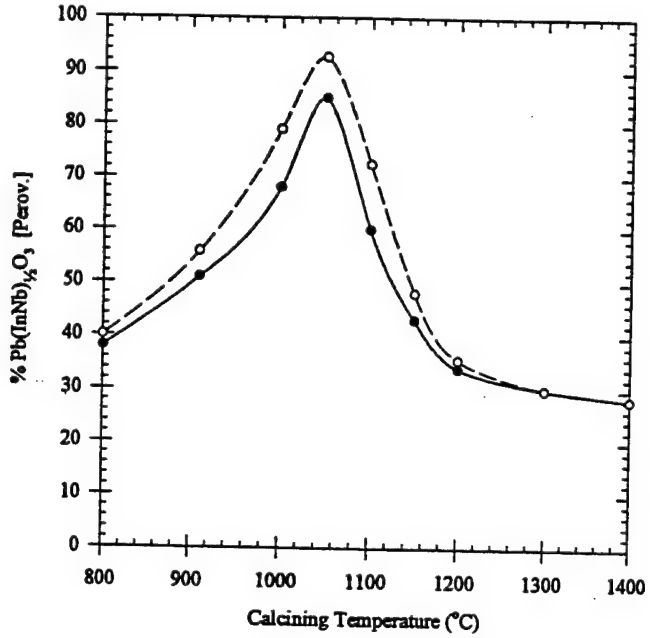

FIGURE 2 Formation of $Pb(In_{1/2}Nb_{1/2})O_3$ with a soak time of 4 hours. ● → stoichiometric, ○ → 3 wt% excess Li_2CO_3.

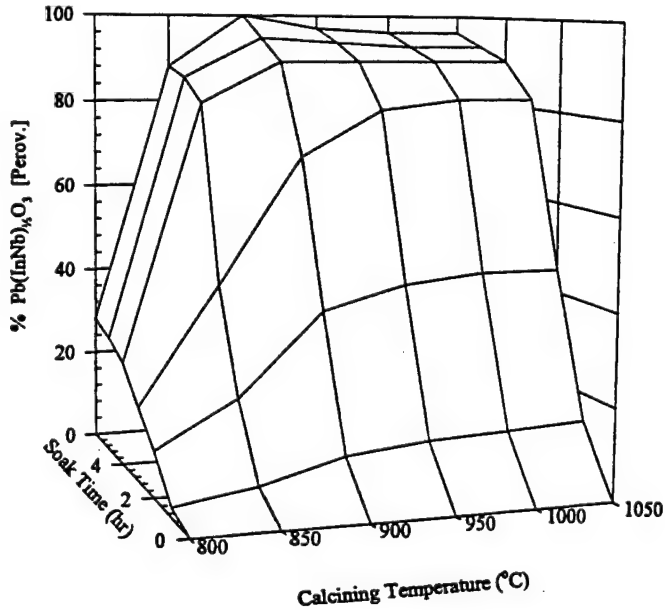

FIGURE 3 Formation of $Pb(In_{1/2}Nb_{1/2})O_3$ with 2 wt% excess In_2O_3 and 3 wt% excess Li_2CO_3. 100% Perovskite forms at 900°C after 6 hours.

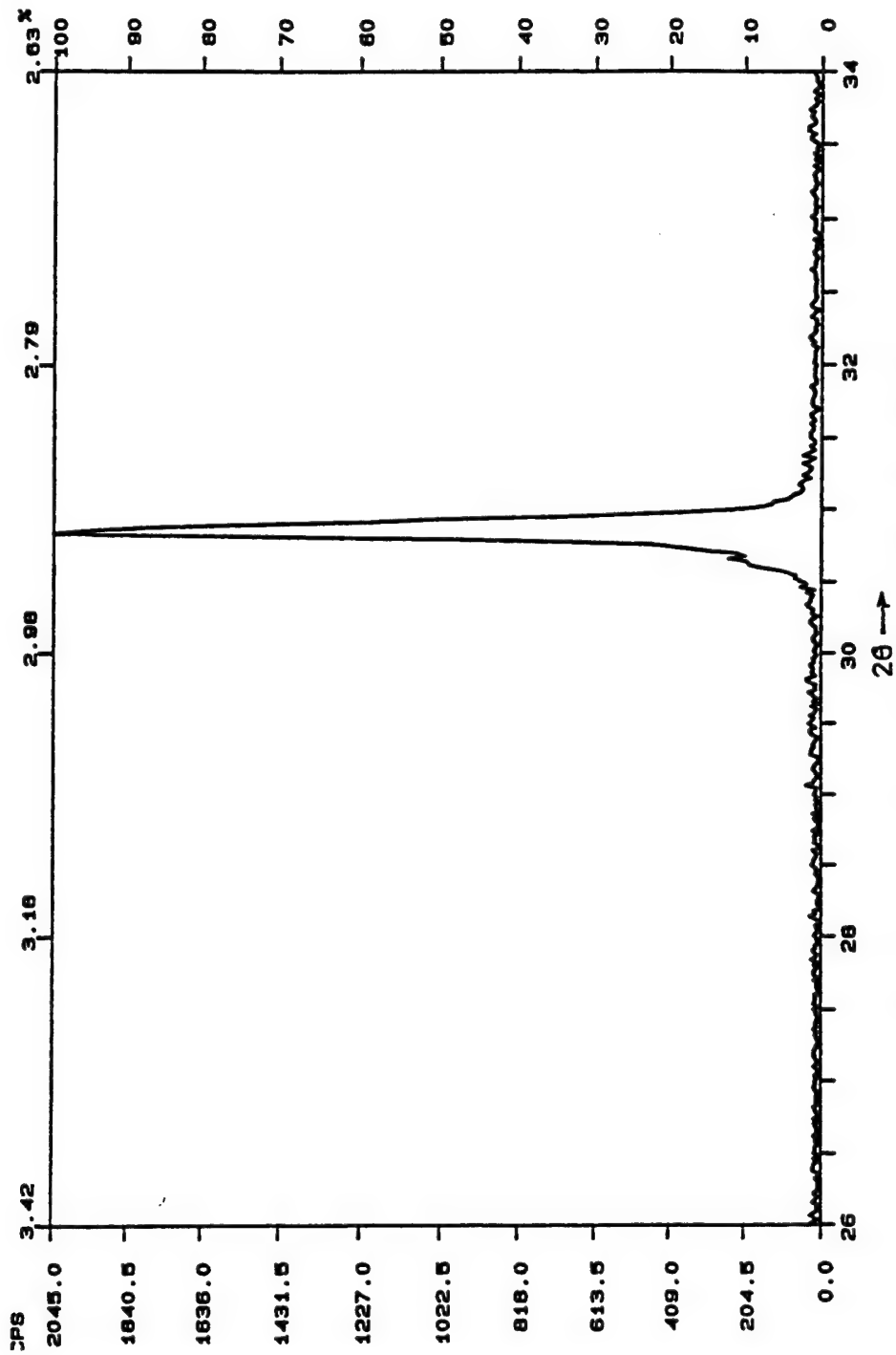

FIGURE 4 X-Ray diffraction pattern of a calcined $Pb(In_{1/2}Nb_{1/2})O_3$ powder.

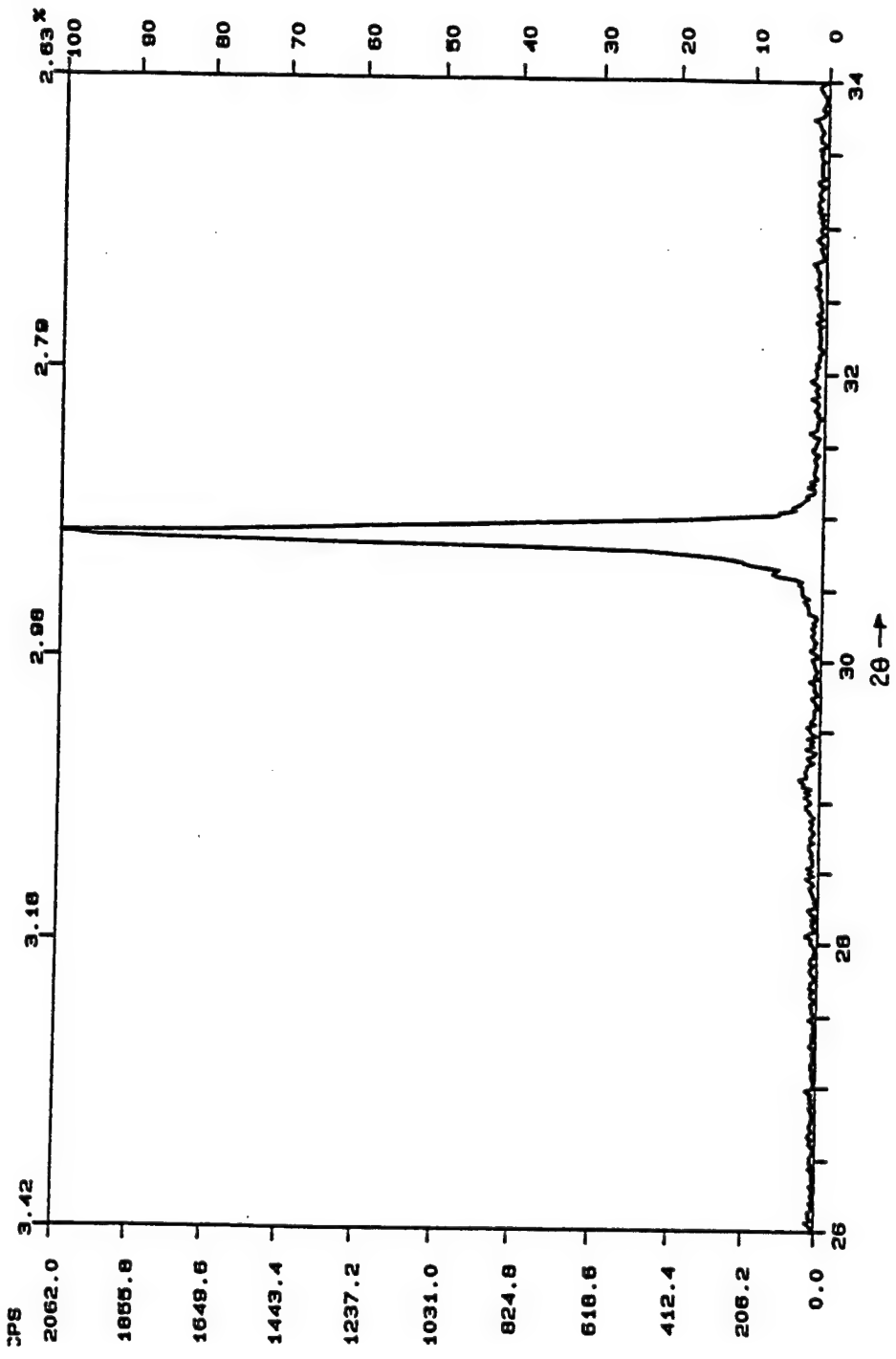

FIGURE 5 X-Ray diffraction pattern of a sintered $Pb(In_{1/2}Nb_{1/2})O_3$ ceramic.

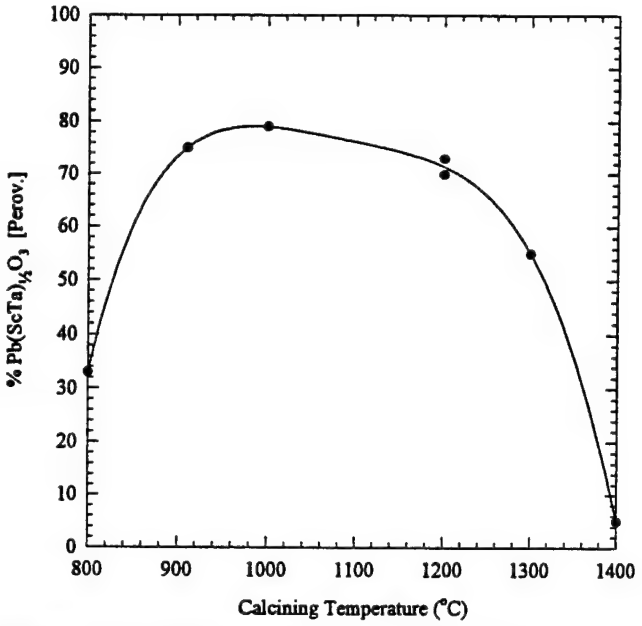

FIGURE 6 Formation of $Pb(Sc_{1/2}Ta_{1/2})O_3$ by the mixed oxide method.

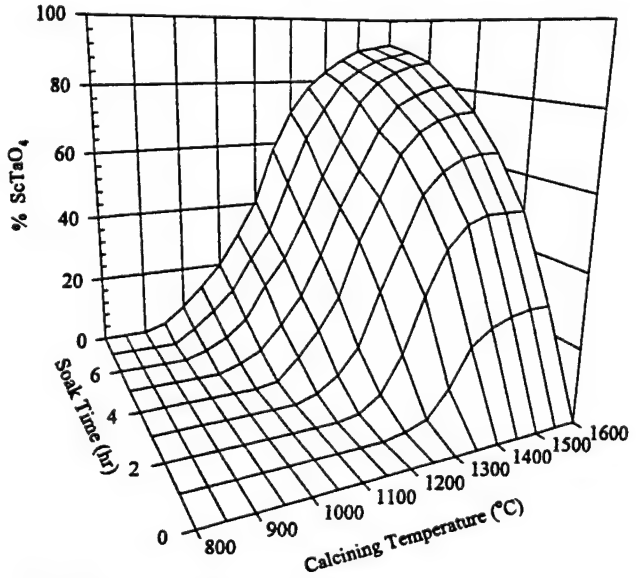

FIGURE 7 Formation of $ScTaO_4$ by the mixed oxide method.

was synthesized and mixed with PbO and re-milled as previously mentioned. After drying the powder, various calcining conditions were evaluated using the sealed crucible method. It was found that soak times longer than four hours lead to increased concentration of the pyrochlore phase. Maximum perovskite phase content was found to be 85% at 1050°C (see Figure 2).

As suggested by Groves (1985) Li_2CO_3 was used to aid in forming PIN. In this

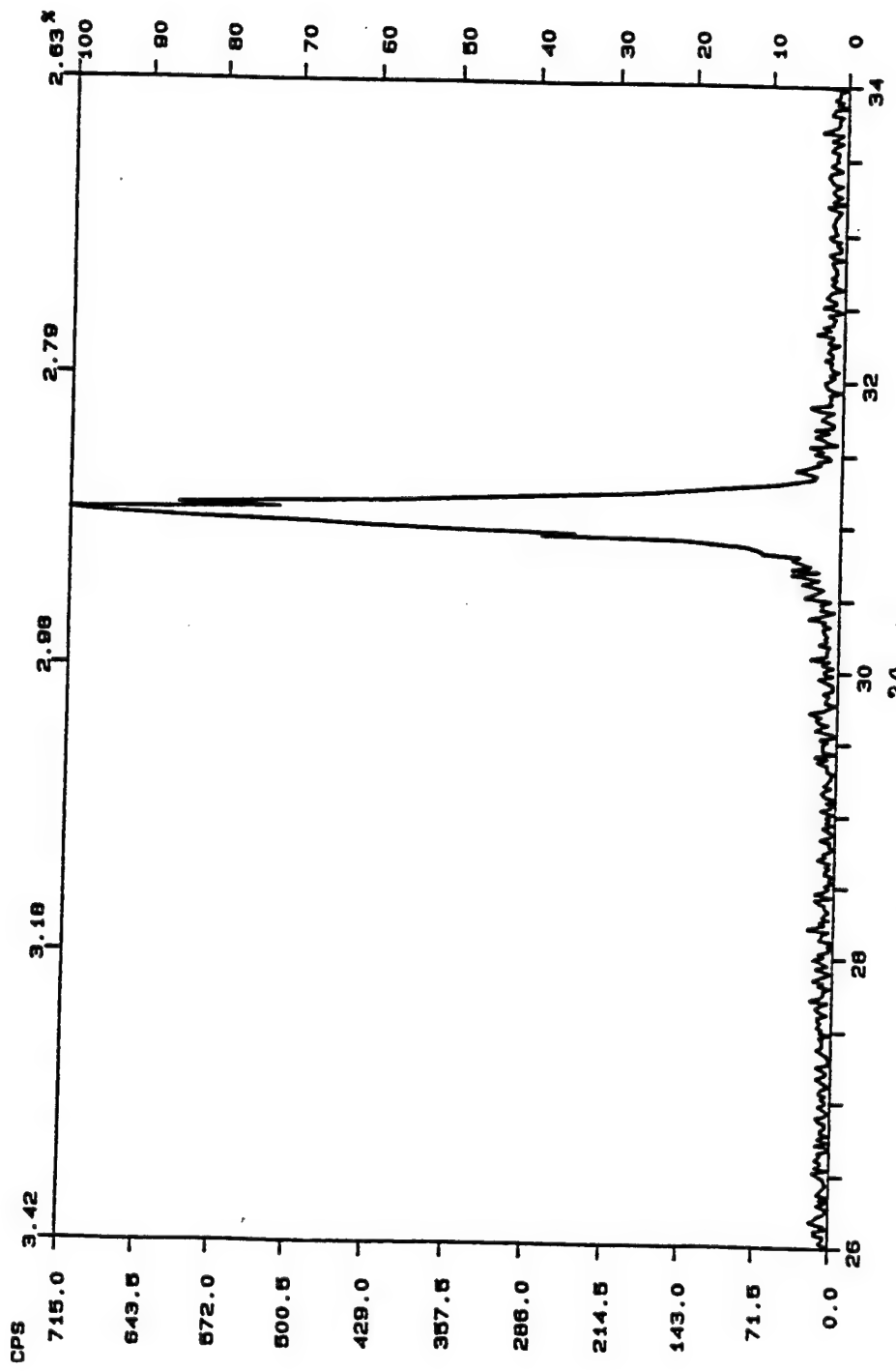

FIGURE 8 X-Ray diffraction pattern of a calcined $Pb(Sc_{1/2}Ta_{1/2})O_3$ powder.

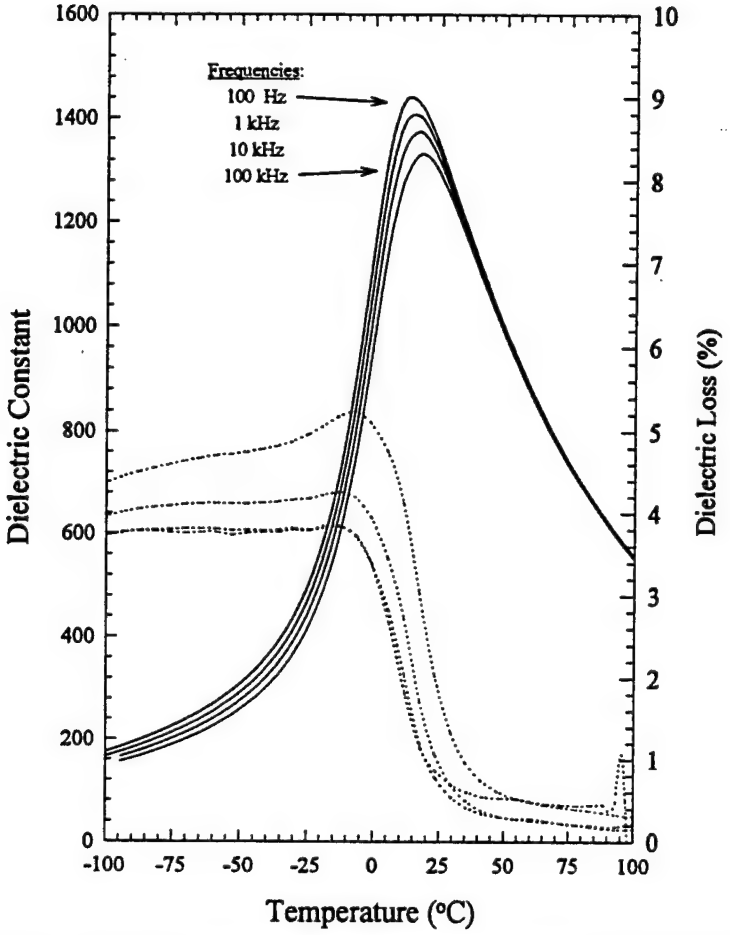

FIGURE 9 Dielectric constant and loss of (a) PIN:PST (2.5) and (b) PIN:PST (97.5).

paper the author reasons that the perovskite phase has a more "open" structure as compared to the pyrochlore. The small lithium ion should, therefore, add to the driving force for perovskite production due to its large kinetic energy at processing temperatures. This does seem to be the case as seen in Figure 2. The addition of 3 weight percent of ultra-pure Li_2CO_3 increased the formation of the perovskite phase to about 90% with the previously mentioned calcining conditions. Another problem realized at this temperature was the tendency for the powders to begin to sinter.

Another useful approach used lithium and excess indium. Figure 1 shows the result of adding 2 excess weight percent In_2O_3 before the processing of $InNbO_4$. It was found that >90% $InNbO_4$ was formed at 1100°C after 4 hours and the product showed greater crystallinity. This precursor was then mixed with PbO and 3 weight percent Li_2CO_3. (Calcined powders and ceramics using this procedure will be referred to as PIN23). Figure 3 is a time and temperature diagram derived from the PIN23 calcination study. At a temperature of 900°C PIN23 phase pure powders were produced after reacting the mixtures for 6 hours. Using this method, the need for sealed crucibles was eliminated; however, lead and indium sources were still used and precise

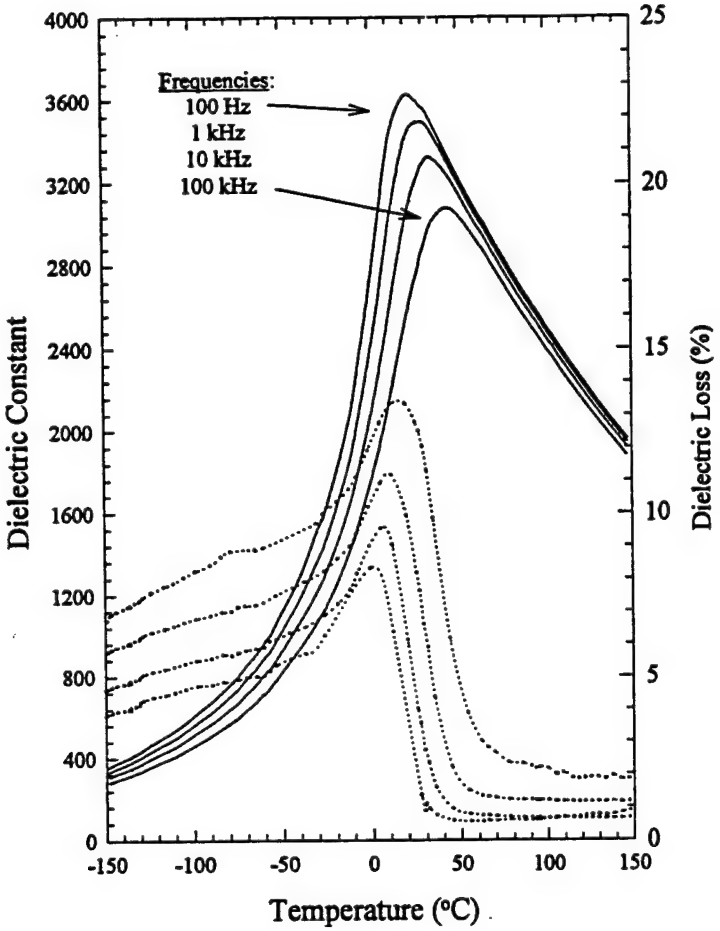

FIGURE 9 (*Continued*)

temperature control was also required. A sample PIN23 XRD pattern is shown in Figure 4.

Currently sol-gel methods are also being investigated (Ravichandran *et al.*, 1995) for the production of PIN powder. It is hoped this will lead to a more robust processing method and larger batch sizes.

Sintering of PIN23 ceramics was done at 1050°C for 2 hours. This temperature was a trade-off between density and phase purity of the resulting ceramics. At 1050°C approximately 89 to 92% theoretical density was achieved while maintaining at least 98% of the perovskite phase in the bulk. Concentration of the pyrochlore phase on the surface tended to be slightly greater but could easily be polished off during sample preparation. Figure 5 shows an XRD pattern of a typical as sintered PIN23 ceramic.

ii. *Lead scandium tantalate ceramics.* The production of PST has also evolved through a number of steps. Similar to PIN, the common mixed oxide method was used initially. Stoichiometric amounts of reagent grade PbO, Sc_2O_3, and Ta_2O_5 was mixed and ball-milled for 12 hours with zirconia media in alcohol. After drying 18

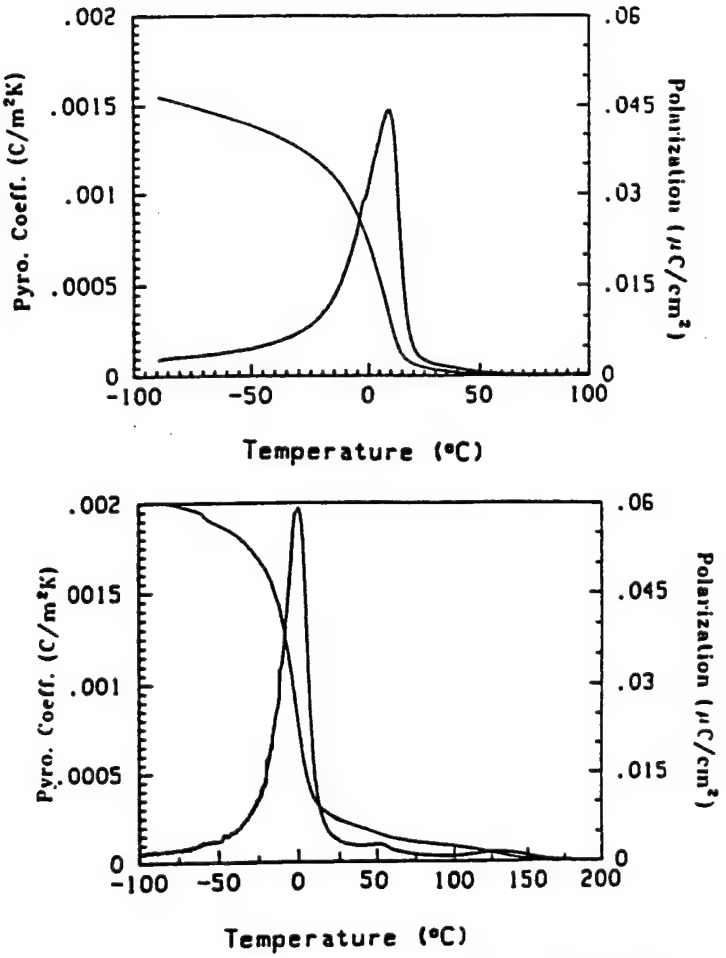

FIGURE 10 Pyroelectric constant and remnant polarization of (a) PIN:PST (97.5) and (b) PIN:PST (2.5).

to 24 hours the powders were ground to 100 mesh and placed on a platinum foil in a closed alumina crucible. An alumina boat containing PbO was also placed in the crucible to control lead losses. The formation of PST is governed by the following formula:

$$4 \cdot PbO + Sc_2O_3 + Ta_2O_5 \rightarrow [\text{perovskite}]4 \cdot Pb(ScTa)_{1/2}O_3$$

This mixed oxide approach did not yield promising results. A maximum of 80% perovskite phase was achieved at 1000°C after calcining 4 hours (see Figure 6). Sealing the crucibles, as done with PIN, was found to have no effect on the amount of pyrochlore phase present.

The wolframite precursor method was also used for the synthesis of PST. The appropriate precursor phase for PST was found to be $ScTaO_4$. 90% Single phase $ScTaO_4$ was produced after calcining the oxides for 8 hours at 1500°C (see Figure 7). It was determined that highly crystalline, single phase $ScTaO_4$ could be produced

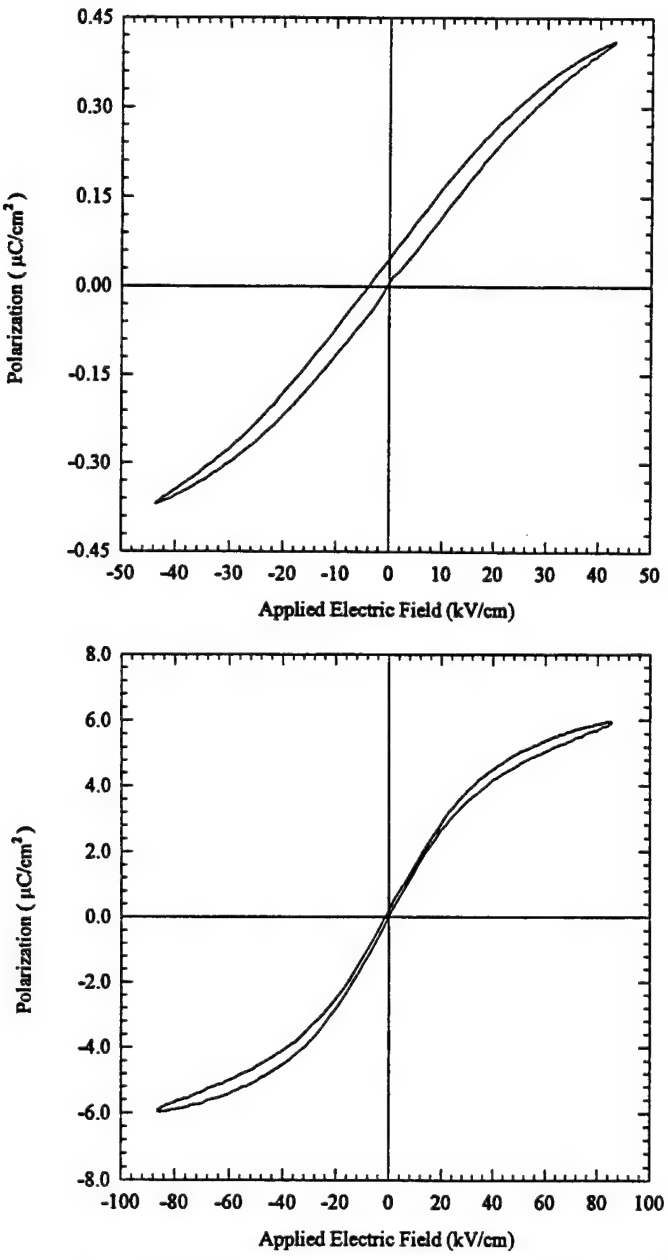

FIGURE 11 Room temperature dielectric hysteresis loop of (a) PIN:PST (97.5) and (b) PIN:PST (2.5).

from a two-step method. The first step was to calcine the powder at 1400°C for 4 hours to obtain 60% single phase $ScTaO_4$. The powder was then re-milled for 12 hours in alcohol and dried for 18 hours. After drying the powder was fully converted to $ScTaO_4$ when soaked at 1500°C for 4 hours.

PbO was added to the $ScTaO_4$ and was milled and dried. It was found that single phase PST could easily be produced at temperatures as low as 800°C and times as

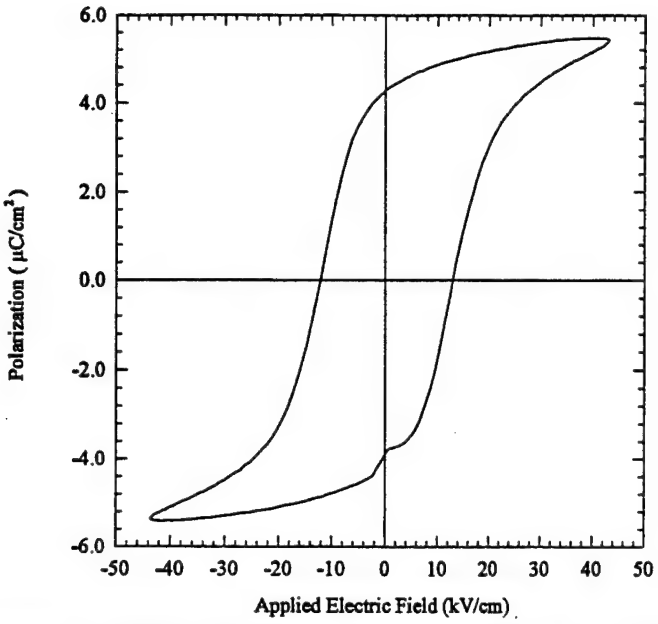

FIGURE 12 Dielectric hysteresis loop of PIN:PST (2.5) measured at −30°C.

short as 2 hours. A sample XRD pattern of a PST powder produced by this method is shown in Figure 8. Sintering of PST ceramics, however, has proven to be more difficult. The maximum density found after sintering for 8 hours at 1400°C was 65 to 70% theoretical. Fielding *et al.* (1995) has shown that highly dense single phase PST ceramics can be produced after sintering pellets between 1500°C and 1600°C in double sealed crucibles. In addition, work by Ravichandran *et al.* (1995) has shown sol-gel derived PST can be sintered in a phase pure perovskite pellets at a temperature of approximately 1400°C.

iii. *PIN:PST ceramics.* PIN:PST (x) ceramics (x representing the concentration of PIN in mole percent) were fabricated using the single phase powders as discussed previously. Appropriate amounts of the end members were mixed and milled for 6 hours and a binder was added. Once the powder was dried it was ground to 100 mesh and pressed. Weight loss of the ceramics was in all cases less than 2%. Pellets were placed in alumina crucibles on platinum foils and lead and indium sources were added. All of the ceramics (x = 100.0, 97.5, 50.0 and 2.5) retained at least 98% of the perovskite phase and were between 95 and 80% of the theoretical density.

2. *Electrical*

Electrical measurements including the dielectric constant and loss, dielectric hysteresis, and pyroelectric coefficient were made on the sintered pellets. The experimental setup to measure the dielectric constant and loss included a Hewlett Packard 4271 A capacitance bridge and liquid nitrogen feed furnace. The Byer-Roundy method was used for the pyroelectric measurements. This setup involved a Hewlett Packard 4192A picoammeter and a similar furnace setup. Data was collected by

Hewlett Packard 200 series micro computer. A modified Sawyer-Tower circuit was used for the hysteresis measurements. It included a Trek 2000 voltage amplifier and an MS-DOS based computer equipped with analog to digital converters for data collection.

Room temperature dielectric constant measured at 1 kHz were found to be 3845 (near the peak) and 1267 (in the paraelectric region) for ceramics with $x = 97.5$ and 2.5, respectively. The transition temperatures for the two ceramics were determined for the two ceramics to be 20°C and 10°C, respectively. Transition temperatures from pyroelectric data were found to be slightly lower, with values of 10°C and 0°C, respectively. As expected from the dielectric and pyroelectric data, only limited room temperature hysteresis was noticed. Upon cooling to −30°C, PIN:PST (2.5) shows a remnant polarization of 4.5 $\mu C/cm^2$, and reaches a saturated value of 5.7 $\mu C/cm^2$. The coercive field was found to be 9.86 kV/cm. No piezoelectric response has been detected in these compositions at room temperature. Further studies on the temperature dependence of the ferroelectric properties and the similar measurements on other compositions across the phase diagram are in progress.

SUMMARY

The experimental approach describes a suitable method for fabricating phase pure perovskite ceramics in the PIN:PST solid solution system. It is shown that high quality ceramics with less than 2% pyrochlore phase can be produced by a suitable multi-step process. Future work will focus on the order-disorder behavior and the electromechanical properties of these and other compositions across the PIN:PST phase diagram.

REFERENCES

1. J. F. Fielding, Proceedings of the Amer. Ceram. Soc. Meeting, April 1995.
2. P. Groves, "Fabrication and Characterization of Ferroelectric Perovskite Lead Indium Niobate," *Ferroelectrics*, **65**, 67–77 (1985).
3. S. S. Park and W. K. Choo, "Pyroelectric and Dielectric Properties of Lead Indium Niobate Ceramics," *Ferroelectrics*, **118**, 117–122 (1991).
4. N. Setter, Ph.D. Thesis, The Pennsylvania State University, 1980.
5. S. L. Swartz and T. R. Shrout, "Fabrication of Perovskite Lead Magnesium Niobate," *Mat. Res. Bull.*, **17**, 1245 (1982).
6. J. Von Liebertz, "Gitterkontanten von $InNbO_4$ und $InTaO_4$," *Acta. Cryst. B*, **28**, 3100 (1972).
7. D. Ravichandran, A. S. Bhalla and R. Roy, "Sol-Gel Derived $Pb(Sc_{0.5}Ta_{0.5})O_3$ Powders," *Materials Letters* (to be published).

THIN FILM FERROELECTRICS

APPENDIX 79

journal

J. Am. Ceram. Soc., 79 [8] 2189-92 (1996)

Fabrication and Electrical Properties of Lead Zirconate Titanate Thick Films

H. Daniel Chen, K. R. Udayakumar,* Christopher J. Gaskey, and L. Eric Cross*

Materials Research Laboratory, The Pennsylvania State University, University Park, Pennsylvania 16802

Jonathan J. Bernstein and Lance C. Niles

The Charles Stark Draper Laboratory, Cambridge, Massachusetts 02139

Thick films of lead zirconate titanate of the morphotropic phase boundary composition, $Pb(Zr_{0.52}Ti_{0.48})O_3$, have been fabricated on platinum-buffered silicon using a modified sol–gel spin-coating technique. Crack-free films of 12-μm thickness can be uniformly deposited on 3-in.-diameter wafers with high yield and properties comparable to those of bulk ceramics. The thickness dependence of film structure and the dielectric, ferroelectric, and piezoelectric properties have been characterized over the thickness range of 1–12 μm. A strong (100) texture develops as film thickness increases above 5 μm; the films were marked by saturation values of longitudinal piezoelectric coefficient d_{33}, 340 pC/N; remanent polarization, 27 μC/cm²; and dielectric permittivity, 1450. PZT films in this thickness range are extremely well-suited to application as electromechanical transduction media in silicon-based microelectromechanical systems (MEMS).

I. Introduction

PIEZOELECTRICITY, the ability of a material to develop an electric moment proportional to an applied mechanical stress, figures prominently in the acoustic transduction process, as many types of transducers make use of the piezoelectric effect to convert efficiently between electrical and mechanical energies. Because of the strong piezoelectric activity found near the morphotropic phase boundary composition, $Pb(Zr_{0.52}Ti_{0.48})O_3$, poled ceramics of this composition have been widely used as an electromechanical conversion medium in transduction applications. One important application is in medical and underwater acoustic imaging systems, the design of which incorporates a high-frequency sonar transducer with two-dimensional arrays of PZT active layers, serving to convert acoustic vibrations from impinging pressure wave fronts into electrical signals, to be processed and imaged. Transducers of this type can be integrated onto a silicon chip with on-board circuitry, in which a ceramic PZT film is deposited on the substrate through one of a number of deposition techniques.

The need for thicker PZT films stems from the figure of merit (FOM) for the response of a piezoelectric element in an acoustic sensing device, given by the sensitivity (M_0) squared times the output capacitance (C_0):[1]

$$\text{FOM} = M_0^2 \cdot C_0$$

Although the capacitance of a PZT film scales inversely with thickness, the lower output capacitance of thick PZT films is more than compensated for by their higher sensitivity, and a greater FOM can be obtained by increasing the film thickness to an optimal level.

The optimal thickness of a PZT film on a patterned silicon wafer is approximately one half of the silicon membrane thickness, or between 5 and 10 μm. This target thickness extends well beyond the upper limit of conventional thin film fabrication methods, which are predominantly used in the deposition of films less than 1 μm in thickness, and well below the lower limit of conventional tape-casting and screen printing thick film techniques, which, in addition, require higher thermal budgets, inappropriate for silicon device fabrication. The development of sol–gel-prepared, thick film devices has previously been

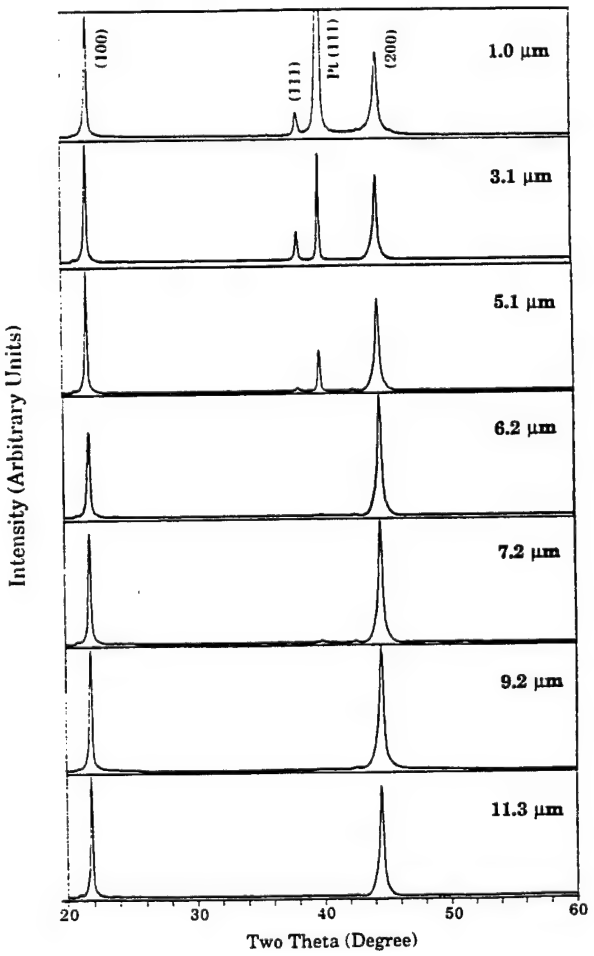

Fig. 1. Evolution of (100) planar orientation with thickness as evidenced by X-ray diffraction patterns of films of increasing thickness.

M. Sayer—contributing editor

Manuscript No. 192209. Received November 6, 1995; approved May 23, 1996.
*Member, American Ceramic Society.

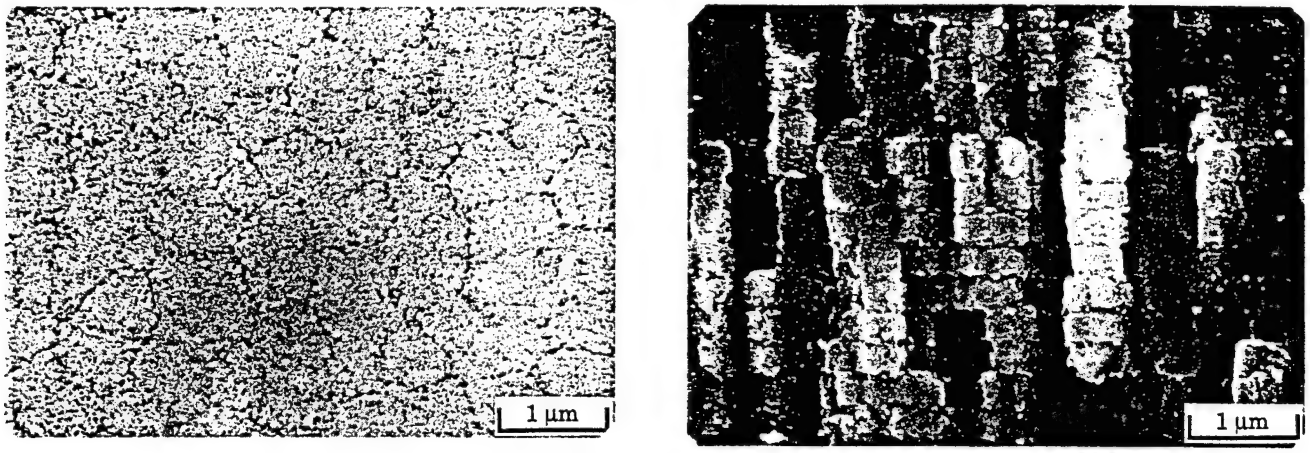

Fig. 2. SEM micrographs of surface and cross-sectional morphologies of a 11.3-μm-thick PZT film.

undermined by the tendency of chemically prepared PZT films to crack beyond a critical layer thickness and, to a lesser extent, a lack of information as to the variation of film properties with thickness in this uncharted range. The thick PZT films prepared in this work are then of major interest for both their device potential and the opportunity for investigation of the scaling of fundamental properties with thickness. There have been reports on the preparation of thicker films that apparently employ a hybrid technique involving the blending of the PZT powder with a solution to obtain a viscous paste, the processing details of which are still unknown.[2]

II. Experimental Procedure

The sol–gel spin-coating procedure used to prepare thick PZT films employs multidentate solvents and/or metal-organic precursors that contain multidentate ligands, rather than an alcohol. The idea behind the use of such solvents and ligands is that, through chelating effects, it is likely that these ligands are removed less easily by hydrolysis and may impart solubility to a growing metal oxide cluster, extending the time to the gel point.[3] It is likely that when many metal alkoxide compounds are dissolved in such multifunctional alcohol solvents, alcoholysis reactions occur, leading to the formation of new species, perhaps prior to hydrolysis and condensation reactions. This idea has been used for film fabrication by Yi *et al.*,[4,5] and a variant of the method using carboxylic acids as solvent has been used to prepare the solution in this study. The elemental precursors used were lead acetate trihydrate, zirconium *n*-propoxide, and titanium isopropoxide. Lead acetate trihydrate is initially dissolved in acetic acid, and the water of hydrolysis is expelled during a period of distillation at 105°C. After cooling to room temperature, the solution is mixed with zirconium and titanium alkoxides in amounts dictated by the morphotropic phase boundary composition, $Pb(Zr_{0.52}Ti_{0.48})O_3$. Solutions were synthesized with excess lead addition of 20 mol%. To the final precursor solutions, ethylene glycol and deionized water are added to control the viscosity and concentration of the sol. The resulting solution, stable in air, and relatively insensitive to moisture, is spin-deposited, at 7500 rpm for 30 s, on 1- and 3-in. platinum metallized silicon wafers using a photoresist spin coater. Each wet layer is initially dried at 150°C to evaporate the solvent, rapidly heated to 400°C to remove residual organics, and preannealed at 600°C to densify the layer and prevent further shrinkage. Finally, the multilayer films of desired thickness are annealed at 700°C for 1 h in a conventional box furnace.

The thicknesses of the PZT films were determined from surface profilometer traces, and compared against values taken from SEM cross-section images. Room-temperature X-ray diffraction data, recorded with a Scintag diffractometer using Cu$K\alpha$ radiation, and plane view SEM images were used to evaluate structure and phase assemblage. Contact electrodes of 0.8- and 1.6-mm diameter are formed by sputter-depositing platinum, 600 Å thick, on the top film surface. Piezoelectric,

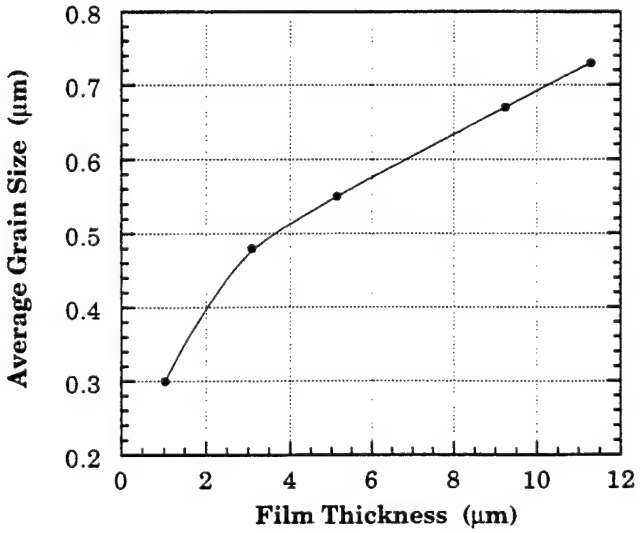

Fig. 3. The average surface grain size tends to increase with film thickness.

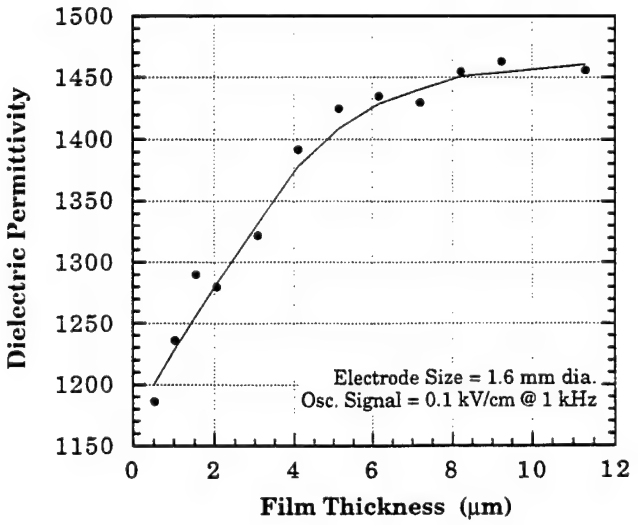

Fig. 4. Weak field dielectric permittivity plotted as a function of thickness. The dissipation losses are in the range of 3% to 4%.

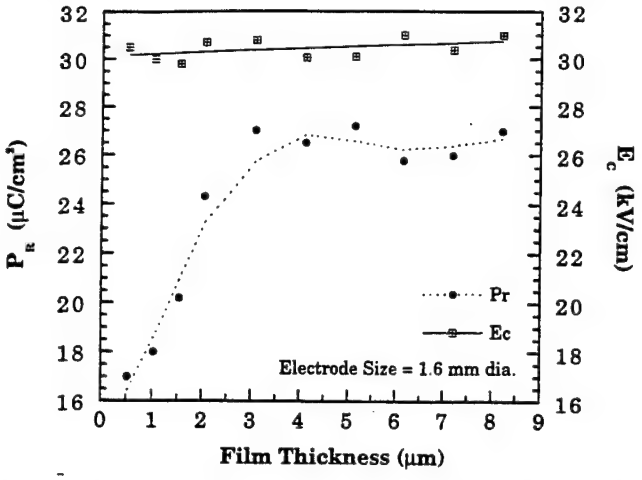

Fig. 5. Plot of the variation of hysteresis parameters, remanent polarization, and coercive field, with thickness.

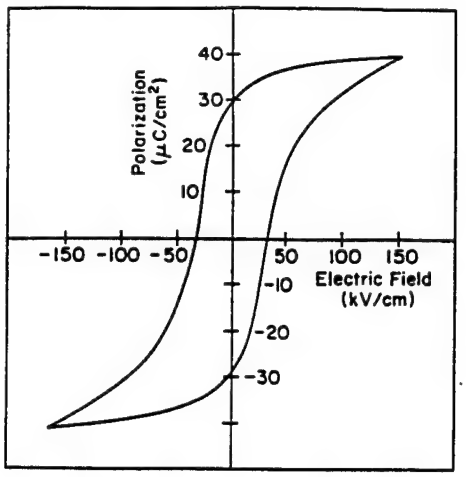

Fig. 6. *P–E* hysteresis trace for a 8.2-μm-thick film. Note the high polarization, and a relatively low coercive field.

hysteresis, and dielectric measurements were made using a double-beam laser interferometer, modified Sawyer-Tower circuit, and LCR bridge, respectively.

III. Results and Discussion

The thickness of each layer was found to be constant at 0.25 μm over the entire range of thicknesses examined; multiple coatings were applied to achieve a thickness of 12 μm. X-ray diffraction (XRD) patterns taken for films of increasing thickness (Fig. 1) demonstrate a pseudocubic perovskite structure with a strong tendency toward textured planar orientation, a tendency which increases with thickness up to 6 μm, beyond which only (100) and (200) reflections are observable. A dense, close-packed surface microstructure is common to films of the entire thickness range investigated, as can be observed from the typical micrograph of a 11.3-μm-thick film (Fig. 2); the film cross section displays a dense layered structure with well-defined grains along columns and within each layer. The surface grain sizes of the films tended to increase with thickness (Fig. 3).

In general, the electrical properties of the PZT thick films under investigation compare favorably with those of a well-prepared bulk ceramic sample; however, scaling effects with film thickness need to be taken into consideration when incorporating films into device designs. The weak field dielectric permittivity at 1 kHz increases with film thickness up to 8 μm, at which point it saturates at a value of 1450 (Fig. 4). A similar tendency is noted in the plot of remanent polarization vs thickness. 27 μC/cm² at film thicknesses above 3 μm, while the coercive field is relatively independent of film thickness (Fig. 5). A representative *P–E* hysteresis trace for a film 8.2 μm thick is shown in Fig. 6.

The longitudinal piezoelectric coefficient, d_{33}, of the thick PZT films, subjected to a poling field of 150 kV/cm for 2 min in air, is determined from the slope of the linear portion of the plot of strain vs ac driving field, displacements being measured by a double beam laser interferometer. From Fig. 7, it may be noticed that at higher driving fields, higher-order terms contribute to the induced strain, the small field assumption being no longer valid. The thickness dependence of the effective d_{33}, plotted in Fig. 8, levels off at approximately 340 pC/N, a value higher than that observed in undoped ceramic PZTs,[6] possibly

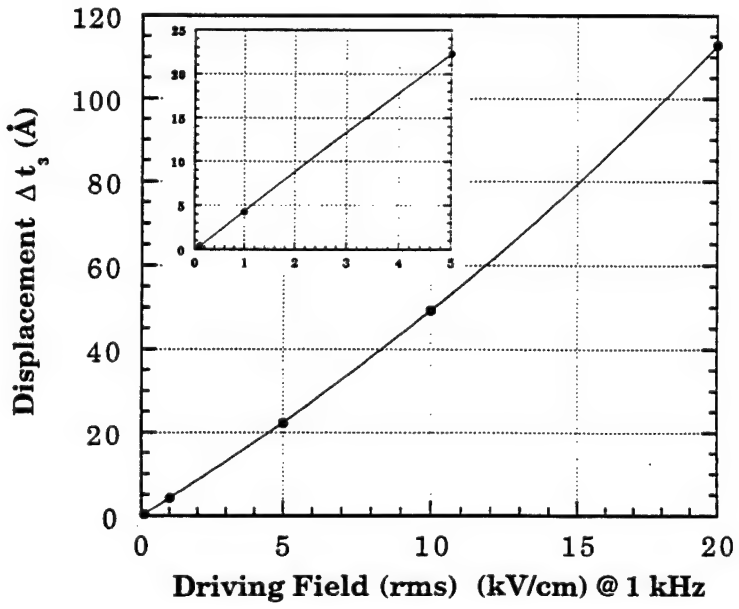

Fig. 7. Film displacement of a 9.2-μm-thick film measured through a double laser interferometer plotted as a function of driving field amplitude.

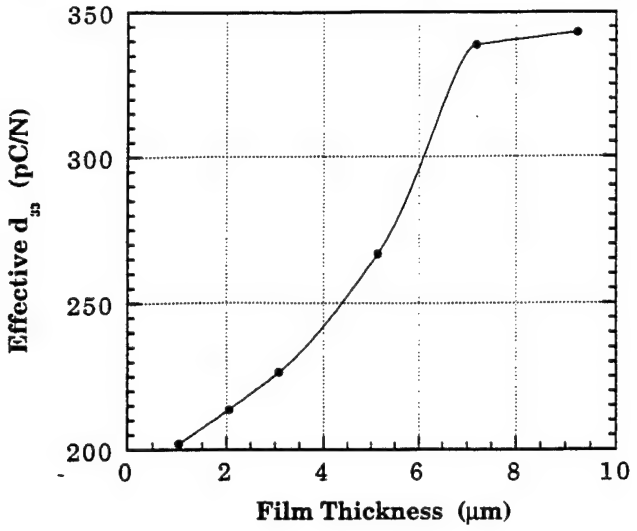

Fig. 8. Effective longitudinal piezoelectric coefficient plotted as a function of thickness.

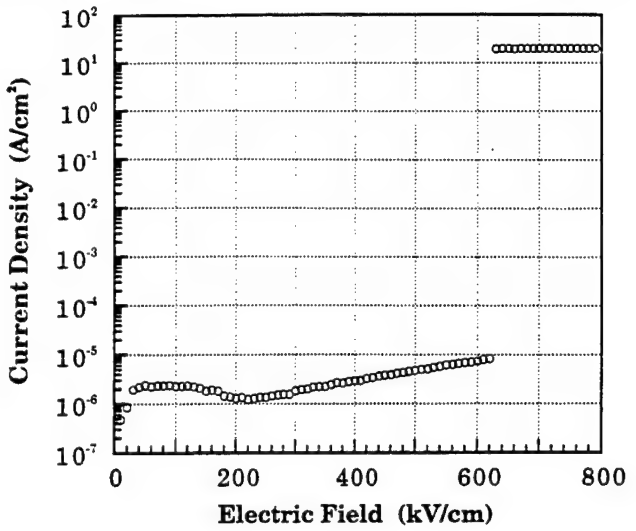

Fig. 9. *I–V* plot of a 8.2-μm-thick film to determine the dielectric breakdown strength of the film.

due to extrinsic effects resulting from the stress boundary conditions imposed by the substrate and surrounding film, as also the film texture.

The dielectric breakdown strength of a material, especially in relation to its projected operating voltage, is a crucial parameter in judging the feasibility of its use in a particular application. The breakdown strength of a 8.2-μm-thick PZT film, determined from the onset of the sharp rise in current density vs dc voltage, is 640 kV/cm (Fig. 9). As expected from thickness considerations, this value of breakdown field is notably higher than values for bulk ceramics (60–100 kV/cm),[7] yet lower than breakdown levels reported for submicrometer thin films (1 MV/cm).[5]

IV. Summary

Integrated piezoelectric elements of thick film PZT(52/48) on platinized silicon have been fabricated using a modified sol–gel spin-on process. Crack-free, dense films 1–12 μm in thickness were characterized to determine variations in structure and electrical properties as a function of film thickness, wherein 20 mol% of excess lead was found to be necessary to stabilize the perovskite phase, and improve electrical properties. Highly textured films of (100) orientation were observed above thicknesses of 5 μm. The dielectric permittivity, remanent polarization, and longitudinal piezoelectric coefficient saturate at values comparable to a ceramic PZT specimen. The high dielectric breakdown strength of thick PZT films will enable the applicability of the films in a number of MEMS structures and smart systems.

References

[1]O. B. Wilson, *Introduction to Theory and Design of Sonar Transducers*; p. 155. Peninsula Publishing, Los Altos, CA, 1988.

[2]D. A. Barrow, T. E. Petroff, and M. Sayer, "Fabrication of Thick, Sol Gel PZT Films: Applications to Macroscopic Piezoelectric Devices," *Mater. Res. Soc. Symp. Proc.*, **360**, 103–108 (1995).

[3]C. D. Chandler, C. Roger, and M. J. Hampden-Smith, "Chemical Aspects of Solution Routes to Perovskite-Phase Mixed-Metal Oxides from Metal-Organic Precursors," *Chem. Rev.*, **93**, 1205–41 (1993).

[4]G. Yi, Z. Wu, and M. Sayer, "Preparation of $Pb(Zr,Ti)O_3$ Thin Films by Sol Gel Processing: Electrical, Optical, and Electro-optic Properties," *J. Appl. Phys.*, **64**, 2717–24 (1988).

[5]G. Yi and M. Sayer, "Sol Gel Processing of Thick PZT Films"; pp. 289–92 in Proceedings of the Eighth IEEE International Symposium on Applications of Ferroelectrics (Greenville, SC, 1992). Edited by M. Liu, A. Safari, A. Kingon, and G. Haertling. Institute of Electrical and Electronics Engineers, Piscataway, NJ, 1992.

[6]B. Jaffe, W. R. Cook, Jr., and H. Jaffe, *Piezoelectric Ceramics*; p. 146. Academic Press, New York, 1971.

[7]R. Gerson and T. C. Marshall, "Dielectric Breakdown of Porous Ceramics," *J. Appl. Phys.*, **30**, 1650–53 (1959).

[8]K. R. Udayakumar, P. J. Schuele, J. Chen, S. B. Krupanidhi, and L. E. Cross, "Thickness-Dependent Electrical Characteristics of Lead Zirconate Titanate Thin Films," *J. Appl. Phys.*, **77**, 3981–86 (1995).

APPENDIX 80

THICKNESS-DEPENDENT ELECTRICAL PROPERTIES IN LANTHANUM-DOPED PZT THICK FILMS

H.D. CHEN, K.K. LI, C.J. GASKEY, and L.E. CROSS
Materials Research Laboratory, The Pennsylvania State University, University Park, PA 16802

ABSTRACT

Lanthanum-doped lead zirconate titanate (PLZT) films, with thickness up to 10 μm, are fabricated on platinized silicon substrates through a modified sol-gel technique. Thickness-dependent piezoelectric properties measured with a double-beam laser interferometer show piezoelectric relaxation in field-induced strain as the ac driving field exceeds 10 kV/cm. In addition, the strain levels of PLZT thick films are approximately one third of those of undoped PZT films under the same fabrication and measurement conditions. For 1 μm PZT(55/45) films doped with 0, 2, and 4 mole% La, the *P-E* hysteresis exhibits decreasing squareness with increasing lanthanum content while the piezoelectric d_{33} coefficient reduces from 130 to 52 pC/N. Residual (tensile) stress in these films and resulted depoling effect may be responsible for this phenomenon.

INTRODUCTION

Lanthanum-modified lead zirconate titanate (PLZT) ceramics have been widely known as the first transparent ceramics suitable for electrooptic applications since 1971 [1]. Because of their excellent electrooptic properties, optically transparent PLZT ceramics have been exploited in an ever-growing number of applications such as light shutters, modulators, switches, color filters, and image storage and display devices [2]. Through proper choice of composition within the PLZT phase diagram, compositions with approximately 4-8 mole% La and located at or near the morphotropic phase boundary (MPB) between the rhombohedral and tetragonal phases are found to be of interest in piezoelectric applications [3]. Compared with undoped PZT materials, La-doped PZT bulk ceramics have shown great enhancement in their electromechanical properties; for example, very high values of planar coupling coefficient k_p and piezoelectric d_{33} coefficient of 0.72 and 710 pC/N, respectively, have been reported for PLZT(7/60/40) ceramics [4].

Since the sensitivity of monomorph-based acoustic image sensors increases with the piezoelectric voltage g_{31} coefficient and the thickness of the active piezoelectric layer, ferroelectric films of 5-10 μm thickness greatly improve the acoustic receiving sensitivity in micromachined high-frequency electroacoustic transducers [5-6]. While these transducers have been made with thick films of the un-modified PZT(52/48) composition, it is hoped that by applying PLZT films with better piezoelectric properties, the acoustic sensitivity can be further improved.

Since there is no study referring to the piezoelectric properties of PLZT thick films up to date, it is the objective of this study to determine if these piezoelectric properties enhancements in PLZT ceramics translate into the PLZT thin/thick film vernacular. Effects of lanthanum doping on associated dielectric and ferroelectric properties of PZT films are also discussed.

Mat. Res. Soc. Symp. Proc. Vol. 433 © 1996 Materials Research Society

EXPERIMENTAL PROCEDURE

In this work, PLZT films with compositions close to the MPB and exhibiting high piezoelectric coefficients in the bulk are deposited on platinum-coated silicon wafers. The sol-gel spin-on technique is applied in this study primarily because of its superb stoichiometric control and its compatibility with silicon microfabrication processes. The precursors used to prepare PLZT films were lanthanum acetate, lead acetate trihydrate, zirconium n-propoxide, and titanium isopropoxide. Details of the fabrication procedure were documented in our earlier paper [7]. Compositions of PLZT films were formulated by assuming the formation of A-site vacancies: $Pb_{1-1.5(X/100)}La_{X/100}[Zr_{Y/100}Ti_{1-(Y/100)}]O_3$ and denoted as PLZT(X/Y/100-Y), where X = 0, 2, and 4, and Y = 55. Solutions were spin-coated on 1" square platinized silicon wafers. Films with thickness ranging from 0.5 to 10 μm were prepared through multiple coatings. For electrical properties evaluations, platinum top electrodes of 1.6 mm diameter and approximately 1200 Å thickness were formed by sputtering.

The effective field-induced piezoelectric displacements of PLZT films were characterized with a highly sensitive double-beam laser interferometer [8]. Weak signal dielectric properties were monitored from an LCR meter; and P-E hysteresis loops were recorded with a modified Sawyer-Tower circuit.

RESULTS AND DISCUSSION

Figure 1 plots the field-induced strain as a function of ac driving field for various thicknesses of PZT(52/48) films reproduced from our earlier study [7]. It is shown that at large driving fields (> 5 kV/cm), higher order terms of ac field contribute to the induced strain, and hence a linear relationship between induced strain and driving force based on the small signal assumption is no longer valid. The piezoelectric d_{33} coefficient is therefore determined from the slope of the linear

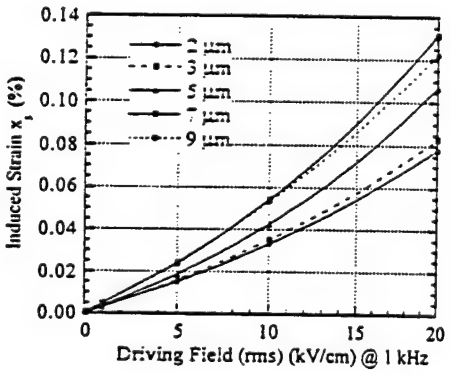

Figure 1. Field-induced strain of various thicknesses PZT(52/48) films through a double beam laser interferometer plotted as a function of ac driving field.

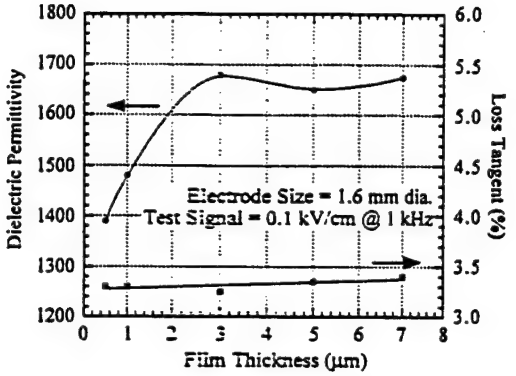

Figure 2. Weak field dielectric permittivity of PLZT(4/55/45) films plotted as a function of film thickness. The loss tangents are in the range of 3 to 3.5 %.

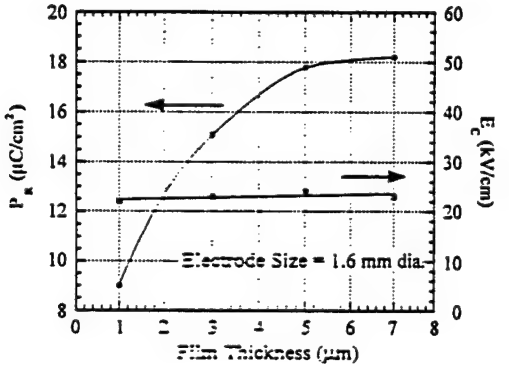

Figure 3. Plot of the variation of hysteresis parameters, remnant polarization and coercive field, of PLZT(4/55/45) films with film thickness.

portion (small driving fields) of the plot of induced strain vs. driving field. As a reference, Figure 1 of undoped PZT films will be used to contrast with the results of La-doped PZT films.

Small signal dielectric permittivities and tangent losses of PLZT(4/55/45) films shown in Figure 2 indicate that the permittivities reach a saturation of 1650 as film thickness exceeds 3 μm; but loss tangents are relatively independent of the thickness. Very similar tendencies are seen in *P-E* hysteresis parameters vs. thickness (Figure 3). The remnant polarization increases with the thickness and saturates at film thicknesses above 5 μm; while the coercive field does not change much with the thickness.

Figure 4 shows the field-induced strain as a function of the ac driving field for PLZT(4/55/45) films of different thicknesses. Two distinct differences can be realized by comparing Figure 4 with Figure 1. First, while higher order terms of the ac driving field promotes the induced strain

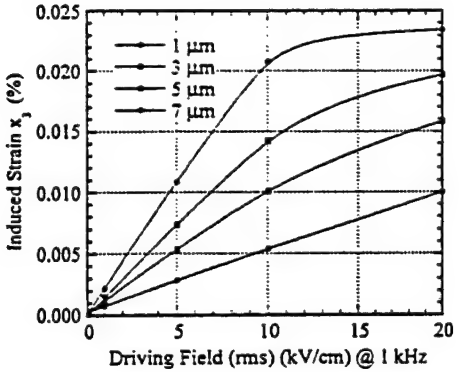

Figure 4. Field-induced strain of various thicknesses of PLZT(4/55/45) films plotted as a function of ac driving field. Notice the difference between this plot and Figure 1.

in PZT films as mentioned above, such phenomenon is reversed in the PLZT samples, especially when the film thickness becomes greater. Second, the strain levels of PLZT films are about one third of those of PZT samples.

Since the piezoelectric d_{33} coefficient is intrinsically proportional to the remnant polarization P_R, it appears that PLZT films experience some depoling effect which affects their piezoelectric performance at high driving fields. In order to maintain the polarization from depoling, dc biasing voltages of various magnitudes are applied when measuring the induced strain with a fixed ac driving field, and the effective d_{33} coefficient is obtained as the ratio of induced strain and driving field. Results in Figure 5 show the effective d_{33} values increase initially with biasing voltage, which confirms that the dc bias did hold the polarization to some extents; as the biasing voltage

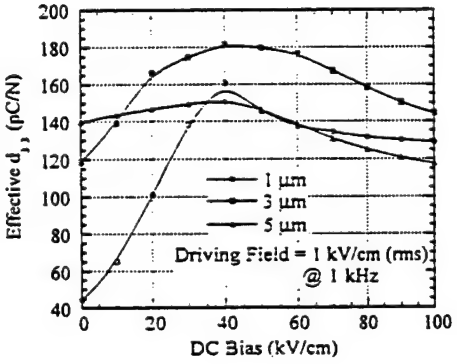

Figure 5. The dc bias dependence of the effective d_{33} plotted for PLZT(4/55/45) films of approximately 1, 3, and 5 μms.

exceeds 40 kV/cm, these values decrease slightly. However, such effect of enhancing effective d_{33} by dc bias is limited on the 5 μm PLZT films, as can be seen by its smaller-curvature profile in Figure 5.

These thickness-dependent piezoelectric relaxation phenomena shown in Figures 4 & 5 were not found in undoped PZT thick films from our earlier study [7]. Thus, lanthanum doping does modify certain mechanisms in PLZT thick films. To further inspect this issue, 1 μm thickness PZT(55/45) films with 0, 2, and 4 mole% lanthanum were prepared. Figure 6 shows that the dielectric permittivity increases with the level of La-doping and loss tangent remains constant. Hysteresis loops shown in Figure 7 display less square loops, and lower remnant polarization, with increasing lanthanum doping level.

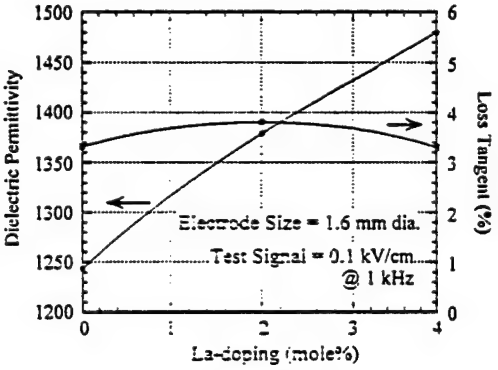

Figure 6. Dielectric permittivity and loss tangent of PZT(55/45) films vs. the level of lanthanum doping. Measurement is performed on HP4274A LCR bridge with test signal set as 0.1 kV/cm at 1 kHz.

From the data of bulk PZT ceramics, lanthanum-doped PZT ceramics show improved electromechanical properties over PZT materials. The incorporation of La^{3+} ions into PZT ceramics produces excess positive charges which are largely compensated by Pb ion vacancies (V_{Pb}''). By forming V_{Pb}'' the maneuverability of the domain walls is greatly enhanced. Lower coercive field and relatively higher squareness of *P-E* hysteresis loop are expected. This is usually termed as a "softening" effect. Other common characteristics include increased dielectric permittivity and higher electromechanical coupling coefficients [9].

Shown in Figure 8 is, however, a decreasing tendency of the slope (which corresponding to piezoelectric d_{33} coefficient) with increasing the molar percentage of La in PZT(55/45) films. This seems to contradict the general expectation from La-doping of PZT ceramics as stated above.

It is recognized that the rigid substrate has the major effect on ferroelectric film properties. Li [10] pointed out that, depending on the substrate materials used, distinctly different *P-E* hysteresis loops can be exhibited by the PLZT films identically processed from the same coating solutions. This has been attributed to the film stresses resulting from thermal expansion mismatch between films and substrates. As the introduction of La into the PZT structure creates cation vacancies and soften the whole lattice, this makes PLZT films more susceptible to stress

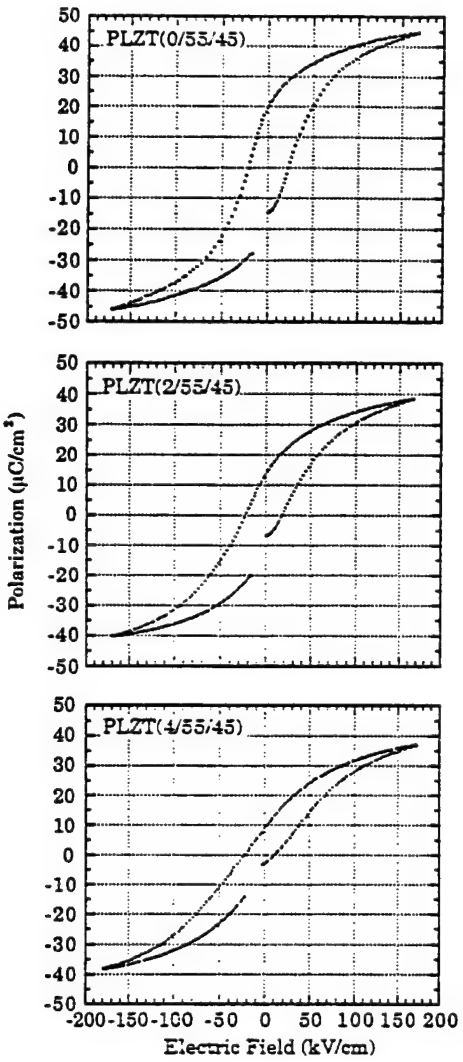

Figure 7. Lanthanum doping effect in hysteresis behavior of 1 μm thickness PZT(55/45) films.

effects and consequently subjected to stress-induced depoling [11].

On the other hand, since it is believed that the film stress will be proportional to the temperature difference between the film annealing temperature and its phase transformation temperature (T_C), and adding lanthanum into PZTs tends to lower T_C, the residual stress level is expected to be greater in PLZT films than in PZT ones. This may elucidate the decreasing P_R and

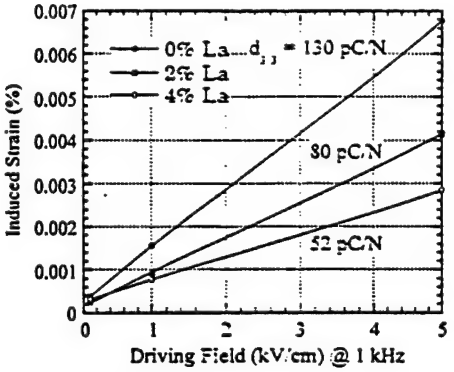

Figure 8. Induced strain of PZT(55/45) films plotted as a function of ac driving field. The piezoelectric d_{33} coefficient drops with increasing La-doping level.

d_{33} coefficients exhibited by PLZT films with increasing La contents. It may also explain the difficulties in depositing PLZT, but not PZT, thick films on larger Si wafers without cracking [12].

Although definite answers to the La-doping effects on the piezoelectric responses of PLZT films cannot be given at this time, it is thought that for piezoelectric applications the La doping concept developed in the bulk PZT ceramics may not apply to their thin/thick film counterparts.

CONCLUSIONS

PLZT films with thickness from 0.5 to 10 μm are fabricated on platinized silicon wafers for piezoelectric properties evaluation. Unlike undoped PZT thick films, PLZT films show piezoelectric relaxation with increasing film thickness, particularly in the high ac driving field region. Besides, the strain levels of PLZT thick films are less than those of the undoped PZT films under the same fabrication and measurement conditions. Attempts have been made to explain the lanthanum doping effect on the piezoelectric responses of PZT films in terms of residual film stresses.

ACKNOWLEDGMENT

The authors acknowledge the financial support from The C. S. Draper Laboratory, Cambridge, MA.

REFERENCES

1. G.H. Haertling and C.E. Land, J. Am. Ceram. Soc., 54, 1 (1971).
2. A.J. Moulson and J.M. Herbert, Electroceramics: Materials, Properties, and Applications, (Chapman and Hall, New York, 1990), p. 362.
3. G.H. Haertling, Ferroelectrics, 75, 25 (1987).

4. S.T. Liu, S.Y. Pai, and J. Kyonka, Ferroelectrics, **22**, 689 (1978).
5. H.D. Chen, K.R. Udayakumar, L.E. Cross, J.J. Bernstein, and L.C. Niles, J. Appl. Phys., **77**, 3349 (1995).
6. J.J. Bernstein, K. Houston, L.C. Niles, K.R. Udayakumar, H.D. Chen, and L.E. Cross, (accepted for publication in IEEE J. Ferroelectrics and Frequency Control).
7. H.D. Chen, K.R. Udayakumar, C.J. Gaskey, L.E. Cross, J.J. Bernstein, and L.C. Niles, (accepted for publication in J. Am. Ceram. Soc. Communication).
8. W.Y. Pan and L.E. Cross, Rev. Sci. Instrum., **60**, 2701 (1989).
9. B. Jaffe, W.R. Cook, Jr., and H. Jaffe, Piezoelectric Ceramics, (Academic Press, New York, 1971), p. 154.
10. K.K. Li, Ph.D. thesis, Clemson University, 1993.
11. J.M. Herbert, Ferroelectric Transducers and Sensors, (Gordon and Breach Science Publishers, New York, 1982), p. 37.
12. Technical Report to The C. S. Draper Laboratory, Cambridge, MA (1995).

APPENDIX 81

Pergamon

Materials Research Bulletin, Vol. 31, No. 7, pp. 817-825, 1996

0025-5408/96 $15.00 + .00

PII S0025-5408(96)00073-6

SOL-GEL SYNTHESIS OF $Ba(Mg_{1/3}Ta_{2/3})O_3$: PHASE PURE POWDER AND THIN FILMS

D. Ravichandran*, R. Meyer Jr., R. Roy, R. Guo, A.S. Bhalla and L.E. Cross
Materials Research Laboratory, The Pennsylvania State University
University Park, PA 16802, USA

(Refereed)
(Received March 4, 1996; Accepted March 13, 1996)

ABSTRACT

Phase pure $Ba(Mg_{1/3}Ta_{2/3})O_3$ (BMT) powders were prepared using Ba metal, $Mg(OC_2H_5)_2$, and $Ta(OC_2H_5)_5$ as metal-organic precursors. Thin films of BMT were spin coated onto Pt-coated Si (100) substrates using the prepared solution and then fired at various temperatures. The X-ray diffraction patterns show that the films crystallize to a single disordered perovskite phase on Si (100) at ~600°C. Scanning electron microscopy reveals that the films 0.3 μm in thickness and approximately 0.1 μm in grain size were essentially crack-free.

KEYWORDS: A. thin-films, A. electronic materials, B. sol-gel chemistry, C. thermogravimetric analysis (TGA), C. X-ray diffraction

INTRODUCTION

The requirements for dielectric materials used in microwave applications usually include (i) a high unloaded Q, (ii) a moderate dielectric constant, and (iii) small temperature coefficient of the resonant frequency. Additionally, good sinterablity and high reproducibility are desirable processing features for these dielectric materials. $Ba(Mg_{1/3}Ta_{2/3})O_3$ (1-4), $Ba(Zn_{1/3}Ta_{2/3})O_3$ (5), $(Zr,Sn)TiO_3$ (6), $Ba(Mn_{1/3}Ta_{2/3})O_3$ (7), and other complex oxides have been reported as promising microwave materials. However,

* To whom correspondence should be addressed.

very high processing temperatures and poor sinterability are known obstacles for production, particularly for BMT. BMT has a melting point of ~3000°C (4) and is difficult to make in the form of high density ceramics and large area crystals. Additives such as Sn or Mn have been used in the synthesis of BMT to reduce the sintering temperatures or prolonged sintering time at high tempratures. Many materials for microwave applications have cations such as Mg, Sn, and Mn that easily form compounds with tantalum during the conventional solid state reactions and possibly resulting in undesirable phases. Sol-gel processing has been used for preparing phase pure bulk ceramics and thin films. Sol-gel techniques ensure homogeneous mixing of cations and low crystallization temperatures.

In this paper, we report the synthesis for the first time of phase pure BMT powders, ceramics, and thin films by the sol-gel process, using Ba metal, $Mg(OC_2H_5)_2$, and Ta $(OC_2H_5)_5$ as metal-organic precursors. The densification of ceramics as a function of sintering temperature without the use of any sintering aids commonly used in solid-state reaction routes is also reported.

EXPERIMENTAL

A schematic reaction sequence for the formation of BMT gels and thin films is shown in Figure 1. Initially, $Ta(OC_2H_5)_5$ (Aldrich Chemicals, 99.99% purity) in stoichiometric amount was dissolved in 20 ml of 2-methoxyethanol in a three-neck flask and refluxed at 125°C for 6 hours in an argon atmosphere.

$$Ta(OC_2H_5)_5 + 5\ CH_3\text{-}O\text{-}CH_2\text{-}CH_2\text{-}OH \rightarrow Ta(OCH_2CH_2OCH_3)_5 + 5\ C_2H_5OH$$
(yellow clear solution)

The required amount of $Mg(OC_2H_5)_5$ (Aldrich Chemicals, 99.99% purity) was dissolved in 15 ml of 2-methoxyethanol along with 3-5 ml of CH_3COOH needed to dissolve the

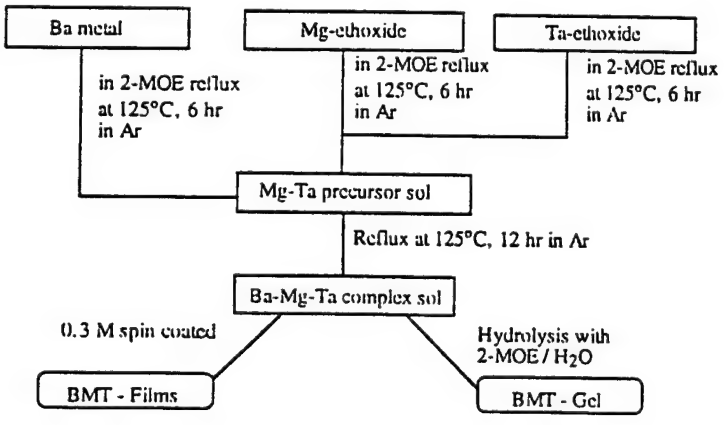

FIG. 1
Schematic reaction sequence for the formation of BMT xero-gel.

$Mg(OC_2H_5)_5$ completely. The mixture was refluxed for 6 hours in an inert atmosphere (e.g., Argon/N_2 gas).

$$Mg(OC_2H_5)_2 + 2\ CH_3\text{-}O\text{-}CH_2\text{-}CH_2\text{-}OH \rightarrow Mg(OCH_2CH_2OCH_3)_2 + 2\ C_2H_5OH$$
(colorless clear solution)

A double alkoxide (6) can be formed by mixing $Mg(OCH_2CH_2OCH_3)_2$ and $Ta(OCH_2CH_2OCH_3)_5$ under inert gas atmosphere. Finally, $Ba(OCH_2CH_2OCH_3)_2$ was formed following the reaction

$$Ba + 2\ CH_3\text{-}O\text{-}CH_2\text{-}CH_2\text{-}OH \rightarrow Ba(OCH_2CH_2OCH_3)_2 + H_2$$
(golden yellow solution)

The Ba-methoxyethoxide was cooled to room temperature and then added to the double alkoxide solution. The clear homogeneous solution obtained was further refluxed at 125°C for 12 hours in argon atmosphere. This process forms the barium-magnesium-tantalum precursor solution. In order to form the BMT gel, a part of the solution was hydrolyzed by adding a theoretical amount of deionized water diluted with 2-methoxyethanol in the volume ratio 1:5. The clear solution was put in a 60°C oven for 3-4 hours to form the gel. The transparent BMT xero-gel thus formed after drying was crushed with a mortar and pestle.

The powder was analyzed using a Perkin-Elmer PC-series thermogravimetric (TGA) analyzer to determine the drying and organic burnout behavior of the gel. Differential thermal analysis (DTA) was done in a Perkin-Elmer PC-7 series differential thermal analyzer interfaced with a computer for determination of crystallization temperature. Phase identification was carried out using a Scintag powder X-ray diffraction (model DMC-15) with Ni-filtered Cu $K_{\alpha 1}$ radiation.

BMT thin films were made by spin coating onto Si substrates, using the sol-gel prepared solution. The BMT solution concentration was diluted to 0.3 M and hydrolyzed with water (1:2 ratio with deionized water). In order to prepare crack-free films, 4% (by volume) formamide was added to the solution. Prior to the spin coating, the Pt-coated Si substrates were thoroughly washed with isopropanol. Thin films were spun at 3000 rpm for 20 seconds using an Integrated Technologies P-6000 spincoater.

The deposited films were pyrolyzed on a hot plate at 400-450°C to remove the volatile organics and then held in a furnace set at 600°C for 3 hours. The films were characterized by thin-film Scintag X-ray diffractometer (model DMICRO8) with a pair of divergence solvo silts ahead of the scintillation detector. A scanning electron microscope (SEM) (model ISI-DS 130, Akashi Beam Tech, Japan) was used to study the microstructures and also to measure film thickness. In order to measure dielectric constant and loss, a pellet of BMT powder was pressed, sintered, and gold sputtered on both sides. The density of the pellet as a function of sintering temperature was determined using the Archimedes method.

RESULTS AND DISCUSSION

The TGA results for the gel dried at 70°C from 30°C to 850°C with a heating rate of 10°C/min in an air atmosphere are shown in Figure 2. The TGA thermograms show a maximum weight loss at 240°C, indicating the decomposition of volatile organics from the

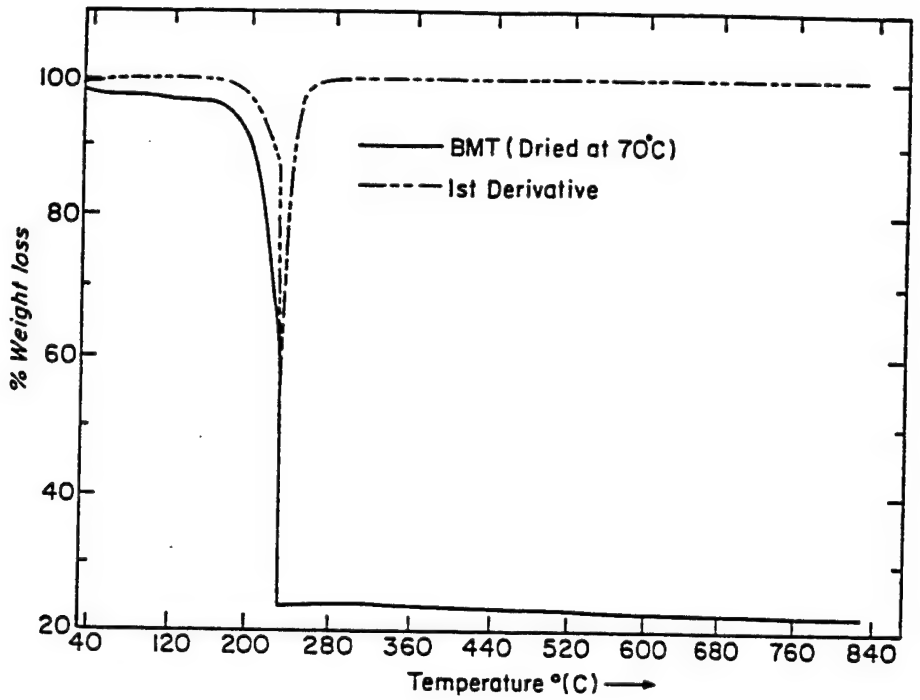

FIG. 2
TGA trace of BMT gel dried at 70°C in an air atmosphere.

gel. To determine the calcination, sintering, and crystallization temperatures of the gel, DTA analysis was done from 100°C to 1000°C with a heating rate of 10°C/min in an air atmosphere. The DTA thermograms show a sharp exotherm with an onset temperature of 278°C and a broad endotherm with an onset temperature of 570°C, as shown in Figure 3. The sharp exotherm at 278°C shows the organic burnout to form the inorganic BMT phase, and the broad endotherm at 570°C is due to the compound formation, which corroborates the X-ray analysis. The gel dried at 60°C was crushed and analyzed by powder X-ray diffraction. It was found to be amorphous with no well-defined diffraction lines. DTA thermograms show a sharp crystallization temperature at 278°C. A powder X-ray diffraction of the amorphous powder heated at 300°C for 6 hours is shown in Figure 4. Most of the diffracted lines could be indexed for the BMT. In addition, a few impurity lines were detected at the low angles. TGA analysis of the BMT powder heated at 300°C for 6 hours (Fig. 5) shows an additional weight loss from organics of 1.64% at 500°C. Reheating the gel powder at a 650°C for 7 hours gave rise to X-ray diffraction patterns in which all the diffraction lines could be indexed in terms of a disordered perovskite structure of BMT. The lattice parameters were calculated using the least-square fitting program with a pseudo cubic perovskite structure $a = 4.0905$ Å.

The values obtained are in accordance with the data reported earlier (4,8) for BMT synthesized by solid-state reaction. The structure of BMT (4) is similar to that of $Ba(Sr_{1/3}Ta_{2/3})O_3$, based on the P3m1 space group. The perovskite structure has close-packed

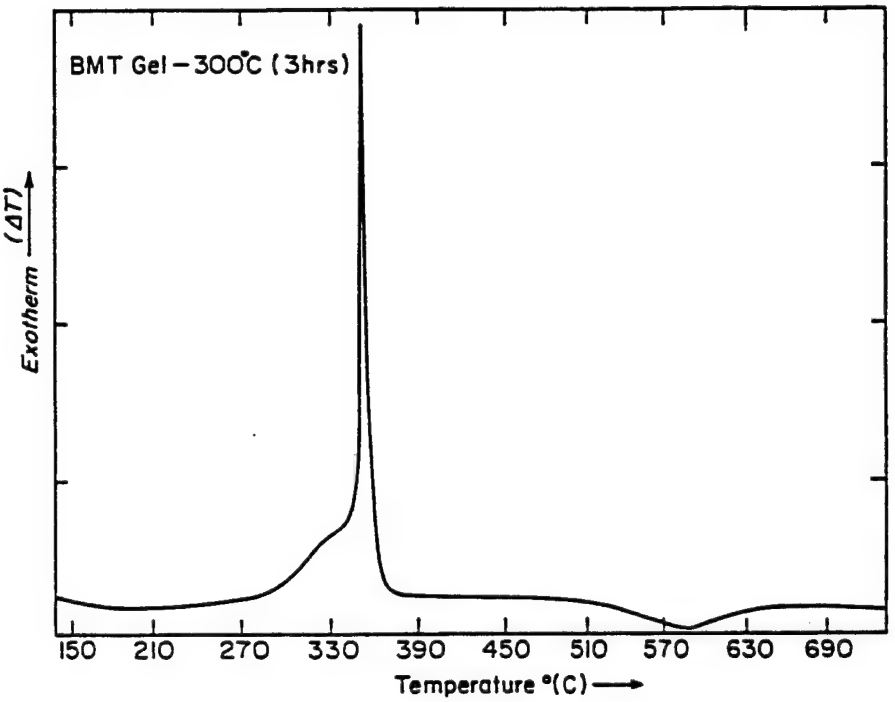

FIG. 3
DTA trace of BMT powders calcined at 300°C for 6 hours in an air atmosphere.

layers of barium and oxygen ions perpendicular to <111>, with Mg and Ta cations occupying the octahedral sites between the layers.

In the case of solid-state reaction, the phase pure BMT phase is obtained at high temperatures ~1600°C (4) or at ~1300°C when precipitated via oxine (2). In contrast, the sol-gel synthesis route produced phase pure BMT powders at 600°C, as shown in Figure 4. The density of sintered pellets as a function of sintering temperature (1300, 1400, and 1500°C) was measured by the Archimedes method. The pellets sintered at 1500°C had high relative density of 98.4% kg/m^3.

Sintering Temperature (°C)	Duration (hours)	Measured Relative Density
1300	24	97.3
1400	24	97.9
1500	24	98.4

X-ray diffraction patterns for the spin-coated thin films on the Pt-coated silicon substrates are shown in Figure 6. The BMT films were transparent with a smooth mirror-like surface after pyrolysis at 600°C for 3 hours. The thickness of the films was measured using SEM. Typical films 0.3 μm in thickness were formed free from cracks.

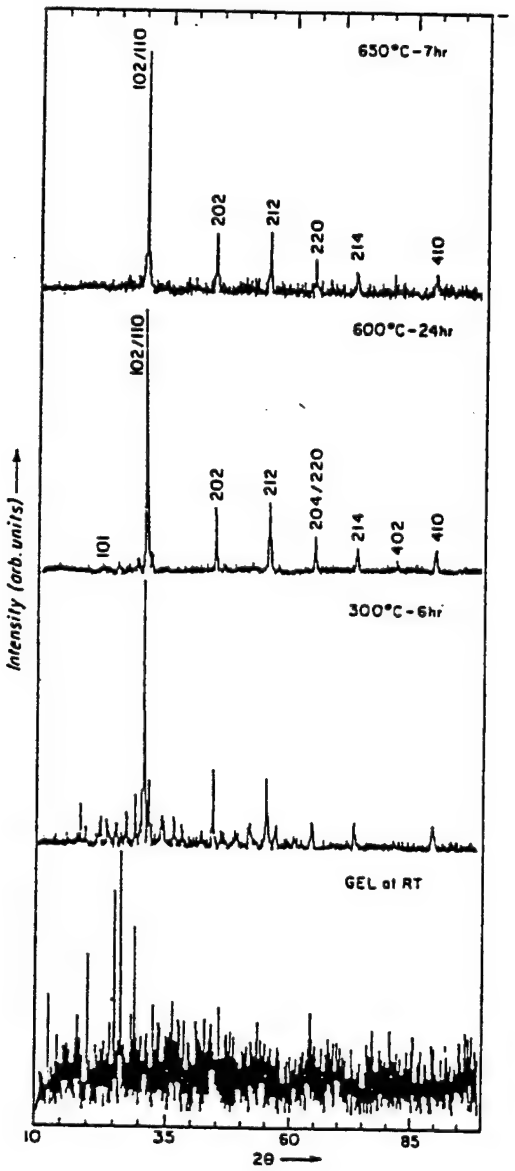

FIG. 4
Powder X-ray diffraction patterns of the BMT powders heated at various temperatures.

CONCLUSIONS

We have synthesized phase pure BMT powder by the sol-gel technique and thin films at a very low temperature (~600°C) instead of by the solid-state reactions usually done at

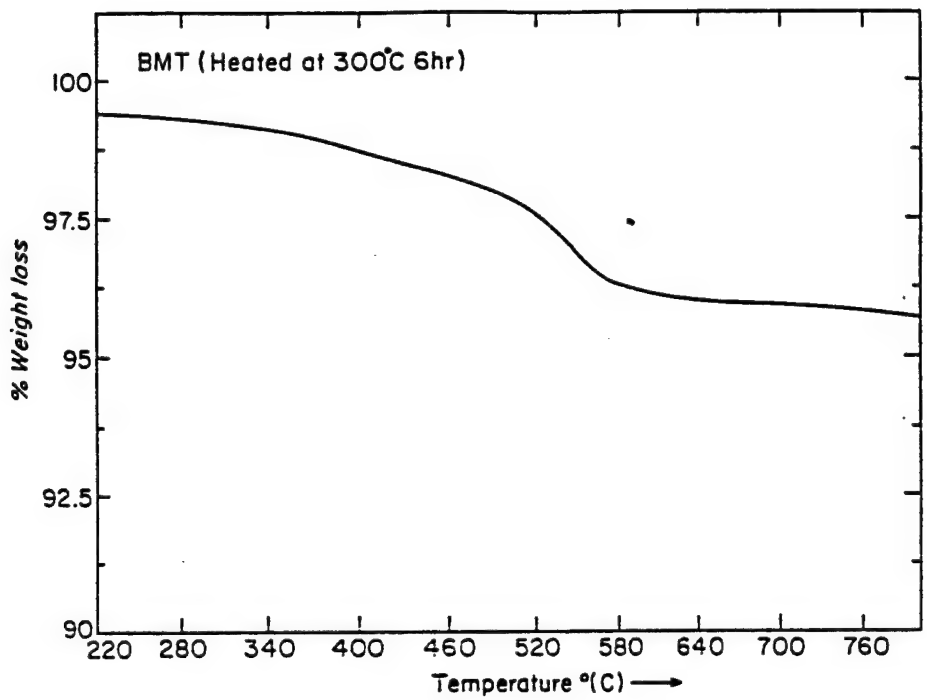

FIG. 5
TGA trace of BMT powders heated at 300°C for 6 hours in an air atmosphere.

high temperature (~1400°C) with very long heating schedules. High quality, crack-free BMT films were prepared on Pt-coated Si substrates for the first time. The relative density of pellets made with sol-gel BMT powder increased with increasing sintering temperature. High relative density (98.4%) kg/m^3 BMT ceramics were formed at 1500°C in 24 hours without the addition of any sintering aid. SEM analysis showed that the films of 0.3 μm in thickness were essentially crack-free.

ACKNOWLEDGMENT

This work was supported by the Defense Advanced Research Projects Agency (DARPA) under the contract number DN 00014-90-J-4140.

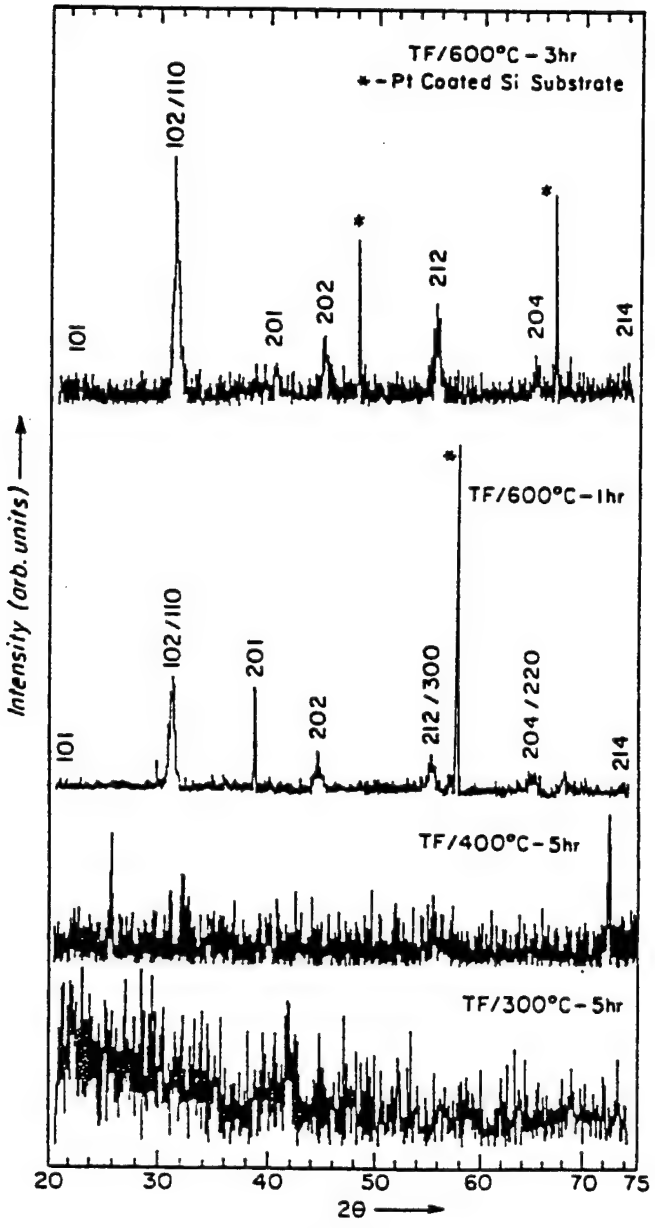

FIG. 6
X-ray patterns of BMT films spin-coated onto a Pt-coated Si substrate.

REFERENCES

1. S. Nomura, K. Toyama and K. Kaneta, *Jpn. J. Appl. Phys.* **21**, L624 (1982).
2. S. Kakegewa, T. Wakabayashi and Y. Sasaki, *J. Am. Ceram.* 69, C-82 (1986).
3. S. Katayama and M. Sekine, *J. Mater. Chem.* **2**, 889 (1992).
4. R. Guo, A.S. Bhalla and L.E. Cross, *J. Appl. Phys.***75**, 4704 (1994).
5. S. Kawashima, M. Nishida, I. Ueda, and H. Ouchi, *J. Amer. Ceram.* 66, 421 (1983).
6. D.C. Bradley, R.C. Mehrotra and D.D. Gaur, *Metal Alkoxides*, p. 308, Academic Press, London (1978).
7. S. Nomura and K. Kaneta, *Jpn. J. App. Phys.* **23**, 507 (1984).
8. F. Galasso and J. Pinto. *J. Inorg. Chem.* **2**, 482 (1963).

APPENDIX 82

THE EFFECT OF ANNEALING TEMPERATURE ON THE FORMATION OF $SrBi_2Ta_2O_9$ (SBT) THIN FILMS

D.Ravichandran, K.Yamakawa, R.Roy, A.S.Bhalla, S.Trolier-McKinstry, R. Guo and L.E. Cross

Materials Research Laboratory
The Pennsylvania State University
University Park, PA 16802, USA

Abstract--In this paper we report on synthesis of SBT thin-films by sol-gel processing. Sr metal, Bi, 2-ethyl hexanoate and Ta-ethoxide were used as precursors. Thin-films with nominal composition $SrBi_2Ta_2O_9$ and SBT +10 % excess Bi content were made. Films were annealed at various temperatures to study the microstructure, crystallization temperature and the polarization values. Good crystallization of SBT was obtained by annealing at 700°C-2hrs, independent of the Bi content in the films. Films annealed in oxygen atmosphere at 800°C-2hrs did not show any significant change in the polarization value. Crack free films were made with film thicknesses of 0.4 μm. Films annealed at 800°C-2 hrs showed a grain size of ~0.2 μm, and reasonably good polarization values of 5 $\mu C/cm^2$. In contrast, films prepared with 10% excess Bi showed a very fine grain size < 0.1 μm with a lower polarization values of 1.5 $\mu C/cm^2$.

I. INTRODUCTION

Bi layered structure ferroelectrics are of great interest for ferroelectric memory device applications because of their excellent fatigue properties compared to lead zirconate (PZT) thin films[1,2]. Newnham et al. [3] studied crystal structure of $Sr_{0.9}Ba_{0.1}Bi_2Ta_2O_9$ was of particular interest, it represents an Aurivillius phase which does not contain Bi^{3+} in the perovskite A site. The compounds of the type $ABi_2B_2O_9$ system, the perovskite-like layers consists of two layers of octahedron. In the case of $Bi_4Ti_3O_{12}$ the perovskite like layer of composition $[(Bi_2Ti_3O_{10})]_x^{2-}$ consists of three layers of octahedron and in compounds $ABi_4Ti_4O_{15}$, it has four layers of octahedron. Cross et al. [4] determined the elastic Gibbs function and its coefficients for $Bi_4Ti_3O_{12}$. The compounds containing perovskite like layers consisting of octahedra NbO_6, TaO_6 and TiO_6 in the lattice of these materials can lead to spontaneous polarization both in the planes and layers [5]. Bi layered structure films such as $SrBi_2T$ the sol-gel method, metal organic deposition (MOD), laser ablation, and laser MBE [6-8]. For all of these methods, it is necessary to study the ferroelectric and dielectric properties,the crystallization behavior, the effects of nonstoichiometry and film microstructure in detail in order to understand the best route to prepare the Bi layered structure films. In this paper we report on the properties of $SrBi_2Ta_2O_9$ (SBT) films with different starting Bi compositions.

II. EXPERIMENTAL PROCEDURE

Fig.1 shows the reaction sequence for the formation of SBT films and gels. The solution was cooled and diluted to 0.3 M with deionized water and 2-methoxyethanol in a ratio of 1:2 [6]. The solution was spin coated on to Pt coated Si substrates after adding 4 % by volume formamide to avoid cracking in the films. The solution was spin coated at 3000 rpm for 20 seconds followed by drying at 400°C. This spin-coating cycle was then repeated to build up the desired thickness. After the depositions the samples were subjected to either conventional furnace annealing or rapid thermal annealing (RTA) at temperatures between 500 and 800°C.

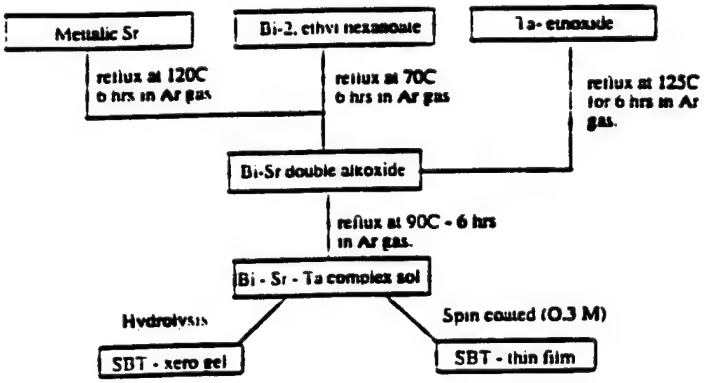

Fig 1. Reaction sequence for the formation of SBT films.

The structural and microstructural characteristics of the films were investigated using an X-ray diffractometer (XRD) and a scanning electron microscope (SEM). The electrical properties were measured using a Radiant Technology RT66A tester and an impedance analyzer. In both cases, sputtered gold top electrode, with a diameter of 0.4 mm, were used.

III. RESULTS AND DISCUSSION

It was found that the crystallization of $SrBi_2Ta_2O_9$ films started at 700°C in both the stoichiometric films and the Bi

rich films. A peak from (115) indexed on the tetragonal unit cell was observed. The stoichiometric film shows better crystallinity than the Bi rich film following annealing at 800°C (fig. 2). For the films annealed at 600°C for 6 hours, a peak from $SrBi_2Ta_2O_9$ was also observed. In any case, the crystallinity of the stoichiometric film was better than that of the Bi rich film. The same tendency was observed for the films annealed at 800°C using RTA.

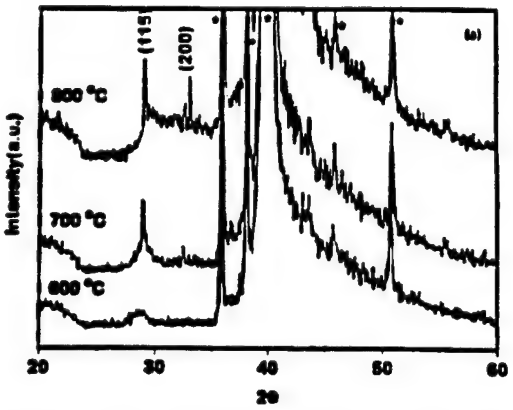

Fig. 2. X-ray diffraction patterns of SBT films.

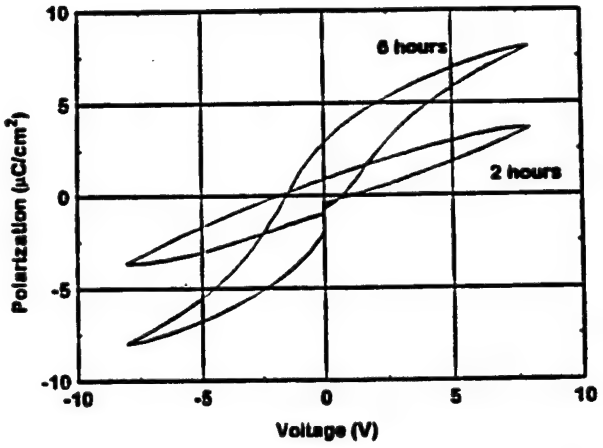

Fig. 3. D-E hysteresis loops for stoichiometric films annealed at 600°C.

The structural properties analyzed using XRD was consistent with the electrical properties. The films that had the layered SBT structure exhibited ferroelectric behavior in a hysteresis loop measurement. Fig.3 shows hysteresis loops for stoichiometric films annealed at 600°C for 2 and 6 hours, respectively. The stoichiometric film exhibits superior ferroelectric properties, with a remanent polariz-ation value of around 5 $\mu C/cm^2$ (fig. 4), while the Bi rich film shows a polarization of 1.5 $\mu C/cm^2$. It is possible that the excess Bi forms a BiO_X layer in the film which functions as a dielectric layer. In addition, the excess Bi leads to a difference in the film grain sizes. The stoichiometric films had rough surfaces and consisted of anisometric grains with grain sizes between 0.1 to 0.2 μm. On the other hand, films with excess Bi showed smooth surfaces and had isometric grains with sizes under 0.1μm. Anisometric grains are generally observed in bulk ceramics of this material.

Asymmetry of the hysteresis loop was also observed as shown in Fig.4. This might be caused by the degradation of the interface between the ferroelectric films and the electrodes due to the high temperatures and long annealing time necessary to crystallize the SBT films. A reaction between Bi and Pt has been reported in previous work [9]. This reaction might affect the crystallinity of the films. Some films were also annealed in a 100 % oxygen atmosphere at 800°C for 2 hours. There was no significant difference in either the structural and electrical properties compared to those annealed in air.

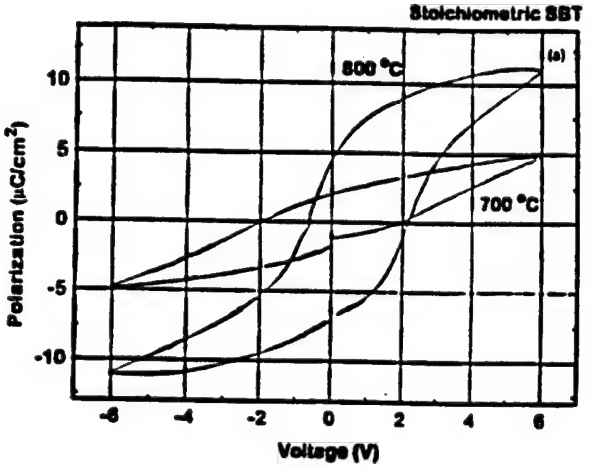

Fig. 4. D-E hysteresis loops stoichiometric films.

Since the crystal structures of Bi layer ferroelectrics are more complicated than the perovskite structure, it is reasonable to expect the two crystallization processes to differ from one another. In the case of room temperature depositions by sol-gel methods, sputter deposition or laser ablation, the atoms in the amorphous as-deposited films must be rearranged significantly to build the Bi layered structures. Each atom in this case needs to move more than in the case of formation of perovskite phase. For example, we observed no crystallized phase in amorphous films prepared by laser ablation at room temperature even after 700°C annealing for 2 hours.

IV. CONCLUSIONS

SBT films have been prepared by a sol-gel method. Stoichiometric films annealed at 800°C showed ferro-electricity with a maximum remanent polarization of 5 $\mu C/cm^2$, while Bi rich films had poor ferroelectric properties. The excess Bi produced difference in grain size and grain shape. The complexity of the Bi layer structure apparently increased the difficulty of crystallization of the films, especially that prepared by PVD methods. Crack free films were produced with a film thicknesses of 0.4 μm.

ACKNOWLEDGMENT

This work was supported by the Defense Advanced Research Project Agency (DARPA) under the contract No : DN 00014-90-J-4140.

REFERENCES

[1] C.A.Paz de Araujo, J.D.Cuchiaro, L.D.McMillan, M.C.Scott and J.F.Scott, Nature, 374, (1995) 627.

[2] K.Amanuma, T.Hase and Y.Miyasaka, Appl.Phys.Lett, 66 (1995) 221.

[3] R.E. Newnham, R.W. Wolf, R.S. Hosey, F.A. Diaz-coln and M.I. Kay, Mater. Res. Bullt. 8 (1993) 1183.

[4] L.E. Cross and R.C. Pohanka, Mater. Res. Bullt. 6 (1976) 939.

[5] I.G. Ismailzade, Proc. III Internl. conf. on ferroelectricity (USSR) Acad.Sci.USSR, Press, Moscow 1960.

[6] D.Ravichandran,K.Yamakawa, A.S.Bhalla and R.Roy, Sol-Gel Sci. & Tech. (To appear in vol. 9, 1997).

[7] P.Y. Chen, R.E. Jones, P. Zurcher, D.J. Taylor, B. Jiang, S.J. Gillespie and Y.T. Lii, J. Mater.Res. 11(1996) 1065.

[8] D.P. Vijay, S.B. Desu, M. Nagata, X. Zhang and T.C. Chen, Mater. Res. Symp. vol 361 (1995) pp.3.

[9] K.Amanuma, T.Hase and Y.Miyasaka Mat.Res.Soc. Symp.Proc., 361, 21 (1995)

INSTRUMENTATION

APPENDIX 83

Sup.
Rev. Sci. Instru.

A Bimorph Based Dilatometer for Field Induced Strain Measurement in Soft and Thin Free Standing Polymer Films

J. Su,[1] P. Moses,[1] and Q. M. Zhang[1,2]*

[1] Materials Research Laboratory, The Pennsylvania State University

[2] Department of Electrical Engineering, The Pennsylvania State University

University Park, PA 16802

Abstract:

A bimorph based dilatometer has been developed which enables one to characterize the electric field induced strain response in the out of plane direction in thin and soft free standing polymer film samples conveniently over a relatively wide frequency range (1 Hz to 1 kHz). The test results demonstrate that the newly developed dilatometer is capable of detecting displacement down to the 0.01 Å range at 100 Hz. The agreement between the test results and the model analysis indicates that the device can indeed be used reliably for these measurement with high sensitivity.

* Corresponding author

I. Introduction.

Polymeric materials have many attractive and unique features for electronic and electromechanical transduction applications. In these applications, how the material behaves under an external electric field is of prime concern in the material selection. Because of the softness of samples to be characterized, currently it is still a great challenge to reliably determine the strain induced by an external electric field in thin polymer films without imposing constraint.

In general, the existing techniques for characterizing the electric field induced strain response in a polymer film can be grouped into two categories: the contact methods and non-contact methods. The contact methods such as the one making use of the change in capacitance between two parallel plates to measure the dimensional change of a polymer film are typically difficult to be used on routine bases.[1,2] In addition, the contacts from the capacitor plates in the capacitance method may impose mechanical constraints in the sample which could be significant for a soft and thin sample and introduce large error in the measurement. For the non-contact measurements, where the laser dilatometer is the one most frequently used, in order to determine the field induced strain in the out-of-plane direction in thin films, two laser beams on the opposite faces of the sample are required. However, again because of the thinness and softness of the films, it is quite easy to excite the flexure motion in the sample which causes severe errors in the results.[3] It appears to us that currently there exists no suitable technique to characterize the electric field induced strain in thin and soft polymeric samples reliably and conveniently.

The recent development of the atomic force microscope has demonstrated the high sensitivity of a cantilever beam in detecting small force, which implies that the similar principle may be transplanted to measure the displacement of soft polymer films without imposing large stress or mechanical constrains in the sample.[4,5] In an even more traditional area, i.e., displacement sensor in a phonograph cartridge, the demands of audiophiles have been forcing the constant improvement of the sensor head and as a result, phonograph cartridges are well developed high sensitivity transducers which require a very small contact force and can be operated over a wide frequency range. Inspired by these advancements, we attempted to develop a high sensitivity

displacement sensor to characterize the electric field induced strain in soft and thin polymeric samples based the piezoelectric bimorph cantilever beam, which in the current device was modified from a phonograph pick-up cartridge, and the results are reported in this paper.

II. Experimental

The schematic of the set-up is shown in figure 1. Under an external electric field, the sample expands and contracts in the z-direction and generates a corresponding motion in the sensor head. Consequently, a bending in the piezoelectric bimorph is produced. Through the direct piezoelectric effect, an electrical output which is proportional to the sensor head displacement is generated. Through a simple calibration procedure, this output signal can be used to quantitatively measure the displacement. In the current set-up, a well aged PZT-4 piezoceramic is used as the displacement standard, whose piezoelectric d_{33} value was measured by both a laser dilatometer and a Berlincourt d_{33} meter.[6,7] By applying a fixed voltage to this standard, typically in the range between 1 to 10 volts, a displacement in the range of 2 - 20 Å is generated to calibrate the device. A typical calibration curve thus obtained is shown in figure 2 where the measured current from a lock-in amplifier vs. the displacement in the PZT-4 standard is presented against the measuring frequency. The dimensions of the PZT-4 standard is 5*5*5 mm^3. The lock-in amplifier used is Model SR830 from Stanford Research Systems which has a current sensitivity down to the fA range.

To assess the performance of this new bimorph based dilatometer in characterizing the field induced strain in soft polymer films, the relationship between the sample surface displacement, the force the sensor head exerting on the sample, and the error thus induced are analyzed based on a static model and results are compared with the experiment. The possible dynamic effect on the measurement is also examined.

III. Analysis of the Performance

Using the constitutive equations for a piezoelectric ceramic material, the relations among the displacement δ^b at the point B, the force F at the tip, and the charge q and voltage output V of a bimorph supported at one end under static condition can be derived (as shown in figure 1(b)):

$$\begin{pmatrix} \delta^b \\ q \end{pmatrix} = \begin{pmatrix} \frac{s_{11}^E h^3}{2wt^3} & -\frac{3d_{31}h^2}{8t^2} \\ -\frac{3d_{31}h^2}{8t^2} & \frac{\varepsilon_{33}^T hw(1-k_{31}^2/4)}{2t} \end{pmatrix} \begin{pmatrix} F \\ V \end{pmatrix} \qquad (1)$$

where s_{11}^E is the elastic compliance of the piezoceramic, w is the width of the bimorph, d_{31} is the transverse piezoelectric coefficient, ε_{33}^T is the dielectric permittivity, and k_{31} is the electromechanical coupling factor, respectively.[8] In our experimental situation, the short circuit condition is used which implies V = 0 in the equation (1).

For the stainless steel (ss) pin attached to the end of the bimorph, a force F at the tip G will produce a bending according to[9]

$$\delta^s = \frac{2L^3 s^{st}}{3\pi r^4} F \qquad (2)$$

where r is the radius of the ss pin which is 0.32 mm in the current device and s^{st} is the elastic compliance of the ss pin. In addition, the bending in the piezoceramic bimorph will also produce a displacement at the point G, which can be shown through the geometric consideration:

$$\delta' = \left(\frac{h^3 s_{11}^E}{2wt^3} + \frac{3h^2 L s_{11}^E}{2wt^3}\right) F \qquad (3)$$

where the first term on the right hand side of the equation is the displacement at the end of the bimorph (point B in figure 1(b)) and the second term is just a geometric amplification effect. Combining this with the bending at the stainless steel pin (eq. (2)) yields the relationship between the force F and displacement Δ at the sensor head (point G):

$$\Delta = \delta^s + \delta' = \mathrm{B}\,\mathrm{F} \qquad (4)$$

where $B = \frac{2L^3 s^{st}}{3\pi r^4} + \frac{3h^2 L s_{11}^E}{2wt^3} + \frac{h^3 s_{11}^E}{2wt^3}$. Similarly, the charge output from the sensor head (piezoelectric bimorph) is given by

$$q = -\frac{3d_{31}h^2}{8t^2}F \qquad (5)$$

Since we are interested in the displacement sensing, combining eqs. (4) and (5) produces

$$q = -\frac{3d_{31}h^2}{8t^2 B}\Delta \qquad (6)$$

In our set-up, L is approximately the same as h and hence, B in eq. (6) is proportional h^3. Eq. (6) indicates that for a fixed displacement Δ at point G, a short length (smaller h and L) in the sensor head will improve the sensitivity. The reason behind this is that for a fixed displacement Δ, a shorter length will result in a large force F in the bimorph (eq. (4)) which results in a high charge output. As a result, the sensitivity of the bimorph sensor is approximately inversely proportional to h and L. However, for the strain measurement in soft polymer films, as will be shown in the next paragraph, a large force at the sensor head will inevitably introduce a large error, which certainly imposes limit on the lengths of h and L in the device.

In order to determine the optimum dimensions for the sensor length (h and L), the possible error induced by the force at the sensor head (point G) in the strain measurement on soft polymer films should be analyzed. From Newton's third law, it can be derived that this force should be equal to that produced in the sample due to the deformation $(\Delta - \Delta_0)$, i.e.,

$$F = A\,(\Delta - \Delta_0)\,/\,(s_{11}^{\,p}\,t_p) \qquad (7)$$

where A is the contacting area of the probe head with the sample, which in our case is about $A = \pi\, 0.3^2$ mm^2, $s_{11}^{\,p}$ is the elastic compliance and t_p is the thickness of the polymer sample, and Δ_0 is the displacement of the polymer without the force F. Clearly, a small error due to the force at the sensor head requires Δ_0/Δ be nearly equal to one. Combining eqs. (4) and (7) yields:

$$\frac{\Delta}{B} = \frac{A(\Delta - \Delta_0)}{s_{11}^p t_p}$$

which, after the rearrangement, becomes

$$\frac{\Delta_0}{\Delta} = 1 - \frac{t_p s_{11}^p}{AB} \qquad (8)$$

To satisfy the condition that Δ is nearly equal to Δ_0, it is required that

$$\frac{A}{t_p s_{11}^p}\left(\frac{2L^3 s^{st}}{3\pi r^4} + \frac{3h^2 L s_{11}^E}{2wt^3} + \frac{h^3 s_{11}^E}{2wt^3}\right) >> 1 \qquad (9)$$

One interesting consequence of the inequality (9) is that the error due to the force F at the sensor head is smaller in a thin film sample (t_p is small) compared with a thick one. Figure 3 presents (Δ_0/Δ -1) vs the compliance of polymer film s_{11}^P for different h (here for the simplicity, h=L and t_p=0.1 mm are assumed) based on eq. (8). Apparently, for soft polymers, in order to reduce the error, a longer length of the bimorph (large h and L) is required.

VI. Experimental Results.

Figure 4(a) presents the relationship between the current output of the sensor head and driving electric field applied to the PZT-4 standard (the displacement is linearly proportional to the driving field). The data shown are at 100 Hz, 400 Hz, and 1 kHz. Since for a fixed displacement Δ, the charge output q is fixed and for a sinusoid signal, the current output I from the bimorph is equal to q ω, where ω is the angular frequency. The sensitivity of the system which is defined as I/Δ, hence, will be directly proportional to the frequency. On the other hand, the environmental noises such as the vibration and air turbulence, which in the current system are the major source limiting the probe sensitivity, will become severe at low frequencies. Due to this reason, the measured sensitivity (or displacement resolution) limit of the system vs. frequency, as shown in figure 4(b), falls off faster than 1/f. The data in figure 4(b) is from the

error bar $\delta\Delta$ ($\Delta \pm \delta\Delta$), which is defined as the half width at half maximum of the displacement data for a given applied voltage. To reduce these noises, the set-up was placed inside a closed chamber during the measurement. The data in figure 4(b) show that the probe has a sub-Angstrom sensitivity over a relatively wide frequency range. For instance, at 100 Hz, it can detect a displacement of 0.01 Å.

The data at 100 Hz were also used to make a comparison between the test result and the performance prediction based on the static model presented in the preceding section. Since in the construction of the sensor head, the exact dimensions such as h and L cannot be controlled precisely, the approximate values of h = 10 mm, and L = 10 mm are used in the calculation. The other parameters are: for the piezoceramic bimorph, t = 0.3 mm, w = 1.5 mm, $s_{11}^{E} = 16.5 * 10^{-12}$ m^2/N, and $d_{31} = -274$ pC/N, and for the ss pin, r = 0.32 mm, $s^{st} = 5.2 * 10^{-12}$ m^2/N. Using these parameters, we obtain the charge output $1.50*10^{-15}$ C for a displacement at the sensor head of 11.04 Å, which is very close to the experimentally measured value of $1.59*10^{-15}$ C (data in figure 4(a)). Such a good agreement between the model prediction and the test result could be a coincidence. However, it does indicate that the probe functions properly with a high sensitivity.

The force exerting on the sample by the sensor head can also be evaluated. For the same displacement of 11.04 Å and charge output of $1.59*10^{-15}$ C, the force F is 2.07 mg (eq. (5)). Making use of eq. (7), the difference between Δ and Δ_0 for a polymer film of thickness 50 μm and a compliance of $5*10^{-8}$ m^2/N is about 0.2 Å which amounts for a 1.8% error in the measured data and indicates the probe in the current configuration is proper for the polymers to be examined.

One of the concerns in operating this new instrument is its operational frequency range. At the low frequency end, the frequency limit is mainly caused by the decrease of the sensitivity as the frequency is lowered. On the other hand, on the high frequency end, it is the resonant frequency of the system which limits how high the probe can be operated. For a cantilever beam, the resonant frequency is inversely proportional to the square of the length (h and l for the

system discussed here).[8,9] Shown in figure 5 is the electric impedance of the probe head (the impedance is from the piezoelectric bimorph) vs. frequency for the system tested where the probe head is in contact with a sample as in the measurement situation. As seen, the first resonance mode appears at a frequency above 2 kHz. From the fixed boundary condition at the two ends, this resonance corresponds to a half-wave length resonance. Hence, the device can be used at frequencies up to 1 kHz without the interference with the resonant mode which was also confirmed by direct experimental results.

As the operation frequency increases, one is also concerned with the possible mass loading on the sample. According to Newton's second law, this force should be proportional to the square of the frequency. To assess this effect, the worst case scenario is considered, i.e., with all the mass m of the stainless steel pin concentrated at the tip so that the force is equal to $m\,\omega^2\,\Delta$, which at 1 kHz is $1.46*10^{-6}$ N for Δ = 11.04 Å and is more than ten times smaller than the force originated from the bending of the sensor arm (the static force). Hence for the current configuration, the probe is capable of operating over a wide frequency range without significant mass loading effect.

After the calibration and evaluation of the device, a series of polyurethane elastomers (DOW 2103-80AE) was characterized as to their field induced strain responses. In the temperature range about room temperature, the compliance of the polyurethane samples is below $5*10^{-8}$ m^2/N and, the device can be used to determine the field induced strain without introducing significant error as has been shown.

It is well known that in this type of material, because of the central symmetry, the strain S is proportional to the square of the applied electric field E, i.e., $S = RE^2$, where R is a coefficient describing the sensitivity of strain change in the material to the external electric field. For a sinusoidal applied electric field $E= E_0 \cos \omega t$, it is the 2f component of the strain response that is measured by the lock-in amplifier,

$$S = R (E_0 \cos \omega t)^2$$

$$= R E_0^2 (1-\cos 2\omega t) / 2 \qquad (9)$$

and the displacement amplitude Δ measured at the probe head at 2f frequency is

$$\Delta = t_p R E_0^2 / 2$$

Shown in figure 6 is the R coefficient for polyurethane films vs. thickness at different frequencies measured at room temperature. The samples are solution cast films of DOW polyurethane 2103-80AE and the electrode is sputtered gold film of about 300 Å thickness. The negative sign of R coefficient shows that the film contracts as an electric field is applied. The device is quite convenient in measuring the electric field induced strain in thin film samples and the thinnest film measured here is 20 μm. From the basic principle of the device and the analysis presented, it is clear that the probe can be used to characterize the strain response in even thinner films. The dependence of R with thickness has been investigated earlier and due to the limitation of the measuring technique (a laser beam dilatometer), the thinnest sample examined was 0.15 mm.[3,10] In the thickness range overlapped, the results from the two measurements are consistent with each other. Figure 7 presents a comparison between the result measured from the current device and that from a double beam laser dilatometer on polyurethane sample of 2 mm thickness.[7] Apparently, the results from the two agree with each other quite well.

The displacement Δ of the polyurethane film of 50 μm thick was also measured as a function of driving field at 100 Hz and the result is shown in figure 8. As expected, the displacement exhibits a V^2 dependence where V is the applied voltage. Clearly, the result demonstrates that at this frequency, the set-up has a resolution much below 10^{-2} Å for a soft thin polymer film.

V. Summary

In summary, a novel bimorph based dilatometer has been developed which enables one to characterize the electric field induced strain response in thin and soft polymer film samples

conveniently over a relatively wide frequency range (1 Hz to 1 kHz). The test results demonstrate that the newly developed dilatometer is capable of detecting displacement much below 0.01 Å at 100 Hz. The agreement between the test results and the model analysis indicates that the device can indeed be used reliably for these measurements with a high resolution.

This work was supported by the Office of Naval Research.

References:

1. M. Zhenyi, J. I. Scheinbeim, J. W. Lee, and B. A. Newman, J. Polym. Sci. Part B: Polym. Phys. 32, 2721 (1994).

2. Ravi F. Saraf, Ho-ming Tong, Tze W. Poon, B. David Silverman, Paul. S. Ho, and Angelo R. Rossi, J. Appl. Polym. Sci. 46, 1329 (1992).

3. H. Wang, Q. M. Zhang, L. E. Cross, R. Ting, C. Coughlin, and K. Rittenmyer, Proc. Int. Symp. Appl. Ferro. 9, 182 (1994).

4. G. L. Miller, J. E. Griffith, E. R. Wagner, and D. A. Grigg, Rev. Sci. Inst. 62, 705 (1991).

5. T. Itoh and T. Suga, J. Vac. Sci. Technol. B12, 1581 (1994).

6. PZT-4 is the trademark of Morgan Matroc Inc. OH for its piezoceramic.

7. Q. M. Zhang, S. J. Jang, and L. E. Cross, J. Appl. Phys. 65, 2807 (1989).

8. J. M. Herbert, "Ferroelectric Transducers and Sensors" (Gordon and Breach Science Publishes, N. Y. 1982).

9. Landau and E. M. Lifshitz, "Theory of Elasticity" (Oxford: Pergamon Press 1986).

10. H. Wang, Ph. D. Thesis, The Pennsylvania State University (1994).

Figure captions:

Figure 1. (a) Schematic of the newly developed high resolution displacement sensor and the electric driving and detection circuits; (b) Schematic of the sensor head consisting of a piezoceramic bimorph and a stainless steel pin. The bending in the bimorph generates an electric output which is proportional to the displacement at the point G.

Figure 2. The calibration curve of the displacement sensor which shows that the sensitivity of the device is proportional to the frequency. Open circles are the experimental data and solid line is a linear fitting curve.

Figure 3. The error in the displacement (Δ_0/Δ -1) caused by the force from the bending in the sensor head vs. the elastic compliance of the polymer film of 100 μm thickness for sensors with different bimorph and ss pin lengths (L=h is assumed) (calculated from eq. (8)).

Figure 4. (a) The current measured by a Lock-in amplifier vs. the displacement in a PZT-4 standard (the displacement in PZT-4 = 2.20 Å * applied voltage) which shows a linear relationship between the displacement and the current output. The sensitivity of the device decreases at low frequency. Open circles, black dots, and crosses are the data points and solid lines are drawn to guide eyes. (b) The displacement resolution limit of the device vs. frequency. Apparently, the resolution limit drops off faster than 1/f. Open circles are the data and solid curve is drawn to guide eyes.

Figure 5. The electric impedance curve measured from the piezoelectric bimorph when the probe head was in contact with a sample. There is no noticeable resonance at frequencies below 2 kHz (the weak resonances are indicated by arrows). Hence, the current device can be used up to 1 kHz without the interference of the resonance. The resonant frequency in the device can be raised by reducing the lengths of the bimorph and ss pin.

Figure 6. R of a polyurethane elastomer (DOW 2103-80AE) as a function of the sample thickness at different frequencies. The negative sign of R coefficient indicates that the film contracts when a voltage is applied. The thinnest sample measured is 20 μm thick. Data points are shown on the figure and the solid curves are drawn to guide eyes.

Figure 7. Comparison of R coefficient of a polyurethane sample (2 mm thick) measured from a double beam laser dilatometer (solid circles) and the newly developed bimorph dilatometer (open circles) as a function of frequency.

Figure 8. The displacement measured from a polyurethane thin film (50 μm) under an electric field of 100 Hz as a function of applied voltage. The black dots are the data and solid line is a fitting: Displacement -- V^2. The data demonstrate the high resolution of the system (much below 0.01 Å).

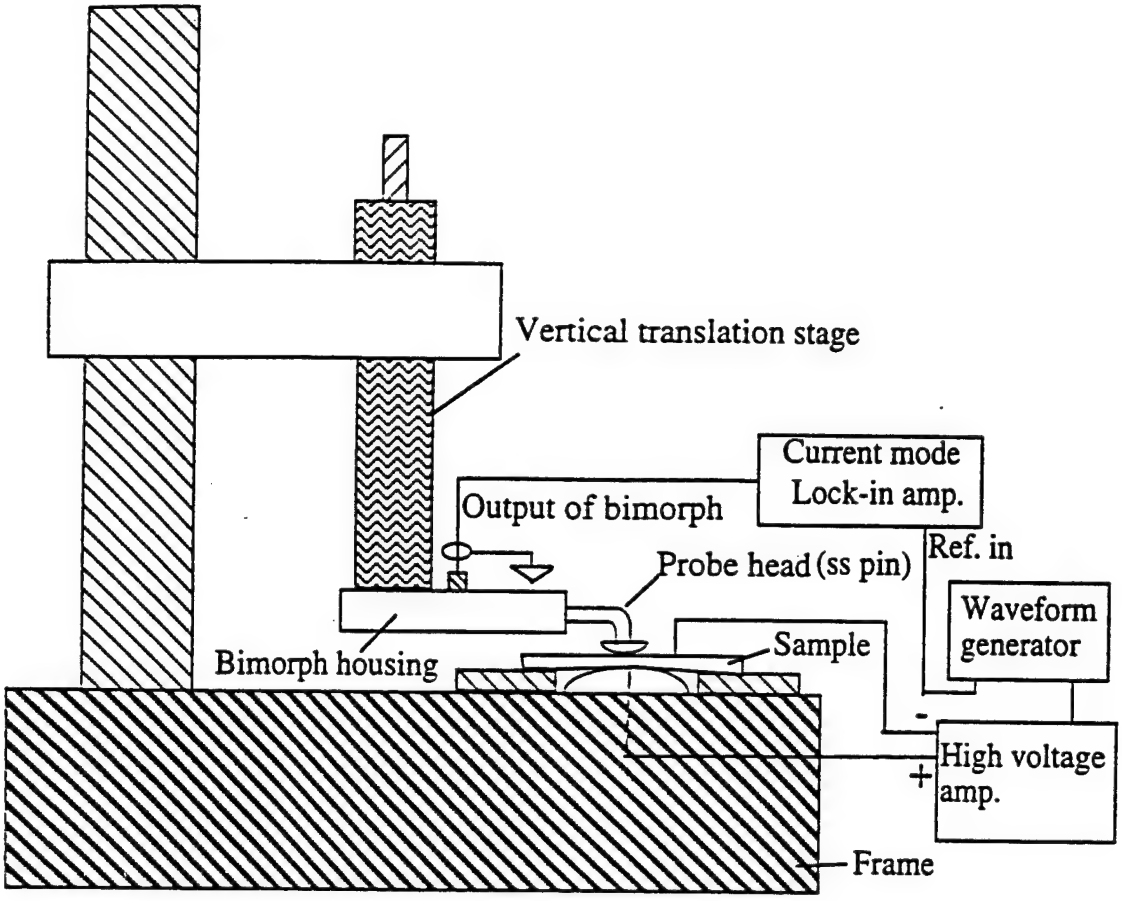
Vertical translation stage
Current mode
Lock-in amp.
Output of bimorph
Ref. in
Probe head (ss pin)
Waveform
generator
Sample
Bimorph housing
-
+
High voltage
amp.
Frame

(a)

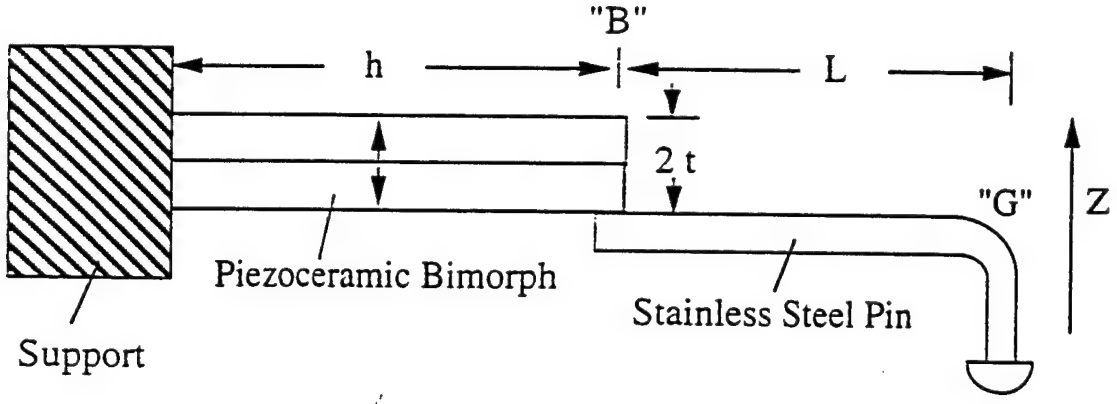
"B"
h
L
2 t
"G"
Z
Piezoceramic Bimorph
Stainless Steel Pin
Support

(b)

J. Su. F. 1

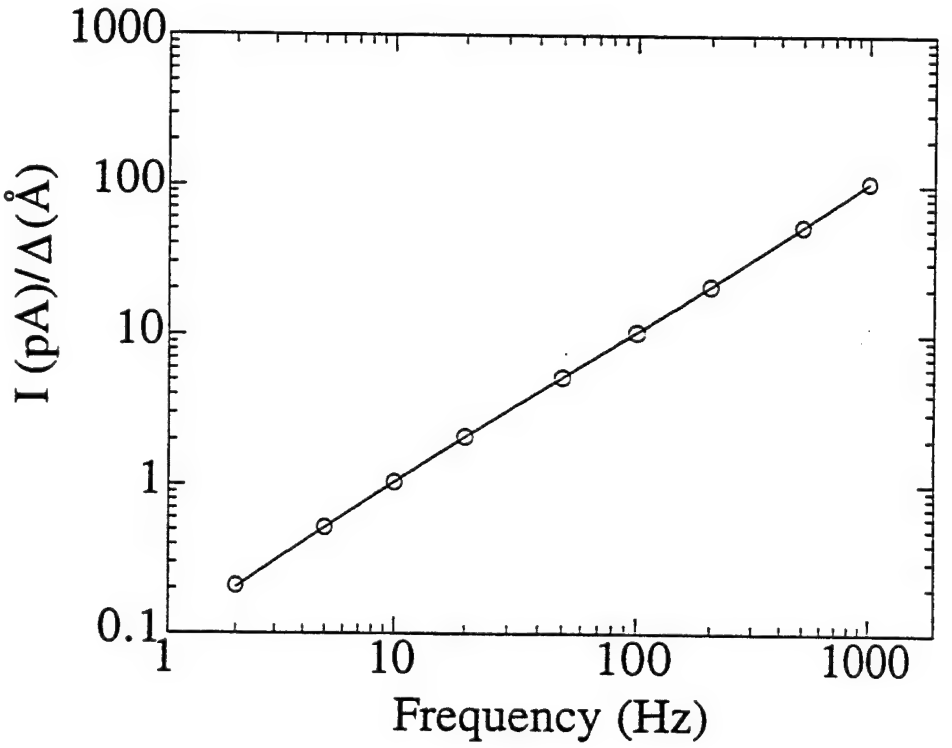

F. 2

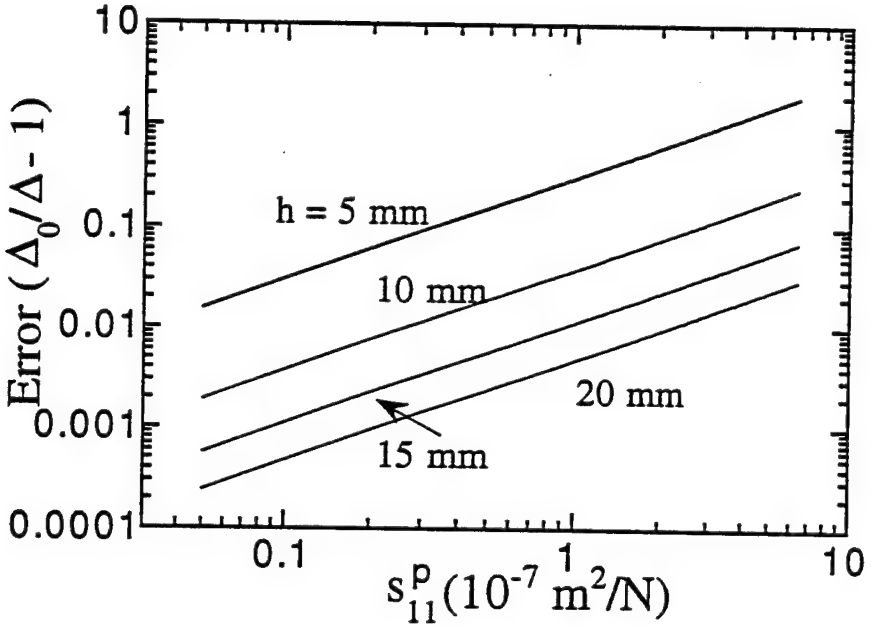
10
1
0.1
0.01
0.001
0.0001
Error (Δ_0/Δ - 1)
h = 5 mm
10 mm
20 mm
15 mm
0.1
1
10
s_{11}^p(10^{-7} m^2/N)

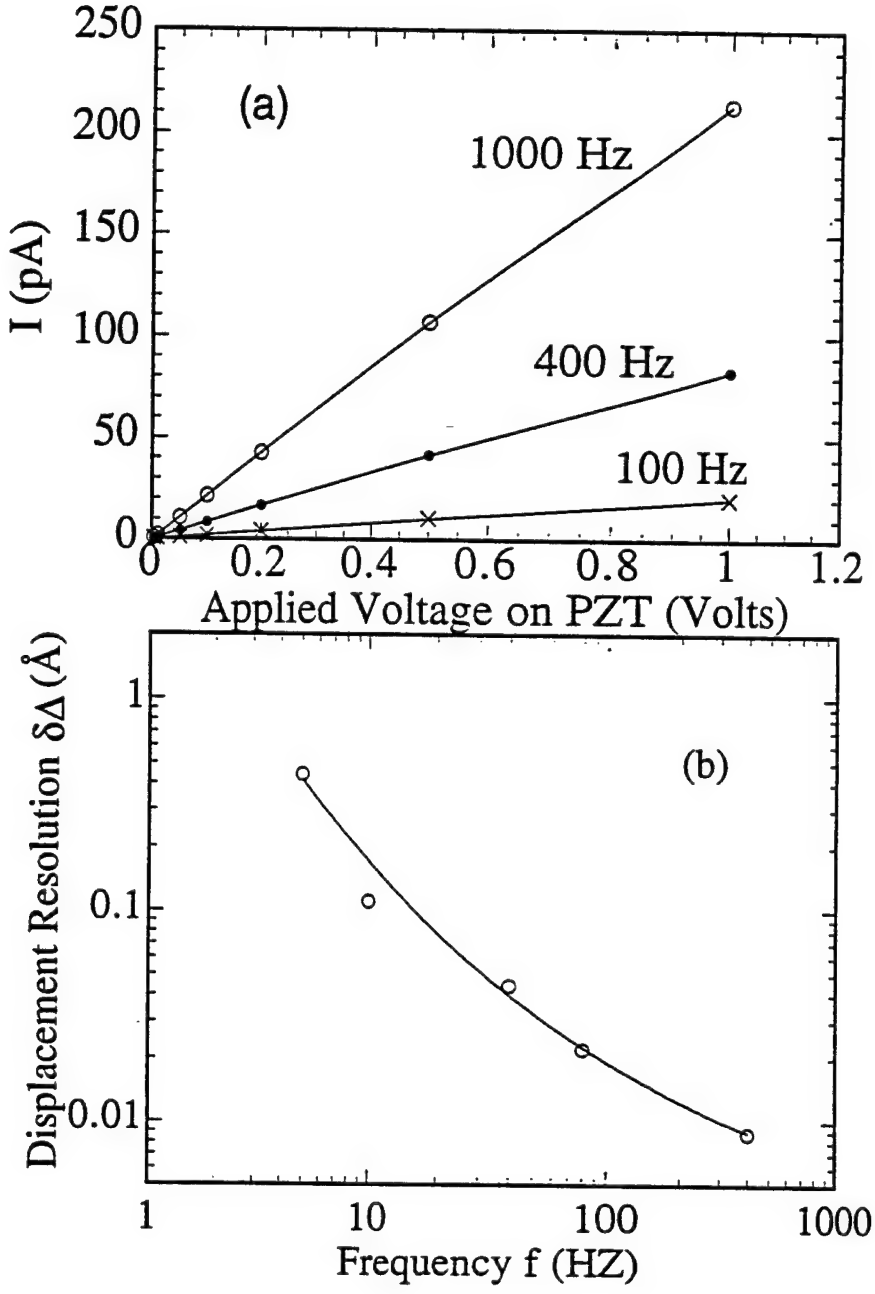
250
200
150
100
50
0
I (pA)
(a)
1000 Hz
400 Hz
100 Hz
0
0.2
0.4
0.6
0.8
1
1.2
Applied Voltage on PZT (Volts)
Displacement Resolution δΔ (Å)
1
0.1
0.01
(b)
1
10
100
1000
Frequency f (HZ)

F. 4

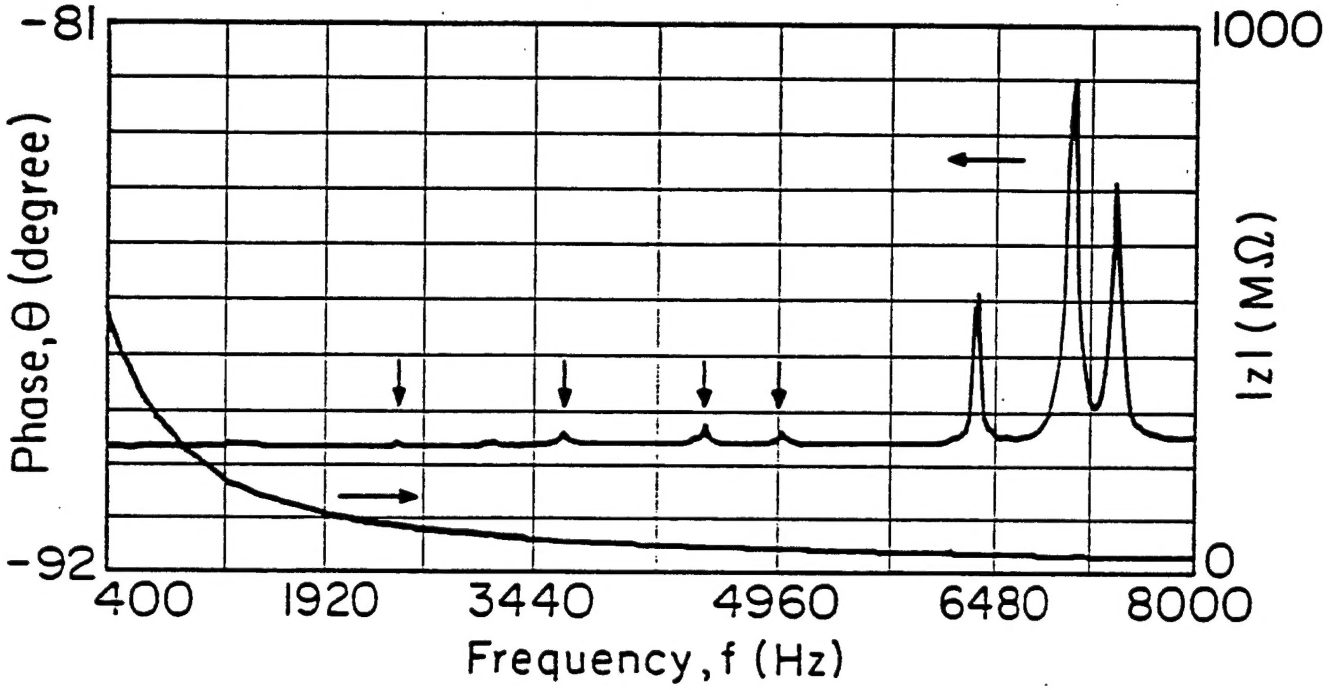
-81
-92
Phase, θ (degree)
1000
0
|z| (MΩ)
400
1920
3440
4960
6480
8000
Frequency, f (Hz)

J. Su F.5

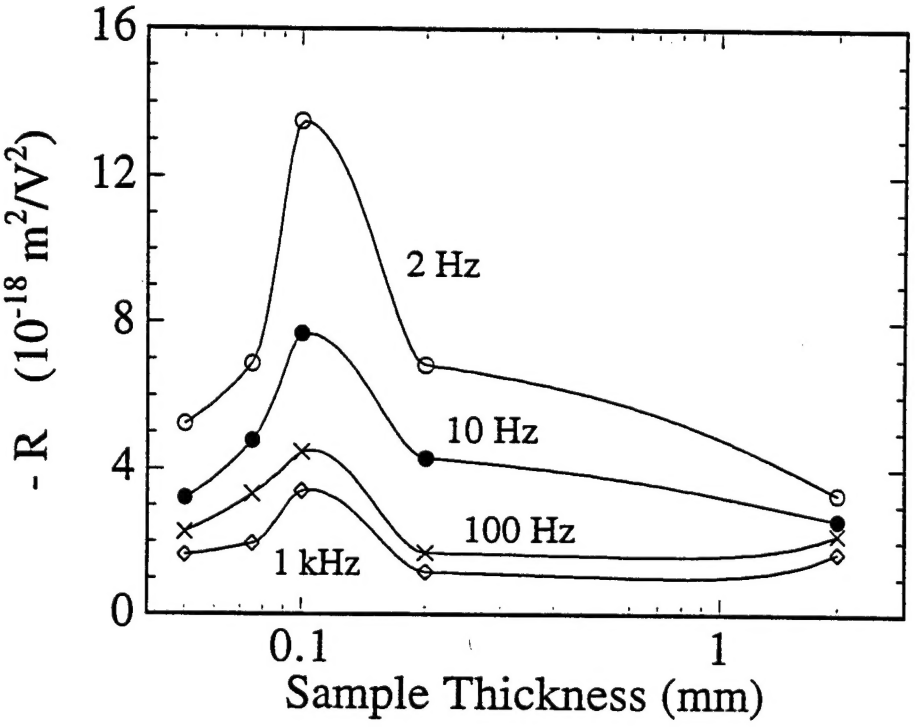
16
12
8
4
0
- R (10^-18 m^2/V^2)
2 Hz
10 Hz
100 Hz
1 kHz
0.1
1
Sample Thickness (mm)

J. Su F.f

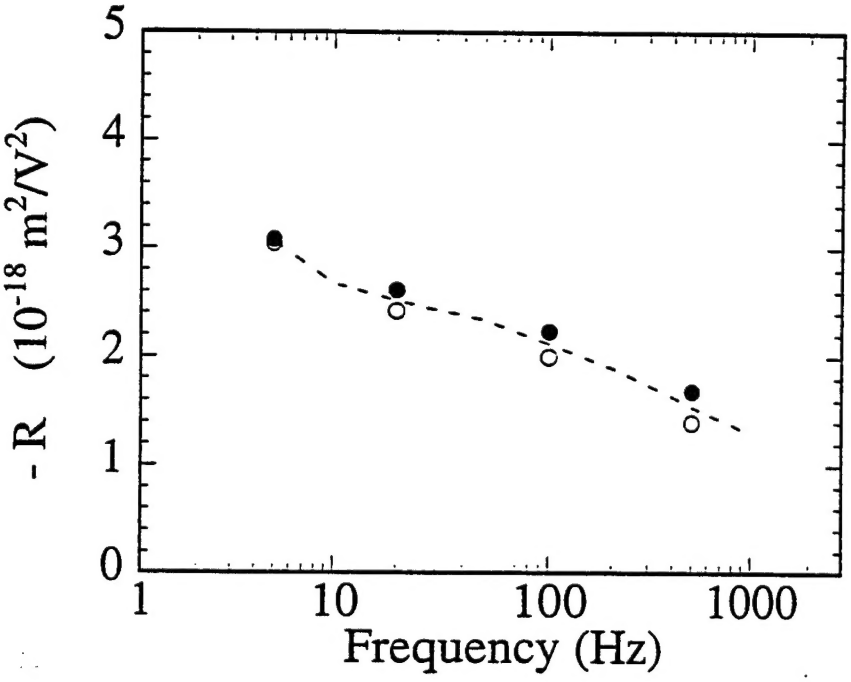

J. Su F.

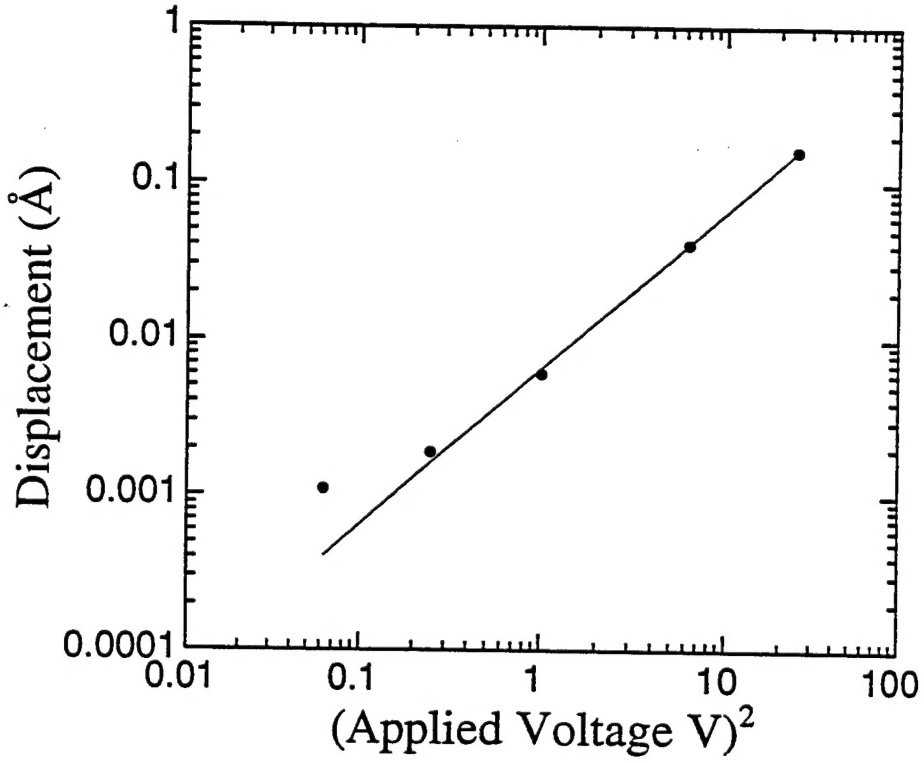
Displacement (Å)
1
0.1
0.01
0.001
0.0001
0.01
0.1
1
10
100
(Applied Voltage V)^2

F. 8.